

**The effects of cell-specific Reelin depletion in
inhibitory interneurons on the dentate gyrus of
adult mice (*Mus musculus*, *Linnaeus 1758*)**

Dissertation

with the aim of achieving the doctoral degree

doctor rerum naturalium (Dr. rer. nat.)

at the Faculty of Mathematics, Informatics and Natural Sciences

Department of Biology

of the University of Hamburg

Submitted by

Jasmine Pahle

from Hochstadt/Pfalz

Hamburg, 2019

Day of the oral defence: 21st February, 2020

The following evaluators recommend the admission of the dissertation:

Gutachter 1/ evaluator 1:

Prof. Dr. Christian Lohr
Martin-Luther-King-Platz 3
20146 Hamburg

Gutachter 2/ evaluator 2:

Prof. Dr. Matthias Kneussel
Falkenried 94
20251 Hamburg

Declaration on oath

I hereby declare, on oath, that I have written the present dissertation by my own and have not used other than the acknowledged resources and aids.

Hamburg, 4th of November 2019

Jasmine Pahle

Eine Erkenntnis von heute kann die Tochter eines
Irrtums von gestern sein.

The knowledge of today can be the daughter of a fallacy
from yesterday.

Marie von Ebner-Eschenbach (*1830- †1916)

(Schriftstellerin/ author)

Abstract

The highly conserved brain matrix protein Reelin is a very important conductor in the well-orchestrated process of brain development. As guidance cue for new born migrating neurons, influencer on cytoskeleton functions or modulator for N-methyl-d-aspartate (NMDA) receptors at synapses, the glycoprotein Reelin plays a critical role. However, little is known about Reelin function in adulthood. Previous studies proposed a participation of Reelin in diseases emerging at adolescence or adulthood. They reported altered amounts of Reelin mRNA and protein in brains of patients suffering from schizophrenia, bipolar disorder, depression, temporal lobe epilepsy and Alzheimer's disease. Thus, it is of great interest to investigate the function of Reelin in an adult brain. To accomplish this, this study established a cell-specific Reelin knockout mouse line, in which Reelin is depleted exclusively in inhibitory interneurons, being the main adult Reelin source in the cortex and the hippocampus. Activation of the loxP/Cre system was accomplished with the interneuron specific *Dlx5/6* promoter, which controlled Cre recombinase expression. An examination with the naturally occurring mutant, the *reeler* mouse, which does not produce any Reelin, would be ineffective, as this mutant has severe developmental defects. However, the cell specific Reelin knockout mouse line displayed an unaffected development, resulting in normal layering and cytoarchitecture in the different brain structures. The main focus of this study was on the dentate gyrus of the hippocampal formation, as this brain area is highly important for pattern integration, learning and memory, and as one out of two hotspots of adult neurogenesis. Furthermore, the dentate gyrus had been shown to be susceptible to Reelin influence. Immunohistochemical staining and quantifications in the inhibitory interneuron specific Reelin knockout revealed a higher number of Reelin-expressing Cajal-Retzius cells at the hippocampal fissure, a significant higher cell number of Calretinin-expressing cells (mossy cells), and less interneuron numbers in the hilar area of the dentate gyrus plus a higher staining intensity of Calretinin and cannabinoid receptor 1 in the inner molecular layer of the dentate gyrus. In contrast, the overall and subgroup specific numbers of interneurons were unaltered. Additionally, no granule cell dispersion was found in the conditional Reelin knockout, although correlations between a loss of Reelin or interference with the Reelin signalling pathway with this phenomenon had previously been published. The examination of the adult neurogenesis in the dentate gyrus was split in two analyses. One addressed the composition and integrity of the stem cell niche, located adjacent to the granule cell layer and

Abstract

the hilar area. The second gathered the quantity of proliferating cells and maturation stages of cells together with an evaluation of cell properties of progenitor cells and young neurons. The stem cell niche was found to be intact and with a normal composition of cells containing in midst a Reelin expressing hilar commissural-associational pathway related (HICAP) cell. The amount of proliferating cells and maturing stages were comparable to the control, and the cell properties of progenitor cells and young neurons were unaltered, too. The performed behavioural tests revealed no abnormal behaviour in the established inhibitory interneuron specific Reelin knockout mouse line. In conclusion, it is to be stated that Reelin derived from inhibitory interneurons has no share of establishing or maintaining cell layering or cytoarchitecture, nor does it influence in a special way the proliferation and maturation in adult neurogenesis. On the other hand the cell specific depletion of Reelin in inhibitory interneurons led to an increased number of Reelin expressing Cajal-Retzius cells, indicating an autocrine influence of Reelin and a possible compensatory effect. The increased number of Calretinin-expressing mossy cells and the increased presence of Calretinin and cannabinoid receptor 1 in the inner molecular layer of the dentate gyrus represent a phenomenon for further investigations. These results were not found in mice genotypically comparable to the heterozygous *reeler* mouse, exhibiting and over all halving of Reelin protein amount, so they can be attributed to the cell specific Reelin depletion in inhibitory interneurons.

This study provided initial insights into the effects of the interneuron-derived Reelin on the adult dentate gyrus. Thereby, it contributed to the elucidation of the cell- and development-specific effects of Reelin.

Zusammenfassung

Das hochkonservierte Gehirnmatrixprotein Reelin ist ein wichtiger Dirigent im gut orchestrierten Prozess der Gehirnentwicklung. Es spielt eine wichtige Rolle als Richtungsweiser für neu geborene, migrierende Neurone, als Beeinflusser der Zellskelettfunktion oder als Modulator des N-Methyl-D-Aspartat (NMDA) Rezeptors in der Synapse. Es ist jedoch wenig darüber bekannt, welche Funktion Reelin im Erwachsenenalter hat. Vorhergehende Studien schlugen eine Beteiligung von Reelin in Krankheiten vor, die in der Jugend oder dem Erwachsenenalter auftreten. Sie berichteten von veränderten Reelin mRNA- und Proteinmengen in Gehirnen von Patienten mit Schizophrenie, Temporallappenepilepsie, bipolarer Störung, Depression und Alzheimer. Daher ist es von

Abstract

großem Interesse, die Funktionsweise von Reelin in einem erwachsenen Gehirn zu erforschen. Um dies zu bewerkstelligen, wurde in dieser Studie eine zellspezifisch konditionale Reelin knockout Mauslinie etabliert, in der Reelin nur in hemmenden Interneuronen dezimiert ist, welche die Hauptquellen für Reelin im adulten Cortex und Hippocampus sind. Die Aktivierung des verwendeten loxP/Cre Systems wurde mit dem interneuronenspezifischen Dlx5/6 Promotor bewerkstelligt, der die Expression der Cre-Rekombinase kontrolliert. Eine Untersuchung anhand der natürlich vorkommenden Mutante der *reeler* Maus, die keinerlei Reelin produziert, wäre nicht zielführend, da diese Mutante schwere Entwicklungsdefizite aufweist. Die zellspezifisch ausgeschaltete Reelin Mauslinie zeigte jedoch eine ungestörte Entwicklung, resultierend in einer normalen Schichtung und Zellarchitektur in den unterschiedlichen Gehirnregionen. Der Hauptfokus der Untersuchung wurde auf den Gyrus dentatus der hippocampalen Formation gelegt, da diese Gehirnregion sehr wichtig ist für die Musterintegration, das Lernen und Erinnern und als einer von zwei Schwerpunkten der adulten Neurogenese gilt. Weiterhin wurde gezeigt, dass der Gyrus dentatus sehr empfänglich für die Beeinflussung durch Reelin ist. Immunhistochemische Färbungen und Quantifizierungen in der Mauslinie mit zellspezifisch ausgeschaltetem Reelin offenbarten eine größere Zahl an Reelin exprimierenden Cajal-Retzius Zellen entlang der hippocampalen Fissur, eine signifikant höhere Anzahl an Calretinin exprimierenden Zellen (Mooszellen) und eine geringere Anzahl an Interneuronen im Hilus des Gyrus dentatus, sowie eine höhere Farbeintensität für Calretinin und den Cannabinoidrezeptor 1 in der inneren Molekularschicht des Gyrus dentatus. Hingegen war die Gesamtzahl und die Anzahl in den Untergruppen der Interneurone unverändert war. Zusätzlich konnte keine Körnerzelldispersion in der zellspezifisch ausgeschalteten Reelin Mauslinie festgestellt werden, obwohl Zusammenhänge zwischen einem Reelin Verlust und der Beeinflussung des Reelin Signalweges mit diesem Phänomen vorher publiziert worden waren. Die Untersuchung der adulten Neurogenese im Gyrus dentatus wurde in zwei Analysen unterteilt. Eine adressierte die Zusammensetzung und Integrität der Stammzellnische, angrenzend an die Körnerzellschicht zur Hilus Region gelegen, die zweite erfasste die Quantität der proliferierenden Zellen und Reifungsstadien der Zellen zusammen mit einer Untersuchung der Zelleigenschaften von Vorläuferzellen und jungen Neuronen. Die Stammzellnische war unversehrt und zeigte eine normale Zusammensetzung an Zellen, in deren Mitte sich eine Reelin exprimierende, hiläre kommissural-assoziierende Bahn verbundene (HICAP) Zelle befand. Die Menge an proliferierenden Zellen und Reifestadien war vergleichbar mit denen der Kontrolle, und die

Abstract

Zelleigenschaften der Vorläuferzellen und jungen Neuronen waren gleichfalls unverändert. Die durchgeführten Verhaltenstests deckten kein abnormes Verhalten in der etablierten Mauslinie auf, in der Reelin zellspezifisch in hemmenden Interneuronen ausgeschaltet wurde. Abschließend ist festzuhalten, dass Reelin von hemmenden Interneuronen nicht beteiligt ist an der Etablierung oder der Aufrechterhaltung von Zellschichten oder der Zellarchitektur, noch beeinflusst es in spezieller Weise die Proliferation und Reifung während der adulten Neurogenese. Andererseits führt die zellspezifische Depletion Reelins in hemmenden Interneuronen zu einer erhöhten Anzahl Reelin exprimierender Cajal-Retzius Zellen, was auf einen autokrinen Einfluss Reelins und einen möglichen kompensatorischen Effekt hindeutet. Die gesteigerte Anzahl Calretinin exprimierender Mooszellen und die stärkere Präsenz von Calretinin und des Cannabinoidrezeptors 1 in der inneren Molekularschicht des Gyrus dentatus stellen ein näher zu untersuchendes Phänomen dar. Diese Ergebnisse wurde nicht in Mäusen gefunden, die genotypisch der heterozygoten *reeler* Maus ähneln, deren Gesamtproteinmenge an Reelin halbiert ist, und können dadurch der zellspezifischen Depletion von Reelin in hemmenden Interneuronen zugeschrieben werden.

Mit dieser Studie konnten erste Einblicke in die Wirkung des von Interneuronen stammenden Reelins auf den adulten Gyrus dentatus gewonnen werden. Damit leistet sie ihren Beitrag zur Aufklärung der zell- und entwicklungsspezifischen Wirkungsweise von Reelin.

Content

Abstract.....	5
Zusammenfassung	6
Content	9
1. Introduction	15
1.1 The natural mutant <i>reeler</i>	15
1.2 Reelin: gene, protein, receptors and canonical pathway	17
1.2.1 The <i>reelin</i> gene	17
1.2.2 The Reelin protein	18
1.2.3 The Reelin main receptors	19
1.2.4 The canonical Reelin signalling pathway	20
1.2.5 Reelin and disease in men	22
1.3 Cajal-Retzius cells in the mouse.....	24
1.4 Inhibitory interneurons in the mouse.....	25
1.5 Adult neurogenesis in the mouse brain	27
1.6 Hippocampal formation of the mouse	30
1.7 Aims and Objectives.....	33
2. Material and Methods.....	34
2.1 Animals.....	34
2.2 Polymerase chain reaction (PCR).....	35
2.2.1 Digestion of tissue	35
2.2.2 Polymerase chain reaction	35
2.2.3 Electrophoresis	38
2.3 Immunohistochemistry (IHC).....	38
2.3.1 Preparation of tissue	38

2.3.2	Fixation of tissue	39
2.3.3	Slicing of tissue	39
2.3.4	Immunohistochemical staining (IHC)	39
2.3.5	Imaging	40
2.4	5-Bromo-2'-deoxyuridine staining (BrdU)	42
2.4.1	Purpose of BrdU staining	42
2.4.2	Application and solution	42
2.4.3	Pilot test BrdU application and drinking amount	42
2.4.4	Main BrdU experiment	43
2.5	Quantifications	44
2.5.1	Quantification of proliferating cells with BrdU marker	44
2.5.2	Quantification of proliferating cells with Ki-67 marker	44
2.5.3	Quantification of cell morphological properties of Doublecortin and Nestin positive cells	45
2.5.4	Quantification of Doublecortin positive cells	46
2.5.5	Quantification of Neuronal Nuclei marker (NeuN) intensity staining	46
2.5.6	Quantification of inhibitory interneurons (iIN)	46
2.5.7	Quantification of Cajal-Retzius cells in the dentate gyrus	48
2.6	Western blot	49
2.6.1	Homogenisation of tissue	49
2.6.2	Electrophoresis	49
2.6.3	Blotting	49
2.6.4	Staining	49
2.6.5	Analysis	50
2.7	Cloning and sequencing of the floxed <i>reelin</i> gene	50
2.8	Behavioural analysis	50
2.8.1	Elevated Plus Maze (EPM)	51

2.8.2 Open Field (OF)	52
2.8.3 Spontaneous Alternation Test Y-Maze (SA).....	52
2.8.4 2-Object Novel Object Recognition Test (OR)	52
2.8.5 Three-Chamber Sociability and Social Novelty Test (SI).....	53
2.8.6 Morris water maze (MWM)	54
2.9 Statistics.....	55
2.10 Software.....	56
2.11 Contributions	57
3. Results	58
3.1 Creation and establishment of the inhibitory interneuron specific conditional Reelin knockout mouse line.....	58
3.1.1 The location of the loxP sites in the $ReIn^{flox/flox}$ mouse line	58
3.1.2 Selection of the Cre recombinase mouse lines	58
3.1.3 Genotyping	60
3.1.4 Optimization of the breeding scheme to avoid inherited deleter alleles caused by spontaneous $Dlx5/6$ -Cre recombinase activity	61
3.2 Confirming the inhibitory interneuron specific conditional knockout of Reelin in the $ReIn^{flox/flox}$ $Dlx5/6$ -Cre positive mouse line.....	62
3.2.1 Reelin expression in different brain areas	62
3.2.2 Reelin depletion in inhibitory interneurons (iIN) of the neocortex and dentate gyrus	66
3.2.3 Reelin depletion in inhibitory interneurons in the developing dentate gyrus.....	69
3.2.4 Western blot analysis of Reelin expression in the different genotypes of the $ReIn^{flox/flox}$ line	71
3.3 Analysis of neuronal layering and morphology in the $ReIn^{flox/flox}$ $Dlx5/6$ -Cre line	73
3.3.1 Brain size and weight of the $ReIn^{flox/flox}$ $Dlx5/6$ -Cre mouse line.....	73
3.3.2 Overview of the gross cell layering across the brain especially in the neocortex, hippocampus and cerebellum of $ReIn^{flox/flox}$ $Dlx5/6$ -Cre positive mice	75

3.3.3 Granule cell orientation and layer thickness in the dentate gyrus of the $Reln^{flox/flox}$ Dlx5/6-Cre positive mice	78
3.4 Behaviour of the $Reln^{flox/flox}$ Dlx5/6-Cre mice	81
3.4.1 Behavioural tasks used for the pilot group consisting of $Reln^{flox/flox}$ Dlx5/6-Cre positive and $Reln^{wt/wt}$ Dlx5/6-Cre negative mice.....	81
3.4.2 Behavioural tasks in cohort 1 including all control genotype groups with main focus on hippocampal-dependent spatial learning and memory	86
3.5 The Reelin-expressing Cajal-Retzius cells in the $Reln^{flox/flox}$ Dlx5/6-Cre mice	91
3.5.1 Quantification of Cajal-Retzius cell numbers in the dentate gyrus of the $Reln^{flox/flox}$ Dlx5/6-Cre mice	91
3.6 Inhibitory interneurons in the $Reln^{flox/flox}$ Dlx5/6-Cre mice	93
3.6.1 Layer specific quantification of inhibitory interneurons in the dentate gyri of $Reln^{flox/flox}$ Dlx5/6-Cre mice expressing tdRFP.....	93
3.6.2 Marker specific quantification of inhibitory interneurons in the dentate gyri and neocortices of $Reln^{flox/flox}$ Dlx5/6-Cre mice expressing tdRFP	95
3.7 The Reelin-expressing Cajal-Retzius cells in the $Reln^{wt/dl}$ mice	102
3.7.1 Quantification of Cajal-Retzius cell numbers in the dentate gyrus of the $Reln^{wt/dl}$ mice	104
3.8 The Reelin-expressing cells in the dentate gyri of $Reln^{wt/dl}$ mice.....	104
3.8.1 Layer specific quantification of Reelin-expressing cells in the dentate gyri of $Reln^{wt/dl}$ mice	104
3.8.2 Cannabinoid receptor 1 and Calretinin quantification in the stratum moleculare and hilus of the dentate gyri of $Reln^{wt/dl}$ mice	105
3.9 Adult neurogenesis and stem cell niche structure in the dentate gyrus of $Reln^{flox/flox}$ Dlx5/6-Cre mice	107
3.9.1 Composition of the hippocampal stem cell niche in the subgranular zone of $Reln^{flox/flox}$ Dlx5/6-Cre mice	108
3.9.2 Pretesting for long time 5-Bromo-2'-deoxyuridine (BrdU) administration to investigate neurogenesis in the $Reln^{flox/flox}$ Dlx5/6-Cre mice	112

3.9.3 Analysis of BrdU uptake via the drinking water in the experimental cohort of $ReIn^{flox/flox}$ $Dlx5/6$ -Cre mice and controls.....	114
3.9.4 Quantification of proliferation in the adult dentate gyrus using BrdU and Ki-67 in the $ReIn^{flox/flox}$ $Dlx5/6$ -Cre mice	117
3.9.5 Cell numbers and morphology of immature neurons and RGLCs in the adult dentate gyrus in the $ReIn^{flox/flox}$ $Dlx5/6$ -Cre mice.....	121
4. Discussion.....	130
4.1. Establishment of an interneuron specific conditional Reelin knockout mouse line with a non inducible loxP/Cre system	130
4.2 Specificity and effectiveness of the loxP/ $Dlx5/6$ -Cre system	131
4.3 Unaltered gross brain morphology and cytoarchitecture in the interneuron specific conditional Reelin knockout mouse line	133
4.4 Lack of granule cell dispersion in the interneuron specific conditional Reelin knockout mouse line.....	135
4.5 Normal behaviour pattern of the interneuron specific conditional Reelin knockout mouse line.....	137
4.6 Higher cell numbers of Cajal-Retzius cells in the dentate gyrus of the interneuron specific conditional Reelin knockout mouse line.....	139
4.7 Distribution and cell numbers of inhibitory interneurons in the interneuron specific conditional Reelin knockout mouse line	141
4.7.1 Analysis of Reelin-expressing inhibitory interneuron cell numbers in the dentate gyrus	142
4.7.2 Analysis of marker protein defined subgroups of inhibitory interneuron cell numbers in the neocortex and dentate gyrus	143
4.8 Stem cell niche composition and adult neurogenesis in the iIN specific conditional Reelin knockout.....	146
4.8.1 Analysis of stem cell niche composition and integrity.....	146
4.8.2 Quantification of adult neurogenesis proliferation.....	147
4.8.3 Analysis of cell properties from progenitor cells and young neurons.....	149

4.9 Refinement of BrdU administration for mice.....	150
4.10 Summary of discussion and prospect	151
Abbreviations	153
Bibliography	157
Publication:.....	181
Appendix	182
A1 Recipes.....	182
A2 Score sheet	185
A3 Hippocampal areas.....	186
A4 Companies	187
Acknowledgements	188

1. Introduction

1. Introduction

1.1 The natural mutant *reeler*

In 1951 D.S. Falconer published the description of two mouse mutants. He named the first “trembler” (symbol Tr), which appeared as a spontaneous mutation in a breeding colony of Dr C. Auerbach at the Institute of Animal Genetics in Edinburgh and the other one “reeler” (symbol rl), which appeared in a mildly inbred stock of “snow-bellied” mice after a brother and sister mating in his colony. Depending on the mating pattern, he concluded the responsible gene to be recessive. The *reeler* homozygote mice he described as physically smaller, less active compared to their siblings and with less aggression towards strangers. Its name giving feature was the reeling gait, where the rear of the animal is swaying from side to side until the animal falls over, meanwhile the general posture of the mice and the swimming were normal, the hearing unimpaired. Falconer assumed the mutants’ short lifespan of around three weeks to be due to difficulties obtaining food and water. He found the male mice mostly sterile and the female unable to raise their offspring normally (Falconer 1951). This publication marked the start of the investigation of the *reeler* mutant. In 1963 Max Hamburg published his study of postnatal developmental defects in the *reeler* mutant brain. He described the disturbed cytoarchitecture of the cortex: a cell-soma-populated molecular layer, scattered distribution of dentate gyrus granule cells and splitting of the Ammon’s horn area 1 pyramidal cell layer, and the missing foliation of Purkinje and granule cell layer in the cerebellum (Hamburg 1963). Various anatomical studies followed, addressing the morphological abnormalities of the *reeler* mutant. Caviness and Sidman first reported the abnormal layering in all cortical areas (Caviness and Sidman 1973), specifying their analysis later by reporting an inversion of the cell layers in the neocortex, but with correct connected intruding fibres to their designated cells (Caviness 1976). 1977 Mariani et al. published a precise analysis of the *reeler* cerebellum. They found that the reduction in size depends on the loss of granule cells. The Purkinje cells were ectopically distributed, with randomly oriented dendrites, and connected with several climbing fibres, instead of only one. The Purkinje cells were connected correctly, but they formed abnormally positioned synapses with granule and mossy cells (Mariani et al. 1977). Stanfield and Cowan compared normal and *reeler* hippocampi and dentate gyri to identify developmental disturbances appearing at embryonic day (E) 15 in the hippocampus and at E18 in the dentate gyrus. In *reeler* mice they found a normal amount of proliferation, an inside-out arrangement of pyramidal cells in the stratum

1. Introduction

pyramidale (Stanfield and Cowan 1979a), and reduced numbers of granule cells, with the dendritic branch appearing normal or quite normal in granule and pyramidal cells. In the molecular layer of the dentate gyrus they discovered a bilaminar instead of a trilaminar pattern and the astrocytes located there showed a more stellate form than in normal mice (Stanfield and Cowan 1979b). Afferents running into the hippocampus and dentate gyrus, were normal in position but wider distributed in the molecular layer (Stanfield et al. 1979). In the same year Goffinet described alterations of nerve cell positions, orientation and axon progression in the cortical plate of the developing *reeler* cortex at E14 (Goffinet 1979). 1982 Simmons published an extensive analysis of the afferent and efferent connectivity in the visual cortex of *reeler* mice, which were found to be normal (Simmons et al. 1982). Then the focus was set on the Cajal-Retzius cells in the cortical molecular layer. A comparison between normal and *reeler* mice uncovered a similar amount of the Cajal-Retzius cells in the *reeler* mutant but positioned a little bit deeper towards layer II of the cortex and often clustered together (Derer 1985). In the 1990ies the gene responsible for the mutation was discovered starting the period of genetical investigation (see below). Nevertheless, pure anatomical studies were still published. 1996 Terashima showed a more scattered distribution of Me5 neurons of the mesencephalic trigeminal nucleus in *reeler* mice (Terashima 1996), while the study of Del Río 1997 found a missing ingrowth of entorhinal afferents after ablation of Cajal-Retzius cells in the dentate gyrus (Del Río et al. 1997). In 2007 the anatomy of *reeler* mice brains was examined with magnetic resonance microscopy, Badea found a smaller brain size and shape differences in the areas of the olfactory bulb, the dorsomedial frontal and parietal cortex, the temporal and occipital lobes, the lateral ventricle and the ventral hippocampus. Badea also showed a diminished thickness of the hippocampus and dentate gyrus and a different density of the septal, middle and ventral hippocampus (Badea et al. 2007). Miyata extended the knowledge of the developmental failure in the *reeler* cerebellum by presenting a missing Purkinje plate forming (Miyata et al. 2010). Finally, Boyle published an analysis of neocortical layering in the *reeler* mouse, stating it more precisely as mirror-image lamination and being more complex than a simple inside-out structure (Boyle et al. 2011).

All in all, the *reeler* mouse, which is lacking the *reelin* gene, suffers from severe developmental defects (Fig. 1). In the brain, these defects are mainly based on altered layering, ectopic cell positions and diminished cell numbers. These anatomical alternations led to the physical appearance of a slight apathetic behaviour and the reeling gate in this

1. Introduction

mouse mutant. Meanwhile, a heterozygous *reeler* appears physically and anatomically normal, but is missing some Purkinje cells in the cerebellum (Biamonte et al. 2009; Magliaro et al. 2016) and some γ -aminobutyric acid (GABA) positive neurons in the cortex (Pappas et al. 2001), the hippocampus (Nullmeier et al. 2011) and in the amygdala (Macrì et al. 2010). Until today numerous reelin mutants have been described differing in alternations of the *reelin* gene, protein structure and signalling pathway (D’Arcangelo and Curran 1998; Bock and May 2016).

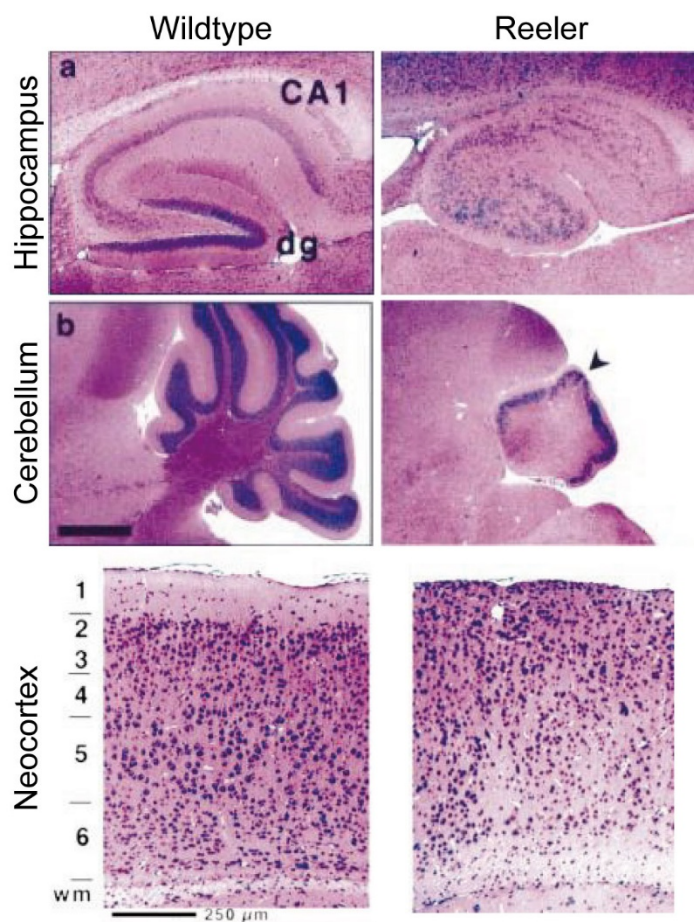


Figure 1: Histologic analysis of wild type and *reeler* mice

Histoanatomy of (a) hippocampus (P20), (b) cerebellum (P20) and neocortex (P13) of wild type and *reeler* mice. Sagittal sections with hematoxylin/eosin staining. P: Postnatal day, CA1: Cornu ammonis area 1, dg: Dentate gyrus. Cerebellum: black arrowhead: Points to the small rim of dysplastic granule cells. Neocortex: Numbers indicate cortical layers, wm: White matter. Scale: 1 mm (Cerebellum), 625 μ m (Hippocampus), 250 μ m (Neocortex). Obtained from Trommsdorff et al. 1999 and modified by the author.

1.2 Reelin: gene, protein, receptors and canonical pathway

1.2.1 The *reelin* gene

In 1994 the *reelin* gene responsible for the autosomal recessive *reeler* mutation was identified and mapped on mouse chromosome 5 (Miao et al. 1994; Bar et al. 1995). The gene was found to encode for an extracellular matrix protein, which was similar to those responsible for cell adhesion (D’Arcangelo et al. 1995). The full genomic structure was published in 1997

1. Introduction

(Royaux et al. 1997) revealing a special organisation. The gene spans over approximately 450 kilobases (kb) of the genomic deoxyribonucleic acid (DNA) and is composed of 65 exons of which 51 encode the eight repeats of the Reelin protein. Different transcripts of the gene were found, resulting from alternative splicing of a micro exon and the use of two different polyadenylation sites. The splicing sites contained the array of GT-AG nucleotides except for the one in intron 30, displaying a GC-AG array. The gene has two transcription starting sites and a TATA and CAAT box free promoter region, containing binding sites for transcription factor SP1 and AP2 and a binding site for Ets-1 (Royaux et al. 1997), being expressed in fetal and neonatal brains (Kola et al. 1993). The *reelin* promoter can also be modified by methylation (Chen et al. 2002; Meadows et al. 2015). The exon 1 of the *reelin* gene contains the initiation codon, the sequence for a signal peptide and part of the F-spondin domain of the protein (Royaux et al. 1997). The nucleotide sequence of the mouse *reelin* gene is to 86 % identical to the rat *reelin* gene (Royaux et al. 1997) and its amino acid sequence shows 94 % similarity to the human amino acid sequence (DeSilva et al. 1997; Chen et al. 2002), derived from the human *reelin* gene located on chromosome 7 (DeSilva et al. 1997). The similarity is most obvious in the nearly identical sequences of the enhancer regions of the *reelin* gene of mice (Royaux et al. 1997) and humans (Chen et al. 2002; Grayson et al. 2006), indicating a highly conserved structure.

1.2.2 The Reelin protein

The protein encoded by the *reelin* gene resembled the extracellular matrix proteins being responsible for cell adhesion (D’Arcangelo et al. 1995). Further analyses revealed that the full length secreted glycoprotein consists of 3461 amino acids (aa) (D’Arcangelo et al. 1995) with a molecular weight of ~450 kilodalton (kDa) (D’Arcangelo et al. 1997). The n-terminal part of the protein contains the epitope for the CR-50 antibody (Ogawa et al. 1995) and the G10 antibody (de Bergeyck et al. 1998), a signal peptide, a F-spondin domain and a unique “H” domain, being followed by eight homologous tandem repeats (A and B), separated by epidermal growth factor (EGF)-like motives (Royaux et al. 1997; Ichihara et al. 2001), representing the central part (Fig. 2). The c-terminal region is highly charged and essential for secretion (D’Arcangelo et al. 1997). Two cleavage sites, the first at aa1244 and the second at aa2688, allow for post-translational processing, resulting in five possible fragments containing n-terminal, central or c-terminal parts or in combination n-terminal and central or c-terminal and central parts (D’Arcangelo et al. 1997; Ranaivoson et al. 2016). The protein

1. Introduction

exhibits many N-linked and O-linked glycosylation sites (D’Arcangelo et al. 1997). The central fragment of the protein is essential for binding to Reelin receptors and to induce the canonical signalling pathway (Jossin et al. 2004). In vivo and in vitro the protein forms homo-polymers, also known to be essential for inducing canonical Reelin signalling (Utsunomiya-Tate et al. 2000). In the extracellular matrix, Reelin displays a serine protease activity on adhesion molecules (Quattrocchi et al. 2002).

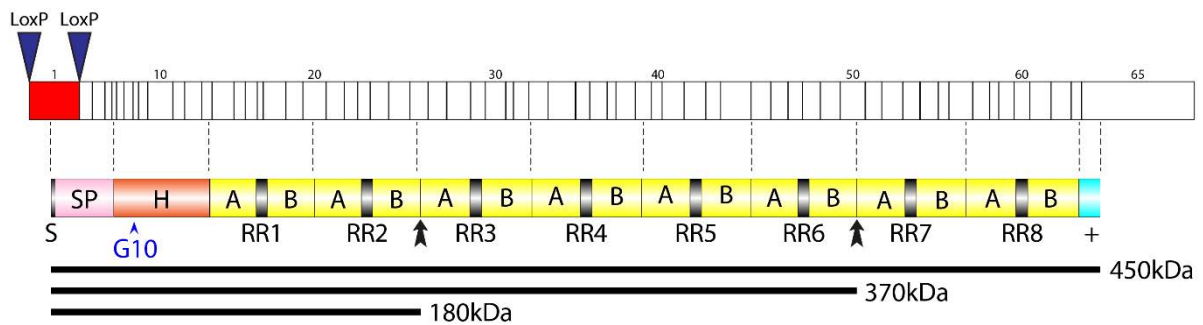


Figure 2: Scheme of the Reelin protein

Scheme of the Reelin protein as opposed to the respective coding exons of the *reelin* gene. Above: Sequence of coding exons, middle: Protein scheme, below: Fragment length with respective weight, resulting from post-translational cleavage. Red: Exon 1 with annotated loxP-sites being present in the $ReIn^{flx/flx}$ mouse line used in this study. S: Signal peptide, SP: F-spondin domain, H: “H” domain, blue arrow G10: Location of epitope of the G10 antibody used in this study, A/B: Homologue tandem sub-repeats, RR: Reelin repeat, grey boxes: EGF-like motives, cyan box: Conserved fragment of c-terminal region. Black arrows: Cleavage sites. Obtained by Royaux et al. 1997 and modified by the author.

1.2.3 The Reelin main receptors

The Reelin protein binds with its central fragment (Jossin et al. 2004) to very-low-density lipoprotein receptor (VLDLR) and apolipoprotein E receptor 2 (ApoER2) (D’Arcangelo et al. 1999) of the low-density lipoprotein receptor gene family (structure Fig. 3). Binding to the ApoER2 requires calcium and is prevented in presence of apolipoprotein E (apoE). Binding to the VLDLR, Reelin is then internalized into vesicles (D’Arcangelo et al. 1999). The linkage to this receptor is blocked, if the CR50 antibody is present (D’Arcangelo et al. 1999) or the c-terminal part of the protein is truncated (Ha et al. 2017). Despite being inherent to the same receptor family, both receptors vary in structural composition, distribution and interaction partners (Trommsdorff et al. 1999; Reddy et al. 2011). To induce the Reelin signalling pathway it is necessary that homo-polymers of the Reelin protein bind to the homo-di/oligomers of the receptors (Utsunomiya-Tate et al. 2000; Dlugosz et al. 2019) to initiate receptor clustering (Strasser et al. 2004) to homo-oligomers, triggering the internal

1. Introduction

phosphorylation of Disabled-1 (Dab1) (Dlugosz et al. 2019). Single knockout mice of VLDLR or ApoER2 display different developmental defects. While a VLDLR knockout mouse shows over-migration of cells in the molecular layer of the neocortex and the dentate gyrus, the ApoER2 knockout mouse displays clustering of cells in the neocortex and the hilar area of the dentate gyrus. In both cases a tendency to cerebellar foliation is present, but the brain area is stunted in development. Meanwhile, a double knockout of both receptors leads to a *reeler* like phenotype (Trommsdorff et al. 1999). This indicates both receptors being important for the canonical Reelin signalling pathway.

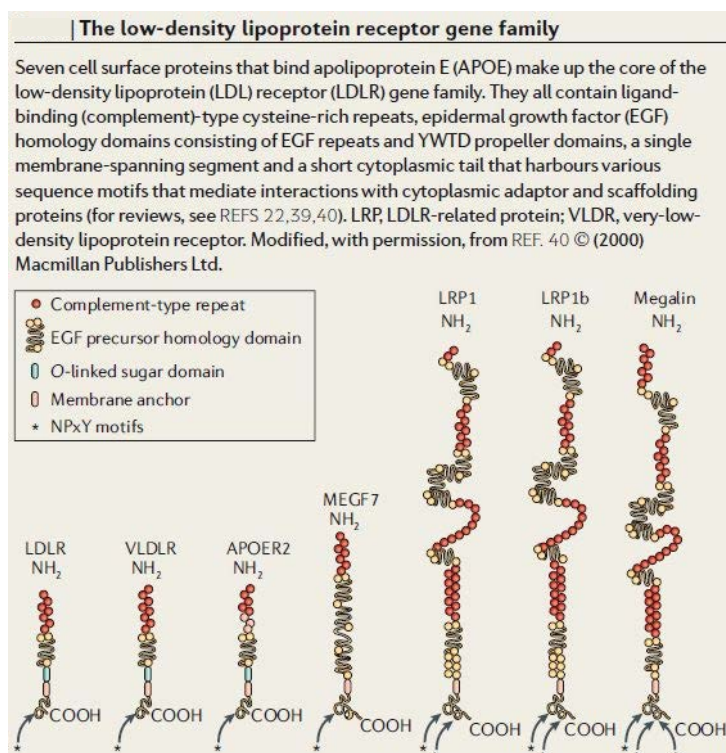


Figure 3: Low-density lipoprotein receptor gene family

Depicted are the various receptors of the low-density lipoprotein receptor family with composition. VLDLR and ApoER2 are the main Reelin receptors conveying the induction of the canonical Reelin signalling pathway. REF40: Herz and Beffert 2000. Scheme obtained from Herz and Chen 2006

1.2.4 The canonical Reelin signalling pathway

The Reelin canonical pathway is quite complex (Fig. 4). To facilitate the understanding it can be subdivided into the realm from the ultimately biological effect. The following descriptions of the different signalling pathways were compiled from four different reviews (Herz and Chen 2006; Bock and May 2016; Chai and Frotscher 2016; Lee and D'Arcangelo 2016).

All signalling cascades start with the Reelin protein binding to its receptors VLDLR and ApoER2. After initial binding to at least one of the receptors, Dab1 connected to the intracellular domain of the receptor is clustered. This activates the Src/Fyn family tyrosine

1. Introduction

kinases (SFK) which phosphorylates Dab1. Here the pathways split, depending on the molecule affected next (Fig. 5).

Neuronal migration and lamination finally influencing cell-cell adhesion and interaction (Fig. 5A):

The phosphorylated Dab1 initiates the CrK adaptor protein pathway by binding CrK. CrK activates guanosine triphosphate (GTP) exchange factor cyanidin-3-glucoside (C3G), which activates GTPase ras-related protein 1 (Rap1). Rap1 then regulates the cell-cell interaction, via $\alpha 5 \beta 1$ integrin the cell adhesion to fibronectin and via Nectin3 and N-Cadherin the direct cell-cell interaction.

Dendrite and spine development and modulation of the cytoskeleton (Fig. 4 and Fig. 5B):

The phosphorylated Dab1 activates a phosphatidylinositol 3-kinase (PI3K), which then recruits on the one hand a GTPase of the Rho family (Cdc42), which activates LIM domain kinase 1 (LIMK1). LIMK1 inactivates n-cofilin by phosphorylation and prohibits the severing of actin molecules. On the other hand PI3K activates protein kinase B (Akt) by phosphorylation. Akt then inactivates the glycogen synthase kinase 3 beta (GSK3 β), preventing phosphorylation of microtubule-associated protein tau, modifying microtubule dynamics. Akt also activates mechanistic target of rapamycin kinase (mTOR), which then modulates protein transcription for dendritic outgrowth.

Synaptic influence by modulating N-methyl-D-aspartate (NMDA) receptor (Fig. 5C):

ApoER2 is associated with postsynaptic density protein 95 (PSD95) and couples to the NMDA receptor. When Reelin binds to ApoER2 which activates SFK this leads on the one hand to phosphorylation of Dab1, which influences the subunit-composition of the NMDA receptor, and on the other hand to phosphorylation of subunit NR2 of the NMDA receptor, causing an increased calcium (Ca^{2+}) influx into the cell. This Ca^{2+} influx activates the calmodulin-dependent protein kinase type II (CaMKII), activating on its part the cyclic adenosine monophosphate (cAMP)-responsive-element binding protein (CREB), which subsequently initiates gene expression. The third effect of SFK activation is the recruitment of Mitogen-activated protein kinase (MEK), which activates the extracellular signal-regulated kinase 1/2 (ERK1/2) that also induces gene transcription. The regulation of Dab1 activity is accomplished by direct ubiquitylation and degradation of phosphorylated Dab1. The pathways described represent the main parts of the canonical Reelin signalling pathway, illustrating the various participations in cell functionality.

1. Introduction

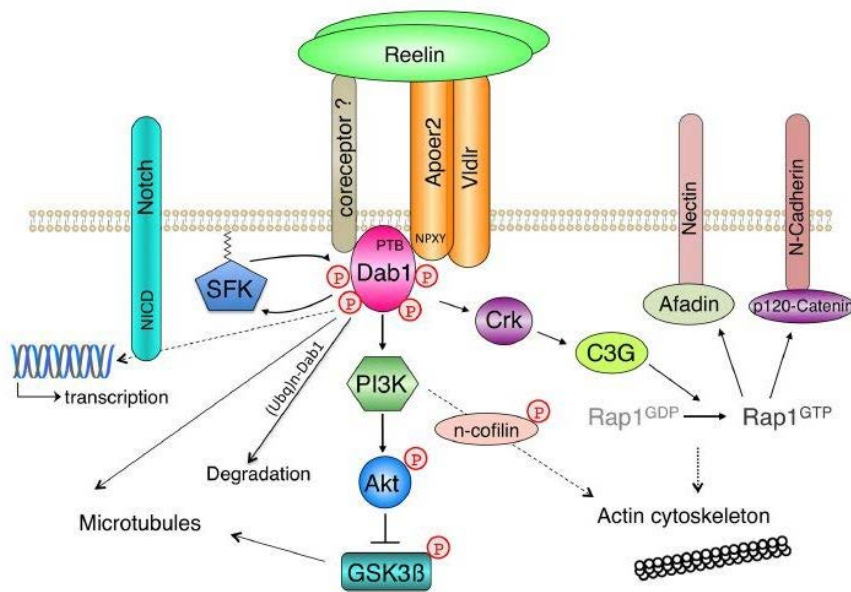


Figure 4: The canonical Reelin signalling pathway

Schematic overview of the canonical Reelin signalling pathway. Obtained from Bock and May 2016

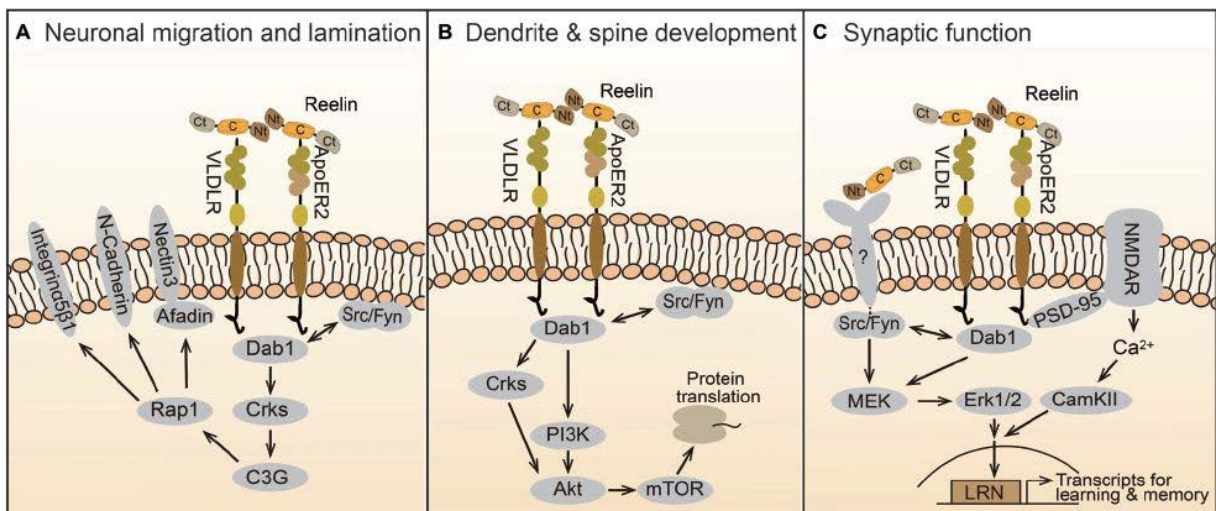


Figure 5: The canonical Reelin signalling pathway split due to biological function

A: Reelin signalling cascade that regulates neuronal migration and lamination via cell-cell adhesion and interaction during development via the Crk-C3G-Rap1 pathway. B: Reelin pathway that modulates dendrite and spine development plus the cytoskeleton via the PI3K-Akt-mTOR cascade. C: Synaptic influence of Reelin on NMDA receptor and other molecules (Erk1/2, CaMKII) regulating gene transcription. Obtained from Lee and D'Arcangelo 2016

1.2.5 Reelin and disease in men

The Reelin protein is associated with various diseases in men. An inherited defect in the *reelin* gene (RELN) causes lissencephaly type III. The affected person suffers from severe ataxia, epilepsy and is mentally retarded. The patient displays a cerebella hypoplasia and a simplified cortical folding, which is the typical symptom of this disease and based on a migration defect in cortical development (Olson and Walsh 2002). Therefore Badaea sees in

1. Introduction

the *reeler* mouse the perfect model to study Norman-Roberts lissencephaly (type III) (Badea et al. 2007). An additional influence and cause for lissencephaly type I, the classical illness, is seen in the interaction of the Reelin pathway with Lis1, the protein of the LIS gene, held responsible for type I lissencephaly (Assadi et al. 2003). Hong discovered in a study with lissencephalic patients a connection between disrupted splicing of Reelin coding deoxyribonucleic acid (cDNA) and the subsequent low level of Reelin protein with this disease (Hong et al. 2000). Lissencephaly is a developmental disease, but there are other connections to diseases affecting adolescence or adulthood. The involvement of Reelin seen in epilepsy is mainly based on the induction of granule cell dispersion (GCD) in the dentate gyrus of epileptic patients (Haas et al. 2002; Haas and Frotscher 2010; Duveau et al. 2011). This GCD was rescued in a kainate-induced epileptic mouse model with the addition of external Reelin (Müller et al. 2009). Heinrich showed a reduced amount of Reelin messenger ribonucleic acid (mRNA) in a kainate-induced epileptic mouse model (Heinrich et al. 2006) and Orcinha recognised additionally a loss of Reelin expressing cells in the hilus of the dentate gyrus (Orcinha et al. 2016). So, there is a connection between the absence of Reelin in the dentate gyrus of epileptic patients and the finding of GCD. The mental illnesses of bipolar disorder, depression, and schizophrenia were also connected to Reelin. The evidence in depression is yet weak but present. Fatemi showed a loss of Reelin expressing cells, albeit not significant, in the hippocampus of patients suffering from depression (Fatemi et al. 2000) and Caruncho recognized the loss of Reelin expressing cells in the subgranular area in a mouse model for depression (Caruncho et al. 2016). Regarding bipolar disorder, there are likewise hints. A loss of Reelin mRNA in the brain of patients (Fatemi et al. 2000; Guidotti et al. 2000; Costa et al. 2001) and the hint of Reelin influencing the vulnerability and adaption to chronic stress in a chronic stress-induced mouse model (Notaras et al. 2017). The same holds true for the schizophrenia topic: the loss of Reelin mRNA and protein in schizophrenic patients (Impagnatiello et al. 1998; Fatemi et al. 2000; Guidotti et al. 2000) and the stress modulation effects of Reelin (Notaras et al. 2017). The lower number of dendritic spines due to Reelin loss was interconnected with schizophrenic dysfunction in the brain by Costa (Costa et al. 2001), while Uribe goes a little further holding Reelin accountable for altered migration of interneurons and their loss in the prefrontal cortex of schizophrenic patients via modulation of the cytoskeleton (Uribe and Wix 2011). Another major syndrome is Alzheimer's disease (AD), but here the interconnection with Reelin is quite different. In AD human brains a higher amount of Reelin levels were found (Botella-López et al. 2006; Cuchillo-Ibañez et al. 2016),

1. Introduction

and an increased mRNA amount in adult Down's syndrome was accompanied by a higher expression of β -amyloid, causing protein plaques (Botella-López et al. 2010). Altered glycosylation of the Reelin protein was analysed in extracts of AD brains (Botella-López et al. 2010) and a loss of Reelin expressing neurons plus an increased deposition of Reelin aggregates found in the hippocampus of aged mice (Knuesel et al. 2009). Lane-Donovan published their findings in a Reelin depleted mouse line, being very vulnerable to synaptic suppression by amyloids and displaying learning and memory deficits but exhibited fewer amyloid deposits in the brain. They determined a protective effect of Reelin towards amyloid β toxicity (Lane-Donovan et al. 2015). Considering all previous publications, the participation of Reelin in pathologic states of the human brain cannot be denied.

1.3 Cajal-Retzius cells in the mouse

The Cajal-Retzius (CR) cells are a special glutamatergic, excitatory (Anstötz et al. 2016), horizontally oriented cell type with a small, ovoid-shaped cell soma. On one cell pole, they sprout a thick main dendrite, which branches until third branching depth. The dendrite is covered with filopodial protrusions (Derer and Derer 1990; Ogawa et al. 1995; Anstötz et al. 2016). They are located in the molecular layer I of the prefrontal cortex (Griveau et al. 2010; Barber et al. 2015; Anstötz et al. 2016) and project in the same layer or the adjacent layer. Seldom they were found to project in a wider range (Anstötz et al. 2016). CR cells gain input from neurogliaform and oriens-lacunosum/moleculare cells (Quattrocchio and Maccaferri 2013) and terminate on GABAergic interneurons and CA1 pyramidal cells (Quattrocchio and Maccaferri 2014). In mice CR cells are born around E10.5 in the pallial-subpallial boundary (PSB) and septum area and the cortical hem (Bielle et al. 2005; Griveau et al. 2010) and migrate between E10.5 and E12.5 to their final destination into the cortical primordium of neocortex (Bielle et al. 2005; Griveau et al. 2010). There they start to express Reelin around E11.5 (D'Arcangelo et al. 1995; Ogawa et al. 1995; Griveau et al. 2010), which plays a major role in cortical development (Marín-Padilla 1998). In the neocortex, they start to decrease in numbers from P8 (Derer and Derer 1990) until there are just 5 % left (Chowdhury et al. 2010; Kilb and Frotscher 2016). In contrast to the hippocampus, where they remain between 15-20 % of their original number in adulthood (Anstötz 2016).

1. Introduction

1.4 Inhibitory interneurons in the mouse

Besides the principal neurons and glial cells of each brain area another main cell type exists, the GABAergic interneurons. They are a heterogeneous group of interconnecting, inhibiting cells and vary in shape, branching, location, connections, electrophysiological properties and marker protein expression (Freund and Buzsáki 1996; Mott et al. 1997; Danglot et al. 2006; Lehmann et al. 2012; Benarroch 2013; Sultan et al. 2013; Harwell et al. 2015; Lim et al. 2018; Mayer et al. 2018; Mi et al. 2018). Reelin, for example, is expressed in various interneuron cell types in different brain areas (Pesold, Impagnatiello, et al. 1998; Markwardt et al. 2011; Hu et al. 2014; Ramos-Moreno and Clascá 2014; Miyoshi et al. 2015). Regarding interneuron types, the actual estimates speak of around 50 different cell types alone within the cerebral cortex (Lim et al. 2018), thus going into detail about the different groups would go beyond the scope of this work, hence, only the most important background information is given. As known to date (2019), all inhibitory interneurons (iIN) are born around E11-17 in the ganglionic eminence (GE) and migrate first tangentially, then radially towards their final destination, where they integrate into the network (Morozov et al. 2009; Sultan et al. 2013; Lim et al. 2018; Mayer et al. 2018; Mi et al. 2018). During birth and migration, they express the Dlx5/6 protein (Simeone et al. 1994; Acampora et al. 1999; Ruest et al. 2003; Monory et al. 2006), its promoter is important for this study. After integration into the network, the iIN terminate on principal cells and other iIN either on the soma, the dendrite or the axon (Freund and Buzsáki 1996; Mott et al. 1997; Benarroch 2013; Lim et al. 2018). The composition of iIN cell types within a special brain area is unique. The schemes below will illustrate the composition for the areas important for this study (Fig. 6, Fig. 7, Fig. 8).

1. Introduction

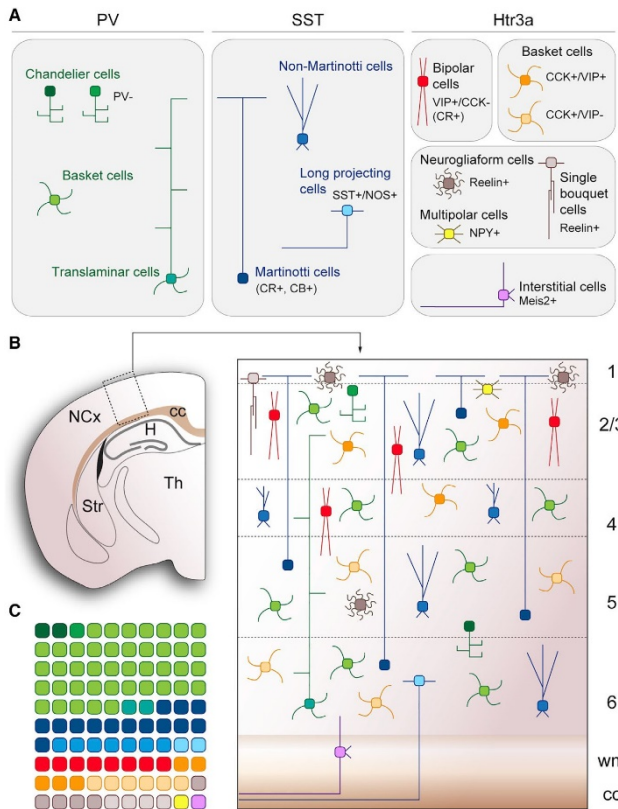


Figure 6: Diversity of inhibitory interneurons in the mouse neocortex

A: Schemes depicting the main classes of iIN. They can be subdivided into three large classes based on the expression of Parvalbumin (PV), Somatostatin (SST), and the serotonin receptor3A (Htr3a). B: Scheme of laminar distribution of the cortical iIN. Some cell types are found in most layers (e.g., PV+ basket cells), whereas others seem to be more restricted regarding their distribution (e.g., Meis2+ cells). C: Scheme representing the approximate relative frequency of the various cell types, color-coded as in A. Of note: not all iIN cell types are covered here with direct estimates of their frequency, instead they are given as relative proportion. NCx: Neocortex, H: Hippocampus, Str: Striatum, Th: Thalamus, cc: Corpus callosum, wm: White matter. Obtained from Lim et al. 2018

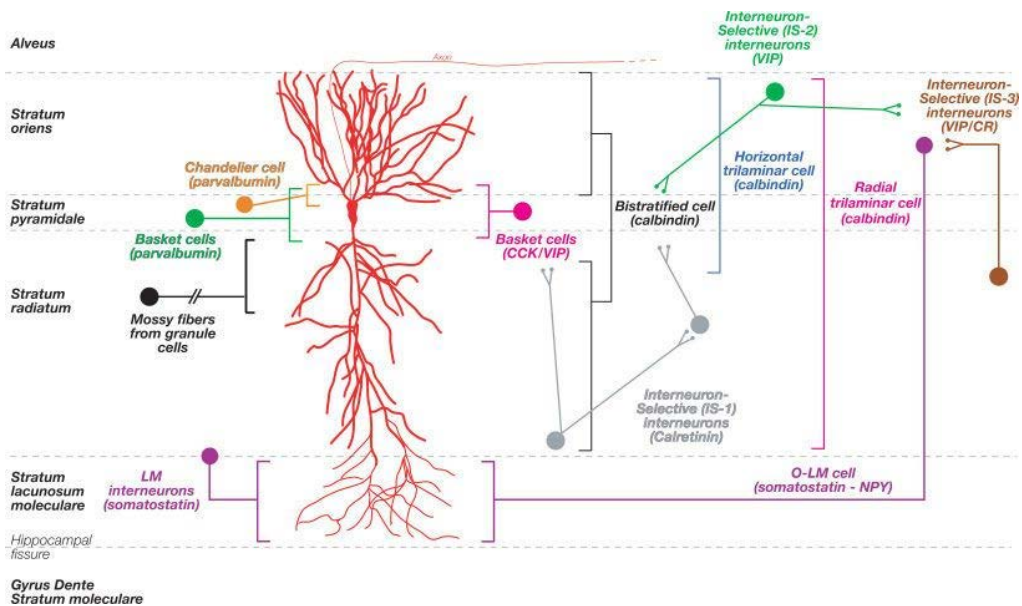


Figure 7: Scheme of Ammon's horn inhibitory interneuron types with afferences on pyramidal cells

The circles correspond to iIN soma and their localisation within the layer, the vertical hooks indicate the zone of input on the pyramidal cell. Annotated below the soma are iIN type and calcium-binding protein plus neuropeptide in parenthesis. The annotation of IS 1, 2, and 3 marks IN inhibiting other interneurons, they can be present in all layers. CCK: Cholecystokinin, CR: Calretinin: IS: Interneuron-selective, LM: Lacunosum-moleculare, NPY: Neuropeptide Y, O-LM: Oriens-lacunosum-moleculare, VIP: Vasoactive intestinal polypeptide. Obtained from Danglot et al. 2006

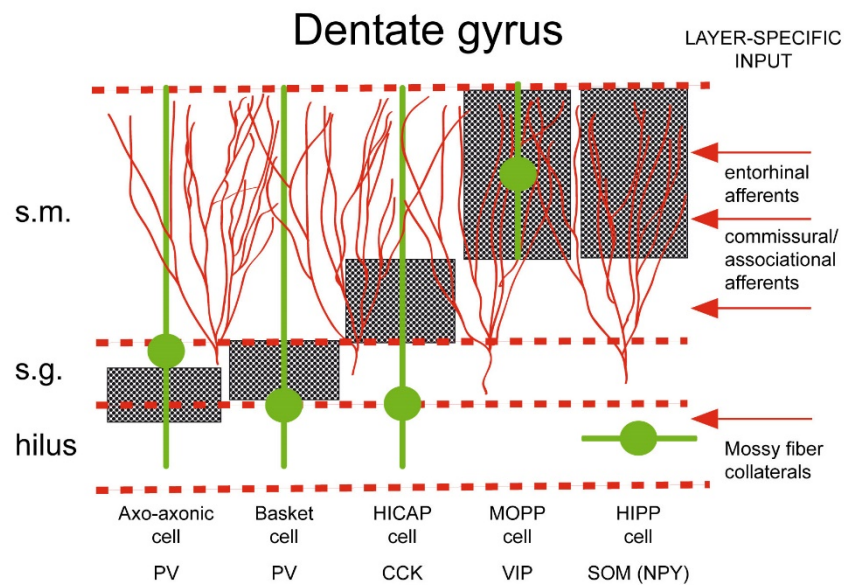


Figure 8: Scheme of inhibitory interneuron types in the dentate gyrus with dendritic and axonal arborisation pattern

The circles represent the interneuron cell soma with their respective location, the thick horizontal or vertical lines represent the main orientation and distribution of the dendritic tree and the patterned boxes represent the area of axonal arborisation. The red ramified lines represent granule cell dendrites. Annotated on the right are afferents positioned at the respective layer they intrude. Below the respective cell, the interneuron type is given together with the typically expressed marker protein. S.m.: Stratum molculare, s.g.: Stratum granulare, PV: Parvalbumin, CCK: Cholecystokinin, VIP: Vasoactive intestinal polypeptide, SOM: Somatostatin, NPY: Neuropeptide Y, HICAP: Hilar commissural-associational pathway-related, MOPP: Molecular layer associated with the perforant pathway, HIPP: Hilar perforant path-associated. Obtained by Freund and Buzsáki 1996 and modified by the author.

1.5 Adult neurogenesis in the mouse brain

In the adult brain, two regions create new cells throughout life (Altman and Das 1965; Eriksson et al. 1998; Doetsch et al. 1999). This phenomenon is called adult neurogenesis. The regions can be located at the rim of the ventricles, the subventricular zone (SVZ), producing cells for the olfactory bulb (Doetsch et al. 1999) and in the hilus area adjacent to the granule cell layer in the dentate gyrus, the subgranular zone (SGZ), producing new granule cells and astrocytes (Cameron et al. 1993; Cameron and McKay 2001). Within these regions, so-called stem cell niches can be found, which are uniquely composed. The stem cell niche in the SVZ consists of a radial glia-like progenitor cell (B cell) (Doetsch et al. 1999; Kriegstein and Alvarez-Buylla 2009; Morrens et al. 2012), surrounded by intermediate progenitor cells (C cell) in a cell wheel of multi-cilial ependymal cells (E cells) making contact to the cerebrospinal fluid (CSF). The progenitor cell is also able to contact the CSF by penetrating the ependymal cell layer with its cilium. In close proximity to the B cells, neuroblasts are

1. Introduction

found (A cells), which leave the stem cell niche via chain migration towards the olfactory bulb, where they differentiate. In between this stem cell niche, some microglia are located and at the rim astrocytes, connecting the stem cell niche to the closest blood vessel. To this blood vessel a process of the B cell extends, connecting the progenitor cell with the circulatory system (Fig. 9A+B) (Ming and Song 2011; Fuentealba et al. 2012; Morrens et al. 2012; Lin and Iacovitti 2015). The different maturation stages can be identified by the marker proteins they express (Fig. 10) (Ming and Song 2011).

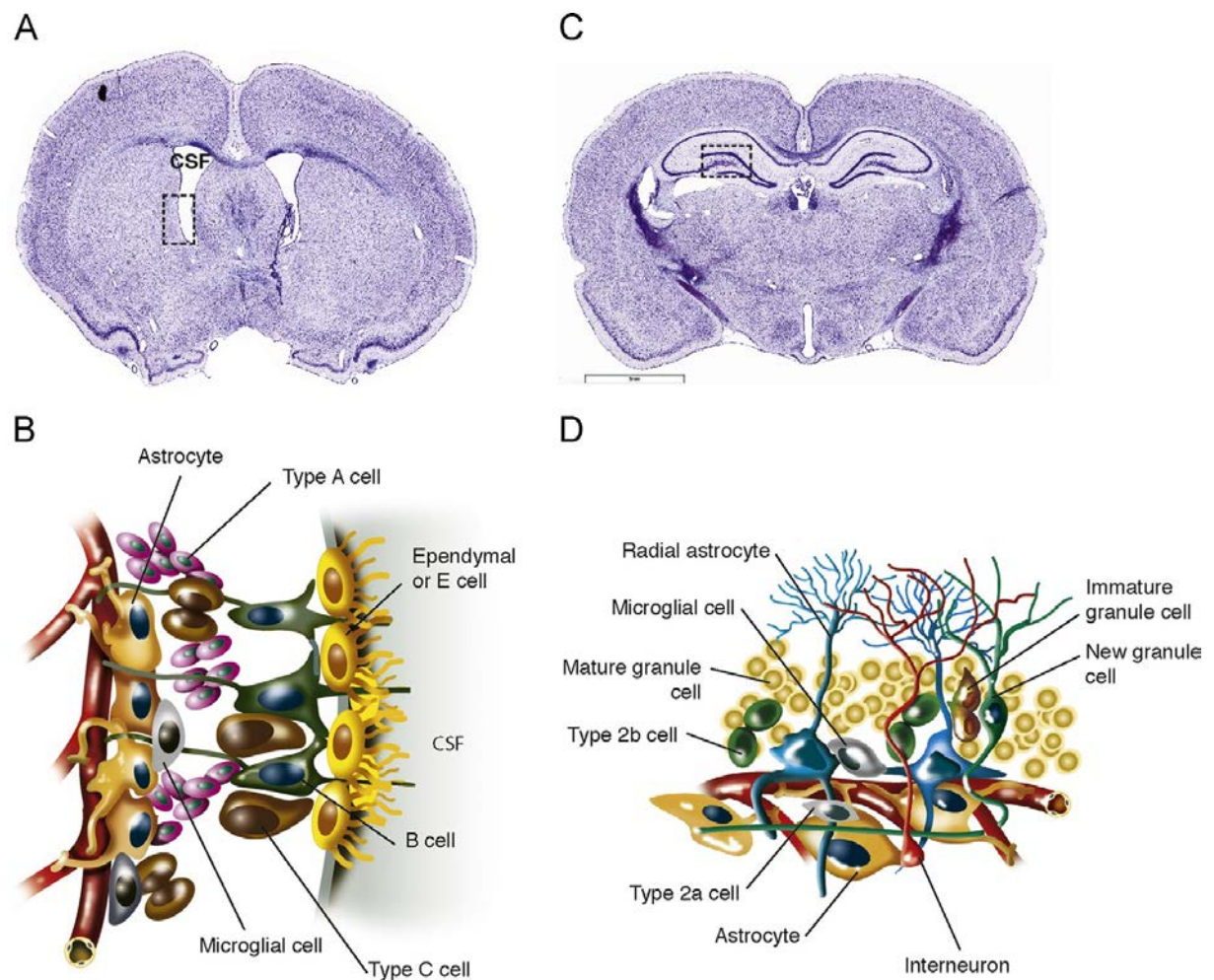


Figure 9: Location in the mouse brain and cell composition of stem cell niches

A+C: Coronal sections of mouse brains stained with cresyl violet. A: Location of stem cell niches in the SVZ. B: Scheme of the cell composition of the SVZ stem cell niche. C: Location of stem cell niches in the SGZ of the dentate gyrus. D: Scheme of the cell composition of the SGZ stem cell niche. Obtained from Lin and Iacovitti 2015

1. Introduction

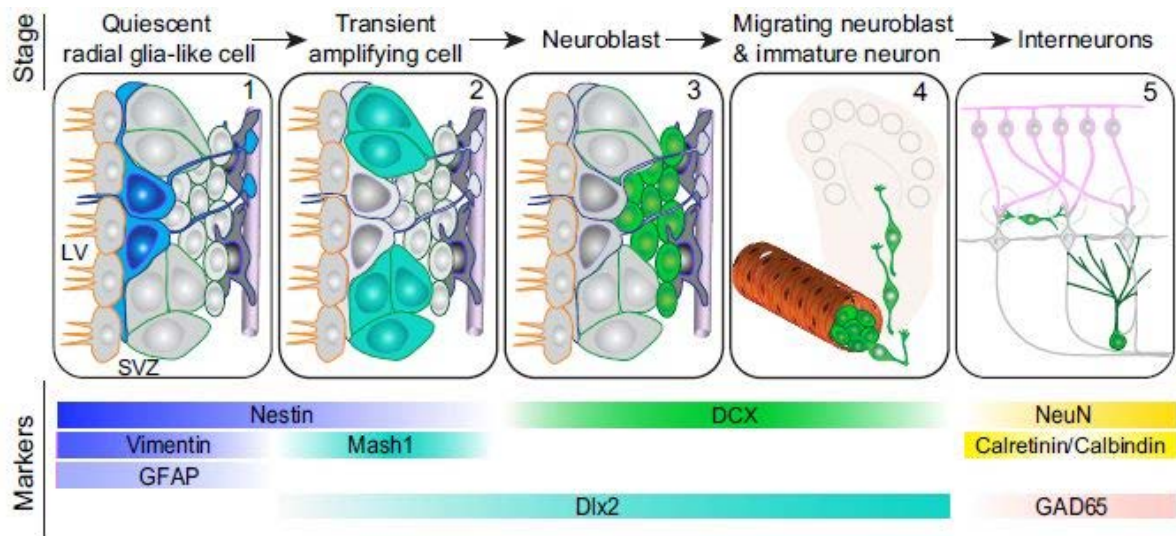


Figure 10: Expressed marker proteins according to the maturation stage in the SVZ

Depicted above are the different maturation stages of cells, at the bottom the respective marker protein expressed by the cells in the respective stage. GFAP: Glial fibrillary acidic protein, Mash1: Mammalian achaete scute homolog-1 also known as ASCL1 (achaete-scute homolog 1), Dlx2: Distalless homeo box 2, DCX: Doublecortin, NeuN: Neuronal nuclei, GAD65: Glutamate decarboxylase isoform 65. Obtained from Ming and Song 2011

The stem cell niche of the SGZ comprises other cell types (Fig. 9C+D). While the progenitor cell is also a radial glia-like cell (also known as type 1 cell synonym: radial astrocyte) (Doetsch et al. 1999; Kriegstein and Alvarez-Buylla 2009; Morrens et al. 2012; Kempermann et al. 2015; Lin and Iacovitti 2015) contacting with its processes blood vessels in the subgranular zone and in the molecular layer (Palmer et al. 2000), this cell is surrounded by two precursor cell types (type 2a synonym: D1, type 2b synonym: D2) (Seri et al. 2004; Kempermann et al. 2015), microglia, astrocytes and interneurons (Ming and Song 2011; Fuentealba et al. 2012; Morrens et al. 2012; Lin and Iacovitti 2015). Above the precursor cell, almost completely integrated into the granule cell layer, the type 3 early postmitotic young granule cell can be found (Fuentealba et al. 2012; Kempermann et al. 2015). This composition is unique to the SGZ stem cell niche. All maturation stages can be addressed by the marker proteins they express in the respective stage (Fig. 11) (Ming and Song 2011; Kempermann et al. 2015; Nicola et al. 2015; Hochgerner et al. 2018). In both stem cell niches, the way of division of the precursor cell, symmetric or asymmetric, destines the cell fate of the daughter cell. If the cell divides asymmetric, the precursor creates a second neuronal progenitor cell. If the division is symmetric, the progenitor amplifies itself (Encinas et al. 2011). The sense and purpose of the adult neurogenesis is still a matter of debate as it evolved lately that it is more than just a part of the learning and memory process (Gould et al. 1999; Ming and Song 2011).

1. Introduction

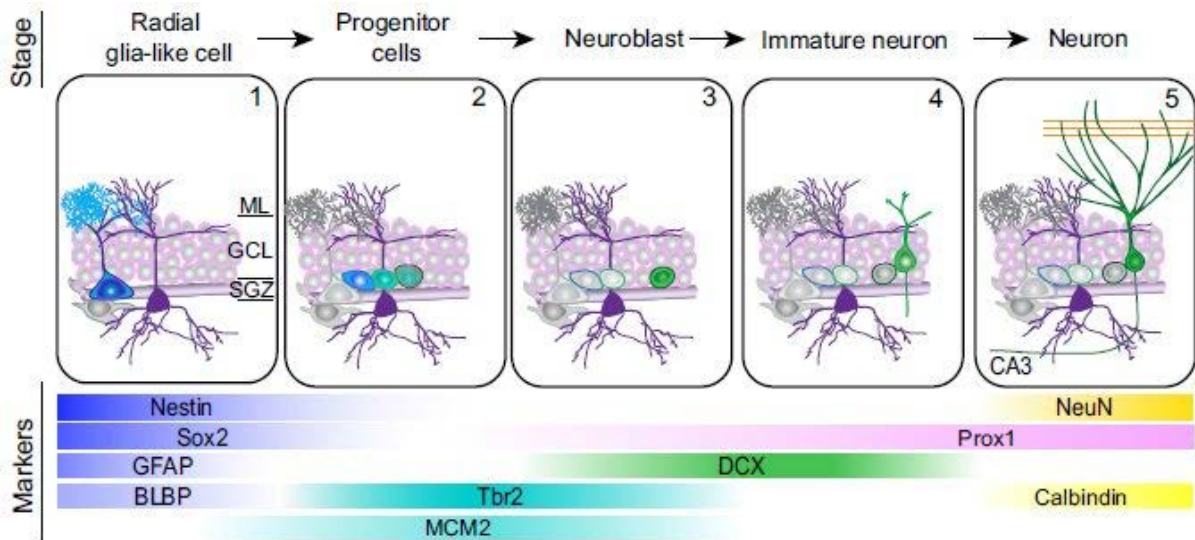


Figure 11: Expressed marker proteins according to the maturation stage in the SGZ

Depicted above are the different maturation stages of cells, at the bottom the respective marker protein expressed by the cells in the respective stage. Sox2: SRY-box transcription factor 2, GFAP: Glial fibrillary acidic protein, BLBP: Brain lipid-binding protein, Tbr2: T-Box Brain2, MCM2: Minichromosome Maintenance Protein 2, DCX: Doublecortin, Prox1: Prospero Homeobox 1, NeuN: Neuronal nuclei, GAD65: Glutamate decarboxylase isoform 65. Obtained from Ming and Song 2011

1.6 Hippocampal formation of the mouse

The hippocampal formation of the mouse is part of the phylogenetic old allocortex and spans with its c-shaped form from the dorsal middle to the lateral ventral of the cortical hemisphere (Fig. 12) (Andersen et al. 2007; van Strien et al. 2009). Through this orientation, it has a septal (dorsal) and a temporal (ventral) pole, which differ in their reception of input and function (Fanselow and Dong 2010). The hippocampal formation consists of the hippocampus proper, the dentate gyrus, subiculum, presubiculum, parasubiculum and entorhinal cortex (Fig. 13) (Amaral and Witter 1989; Förster et al. 2006; Andersen et al. 2007; van Strien et al. 2009).

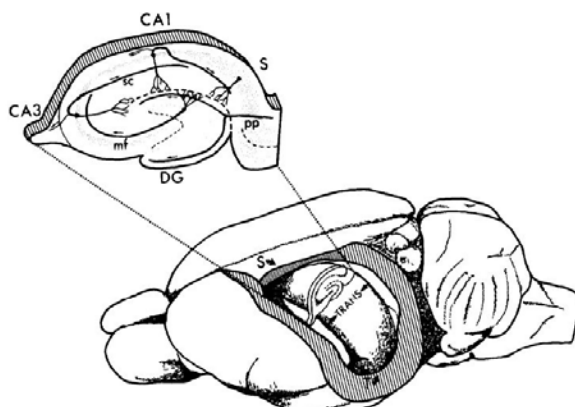


Figure 12: Position of the hippocampal formation in the rat brain

The location of the hippocampal formation in the rat brain. Magnification illustrates the lamellar organisation of the hippocampal formation. CA: Cornu ammonis area 1,3, DG: Dentate gyrus, S: Subiculum, pp: Perforant path, mf: Mossy fibre, sc: Schaffer collaterals. Obtained from Amaral and Witter 1989

1. Introduction

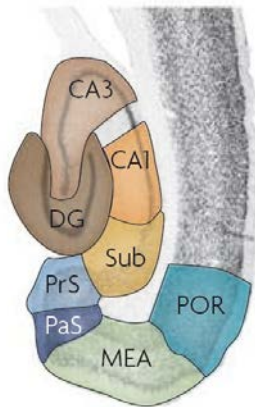


Figure 13: The parts of the hippocampal formation

The compound of the hippocampal formation. CA3 and CA1 represent the hippocampus proper. DG, dark brown: Dentate gyrus, CA3, light brown: Cornu ammonis (CA) area 3, CA1, orange: CA area 1, Sub, yellow: Subiculum, PrS, light blue: Presubiculum, PaS, dark blue: Parasubiculum, MEA, light green: Medial entorhinal cortex, POR, cyan: Postrhinal cortex. Obtained from van Strien et al. 2009

When spoken of the hippocampus in this study, the regions of the hippocampus proper and dentate gyrus are meant. The hippocampus proper is subdivided into the three regions of cornu ammonis (CA) CA1, CA2 and CA3 (Fig. 13). The principal cells in these subregions are pyramidal cells. They are arranged in just one layer and of smaller size in CA1 and larger in CA3. In comparison to CA3 pyramidal cells the CA2 pyramidal cells are lacking the input from mossy fibres of the granule cells and are midsize (Fanselow and Dong 2010). The CA subregions can be subdivided into layers: adjacent to the cortex the alveus with stratum oriens containing basal dendrites of the pyramidal cells and efferents running to the entorhinal cortex and subiculum, followed by the stratum pyramidale with the one layer of pyramidal neurons, the stratum radiatum containing apical dendrites of the pyramidal neurons, mossy fibres, Schaffer collaterals and interneurons, followed by, abutting to the dentate gyrus, the stratum lacunosum-moleculare with entorhinal afferents and interneurons (Andersen et al. 2007) (Fig. 7). The dentate gyrus is comprised of three layers. Adjacent to the stratum lacunosum-moleculare, separated by the hippocampal fissure, the stratum moleculare (molecular layer) is the outermost layer. Here a sparse amount of cells can be found, namely Cajal-Retzius cells and some interneurons. In the outer part of the stratum moleculare, being closer to the hippocampal fissure, the entorhinal afferents (perforant path) terminate on granule cell dendrites and in the inner part the commissural/associational afferents. The next layer contains the principal cells of the dentate gyrus, the granule cells, and therefore is called the stratum granulosum or granule cell layer. The granule cells form a multi-layered, densely packed, u-shaped layer encompassing the pyramidal cell layer of CA3. The part of the granule cell layer positioned between the CA1 and CA3 area is called the suprapyramidal part and the one below the CA3 pyramidal cell layer infrapyramidal part, the turning point of the U is named the crest (Fig. 14). Enclosed by the granule cell layer lies the hilar area or polymorphic layer. Here the mossy cells, mossy fibre collaterals, interneurons and sometimes half of the

1. Introduction

cell soma of radial-glia like cells can be found (Amaral et al. 2007; Amaral and Witter 1989; Andersen et al. 2007; Kassab and Alexandre 2018) (Fig. 8, Fig. 14). Besides its cytoarchitectonical organisation, the hippocampus displays another anatomical singularity. The connectivity is equal in every slice. These slices taken together, amount for the unique laminar structure of the hippocampus (Amaral and Witter 1989) (Fig. 12). The slice internal connectivity is called the trisynaptic pathway and starts with the incoming afferents of the perforant path, terminating on the dendrites of granule cells. The granule cells project on the apical dendrites of pyramidal cells in CA3 with their axons, the mossy fibres. Then the CA3 pyramidal neurons terminate with their axons, the Schaffer collaterals, on the apical dendrites of CA1 pyramidal cells. The CA1 pyramidal cells then invade the subiculum and entorhinal cortex terminating there (Fig. 14) (Amaral and Witter 1989; Amaral et al. 2007; van Strien et al. 2009; Kassab and Alexandre 2018). This anatomical singularity makes the hippocampal formation a popular object for studies.

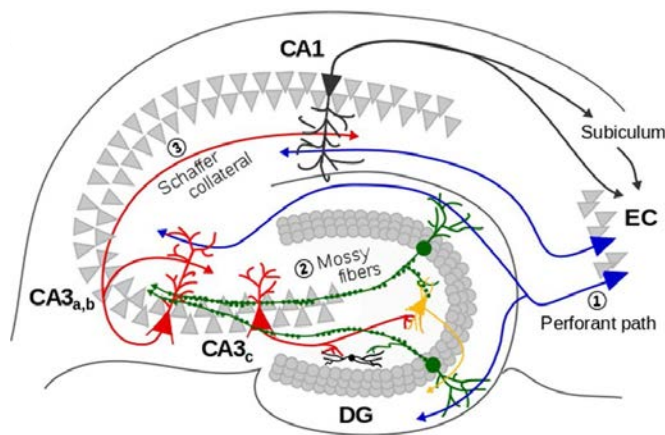


Figure 14: The trisynaptic pathway

This scheme illustrates the trisynaptic pathway of the hippocampal formation. It starts at (1) with the perforant path terminating on granule cells, progress on to (2) where the mossy fibres of the granule cells terminate on CA3 pyramidal cells and finally to (3) the Schaffer collaterals of the CA3 pyramidal cells terminating on CA1 pyramidal cells. EC: Entorhinal cortex, DG: Dentate gyrus, CA: Cornu ammonis area 1-3, blue: Entorhinal cells, green: Granule cells, yellow: Mossy cells, red: CA3 pyramidal cells, black: CA1 pyramidal cells. Obtained from Kassab and Alexandre 2018

1. Introduction

1.7 Aims and Objectives

Two main aims were pursued by this work: first, to establish a conditional, inhibitory interneuron specific Reelin knockout mouse line, to deplete Reelin at adolescence, but leave expression in Cajal-Retzius cells unaltered during development. Additionally, it was aspired to avoid the necessity of drug application, for example, tamoxifen, due to the fluctuating effectiveness of a drug based knockout.

Second, after the successful establishment of this conditional, cell-specific knockout mouse line, to investigate the hypothesised influence of Reelin on cytoarchitecture, layering, cell morphology, cell motility and neurogenesis. The emphasis of the investigation was laid on the dentate gyrus of the hippocampal formation, as this brain area is highly important for integrating patterns, learning and memory and as one out of the two hotspots of adult neurogenesis. The purpose of this study was to gain initial insights on the function of Reelin derived from inhibitory interneurons in an adult dentate gyrus.

2. Material and Methods

2. Material and Methods

2.1 Animals

The animals used in this study were housed and bred in the animal facility of the Centre for Molecular Neurobiology Hamburg (ZMNH) within a restricted hygienic barrier. The mice were housed in type II long standard cages in sex specific groups under standard conditions, such as a light-dark cycle with 12 h light/12 h dark (6 am to 6 pm), a temperature maintained at 20±2 °C and humidity of 50-70 %. The food and tap water were provided ad libitum. Animals were biopsied with 7 days postnatal (P) and weaned at P21.

For experimental purpose the following lines were used:

Table 1: Mouse lines of this study

Mouse line	Abbreviation	Genetic modification	Published by	Provider	Stock number
<i>Reln</i> ^{flox/flox}	Reln ^{flox/flox}	Exon 1 at the <i>reelin</i> gene, containing the information of the secretion signal, is flanked by loxP sites via homolog recombination	Lane-Donovan et al. 2015	Herz, Joachim	none
Tg(dlx5a-cre)1Mekk/J	Dlx5/6-Cre	Random integration of Cre recombinase under the expression of the Dlx5/6 promoter into the genome	Monory et al. 2006	Jackson Laboratory	008199
B6.C-Tg(CMV-cre)1Cgn/J	CMV-Cre	Random integration of Cre recombinase under the expression of the CMV promoter into the genome	Schwenk et al. 1995	Jackson Laboratory	006054
R26tdRFP	tdRFP	Insertion by homolog recombination of tandem dimer red fluorescent protein into the ROSA26 locus	Luche et al. 2007	Fehling, Hans Jörg	none
Tg(Thy1-EGFP)Mjrs/J	Thy1eGFP	Random integration of green fluorescent protein under the expression of the Thy1 promoter into the genome	Feng et al. 2000	Jackson Laboratory	007788
POMC-EGFP	POMCeGFP	Random integration of green fluorescent protein under the expression of the POMC promoter into the genome	Overstreet et al. 2004	Westbrook, Gary	none

All mouse strains were backcrossed at least over five generations and kept on a C57BL/6J background. Animals have been sacrificed at different ages: postnatal day (P) 3, 6 and 10 as developmental states, P21 as the beginning adulthood and at the age of 12 weeks (w), 15 w, 24 w or older as the adult representative stages. Knockout and control animals (except wild type) in comparative experiments were of the same litter. Unless it was otherwise possible to obtain the required number of animals, siblings were also bred together. The breeding of Reln^{flox/flox}-mice with CMV-Cre mice resulted in Reln^{dl/dl}-mice, with a deleted *reelin* gene in all cells indicated by dl abbreviation.

2. Material and Methods

All animal experiments conducted in this work were in compliance with European Union regulations 2010/63/EU and the German TierSchG. The experiments were approved within license G14 111, Org604 and Org850.

All solutions referred to as “in house produced” are listed with precise consistencies in table A1 in the appendix. The following consumables were used: 1.5 ml, 5 ml reaction tubes and pipette tips from Eppendorf, 1.5 ml reaction tubes, 12-/24-Well plates from Sarstedt, Falcon 15 ml/50 ml tubes, 12-/24-well plates from Corning Incorporated, PCR plates and caps by Peqlab Biotechnologies GmbH.

2.2 Polymerase chain reaction (PCR)

2.2.1 Digestion of tissue

Small tail biopsies as genetic source of the experiment animals were digested in a tail digest buffer consisting of 10x Modified Gitschier buffer (dilution 1:10) in house produced, 10 % Triton X-100 (dilution 1:20) by Merck Millipore and two times demineralised water with proteinase K (Genaxxon) 10 mg/ml stock solution (dilution 1:12.5) for 3.5 hours at 55 °C in an incubator. Afterwards the solution was cooked at 95 °C for 30 min in a thermomixer from Eppendorf to inactivate the enzyme. Centrifugation at 10,000 rpm for 5 min at room temperature in an Eppendorf desk centrifuge prevented accidental pipetting of floating last hair particles to be pipetted accidentally.

2.2.2 Polymerase chain reaction

The follow up polymerase chain reactions (PCR) had to cover the full genotype of the animal, so up to five different PCRs had to be performed. The first one had to check for the presence of the loxP sites in the *reelin* gene (Flox PCR) and was performed with a master mix of Soriano buffer in house produced, dimethyl sulfoxide (DMSO) by Carl Roth, bovine serum albumin (BSA) by Fermentas and the Primers PR_069_G_relnfl_wt_PR1 and PR_070_G_relnfl_wt_PR2. The second was performed to check the presence of the Cre recombinase (Cre TG PCR) in the genome. This was performed with a standard 10x PCR buffer by Roche, added magnesium chloride (MgCl₂) by Roche and Primers PR_098_G_Cre1 and PR_099_G_Cre2. A PCR for the deleted *reelin* gene (Deleter PCR) was performed to check for the proper activity of the Cre recombinase. This PCR was performed also with a Master Mix of Soriano Buffer, DMSO, BSA and the Primers PR_089_G_RF_for and

2. Material and Methods

PR_070_G_relnfl_wt_PR2. Two different PCRs had been executed to check for the incorporation of the fluorescent proteins. The eGFP TG PCR was performed with a master mix of standard 10x PCR buffer by Roche, MgCl₂ and Primers PR_081-G_eGFP_for and PR_082 G_eGFP_rev and the ROSA KI PCR to see the presence of red fluorescent protein tdRFP in the ROSA26 locus, was executed with a master mix of standard 10x PCR buffer from Roche, MgCl₂ and the primers PR_095-G_Rosa_WT_Kl and PR_097-G_Rosa_WT for the wild type allele and PR_095-G_Rosa_WT_Kl plus PR_096-G_Rosa_Kl for the knock in allele. All primer sequences are listed below in table 2, the composition of all master mixes in table 3-4 and the settings for the thermo cycler in table 5-6. The water Aqua ad iniectabilia by Braun was used as liquid basis in the master mixes.

Table 2: Primer sequences

PCR	Allel/Insert	Primer name	Primer sequence	Direction	Resulting fragment
Flox	wt+ki	PR_069_G_relnfl_wt_PR1	5'-ATAAACTGGTGCTTATGTGACAGG-3'	forward	424 bp (wt)
Flox	wt+ki	PR_070_G_relnfl_wt_PR2	5'-AGACAATGCTAACAAACAGCAAGC-3'	reverse	561 bp (ki, 3'-loxP)
Deleter	del	PR_089_G_RF_for	5'-CAACGCGTAAATACAGAGTCCGGCGAAG-3'	forward	
Deleter	del	PR_070_G_relnfl_wt_PR2	5'-AGACAATGCTAACAAACAGCAAGC-3'	reverse	563 bp (del)
Flox /	loxP	PR_246_Relnl2_rev	5'-CCGCCCCCTCCGCACCTTCTTAAAG-3'	reverse	
Deleter	loxP	PR_089_G_RF_for	5'-CAACGCGTAAATACAGAGTCCGGCGAAG-3'	forward	660 bp (5'-loxP)
Cre TG	cre	PR_098_G_Cre1	5'-TAA CAT TCT CCC ACC GCT AGT ACG-3'	forward	
Cre TG	cre	PR_099_G_Cre2	5'-AAA CGT TGA TGC CGG TGA ACG TGC-3'	reverse	214 bp (Cre TG)
ROSA KI	wt	PR_095-G_Rosa_WT_Kl	5'-AAA GTC GCT CTG AGT TGT TAT-3'	forward	
ROSA KI	wt	PR_097-G_Rosa_WT	5'-GGA GCG GGA GAA ATG GAT AT-3'	reverse	600 bp (wt)
ROSA KI	ki	PR_095-G_Rosa_WT_Kl	5'-AAA GTC GCT CTG AGT TGT TAT-3'	forward	
ROSA KI	ki	PR_096-G_Rosa_Kl	5'-GCG AAG AGT TTG TCC TCA ACC-3'	reverse	250 bp (ki)
eGFP	eGFP	PR_081-G_eGFP_for	5'-CGCACCATCTTCTTCAAGGACGAC-3'	forward	
eGFP	eGFP	PR_082 G_eGFP_rev	5'-AACTCCAGCAGGACCATGTGATCG-3'	reverse	383 bp (GFP TG)

Table 3: Flox/Deleter master mix recipe

PCR	Flox/Deleter
Substance	in µl
Aqua ad iniectabilia	10.95
10x Soriano buffer	2.00
DMSO	2.00
10 mmol/l each dNTP (Roche)	2.50
BSA	1.25
Primer 1	0.10
Primer 2	0.10
Taq Polymerase (pqlab)	0.10
Total volume without	19.00
DNA sample	1.00

2. Material and Methods

Table 4: Cre/Rosa/eGFP master mix recipe

PCR	Cre TG	Rosa KI	eGFP TG
Substance	in μ l	in μ l	in μ l
Aqua ad iniectabilia ²	18.80	18.70	17.60
10x PCR buffer without MgCl (Roche)	2.50	2.50	2.50
MgCl (Roche)	2.00	2.00	3.00
10 mmol/l each dNTP (Roche)	0.50	0.50	0.50
Primer 1	0.05	0.10	0.10
Primer 2	0.05	0.10	0.10
Taq Polymerase (Roche)	0.1	0.10	0.20
Total volume without sample	24.00	24.00	24.00
DNA sample	1.00	1.00	1.00

Table 5: Thermo cycler settings for flox, deleter, Rosa and eGFP PCR

PCR	Flox		Deleter	
Step	Temperature	Time	Temperature	Time
1st Step	94°C	3 min	94°C	3 min
2nd Step	55°C	2 min	50°C	2 min
3rd Step	65°C	2 min	65°C	2 min
4th Step	94°C	30 sec	94°C	30 sec
5th Step	55°C	30 sec	50°C	30 sec
6th Step	65°C	2 min	65°C	2 min
7th Step	4 to 6 40 circles		4 to 6 40 circles	
8th Step	65°C	10 min	65°C	10 min
9th Step	4°C	forever	4°C	forever

PCR	Rosa KI		eGFP TG	
Step	Temperature	Time	Temperature	Time
1st Step	94°C	3 min	94°C	3 min
2nd Step	45°C	1 min	60°C	1 min 30 sec
3rd Step	72°C	1 min	72°C	1 min 30 sec
4th Step	94°C	30 sec	94°C	30 sec
5th Step	50°C	30 sec	60°C	30 sec
6th Step	72°C	1 min	72°C	1 min
7th Step	4 to 6 40 circles		4 to 6 40 circles	
8th Step	72°C	10 min	72°C	10 min
9th Step	4°C	forever	4°C	forever

2. Material and Methods

Table 6: Thermo cycler settings for Cre PCR

PCR	Cre TG	
Step	Temperature	Time
1st Step	94°C	5 min
2nd Step	X	X
3rd Step	X	X
4th Step	94°C	30 sec
5th Step	55°C	30 sec
6th Step	72°C	45 sec
7th Step	4 to 6 40 circles	
8th Step	72°C	7 min
9th Step	4°C	forever

2.2.3 Electrophoresis

The final PCR construct was differentiated by gel electrophoresis. First 5 µl of loading dye in house produced consisting of Orange G by Sigma-Aldrich, sucrose by Merck Millipore and millipore water was added to the PCR construct. This mixture was pipetted with a volume of 7.5 µl into a pocket of a 1.5 % agarose (Genaxxon) gel on the basis of Tris-acetic acid-EDTA buffer (TAE) in house production with a drop of 0.025 % ethidium bromide by Carl Roth added into the 150 ml total gel volume. The first line always contained the GeneRuler (250-10 000 base pairs (bp)) marker from Thermo Fisher Scientific and at the end the proper controls either wild type, heterozygous, knock in or positive and negative plus the water control. The electrophoresis was run for 30 min at a voltage of 130 V with amperage between 133-142 mA. Illuminated under a UV-lamp an image of the gel was taken and later analysed.

2.3 Immunohistochemistry (IHC)

2.3.1 Preparation of tissue

The animals had been anesthetized with a mixture of 20 % oxygen and 80 % carbon dioxide. While in deep anaesthesia the animals were killed with 100 % carbon dioxide. After death the animals were immediately perfused intra cordial with 0.01 mol/l phosphate buffered saline (1x PBS) pH 7.4, diluted from a 10x PBS stock solution in house produced. An amount of 40 ml 1x PBS was used for animals of the adult stage P21 and older, for the younger animals 20 ml of 1x PBS was enough. Animals at the age of P3 until P7 had been decapitated according to animal welfare regulations. After perfusion respectively decapitation the brain was extracted of the skull by cutting laterally left and right along the occipital, parietal and frontal bone to the start of the orbita. Then the nasal was separated on height of the orbita. This was

2. Material and Methods

followed by a cut along the median suture of the skull which opened up the whole skull capsule. With a pincer both sides of the skull capsule were removed carefully to free the brain. The brain was removed with a spatula from the bottom of the skull and transferred into a Petri dish filled with 1x PBS. There the two hemispheres were separated along the cerebral fissure by a scalpel.

2.3.2 Fixation of tissue

Both hemispheres were put into 1.5 ml of 4.5 % paraformaldehyde (PFA) by Carl Roth in 1x PBS for 48 hours (h) at 4 °C. After three rinsing rounds with 1.5 ml 1x PBS, one of the hemispheres was used directly while the other was put into 1x PBS with 0.02 % of sodium azide (NaN_3) by Merck Millipore for storage at 4 °C.

2.3.3 Slicing of tissue

The brain hemisphere was embedded in 4.5 % agarose dissolved in 1x PBS. After being solid the agarose block was trimmed for better cutting results. Then the tissue within the agarose was fixed with tissue glue Histoacryl by Braun on a probe plate of the Leica VT1000S vibratome. For best cutting results just Gillette 7 o'clock Super Platinum blades were used. At a speed of 8 (1 mm/s) and a frequency of 8 (80 Hz) the hemisphere was cut sequentially in 50 μm thick slices of the hippocampus, following the septal-temporal axe for coronal sections, or the middle-lateral axe of the hemisphere for sagittal sections. Coronal slices were collected in a Falcon 24-well plate from Corning, the sagittal sections in a Falcon 12-well plate from Corning. Each well was filled with either 1x PBS, if the slices were immediately put into staining, or with 1x PBS with 0.02% NaN_3 for storage purpose. For a 24-well plate a volume of 1 ml per well was used and for the 12-well plate 1.5 ml per well was filled in.

2.3.4 Immunohistochemical staining (IHC)

For the here performed floating and indirect immunohistochemical staining (IHC) the slices were first put into a blocking solution of 1x Dulbecco's phosphate-buffered saline (DPBS) from Thermo Fisher Scientific with 10 % horse serum by Thermo Fisher Scientific and 5 % Triton X 100 for one hour plus minus five minutes. The exception here was the 5-Bromo-2'-deoxyuridine (BrdU) (Sigma-Aldrich) staining, which required before blocking a 30 min incubation at 37 °C with 2 mol/l hydrochloric acid (HCl) (stock solution by Carl Roth) followed by three washing steps with 0.1 mol/l phosphate buffer (PB) in house produced. After blocking the slices were transferred with a glass hook into the primary antibody solution consisting of 1x DPBS, 10 % horse serum and the primary antibody in the appropriate

2. Material and Methods

dilution. All primary antibodies with dilution and providing company used in this work are enlisted in table 7. For coronal slices an amount of 250 μ l per well of primary antibody solution was used as for the sagittal slices 500 μ l per well was used. All following amounts given are in the order of 24-well plates (coronal) then 12-well plates (sagittal slices). The slices were incubated 48 h over night at 4 °C on a shaker. After three washing steps with 1x PBS (1 ml per well (24-well plate) or 1.5 ml per well (12-well plate)) for 15 min on a shaker at room temperature the slices were transferred into the secondary antibody solution. This consisted of 1x DPBS and the amount of secondary antibody to obtain the necessary dilution of 1:1,000. All secondary antibodies used here are enlisted with dilution in table 8. The amount of secondary antibody solution was 250 μ l per well (24-well plate) or 500 μ l per well (12-well plate). The slices were incubated over night at 4 °C on a shaker. After that, a 4',6-diamidino-2-phenylindole dihydrochloride (DAPI) staining was applied in most cases. The slices were transferred directly into a DAPI solution of 1x DPBS and DAPI in a 1:5,000 dilution (1 ml per well (24-well plate) or 1.5 ml per well (12-well plate)). The DAPI stock solution used contained 5 mg/ml DAPI by Merck Millipore. After an incubation interval of 30 min at room temperature on a shaker, the slices were subsequently rinsed in 1 ml (24-well plate) or 1.5 ml per well (12-well plate) with 1x PBS three times for 30 min at room temperature on a shaker. Then the slices were mounted with a brush on a slide of glass (76 x 26 x 1 mm) from R. Langenbrinck and sealed with 80-120 μ l Mowiol 4-88 (Carl Roth), dissolved in millipore water with glycerol and 0.2 mol/l Tris-HCl pH 8.5 (in house produced), depending on the amount of slices on the slide. A 0.17 mm cover glass by Menzel was applied atop the Mowiol to enable imaging of the slides. The Mowiol was given one night time to harden at 4 °C before first imaging session was applied.

2.3.5 Imaging

According to the requirements of the experiments two different microscopes had been chosen. For whole brain or large overview images the Keyence BIOREVO BZ-9000 was used. This is an inverted, automated fluorescence microscope with mosaic, z-stack and multichannel imaging properties. The item used was equipped with the following objectives: PlanApo 10x NA0.45 water, PlanApo 20x 0.75NA water, PlanFluor EL Ph1 20x NA0.45 water, PlanApo 40x NA0.95, PlanApoVL 60x NA1.40 oil and PlanApo VL 100x NA1.40 oil by Nikon.

2. Material and Methods

The microscope (machine version 3D210009.-----1.0025.0086) was controlled by the software BZ-II Viewer version 2.1.00a0.0100.0101.0100.0006 and the final arrangement of the mosaic was done by the BZ-II Analyser software (same version) together with the microscope by Keyence company.

All other images were taken at the Olympus FV1000 confocal laser scanning microscope. This microscope was equipped with UPlanS Apo 10x NA0.40 water, UPlanS Apo 20x NA0.85 oil and UPlanS Apo 60x NA1.35 oil Olympus objectives. Three lasers provided the necessary light input: Argon laser: FV5-LA-MAR, a Helium-Neon Green/Red Laser: FV5-LA-HEG/HER and a LD405/440 laser: FV10-LD405/440.

The software controlling the microscope and imaging was FLUOVIEW 4.2.1.20 provided by Olympus. For imaging with the oil objectives the immersion oil Immooil F30CC Type F by Olympus was used. For imaging the following settings were chosen: sequential imaging of channels, line scan setting as well as frame per frame imaging, 1x optical magnification and a size of 1024 x 1024 pixels (px).

Images for the purpose of direct comparison (e.g. for quantification) were taken with the same properties, settings and at the same day.

Table 7: Primary antibodies

Immunogen	Clone	Isotype	Clonality	Host	Company	Order no.	Dilution IHC	Dilution WB	Available
BrdU	BU175 (ICR1)	IgG2a	monoclonal	Rat	Bio-Rad	MCA2060	1:300		no
Doublecortin	(C-18)	IgG	polyclonal	Goat	Santa Cruz	sc-8066	1:100, 1:300		no
Glial Fibrillary Acidic Protein	x	IgG	polyclonal	Rabbit	Agilent (DAKO)	Z033401-2	1:600		yes
NeuN	A60	IgG	monoclonal	Mouse	Merck-Millipore (Chemicon)	MAB 377	1:200, 1:300, 1:500, 1:1000		yes
Prox1	x	IgG	polyclonal	Rabbit	Merck-Millipore (Chemicon)	AB5475	1:500		yes
Reelin	G10	IgG	monoclonal	Mouse	Merck-Millipore (Chemicon)	MAB 5364	1:250, 1:500, 1:600	1:2000	yes
Parvalbumin	PARV19	IgG1	monoclonal	Mouse	Sigma-Aldrich	P3088-.2ML	1:2000		yes
Calretinin	x	IgG	polyclonal	Rabbit	Swant	7699/3H	1:2000		yes
Calbindin	D-28k	IgG	polyclonal	Rabbit	Swant	CB38	1:10 000		yes
Ki-67	SP6	IgG	monoclonal	Rabbit	Thermo Fischer	RM-9106-SO	1:600, 1:1000		no
FOXP2	x	IgG	polyclonal	Rabbit	Abcam	ab16046	1:1000		yes
Nestin	rat-401	IgG	monoclonal	Mouse	Merck-Millipore	MAB353	1:300, 1:500, 1:1000		yes
GAD-67	1G10.2	IgG	monoclonal	Mouse	Merck-Millipore	MAB5406	1:200		yes
Somatostatin	28	IgG	polyclonal	Rabbit	Abcam	ab22682	1:250		no
Vasointestinal peptide	x	IgG	polyclonal	Rabbit	Abcam	ab43841	1:2000		no
Cannabinoid receptor 1	N-15	IgG	polyclonal	Goat	Santa Cruz	sc-10066	1:600		no
Cannabinoid receptor 1	x	IgG	polyclonal	Rabbit	Abcam	ab23703	1:100		yes
BRN2	C-20	IgG	polyclonal	Goat	Santa Cruz	sc-6029	1:250		no
Parvalbumin	x	IgG	polyclonal	Rabbit	Abcam	ab11427	1:600, 1:2000		yes
Red Fluorescent Protein	x	IgG	polyclonal	Rabbit	Abcam	ab62341	1:500		yes
Sox-2	Y-17	IgG	polyclonal	Goat	Santa Cruz	sc-17320	1:100		no
Cholecystokinin	x	IgG	polyclonal	Rabbit	Biozol	LS-C414751-100	1:50		no
Parvalbumin	x	IgY	polyclonal	Chicken	SYSY	195006	1:250		yes
Calretinin	x	IgY	polyclonal	Chicken	SYSY	214106	1:250		yes
Actin	x	IgG	polyclonal	Rabbit	Sigma-Aldrich	A-2066		1:1000	yes

2. Material and Methods

Table 8: Secondary antibodies

Name	Immunogen	Isotype	Clonality	Host	Company	Order no.	Dilution IHC	Dilution WB
AlexaFluor 488	IgG mouse	IgG	polyclonal	Donkey	Life Technologies	A-21202	1:1000	
AlexaFluor 568	IgG mouse	IgG	polyclonal	Donkey	Life Technologies	A-10037	1:1000	
AlexaFluor 488	IgG rabbit	IgG	polyclonal	Donkey	Life Technologies	A-21206	1:1000	
AlexaFluor 568	IgG rabbit	IgG	polyclonal	Donkey	Life Technologies	A-10042	1:1000	
AlexaFluor 488	IgG goat	IgG	polyclonal	Donkey	Life Technologies	A-11055	1:1000	
AlexaFluor 568	IgG goat	IgG	polyclonal	Donkey	Life Technologies	A-11057	1:1000	
Alexa Fluor 568	IgG rat	IgG	polyclonal	Goat	Thermo Fisher	A-11077	1:1000	
Alexa Fluor 647	IgG mouse	IgG	polyclonal	Goat	Thermo Fisher	A-21235	1:1000	
Alexa Fluor 647	IgG rabbit	IgG	polyclonal	Goat	Life Technologies	A-21245	1:1000	
Alexa Fluor 647	IgG mouse	IgG	polyclonal	Donkey	Life Technologies	A-31571	1:1000	
DyLight 488	IgY chicken	IgG	polyclonal	Goat	Abcam	ab96947	1:500	
AlexaFluor 647	IgG goat	IgG	polyclonal	Donkey	Life Technologies	A-21447	1:1000	
HorseRadish Peroxidase conjugated	IgG mouse	IgG	polyclonal	Goat	Abcam	ab97023		1:5000
HorseRadish Peroxidase conjugated	IgG rabbit	IgG	polyclonal	Donkey	Dianova	711-035-152		1:5000

2.4. 5-Bromo-2'-deoxyuridine staining (BrdU)

2.4.1 Purpose of BrdU staining

The 5-Bromo-2'-deoxyuridine (BrdU) staining was chosen to tag cells in proliferative stage (e.g. progenitor cells) at the time point of incorporation of the chemical.

2.4.2 Application and solution

Two different application methods were used within this study. The first was a single intraperitoneal BrdU injection with 50 mg/kg bodyweight for the first main experiment. The second long time application method was chosen for being the least stressful for the mice (Gray 1988; Santoso et al. 2006). A solution of 0.1 % BrdU by Sigma-Aldrich, 1 % sucrose (Buffo et al. 2005; Santoso et al. 2006) dissolved in tap water was prepared for each day for each mouse. The amount was calculated regarding the drinking habit of the C57BL/6J mice published by Bachmanov (Bachmanov et al. 2002) and based on the pilot test. Because of its light sensitivity the BrdU solution was administered via brown drinking bottles in the cages and renewed every day to prevent a high amount of disintegrated BrdU.

The amount of 1 % sucrose added was high enough to mask the taste of BrdU but was not too high to affect the normal water intake of the mice (Bachmanov et al. 2001).

2.4.3 Pilot test BrdU application and drinking amount

To validate the drunken amount of water per day per mouse published by Bachmanov (Bachmanov et al. 2002) for C57BL/6J and the acceptance of the BrdU-sucrose-water mixture as water source, a pilot test was run beforehand with the Reelin conditional knockout mouse line. Four male mice were tested with the two-bottle choice test for preference and drinking amount. The animals were transferred from the mouse colony room into the experimental lab with standard conditions of light dark circle with 12 h light/12 h dark (7 am to 7 pm),

2. Material and Methods

temperature of 21 ± 2 °C and humidity of 50-70 %. Standard food pellets were available ad libitum. After two days for acclimation to the new surroundings, the animals were exposed to the custom made drinking tubes with scale and drinking tips from a standard water bottle. Located besides the used drinking bottle with tap water, the tubes were filled with 2 % sucrose-water solution to encourage drinking. After a period of 24 h, the animals were used to the drinking tubes and the normal drinking bottle was removed. While the testing phase the animals were given two drinking tubes left and right of the food tray enwrapped with aluminium foil to shield them from light. The tubes were filled with water and alternating four solutions containing 1 mg/ml (0.1 %) BrdU dissolved in water and sucrose concentrations from 0.5 %, 1 %, 1.5 % to 2 %. The solutions were exchanged every 24 h because of the light sensitivity of BrdU. The animals always had water in one tube to avoid dehydration. The alternation of tubes every 24 h prevented side preference. The mice could choose freely the tube from which to drink. Beginning with the lowest concentration of the dilution series, it was administered for 48 h, then the next concentration was tested. Following a precise score sheet (see appendix A2), the body weight and general health signs were monitored on a daily basis. At the end the mean drinking amount per day and concentration preference were calculated and used as basis for calculations of the main test.

2.4.4 Main BrdU experiment

The first experiment was performed with standard application of single intraperitoneal injection of BrdU 50 mg/kg bodyweight dissolved in DPBS. 20 mice, all female, 5 mice per genotype at the age of 12 w postnatal, housed in gender separated groups were injected once and brought back into their home cage. Three weeks time were granted to give labelled cells time to mature. 21 days past injection (see time schedule Fig. 15 below) the animals were sacrificed at the age of 15 w, perfused with 1x PBS, the brain fixed in 4.5 % PFA in 1x PBS, then sectioned in 50 μ m coronal slices and immunohistochemically stained for BrdU.

For the long term application of BrdU, 35 mice, 7 per genotype, with 11 weeks of age, mixed gender, housed in gender separated groups were administered the 0.1 % BrdU- 1 % sucrose-water solution via the brown drinking bottle in the cage. The solution was refreshed daily. The application period of 14 days (see time schedule Fig. 15 below) was followed by 14 days of maturation time for labelled cells, meanwhile the animals were given just tap water to drink. At the end of the maturation phase the animals were sacrificed at the age of 15 w, perfused

2. Material and Methods

with 1x PBS, brains fixed in in 4.5 % PFA in 1x PBS, then sectioned in 50 μm coronal slices and immunohistochemically stained for BrdU.

Day	1	2	3	4	5	6	7	8	9	10	11	12	13	14	15	16	17	18	19	20	21	22	23	24	25	26	27	28
1st group								ij	no treatment																		S	
2nd group	BrdU-sucrose-water														water													S
Age	11 w						12 w						13 w						14 w						15 w			

Figure 15:

Schedule for both BrdU experiments. The first (1st) group got a single injection (ij) and no further treatment, the second (2nd) group was treated with BrdU-sucrose-water for two weeks, then got water again for additional two weeks. At the end the animals were sacrificed (S). w: Weeks

2.5 Quantifications

All quantifications were analysed blinded. The areas quantified are depicted exemplarily in figure A3 in the appendix chapter. Summary of statistical relevant data are listed in table 10. Images were taken by the Olympus FV1000, exception the images for the Ki-67 count, which had been taken by the Keyence BIOREVO BZ-9000.

2.5.1 Quantification of proliferating cells with BrdU marker

For quantification of the stained BrdU positive cells in the first main experiment ImageJ FIJI bundle version 1.47s cell counter was used. The coronal 50 μm images were taken along hippocampal septal-temporal axe, one per area and as 7 x 4 μm z-stacks. The images were loaded and cells counted manually with the cell counter plug in. Afterwards the length of subgranular zone was measured with the segmented line tool. The numbers of BrdU positive cells from every area were calculated in reference to the length of the subgranular zone.

The second main experiment was analysed with Imaris version 8.1.1 and the volume reconstruction tool. The image of the coronal 50 μm slices of middle hippocampus taken as 10 x 2 μm z-stacks were opened in Imaris and the volume of BrdU positive cells reconstructed. The areas of counting were measured and the cell number calculated as a reference. The data was coded and statistically analysed with the fitting test required by the data set.

2.5.2 Quantification of proliferating cells with Ki-67 marker

The analysis was based on a series of coronal slices of 50 μm thickness, sequentially cut along the septal-temporal axe of the hippocampus and immunohistochemically stained for Ki-67, a nuclear proliferation marker. The mosaic and z-stack (4 x 3 μm) three channel images of

2. Material and Methods

whole dentate gyrus from Keyence microscope were loaded into ImageJ FIJI version 1.47s. After checking the correct acquisition of the image properties by the programme, the tip of the dentate gyrus, the crest, was marked with a white dot of 10 pixel (px) size. Then the length of whole granule cell layer along the rim to the hilus of the dentate gyrus was measured with segmented line tool. The drawn line was widened to 100 px and defined as subgranular zone. According to the minimizing factor resulting in the composition function of the Keyence software while assembling the mosaic image, the width of the line was adapted consistent with the original image (e.g. instead of 100 px the line was 80 px). Length and height of the subgranular zone were noted. This line selection was then straightened and separated into an individual image. At the zoom factor 400 each single cell was encircled with the ellipse tool always beginning at the end of the suprapyramidal to infrapyramidal cell layer. Then the clusters of cells were encircled with the same tool. The number of cells within the cluster and the number of clusters were noted. Subsequently, the beginning of the suprapyramidal layer, the middle of the crest and the end of infrapyramidal layer were marked with the straight line tool (4 px wide to 10 px height), added to the region of interest (ROI) manager and stored as landmarks. The dot in the middle of the crest was encircled, too, and like all encircled cell bodies and clusters stored as ROI with x and y coordinates, size and number. By splitting the channels of the image into stacks, the correct selection of positive cells was checked in the resulting grey scale image. Subsequently the whole ROIs were measured by the analysis feature of FIJI, exported and stored as data table. The following data were determined: length of granule cell layer, length of supra- and infrapyramidal layer, number of cells in sum, along the supra- or the infrapyramidal layer, the number of cells within a cluster, the number of clusters, the position of clusters within the supra- or infrapyramidal layer, the size and intensity of staining of the cell and the septo-temporal position of the analysed slice. The number of cells and clusters were normalized to the length of the granule cell layer, suprapyramidal or infrapyramidal layer regarding the comparison. The data was coded and statistically analysed with the appropriate test.

2.5.3 Quantification of cell morphological properties of Doublecortin and Nestin positive cells

An immunohistochemical staining for Doublecortin (DCX) and Nestin (Nest) of a series of coronal slices with 50 μm thickness, sequentially cut along the septal-temporal axe of the hippocampus were used for this analysis. The z-stack (40-57 x 0.5 μm or 17-64 x 0.5 μm)

2. Material and Methods

images of middle hippocampus were loaded into Imaris software version 8.4.1. The image was opened and via “edit all channels”, except the one used for analysis, were deleted. With the filament tracer tool of Imaris the Doublecortin or Nestin positive cells with their visible branches of dendrites or processes were reconstructed along the z-axis. Meanwhile the auto depth function was enabled furthermore the cylindrical shape for reconstructing the cell filaments. The reconstructed branches were centred and smoothed five times. Branching depth, branching points and filament length were requested from the software and saved as data table. The data was coded and statistically analysed with the fitting tests required by the data set.

2.5.4 Quantification of Doublecortin positive cells

For this quantification with ImageJ FIJI bundle version 1.47s coronal slices of the middle hippocampus of 50 μm thickness, sequentially cut along the septal-temporal axis were used. Immunohistochemically stained for Doublecortin, the z-stack (10 x 2 μm) three channel images were load into FIJI and visualized as greyscale image. The brightness and contrast setting were maintained at minimum equals zero and maximum equals 1,100, to keep the full range of greyscales. With the segmented line tool and the analysis feature, the supra- and infrapyramidal length and the full length of the granule cell layer along the rim adjacent to the hilus were measured. With the cell counter plug in Doublecortin positive cells along the whole granule cell layer and specific in supra- and infrapyramidal layer were counted. The data was stored as table, coded and statistically analysed.

2.5.5 Quantification of Neuronal Nuclei marker (NeuN) intensity staining

The analysis for the intensity of NeuN staining was done with Imaris version 8.1.1 and the volume reconstruction tool. The coronal slices of the middle hippocampus of 50 μm thickness z-stack 10 x 2 μm , sequentially cut along the septal-temporal axis were used. The volumes of BrdU positive cells were reconstructed with the tool and with the analysis feature of Imaris the median grey intensities for the NeuN staining within each BrdU labelled volume were calculated and summed in a table. The data was stored as table, coded and statistically analysed.

2.5.6 Quantification of inhibitory interneurons (iIN)

Four quantifications regarding the inhibitory interneurons were performed. First was the total quantification for neocortex and hilus of the dentate gyrus with the tandem dimer red fluorescent protein (tdRFP) marker, the second with inhibitory interneuron (iIN) specific

2. Material and Methods

markers, the third an intensity analysis of calretinin (CRET) and cannabinoid receptor 1 (CB1) staining, and the fourth a dentate gyrus layer specific iIN count in combination with Reelin staining. Coronal hippocampal slices out of the middle with 50 μm thickness, z-stack 10 x 2 μm , sequentially cut along the septal-temporal axe were used for these quantifications.

2.5.6.1 Quantification of iIN according to tdRFP and iIN markers in neocortex and hilus of the dentate gyrus

The images were loaded into ImageJ FIJI bundle version 1.47s and opened as z-projection. With the polygon tool the area of the whole hilus and the area of the neocortex were measured and saved as ROI via the ROI manger. For counting, the cell counter plug in was used. All positive cells for tdRFP and the different markers in the hilus or neocortex were individually counted.

The locations of the cells and numbers were stored as cell counter file and as data table. Afterwards the data was coded and statistically analysed with the fitting test required by the data set.

2.5.6.2 Intensity analysis for calretinin and cannabinoid receptor 1 staining

The staining intensities in the stratum moleculare adjacent to the suprapyramidal granule cell layer were also measured with the ImageJ FIJI bundle 1.47s. The images of the first focus plane were loaded as hyperstack and with the channel of the staining open. Predefined ROIs were loaded into the ROI manager, opened and positioned. After that the area, mean grey value, modal grey value and min & max grey value were measured with the analysing tool. Then the image with the second focus plane was opened and measured in the same way. The resulting data table was stored, coded and statistically analysed.

The following ROIs had been predefined and were meant for the indicated position: three rectangles 20 μm x 60 μm for three different positions along the granule cell layer. Three lines to measure the height of the granule cell layer at three different spots. Three rectangles with 15 μm x 50 μm for measuring the intensities in the molecular layer adjacent to the granule cell layer at three different positions. Finally three lines to capture the height of the stained area were positioned along the stripe above the granule cell layer. Out of the measurements of the three rectangles or lines the mean was calculated, then the data was coded and statistically analysed with the fitting test required by the data set.

2. Material and Methods

2.5.6.3 Quantification of iIN also positive for Reelin along hippocampal layers

Again ImageJ FIJI bundle 1.47s was used for this quantification. The image was opened as hyperstack greyscale and the brightness & contrast setting was defined with minimum equals zero and maximum equals 2,000 grey levels. Then the red channel was opened and the middle plane of the z-stack (14 x 2 μm) chosen (seven). Here the measurements were done with the segmented line tool, the polygon tool and the analysis feature for calculation. The area of stratum lacunosum-moleculare, hippocampal fissure, stratum moleculare, the inner rim (25 micrometres (μm)) of the stratum granulare adjacent to the hilus as subgranulare, and the hilus region were measured. The stratum moleculare was halved to separate between the outer (adjacent to the hippocampal fissure) and the inner layer (adjacent to the granule cell layer). The information was stored as data table. Then cell counter plug in was opened. With this tool the following categories of cells were counted see table 9.

Table 9: Classification of cell categories for quantification

iIN: Inhibitory interneurons, tdRFP: Tandem dimer red fluorescence protein, str.: Stratum

Group	cell type	positive for	localisation
1	Cajal-Retzius	Reelin	hippocampal fissure, str. lacunosum-moleculare, str. moleculare
2	iIN	tdRFP	str. lacunosum-moleculare
3	iIN	tdRFP	hippocampal fissure, outer str. moleculare
4	iIN	tdRFP	inner str. moleculare
5	iIN	tdRFP	subgranular zone with contact to str. granulare
6	iIN	tdRFP	hilus and without contact to str. granulare
7	iIN	tdRFP + Reelin	str. lacunosum-moleculare
8	iIN	tdRFP + Reelin	hippocampal fissure, outer str. moleculare
9	iIN	tdRFP + Reelin	inner str. moleculare
10	iIN	tdRFP + Reelin	subgranular zone with contact to str. granulare
11	iIN	tdRFP + Reelin	hilus and without contact to str. granulare

The counted cell numbers were put in relation to the measured areas. Subsequently the data were coded and statistically analysed.

2.5.7 Quantification of Cajal-Retzius cells in the dentate gyrus

The quantification was done as described under 2.5.6.3 above.

2. Material and Methods

2.6 Western blot

2.6.1 Homogenisation of tissue

The glass homogenisers HOG2 from Hartenstein were cooled on ice before usage. The tissue was added to 0.75 ml solution of M-PER (Mammalian Protein Extraction Reagent) and HALT (Protease Inhibitor Cocktail, EDTA-free both by Thermo Fisher Scientific) 1:100 and homogenised on ice. The homogenate was then centrifuged for 15 min with 14,000 times gravity (g) at 4 °C. The supernatant was removed and either SDS-running buffer or Laemmli buffer was added (1:5) (both in house produced). Subsequently, the solution was cooked at 95 °C for 10 min in an Eppendorf thermo cycler, and afterwards immediately put on ice for 2 min. This was followed by another centrifugation step for 5 min and 8,000 rounds per minute (rpm). The amount of protein of every sample was measured via photometry.

2.6.2 Electrophoresis

For the electrophoresis the BIORAD Mini-PROTEAN Tetra System was used. The (in house produced) 4 % stacking and 8 % and 15 % running acrylamide gels were loaded with 10 µl Page Ruler Prestained by BIORAD (10-250 kilodalton (kDa)) in the first lane and the samples amounted to 25 µg protein per pocket in the following lanes. The electrophoresis was performed with (in house produced) SDS-running buffer at 130 V and 90-80 mA for 1.5 h.

2.6.3 Blotting

The proteins were then blotted to a nitrocellulose membrane by BIORAD with (in house produced) transfer buffer at 100 V for 60 min. At the end the correct blotting was checked with PonceauS solution by Applichem.

2.6.4 Staining

First the blotted membrane was given into a blocking solution of 5 % milk powder (Sucofin 0.1 % fat, customary) in Tris buffered saline with 10 % Tween20 (TBST20) for one hour at room temperature. Then the blocking solution was decanted and the antibody solution (antibody diluted in 5 % milk powder in TBST20) was poured onto the membrane and incubated over night on a shaker at 4 °C. All antibodies used are listed in 7 and 8. After incubation the membrane was washed three times with TBST20 for five minutes at room temperature. Then the horseradish peroxidase secondary antibody solution was mixed in 5 % milk powder TBST20 solution according to the default dilution and given onto the membrane. The secondary antibody was incubated for approximately two hours at room temperature on a

2. Material and Methods

shaker. Then the membrane was rinsed with TBST20 and washed three times for 15 min with TBST20 at room temperature at the shaker. At the end chemiluminescence reagent SuperSignal West Pico Chemiluminescent Substrate by Thermo Fisher Scientific was added according to the supplier's instruction, and the membrane imaged by ImageQuant LAS-4000 with Intas ChemoStar Imager. If the signal was too weak, the membrane was again incubated with SuperSignal West Femto Maximum Sensitivity Substrate by Thermo Fisher Scientific.

2.6.5 Analysis

The gels were analysed with ImageJ FIJI bundle 1.47s and gel analyser plugin. The signal was normalized to the actin loading control and indicated as percentage of the corresponding control.

2.7 Cloning and sequencing of the floxed *reelin* gene

To check the positions of the loxP-sides in the *reelin* gene a Flox PCR was performed. The two PCR products, one around the 3'-loxP-side the other around the 5'-loxP-side, were cloned with the TOPO TA Cloning Kit for Subcloning by Thermo Fisher Scientific into a TOPO-TA vector. Subsequently, One Shot TOP10 chemically competent *Escherichia coli* (*E. coli*) by Thermo Fisher Scientific were transformed with this vector. The *E. coli* were plated on a X-gal selection agar plate and incubated at 37 °C over night. The white colonies were picked and screened for the construct via PCR. The colonies with the correct construct were cultured in selective Luria-Bertani-media (LB) 5 ml/tube with Ampicillin (1:1000) by Carl Roth as preculture. After one day of incubation at 37 °C on a shaker, the preculture was harvested and a plasmid preparation with the Quiagen QIAprep Spin Miniprep Kit was performed. The resulting plasmid was then sent to GATC Biotech AG Jakob-Stadler-Platz 7 Konstanz, 78467 Germany for sequencing. The position of the two loxP-sides within the *reelin* gene is shown in the sequence figure 17 in the results chapter.

2.8 Behavioural analysis

Behavioural experiments were performed with two groups of animals. The first (pilot group) was used to check for basic parameters of behaviour. The second group (cohort 1) was tested with specific focus on anxiety, learning and memory. Both groups consisted of just male naïve mice to prevent hormonal influence of estradiol (Bender et al. 2010). The conditions in the mouse housing room were kept at 24±1 °C, 55±5 % humidity and a reversed light/dark cycle (12 h/12 h) with light phase from 7 pm to 7 am. The animals were housed with

2. Material and Methods

littermates at 2-4 animals per type II long standard cage (20.5 x 36.5 x 14.5 cm). Food and water were provided ad libitum and tissue was given for nest building. After the transfer to the behaviour lab from the breeding and housing facility, the animals were given three (pilot) and four weeks (cohort 1) to acclimate to the new conditions. Then the animals were handled weekly to become attuned to handling and to reduce stress while being touched by the experimenter. The pilot group consisted of $Reln^{flox/flox}$ Dlx5/6-Cre positive and $Reln^{wt/wt}$ Dlx5/6-Cre negative mice while in cohort 1 four genotypes were used: $Reln^{flox/flox}$ Dlx5/6-Cre positive, $Reln^{flox/flox}$ Dlx5/6-Cre negative, $Reln^{wt/wt}$ Dlx5/6-Cre positive and $Reln^{wt/wt}$ Dlx5/6-Cre negative. The mice were 15 to 22 weeks of age at the start of the experimental cascades, that were arranged in the following order: Elevated Plus Maze (EP), Open Field (OF), Spontaneous Alternation Test Y-Maze (SA), 2-Object Novel Object Recognition Test (OR), Three-Chamber Sociability and Social Novelty Test (SI) for the pilot group and Elevated Plus Maze (EPM), Open Field (OF) and Morris water maze (MWM) for cohort 1. The basic parameters for testing were adapted by Moy, Muhia and Hausrat (Moy et al. 2004; Muhia et al. 2010; Hausrat et al. 2015) and modified. The experimenter was blinded regarding the genotype of the mice during the whole experimental sequence. All experiments were performed in the dark phase of the circadian cycle. The arenas were cleaned before the first trial and after every trial with first 30 % ethanol, followed by water and dried properly. All tests were recorded with a digital camera centred above the experimental setting. The data were collected and analysed with the EthoVision XT software 8.5.614 by Noldus and statistics calculated with SPSS 22 by IBM.

2.8.1 Elevated Plus Maze (EPM)

The elevated plus maze was custom made of white polyvinyl chloride (PVC) with four arms of 30 cm length and 5 cm width, crossing in a 5 x 5 cm area (centre zone). Two opposing arms were surrounded by a 15 cm high wall of white PVC (closed arms), while the other two arms were bordered by a small rim of 2 mm height (open arms). The arena was elevated 70 cm above the floor on a metallic stand and evenly illuminated with 70-75 lux by two dimmable floor uplighters. The trial started immediately after the mice were positioned in the centre zone facing an open arm. Now the animals were allowed to explore the maze freely for 5 min. Every mouse passed one trial on one day. The automated measurements of distance moved over time bins, frequency of entering the open arms and the time spent in the open arms (anxiety-related behaviour) were analysed.

2. Material and Methods

2.8.2 Open Field (OF)

The single open field arena was a custom made box of white PVC with the dimensions 50 x 50 x 50 cm. The bottom was divided within the software into three areas; the centre zone (15 x 15 cm), the adjacent middle zone (30 x 30 cm) and the outer zone along the wall of the arena (circular area of 7.5 cm width). A single, dimmable light was positioned vertically above the arena, providing evenly 50 lux. For trial start the mice were positioned in the outer zone facing the wall and were released then. The animals were allowed to explore the box freely for 40 min with the frequency of one trial on one day per animal. The time spent in the centre zone (anxiety-related behaviour) and the distance moved (spontaneous locomotor activity) were recorded in consecutive time bins of 5 min for better analysis. Time was displayed as percentage.

2.8.3 Spontaneous Alternation Test Y-Maze (SA)

The Y-maze for the Spontaneous Alternation Test was custom made of white PVC. The three arms were 39 cm in length and 9 cm wide and spread in an angle of 120 ° from each other. Every arm was surrounded by a white PVC wall of 16 cm height. The point of encounter of the arms was defined as centre zone. Four equally distributed lights above the arena illuminated evenly with 20 lux. The trial started with positioning the mouse at the closed end of the start arm facing the open of the arm. The animals were allowed to move freely in the maze for 5 min. The sequence of arm entering (all four paws were in the arm) was noted by the experimenter. The order of entering the arms, the total alternations possible and the true alternations done by the mouse were determined. The ratio of true alternations and total possible alternations were calculated as an indication of working memory and given as percentage.

2.8.4 2-Object Novel Object Recognition Test (OR)

The arena for 2-Object Novel Object Recognition test was a custom made white box of PVC with the dimensions 50 x 50 x 50 cm. Within the box four positions for the objects were marked with equal distance to each other and the wall (16.6 cm). Around the object position a 2 cm area was defined in the software as active exploration zone. Four vertical lights illuminated the OR box evenly with 20 lux. This test was composed of three phases. First the habituation phase to acclimate to the box, then the sample phase, where the animals became familiar with the two identical objects directly followed by the recognition phase, where the mice were exposed to a familiar besides an unfamiliar object. All trials started with placing

2. Material and Methods

the mice at a starting point, facing the wall of the box. The starting positions and the object positions were balanced and alternated between the genotypes. The four objects used were two towers of LEGO blocks of 4.78 x 4.78 cm quadratic base and 5.86 cm height, and two objects comprising two glued together bottle caps from Schott 11 bottles with 5.38 cm diameter and 5.10 cm height (see Fig. 16). The habituation was performed with the empty box, which the animal was allowed to explore freely for 10 min with the frequency of one trial per day at two consecutive days. The sample and recognition phases were performed together on the third consecutive day with one trial per mouse per day each.

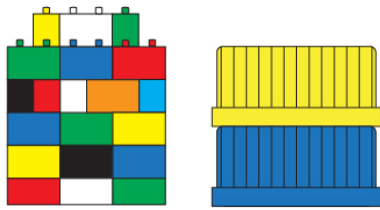


Figure 16:

Objects used for 2-Object Novel Object Recognition Test. Left the LEGO block tower of 4.78 x 4.78 x 5.86 cm, right the two glued together bottle caps from Schott 11 bottles with 5.38 cm diameter and 5.10 cm height.

For the sample run the two equal objects were set at the previously marked positions. After release the mice were allowed to explore the objects freely for 10 min. After 60 min inter trial time at the home cage, the recognition phase was performed. One familiar object and one unfamiliar object were previously set on the marked positions. The mice were given 5 min to explore the two objects freely. The time spend in the exploration zone at the objects was taken as indication of recognition and presented as percentage.

2.8.5 Three-Chamber Sociability and Social Novelty Test (SI)

The Three-Chamber Sociability and Social Novelty Test were performed with a Crawley box. The box was custom made of white PVC with the dimensions 65 cm x 38 cm and 22 cm height and divided into three compartments. The dimensions of the two outer compartments were 22 cm x 38 cm, the ones for the middle compartment 16 x 38 cm. The dividing walls had in each case one small passages of 7 x 7 cm for the mice. Within the two outer compartments, 12.5 cm away from the rear wall, two containers for holding the interaction mice were positioned. Around the container positions a 2 cm circular encounter zone was defined in the software. The Crawley box was illuminated evenly with 40-45 lux by two dimmable floor uplighters. Four extra mice were used as interaction mice and a black sponge as object. The positions of the object, the interaction mouse, the familiar and unfamiliar mouse alternated in a balanced fashion for the genotypes. This test was composed of three phases: the habituation phase, the sociability phase and the social recognition phase. All trials started with placing the mice in the middle compartment facing the open of the box. The

2. Material and Methods

habituation phase was performed on two consecutive days with one trial per mouse per day with the Crawley box containing just both containers. The animals were allowed to explore all compartments freely for 10 min. On the third consecutive day, the sociability and social recognition phase were performed in a row. For the sociability phase one container held the sponge the other held the interaction mice. Both containers were placed in the compartments at the marked positions. After release the mice were given 10 min free exploration time. During the two minutes inter trial time, the sponge was replaced by a novel mouse. The recognition phase was started and the mice were allowed 10 min time for free exploration. The time spent in the two encounter zones at the containers was analysed as indication of social preference and social recognition and given as percentage.

2.8.6 Morris water maze (MWM)

For the Morris Water Maze test the cohort 1 was composed of 39 male mice consisting of 10 $Reln^{lox/lox}$ $Dlx5/6$ -Cre positive, 9 $Reln^{lox/lox}$ $Dlx5/6$ -Cre negative and 10 $Reln^{wt/wt}$ $Dlx5/6$ -Cre positive mice. The test was subdivided in four phases: habituation to water, visible platform, hidden platform (acquisition) and the probe trials (transfer). During all phases the water was coloured opaque by biocompatible, nontoxic tempera paint by Lefranc & Bourgeois ColArt International s.a. and kept at 22-24 °C temperature. The habituation to water was performed in a type II long standard cage in which the mice first learned to get used to water and subsequently learned to swim in it combined with mounting a platform (6 cm diameter) as escape point at alternating positions. The frequency was eight trials per mouse for one day with inter trial interval (ITI) of 8 min. All other phases were performed in a pool of 150 cm diameter and 50 cm height. It was illuminated evenly by wall lights with 80 lux. Four arbitrary cardinal points (N, S, E, W) at its rim divided the pool in inter point quadrants of equal sizes (NE, NW, SE, SW). Around the pool, distant and proximal spatial cues were positioned in the room. The 14 cm diameter, round escape platform consisted of white PVC with a rough surface and was submerged 1 cm when the pool was filled. This general setting was used for the visual platform and the hidden platform tests. The probe trials were lacking the escape platform in the setup. At trial start, the mice were placed into the water, facing the pool wall, and were released then. During the visual platform phase the escape platform was flagged with a prominent cue while the outer maze cues were cloaked by an opaque curtain encircling the pool. The position of the platform and the starting points alternated in a balanced way for all trials and animals. Four trials per mouse at one day were performed with

2. Material and Methods

an ITI of 8 min in a waiting cage on two consecutive days. The trials ended after the mouse reached the platform with a dwelling time of 15 s on it or lasted at maximum 60 s, thereafter the mouse was guided to the platform. Before the hidden platform tests (spatial acquisition) curtain and cue on the platform were removed, the position of the platform fixed in the target quadrant and marked as area in the software. Thus, with the surrounding spatial cues the mice could learn to navigate to the platform. The end of trial was attained, if the mouse reached the platform and dwelling there for 15 s or after 60 s with being guided to the platform. The starting positions were randomly shuffled for every mouse and different for every trial and day. Sufficient acquisition was achieved when the platform was found within 15-20 s latency in four consecutive trials, then the first probe or transfer test was performed 24 hours later. The acquisition was performed for 10 days in a row with four trials per mouse per day with 8 min ITI followed by the first probe test after 24 h. At every probe test the starting position was equal for every mouse opposing the target quadrant and the duration of the trial lasted 90 s (one per mouse and day). After the elapsed time the animal was removed from the water. Two succeeding probe trials were performed 7 and 28 days (d) after the end of acquisition training without reinforcement in between. Latency to platform was used as indication of spatial memory acquisition, time in target quadrant as percentage of trial time, and frequency of crossing platform area were taken for retaining long term spatial reference memory.

2.9 Statistics

Statistical analysis was performed with the statistic software IBM SPSS 22.0 for Windows. The parameters of normal distribution and homoscedasticity of variance were tested with Levene's test and Kolmogorov-Smirnov/Shapiro-Wilk's *W* test. Two-tailed Student's *t*-test was used to compare means of two independent groups with normal distribution. If the parameter of normality was violated, Mann-Whitney-U test was utilized. The analysis of three and more normal distributed, independent group means was performed with one-way analysis of variance (ANOVA) and in the case of violation of normality, Kruskal-Wallis-Test was applied. Datasets from repeated measures were analysed with mixed-design ANOVA with time-bins, days, latency or frequency per trial time as within-subjects factor and genotype as between-subjects factor. A violation of sphericity, evaluated with Mauchley's test, was corrected in degrees of freedom with Greenhouse-Geisser estimate. The data presented in the text and graphs are given as mean \pm standard error of the mean (sem). Table 10 below summarizes the statistical relevant background data for all experiments done. The test

2. Material and Methods

underlying the presented data is annotated in the corresponding figure legends and texts. Type I error rate was set at $P < 0.05$ and served as threshold for significance.

Table 10: Summary of basic experimental data

Experiment	BrdU 1st main experiment	BrdU 2nd main experiment	Ki-67 count	Reconstruction of DCX positive cells	Reconstruction of Nestin positive cells	DCX positive cells count	Intensity of NeuN	iIN count (tdRFP + markers)	Calret and CB1 intensity	iIN count GD layers + Reelin	Cajal-Rezcius cells count	Westernblot	Behaviour pilot group	Behaviour cohort 1
Animals	10	28	23	14	10	14	35	10	10/8	10/8	10/8	19	12	40
Animal/genotype	5	7	5-8	7	5	7	7-11	5	5/4	5/4	5/4	4	6	10
Genotypes														
Rein ^{flox/flox} Dlx5/6-cre pos.	5	7	5	7	5	7	8	5	5/	5/	5/	4	6	10
Rein ^{flox/flox} Dlx5/6-cre neg.		7	6				9					4		10
Rein ^{wt/wt} Dlx5/6-cre pos.		7		7	5	7	11					4		10
Rein ^{wt/wt} Dlx5/6-cre neg.	5	7					7	5	5/	5/	5/	4	6	10
Rein ^{wt/flox} Dlx5/6-cre pos.			4											
Rein ^{wt/flox} Dlx5/6-cre neg.			8											
Rein ^{wt/dl}									/4	/4	/4			
Rein ^{wt/wt}									/4	/4	/4			
Male/ female	0/10	14/14	9/14	7/7	0/10	7/7	15/20	6/4	6/4 / 7/1	6/4 / 7/1	6/4 / 7/1	6/13	12/0	40/0
Age of animals	15 w	15 w	24-30 w	15 w	15 w	15 w	15 w	24 w + 30 w	24 w + 30 w	24 w + 30 w	24 w + 30 w	3, 8, 9 w	15 w	15 w
Slices counted	3/animal 1/region (s,m,t)	1 middle	8/animal various per region	1 middle	1 middle	2 middle	1 middle	1 middle	1 middle	1 middle	1 middle			
Cells constructed per slice	#	#	#	3	2	#	#	#	#	#	#			
Z-stack	7 x 4 µm	10 x 2 µm	4 x 3 µm	40-57 x 0.5 µm	17-64 x 0.5 µm	10 x 2 µm	10 x 2 µm	10 x 2 µm	10 x 2 µm	14 x 2 µm	14 x 2 µm			

2.10 Software

The following software had been used:

Adobe Illustrator CS 5.1 15.1.0 1987-2011 by Adobe

Adobe Photoshop CS 5.1 12.1 1990-2011 by Adobe

Adobe Illustrator CC 22.1 2018 by Adobe

Autodesk 3ds max 2019 by Autodesk

2. Material and Methods

BZII-Viewer and BZII-Analyzer 2.1.00a0.0100.0101.0100.0006 by Keyence

EthoVision XT 8.5.614 2011 by Noldus information technology, Wageningen, Netherlands

FluoView 4.21a.20 2015 by Olympus

Imaris 8.1.1 2015; 8.4.1 2016 by Bitplane

ImageJ FIJI 1.47s 2012 by (Schindelin et al. 2012)

Intas ChemoStar Imager by Intas

SigmaPlot 12.5 2013 by Systat Software GmbH

SPSS 22 1989/2013 by IBM

2.11 Contributions

Sequencing of the exon 1 area of the *reelin* gene: GATC Biotech AG

Cloning and preparation of the template: Jasmine Pahle

Support with the conception of the behavioural part: Dr. Mary Muhia

Performance and analysis of the behavioural part: Jasmine Pahle

Transfer of the 2D scheme of the stem cell niche into 3D: Alf Neu, Wackernheim

Compiling of 2D scheme on the basis of immunohistochemical data and publications:
Jasmine Pahle

3. Results

3. Results

3.1 Creation and establishment of the inhibitory interneuron specific conditional Reelin knockout mouse line

3.1.1 The location of the loxP sites in the *Reln*^{flx/flx} mouse line

The inhibitory interneuron specific conditional Reelin knockout mouse line presented in this work, was the result of breeding two already existing mouse lines. The conditional *Reln*^{flx/flx} mouse line from Joachim Herz and Hans Bock (Lane-Donovan et al. 2015) contains two loxP sites, inserted up- and downstream of the exon 1 of the *reelin* gene. To confirm the correct positioning of the loxP sites before breeding, the corresponding nucleotide sequence around exon 1 was cloned and sequenced (sequencing by GATC Biotech AG). The resulting nucleotide sequence is shown in figure 17. The correct positions of the loxP sites (light green brackets) flanking the exon 1 (red underlining) of the *reelin* gene were confirmed. Alignment with the published sequence of the human *reelin* promoter region (Chen et al. 2002; Grayson et al. 2006), framed by red triangles in figure 17, differing nucleotides were highlighted as red letters, allows the identification of transcription factor binding sites for SP1, T-Box Brain 1 (*Tbr1*) and Pax6. These sites have been described for the mouse and human *reelin* promoter (Royaux et al. 1997; Chen et al. 2002; Grayson et al. 2006). This sequential analysis revealed a close proximity between the 5' loxP site and the promoter region of the *reelin* gene.

3.1.2 Selection of the Cre recombinase mouse lines

For this study two Cre recombinase expressing mouse lines were chosen. One to induce a specific Reelin knockout in inhibitory interneurons, the other to create a control group of inheritable reelin knockout mice with the same genetic modification. For the targeting of inhibitory interneurons, the *Dlx5/6*-Cre mouse line was used (Monory et al. 2006). The mouse line expresses Cre recombinase under the distal-less homeobox5/6 promoter (*Dlx5/6*), which is cell-specific for inhibitory interneurons being born in the ganglionic eminence (Zerucha et al. 2000; Kamprath et al. 2006). The breeding of this line with the *Reln*^{flx/flx} mouse line resulted in the inhibitory interneuron specific conditional Reelin knockout. The advantage of this mouse line was the cell specificity of the Cre recombinase expression, the pre transcriptional depletion caused by embryonic activity of the Cre recombinase and the avoidance of any induction method, whatsoever.

3. Results

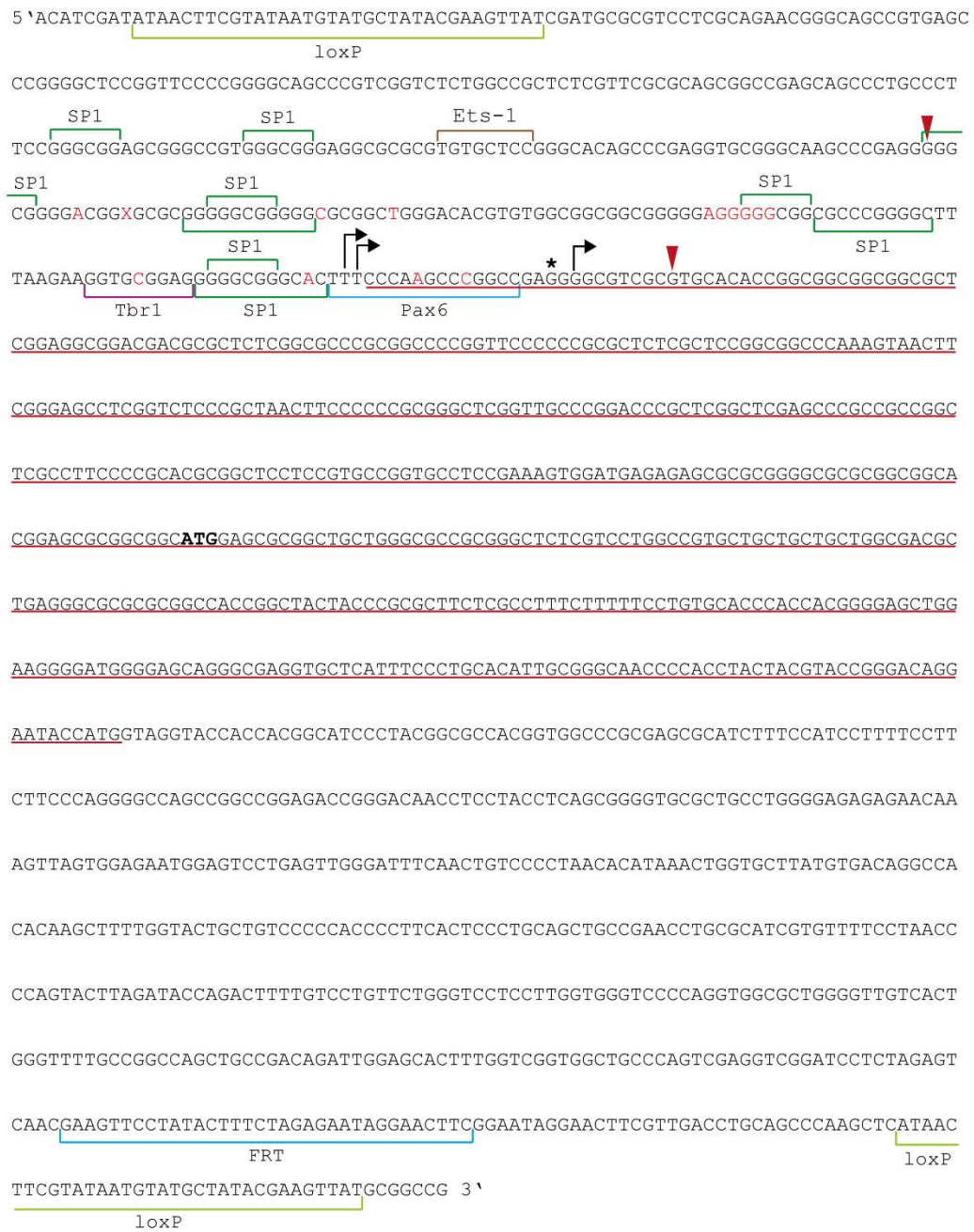


Figure 17: Nucleotide sequence with positions of the loxP sites in the *reelin* gene of the *Reln^{flox/flox}* mouse line

Shown above is the sequencing result of the *reelin* gene of *Reln^{flox/flox}* mice as nucleotide sequence. The positions of the loxP sites are annotated with light green brackets, the remaining FRT (flippase recognition target) site, from homologue recombination, is annotated in blue brackets. The sequence of *reelin* exon 1 is marked with red underlining and the start codon is written in bold letters. Further annotations resulted from a comparison with the nucleotide sequence of the published mouse and human *reelin* promoter (Royaux et al. 1997; Chen et al. 2002; Grayson et al. 2006). The retrieved sequence is framed by two red triangles, deviations are marked with red letters. Additionally annotated are four transcription factors with binding sites: brown brackets: Ets-1 binding site, dark green brackets: Specificity protein 1 (SP1) binding sites, red bracket: T-Box, Brain 1 (Tbr1) binding site, blue bracket: Paired box 6 protein (Pax6) binding site. They are part of the enhancer region (Royaux et al. 1997; Chen et al. 2002) and are also dissected by the Cre-activity in the gene. Arrows indicating initiation sites.

3. Results

The other mouse line chosen was published by Schwenk (Schwenk et al. 1995) and expressed the Cre recombinase under the ubiquitously transcribed cytomegalovirus promoter (CMV-Cre). Bred with the $ReIn^{flox/flox}$ mouse line, the resulting animals provided a genetically comparable direct control for a total *reelin* depletion in all cells.

3.1.3 Genotyping

Based on the sequencing results (Fig. 17) optimised primers and PCR protocols for the genotyping of the experimental animals were designed. For the exact genotyping three different PCRs had been performed (exemplary results are presented in Fig. 18): the first PCR (Flox PCR) was conceptualized to detect the presence of the loxP sites in the genome. The primers used here were positioned up- and downstream flanking the 3' loxP site. After transcription, the resulting two fragments had 424 base pairs (bp) for the wild type allele (lower band) and 561 bp for the allele with incorporated loxP sites (upper band). The presence of both bands in the PCR product indicates the heterozygosity of the animal. The missing transcript in the lane labelled "deleted" was due to the already excised primer location before the 3' loxP site in animals expressing the Cre recombinase under the CMV promoter. The second PCR (deleted allele, Deleter PCR) was conceptualized to detect the *reelin* allele with excised exon 1. The one primer downstream the 3' loxP site from the Flox PCR was reused and combined with a primer located upstream the 5' loxP site. The resulting transcript of 563 bp represented the deleted allele. $ReIn^{flox/flox}$ Dlx5/6-Cre positive animals always display a weak deleted band. This was due to the fact that Dlx5/6-Cre recombinase was expressed also in some ectodermal cells of the apical ectodermal ridge of developing limbs and in skeletal elements (Simeone et al. 1994; Robledo et al. 2002) and thus cells which have undergone recombination were also present in tail biopsies taken for genotyping.

To detect the inserted nucleotide sequence of the Cre recombinase, a standard PCR protocol was used. The primers were located within the coding sequence of the inserted deoxyribonucleic acid (DNA) of the Cre protein. The transcription results in one 214 bp fragment, corresponding to a section of the Cre coding DNA (cDNA) and therefore indicates a positive result. Of Note: the deletion caused by the CMV-Cre recombinase will be inherited from the parents, as CMV-Cre recombinase was active in all cells including the germ cells. Thus the $ReIn^{flox/flox}$ CMV-Cre line was continued as an independent $ReIn^{dl/dl}$ line without inheriting Cre recombinase anymore. The results of all three PCRs allow the exact assignment of the genotype (Fig. 18 – 'Resulting Genotypes').

3. Results

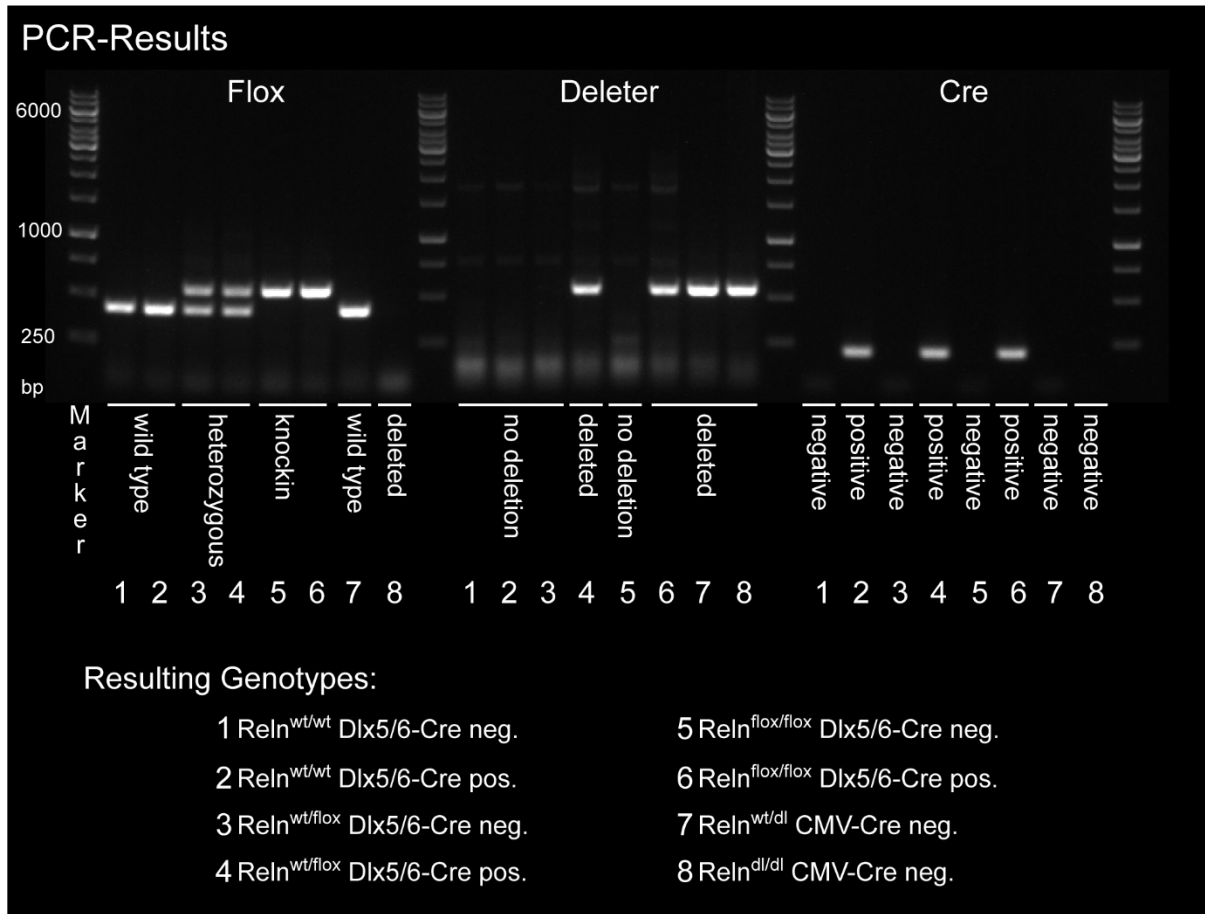


Figure 18: Results of the three main polymerase chain reactions to distinguish the genotypes

Displayed are three main polymerase chain reactions (PCR) for genotyping. Left: The Flox PCR detects the presence of the loxP sites in one or both alleles. The wild type sequence lacking the loxP sites is, therefore, smaller (424 bp) compared to the corresponding flox PCR product (561 bp). The deleted genotype, which has already been modified by the Cre recombinase, does not result in a PCR product in this PCR, as one of the primer binding sites is located within the excised sequence. Middle: The Deleter PCR was used to detect the already recombined allele. It is based on two primers flanking the DNA part, which will be excised by Cre recombinase, resulting in a normal-sized PCR product of 563 bp, if the DNA is not recombined, the PCR product will be 1773 bp (wt) or 1953 bp (flox). Due to their size, these latter products usually do not show up in the PCR. Thus the PCR results in either a 563 bp band or no band. Right: The Cre TG PCR detects the presence of the Cre recombinase coding sequence in the DNA, resulting in either a 214 bp band or no band. Following the results of the PCRs from left to right, the animals can be given a precise genotype, displayed under “Resulting Genotype”:

$Reln^{wt/wt}$: both Reelin alleles are lacking the loxP sites, $Reln^{wt/lox}$: one allele contains the loxP sites one does not, $Reln^{lox/lox}$: both alleles contain the loxP sites, Dlx5/6-/CMV-Cre neg.: Cre recombinase coding sequence is not present, Dlx5/6-/CMV-Cre pos.: Cre recombinase is present, $Reln^{wt/dl}$: animal inherited one allele with the DNA the already excised between the loxP sites by the Cre recombinase, $Reln^{dl/dl}$: animal inherited two excised alleles (deleter).

3.1.4 Optimization of the breeding scheme to avoid inherited deleter alleles caused by spontaneous Dlx5/6-Cre recombinase activity

In the course of breeding, it occurred that animals being Dlx5/6-Cre negative displayed a band in the PCR detecting for the deleted allele. This effect was due to the sometimes occurring,

3. Results

spontaneous activity of the Dlx5/6-Cre recombinase in the germ cell line (Eckardt et al. 2004; Heffner et al. 2012). Thus, the animals inherited a deleted *reelin* gene by their parents, namely by the mother. If the Dlx5/6-Cre recombinase was inherited by the male parenting line, this effect did not arise. Due to this finding, the breeding scheme was optimized by choosing just male $\text{ReIn}^{\text{wt/flox}}$ Dlx5/6-Cre positive and female $\text{ReIn}^{\text{flox/flox}}$ Dlx5/6-Cre negative genotypes as breeder pairs for experimental animals. Successful breeding resulted in inhibitory interneuron specific conditional Reelin knockout animals.

3.2 Confirming the inhibitory interneuron specific conditional knockout of Reelin in the $\text{ReIn}^{\text{flox/flox}}$ Dlx5/6-Cre positive mouse line

3.2.1 Reelin expression in different brain areas

The Reelin protein could be found being expressed in different brain areas namely the olfactory bulb, the neocortex, the hippocampus, the cerebellum, the nucleus of the optic tract, the substantia nigra and the ventral tegmental area (Ikeda and Terashima 1997; Ramos-Moreno et al. 2006). But the cell types expressing Reelin were quite different in the various areas. The first step to prove the proper Reelin depletion was to check the expression in the different brain areas via immunohistochemical staining against Reelin in sagittal brain slices of adolescent mice. They gave an overview of the Reelin expression in the brain (Fig. 19). The slices of $\text{ReIn}^{\text{wt/wt}}$ Dlx5/6-Cre negative (control, Fig. 19A) and $\text{ReIn}^{\text{flox/flox}}$ Dlx5/6-Cre positive (interneuron specific Reelin knockout, Fig. 19B) were displayed as greyscale image for better discrimination of the Reelin immunoreactive (ir) cells in the different brain areas. Even in this magnification, the Reelin positive cells could be seen very clearly in the olfactory bulb, the neocortex, the hippocampus (cornu ammonis 1-3 (CA1-3) areas with dentate gyrus), and the region of the nucleus of the optic tract and substantia nigra, as well as in the ventral tegmental area in the control condition (Fig. 19A). In the interneuron specific Reelin knockout (Fig. 19B), just the mitral cell layer in the olfactory bulb was distinguishable as Reelin positive. Since the olfactory bulb (OB), the neocortex (NC), the hippocampus (HC) and the cerebellum (CB) were the brain areas best described regarding Reelin expression and the effects of Reelin loss in the natural mutant the *reeler* mouse, the focus of magnification was set on these areas. Figure 20 shows the details of these four main areas for four different genotypes. All details were taken out of a sagittal adolescent mouse brain slice of P19/P20, stained immunohistochemically against Reelin, and displayed as greyscale, similar to figure 19. As previously mentioned, the mitral cell layer in the olfactory bulb were evidently Reelin

3. Results

ir positive and present in the $\text{ReIn}^{\text{wt/wt}}$ Dlx5/6-Cre negative (Fig. 20a) and the $\text{ReIn}^{\text{flox/flox}}$ Dlx5/6-Cre negative control (Fig. 20c), as well as in the interneuron specific Reelin knockout $\text{ReIn}^{\text{flox/flox}}$ Dlx5/6-Cre positive (Fig. 20b). The $\text{ReIn}^{\text{dl/dl}}$ genotype (Fig. 20d) displayed no Reelin ir cells at all, confirming the complete Reelin depletion in this ubiquitous knockout mouse line. With no Reelin expression anywhere in the brain (compare Fig. 20d-d''') it could have been expected, that these animals would display a *reeler* like phenotype, too. This was confirmed by the smaller size of the cerebellum (Fig. 20d''') referring to the control (Fig. 20a'''). Comparing all other cerebella (Fig. 20a'''-c''') it was to be mentioned, that nowhere any Reelin ir positive cell was detected at this stage of development, neither in the control situations (Fig. 20a''', Fig. 20c''') nor in the interneuron specific Reelin knockout (Fig. 20b'''). In contrast to the other two areas, the specific knockout of Reelin in the newly established mouse line becomes obvious in the neocortex and hippocampus. The conditional Reelin knockout showed no Reelin-expressing cells in the neocortex (Fig. 20b') but some in the range of the hippocampal fissure in the hippocampus (thin line in Fig. 20b''). This pattern resembles a pattern expected, if just inhibitory interneurons were affected by the interneuron specific Reelin knockout. The missing Reelin expression in the neocortex (Fig. 20b') indicating that the inhibitory interneurons were affected, as they were the main Reelin source at that age in this brain region (Alcántara et al. 1998). The presence of the Reelin-expressing cells around the hippocampal fissure in the hippocampus (Fig. 20b'') was explainable, as there were still Cajal-Retzius cells present below the hippocampal fissure of the hippocampus, which express Reelin until late adulthood (Chowdhury et al. 2010; Anstötz et al. 2016) and were not affected by the conditional knockout, as they were excitatory neurons. Meanwhile the distribution pattern of the Reelin-expressing cells along the neocortex and hippocampus in the two control situations (Fig. 20a', Fig. 20c' and Fig. 20a'', Fig. 20c'') were very similar. This illustrates that the Reelin expression in the two control situations was comparable, meaning that neither the insertion of the loxP sites nor Cre recombinase on its own affected the Reelin expression pattern. The ubiquitous knockout $\text{ReIn}^{\text{dl/dl}}$ showed no Reelin expression at all, confirming the functionality of the loxP sites constructs. The unaffected Reelin expression in excitatory neurons, as mitral and Cajal-Retzius cells and a complete lack of Reelin in inhibitory interneurons (iIN) in the neocortex and hippocampus (Fig. 20b-b'') showed the cell specificity of the Reelin depletion in the interneuron specific Reelin knockout.

3. Results

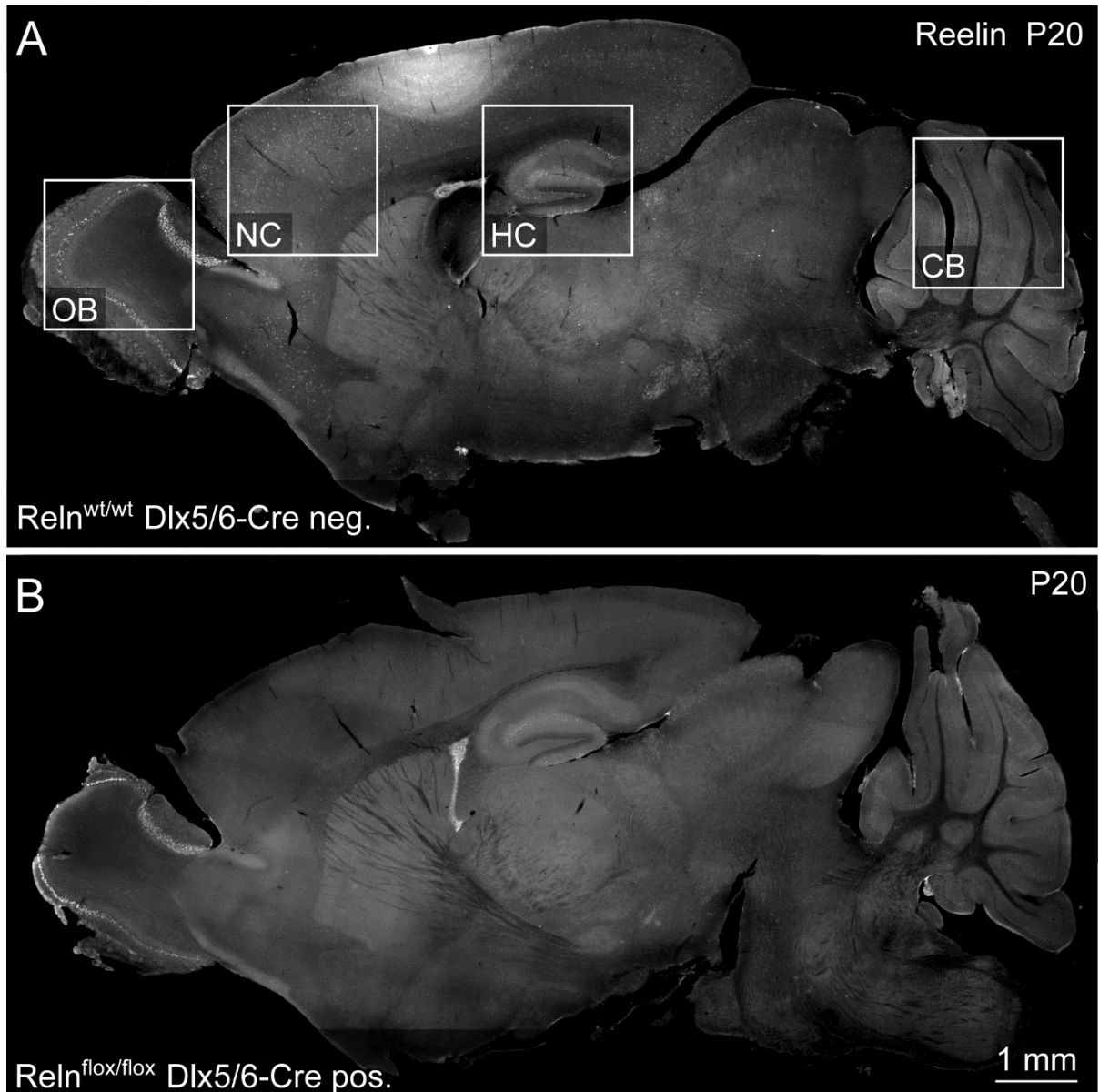


Figure 19: Reelin expression pattern in the brain of $Rein^{flox/flox}$ Dlx5/6-Cre positive mice
Immunohistochemical staining for Reelin presented as greyscale of sagittal brain slices of 20 days old (P) animals. The white punctae along the brain and in the different areas constitute immunoreactive (ir) cells. The white squares in A indicate the areas most affected in the *reeler* mouse. OB: Olfactory bulb, NC: Neocortex, HC: Hippocampus, CB: Cerebellum. A: The control ($Rein^{wt/wt}$ Dlx5/6-Cre neg.) displayed Reelin-expressing cells in the olfactory bulb, the neocortex, the hippocampal formation, the nucleus of the optic tract, the substantia nigra and the ventral tegmental area. B: The conditional Reelin knockout ($Rein^{flox/flox}$ Dlx5/6-Cre pos.) exhibited Reelin-expressing cells just in the olfactory bulb and slight ones in the hippocampus, whereas all other areas lack Reelin-expressing cells.

3. Results

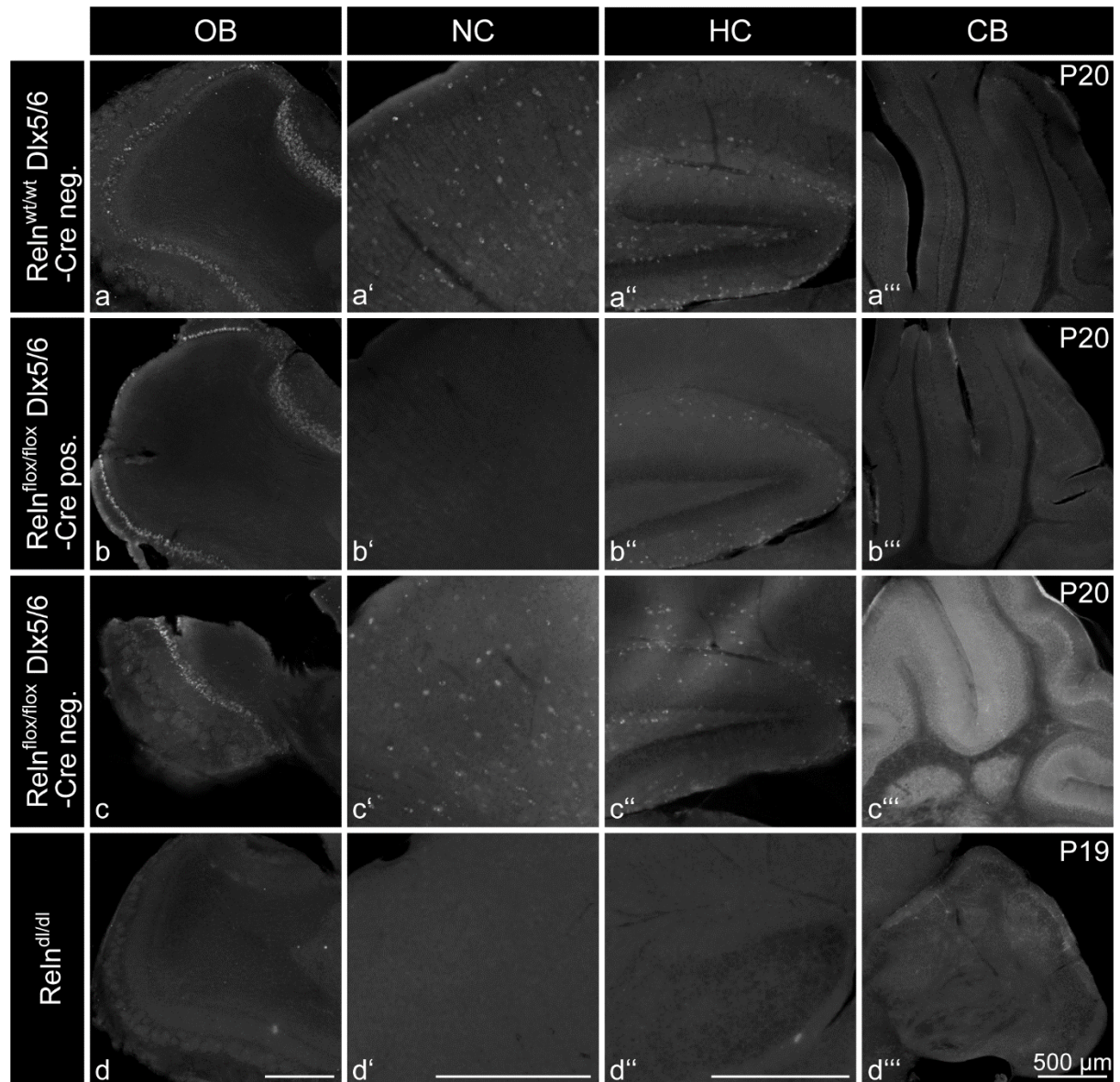


Figure 20: Details of Reelin expression pattern in the brain areas most affected in the *reeler* mouse

The brain areas indicated in Figure 19 as white squares (olfactory bulb (OB), neocortex (NC), hippocampus (HC) and cerebellum (CB)) were exposed and magnified. The immunohistochemical staining against Reelin is presented as greyscale images. Four genotypes are presented for comparison: The $\text{ReIn}^{\text{wt/wt}} \text{Dlx5/6-Cre neg.}$ (a-a'') resembling the wild type, the $\text{ReIn}^{\text{flox/flox}} \text{Dlx5/6-Cre pos.}$ (b-b'') the interneuron specific Reelin knockout, the $\text{ReIn}^{\text{flox/flox}} \text{Dlx5/6-Cre neg.}$ (c-c'') representing the closest control to the interneuron specific Reelin knockout and the $\text{ReIn}^{\text{dl/dl}}$ genotype (d-d''), representing the ubiquitous Reelin knockout comparable to the *reeler* mouse. The $\text{ReIn}^{\text{dl/dl}}$ genotype exhibited no Reelin immunoreactivity in all four brain areas (d-d''). All other genotypes displayed Reelin expression alongside the mitral cell layer of the olfactory bulb (OB) (a, b, c) but none in the cerebellum (CB) (a'', b'', c''). Regarding the neocortex (NC) $\text{ReIn}^{\text{wt/wt}} \text{Dlx5/6-Cre neg.}$ (a') and the $\text{ReIn}^{\text{flox/flox}} \text{Dlx5/6-Cre neg.}$ (c') genotypes exhibited both a variety of scattered Reelin-expressing cells. The $\text{ReIn}^{\text{flox/flox}} \text{Dlx5/6-Cre pos.}$ genotype (b'), by contrast, showed no Reelin-expressing cells in the neocortex (NC). In the hippocampus the $\text{ReIn}^{\text{wt/wt}} \text{Dlx5/6-Cre neg.}$ (a'') and the $\text{ReIn}^{\text{flox/flox}} \text{Dlx5/6-Cre neg.}$ (c'') demonstrated a similar distribution pattern of Reelin-expressing cells all over the hippocampus, while in the $\text{ReIn}^{\text{flox/flox}} \text{Dlx5/6-Cre pos.}$ genotype (b'') the Reelin-expressing cells were just found around the hippocampal fissure surrounding the dentate gyrus.

3. Results

3.2.2 Reelin depletion in inhibitory interneurons (iIN) of the neocortex and dentate gyrus

A reporter mouse line was used to distinguish inhibitory interneurons in the neocortex and dentate gyrus and to confirm the Cre recombinase activity in these cells. The reporter mouse line accommodated the genetic information of a tandem dimer red fluorescent protein (tdRFP) in its *Rosa26* locus. Closely upstream of the promoter region of this tdRFP DNA, a stop codon was located, which was flanked by two loxP sites. Thereby the stop codon was excised if a Cre recombinase had been active in the cell. This resulted in the transcription and translation of the tdRFP information and a red labelling of the cell. The reporter mouse line was bred with the *Reln^{flox/flox}* mouse line. The resulting mice should, if expressing Cre recombinase in a special cell type (here the inhibitory interneurons), display a distinct pattern of red labelled cells along the different brain areas. The ROSA KI PCR (data not shown) was used to identify tdRFP reporter positive animals. Using this reporter positive animals in immunohistochemical staining against Reelin, it could be shown that all Reelin-expressing cells in the neocortex of adult *Reln^{wt/wt} Dlx5/6-Cre* positive mice were also tdRFP positive (Fig. 21a-c and Fig. 21a'-c'). Since the *Dlx5/6* promoter is specifically active in inhibitory interneurons, all tdRFP positive cells could be addressed as inhibitory interneurons (iIN, highlighted with dovetail arrows). In contrast, the interneuron specific Reelin knockout displayed no Reelin in cells in the neocortex, but tdRFP labelled iIN (Fig. 21d-f and Fig. 21d'-f'). This additionally gave proof of the proper function of the *Dlx5/6-Cre/loxP* system in the mouse line, depleting Reelin in all iIN effectively.

The results for the dentate gyrus are presented in figure 22. The immunohistochemical staining against Reelin of 12 week old, tdRFP positive control mice (*Reln^{wt/wt} Dlx5/6-Cre* positive) (Fig. 22a-c, Fig. 22a'-c' and Fig. 22a''-c'') and interneuron specific Reelin knockout mice (*Reln^{flox/flox} Dlx5/6-Cre* positive) (Fig. 22d-f, Fig. 22d'-f' and Fig. 22d''-f'') displayed a similar staining pattern as in the neocortex. Distributed along the layers of the dentate gyrus red labelled iIN were found in both genotypes (Fig. 22a-b and Fig. 22d-e). The Reelin staining revealed two different cell types being immunoreactive for Reelin. One, also labelled in red, could be addressed as iIN (highlighted with dovetail arrows), the other cell type was negative for the tdRFP and had smaller, oval-shaped cell soma (arrowheads). Their narrow distribution along the hippocampal fissure (intermittent white line) of the dentate gyrus, the form of their cell soma and the expression of Reelin identified these cells as Cajal-Retzius (CR) cells.

3. Results

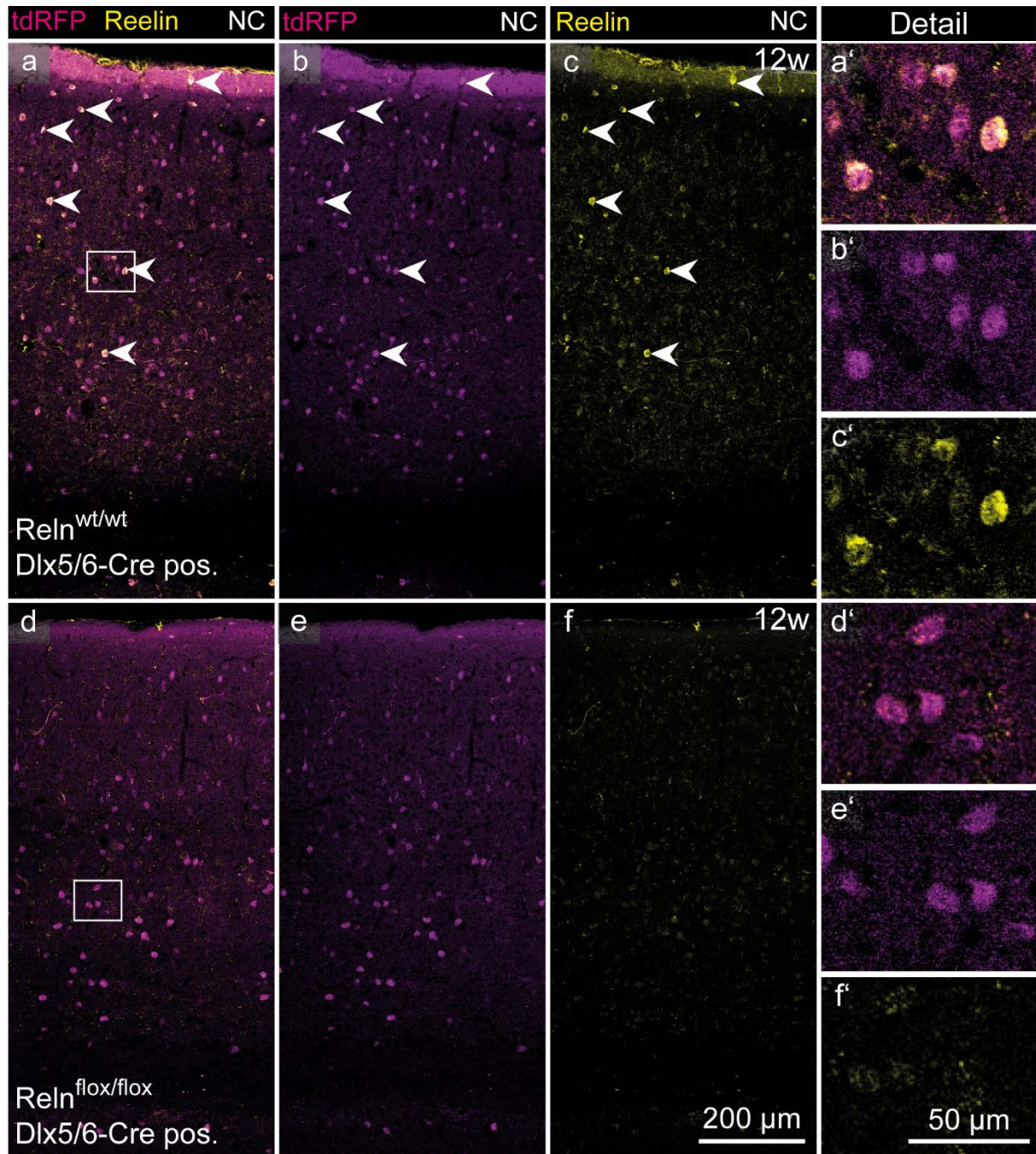


Figure 21: Coexpression of Reelin in tdRFP positive inhibitory interneurons in the neocortex

The breeding of R26tdRFP mice (tdRFP) (Luche et al. 2007) with the Dlx5/6-Cre pos. mice resulted in tdRFP marked inhibitory interneurons. Immunohistochemical staining against Reelin in 12 weeks old (w) tdRFP pos. animals showed the coexpression of Reelin with the tdRFP marker protein in the neocortex of the control genotype $Rein^{wt/wt}$ Dlx5/6-Cre pos. (a-c, dovetailed arrowheads hint positions of inhibitory interneurons). All Reelin-expressing cells in the neocortex were tdRFP positive and with that underwent Cre mediated DNA recombination. In the $Rein^{lox/lox}$ Dlx5/6-Cre pos. genotype (d-f) a clear tdRFP expression was seen along the whole area of the neocortex (d, e), but no Reelin expression (f). The white squares in a and d mark the area of magnification. In images a'-c' of the control, the coexpression of marker protein and Reelin in the same cells is evident. The interneuron specific Reelin knockout ($Rein^{lox/lox}$ Dlx5/6-Cre pos.), however, showed a clear reporter protein expression (d', e'), but no Reelin expression within the cells (f').

3. Results

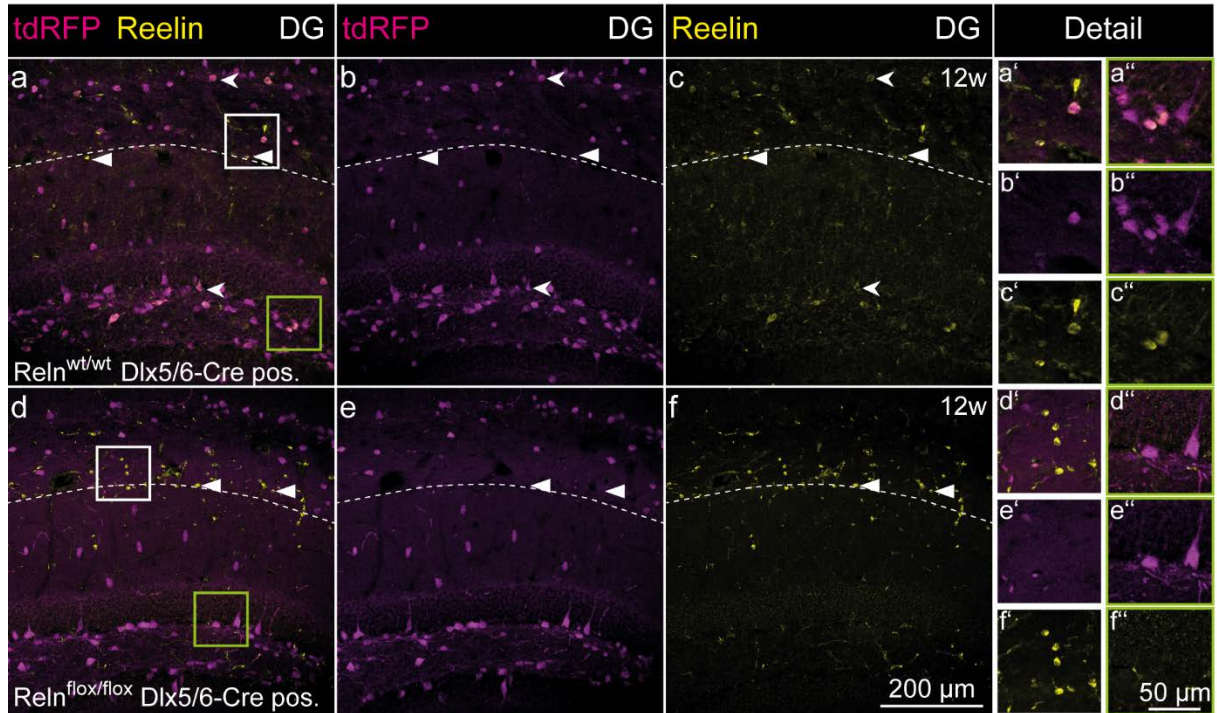


Figure 22: Coexpression of Reelin in tdRFP positive inhibitory interneurons in the dentate gyrus

Immunohistochemical staining for Reelin of dentate gyri (DG) in 12 week old tdRFP pos. $ReIn^{wt/wt}$ Dlx5/6-Cre pos. (a-c, a'-c', a''-c'') and $ReIn^{lox/lox}$ Dlx5/6-Cre pos. (d-f, d'-f', d''-f'') mice showed a similar coexpression pattern to the neocortex. In the dentate gyrus both Reelin sources were present, the Cajal-Retzius cells (arrowheads) along the hippocampal fissure (dotted line) and the inhibitory interneurons (dovetailed arrowheads). The white square in a and d corresponds with the magnifications in a'-c' and d'-f' while the green square (a, d) represents the magnified areas in a''-c'' and d''-f''. The control exhibited Reelin expression in Cajal-Retzius cells (a-c, a'-c') and tdRFP pos. interneurons (a-c, a''-c'') along the whole dentate gyrus. The $ReIn^{lox/lox}$ Dlx5/6-Cre pos. genotype displayed the Reelin expression just in Cajal-Retzius cells (d-f, d'-f') but not in the tdRFP pos. interneurons (d-f, d''-f'').

This cell type could express Reelin in the $ReIn^{wt/wt}$ Dlx5/6-Cre positive (Fig. 22a-c, arrowheads) as well as in the $ReIn^{lox/lox}$ Dlx5/6-Cre positive conditional knockout (Fig. 22d-f, arrowheads). The detail of the white squares in Fig. 22a and Fig. 22d clearly illustrates the difference between the two cell types (Fig. 22a'-c' and Fig. 22d'-f'). The Reelin-expressing iIN were just present in the $ReIn^{wt/wt}$ Dlx5/6-Cre positive control (Fig. 22a-c green square, detailed Fig. 22a''-c''), but not in the $ReIn^{lox/lox}$ Dlx5/6-Cre positive iIN specific Reelin knockout (Fig. 22d-f green square, detailed Fig. 22d''-f'').

In summary, the interneuron specific Reelin knockout ($ReIn^{lox/lox}$ Dlx5/6-Cre positive) had no Reelin expression in the inhibitory interneurons, neither in the neocortex nor in the dentate gyrus. In contrast, Cajal-Retzius cells in the dentate gyrus show normal Reelin expression.

3. Results

3.2.3 Reelin depletion in inhibitory interneurons in the developing dentate gyrus

It was confirmed that, in adulthood, inhibitory interneurons were the main source of Reelin expression in the neocortex and one of two sources, although the strongest in expression, in the dentate gyrus. In the case of the iIN specific Reelin knockout, the cell-specific depletion of Reelin in iIN could also be confirmed for the adult stage. The next focus was laid on the developing situation. Since the expression of Reelin by inhibitory interneurons starts around P5 in the developing dentate gyrus (Alcántara et al. 1998), a series of immunohistochemical staining against Reelin combined with chemical DAPI staining encompassing this time course were performed. In figure 23 the developmental stages of P3, P6 and P10 were displayed for the control $Reln^{wt/wt}$ $Dlx5/6$ -Cre positive (Fig. 23a-c and Fig. 23a'-c') and the conditional knockout $Reln^{flox/flox}$ $Dlx5/6$ -Cre positive (Fig. 23d-f and Fig. 23d'-f'). At P3 a sharp defined band of Reelin positive CR cells (arrow heads) were located around the hippocampal fissure in both genotypes, control (Fig. 23a, Fig. 23a') and interneuron specific Reelin knockout (Fig. 23d, Fig. 23d'). The granule cell layer was not yet formed but the first assembling cells could be determined below the line of Reelin positive CR cells (Fig. 23a, Fig. 23d). Three days later at P6 the CR cells expressing Reelin were still very common around the hippocampal fissure in both genotypes (Fig. 23b, Fig. 23e), but in the control situation there was a faint staining of cell bodies below the forming granule cell layer (GCL) in the hilar area (Hi, dovetailed arrows Fig. 23b, Fig. 23b'). In the interneuron specific conditional knockout, no stained cell somas were detectable in the hilar region (Fig. 23e'). At P10 the number of CR cells expressing Reelin seemed, in both genotypes, to be less compared to the time points before (Fig. 23a-c, Fig. 23a'-c', Fig. 23d-f, Fig. 23d'-f'). In the hilar region of the control situation there were salient Reelin positive cells (Fig. 23c, Fig. 23c' dovetailed arrows), which were completely absent in the interneuron specific Reelin knockout mouse (Fig. 23f, Fig. 23f'). Regarding the Reelin-expressing CR cells, were a comparable expression pattern along the development of the dentate gyrus between the control and the interneuron specific conditional knockout, confirming that this cell population was not affected during development. The published start of Reelin expression in iIN around postnatal day seven was also found in the control situation of the $Reln^{wt/wt}$ $Dlx5/6$ -Cre negative animals. This expression was absent in the $Reln^{flox/flox}$ $Dlx5/6$ -Cre positive genotype directly from the start. Thus, the main developmental Reelin source, the CR cells, were unaltered in both genotypes during development, while the iIN lack Reelin already at this early developmental stage.

3. Results

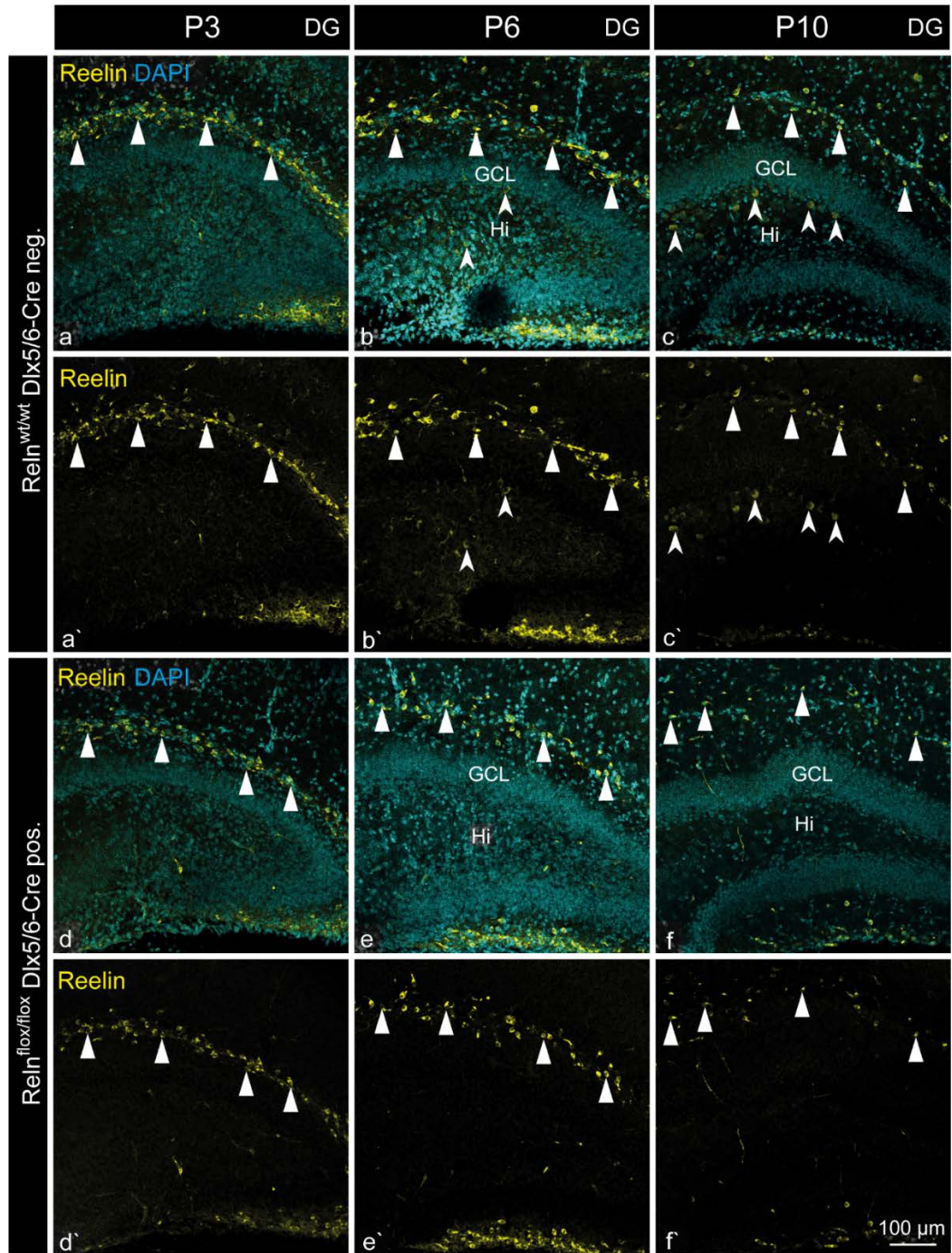


Figure 23: Postnatal timeline of Reelin expression pattern in the dentate gyrus

Postnatal days 3, 6 and 10 dentate gyri (DG) were stained immunohistochemically against Reelin to illustrate the expression switch from Cajal-Retzius cells (CR) (arrowheads) to inhibitory interneurons (dovetailed arrowheads). A counterstaining with DAPI (a marker for DNA) was used to highlight cell positions in the developing DG. In the control genotype ($Rein^{wt/wt}$ Dlx5/6-Cre neg.) a distinct Reelin expression from CR cells along the hippocampal fissure above the granule cell layer (GCL) was present at P3 (a, a') becoming fainter with timely progress from P6 (b, b') to P10 (c, c'). At P6 (b, b') a faint Reelin staining within the hilar area (Hi) could be detected, becoming more intense and numerous at P10 (c, c'), due to the onset of Reelin expression in interneurons (dovetailed arrowheads). This expression in the hilar area at P6 (e, e') and P10 (f, f') was completely missing in the interneuron specific knockout ($Rein^{flx/flx}$ Dlx5/6-Cre pos.). However, the expression pattern from CR cells (arrowheads) resembled the control situation at all time points (d, d', e, e', f, f').

3. Results

3.2.4 Western blot analysis of Reelin expression in the different genotypes of the **ReIn^{flox/flox}** line

Immunohistochemical staining has the inherent quality to give information about the location and an impression of the intensity of expression but was lacking the quantitative evidence. To acquire the quantitative information of the amount of Reelin protein still present in the tissue, Western blot analysis was performed. The focus was set on the most severely affected brain areas in the natural mutant *reeler* brain, the neocortex and the hippocampus. Figure 24 shows an exemplified image of a Reelin Western blot with neocortical and hippocampal tissue samples. Seven different genotypes had been blotted and analysed: the interneuron specific Reelin knockout (ReIn^{flox/flox} Dlx5/6-Cre positive), the control situation with incorporated loxP sites without Cre recombinase (ReIn^{flox/flox} Dlx5/6-Cre negative), the wild type genotype (ReIn^{wt/wt} Dlx5/6-Cre negative), the Cre control (ReIn^{wt/wt} Dlx5/6-Cre positive), that will uncover for Cre effects, and the three genotypes from the ReIn^{flox/flox} CMV-Cre line, the total Reelin knockout ‘deleter’ (ReIn^{dl/dl}), the heterozygous situation (ReIn^{wt/dl}) and the control animal (ReIn^{wt/wt}). The loading control was Actin protein with its band at 42 kilo Dalton (kDa). The Reelin protein has two cleavage sites for posttranscriptional processing (Royaux et al. 1997), which will result in five different cleavage products in addition to the full length protein. Possible products were the small N-terminal part, the N-terminal plus the central part, the central part, the central plus C-terminal part and the small C-terminal part (Fig. 2). The antibody used in these Western blot analyses binds to the N-terminal part of Reelin and hence detects only those three fragments containing this N-terminal part: the 450 kDa band representing the full-length Reelin, the 370 kDa band representing the N-terminal part with the central part and the 180 kDa band representing the N-terminal part. Regarding these Western blots, there was a total Reelin loss in the ‘deleter’ situation ReIn^{dl/dl}. The interneuron specific Reelin knockout displayed a nearly complete loss of Reelin in the neocortex with only a very faint signal being left. The other genotypes (ReIn^{flox/flox} Dlx5/6-Cre negative and ReIn^{wt/wt} Dlx5/6-Cre positive) showed comparable Reelin expression similar to the wild type animals (ReIn^{wt/wt} Dlx5/6-Cre negative). Regarding the hippocampus, there was an obvious difference in the ReIn^{flox/flox} Dlx5/6-Cre positive genotype.

3. Results

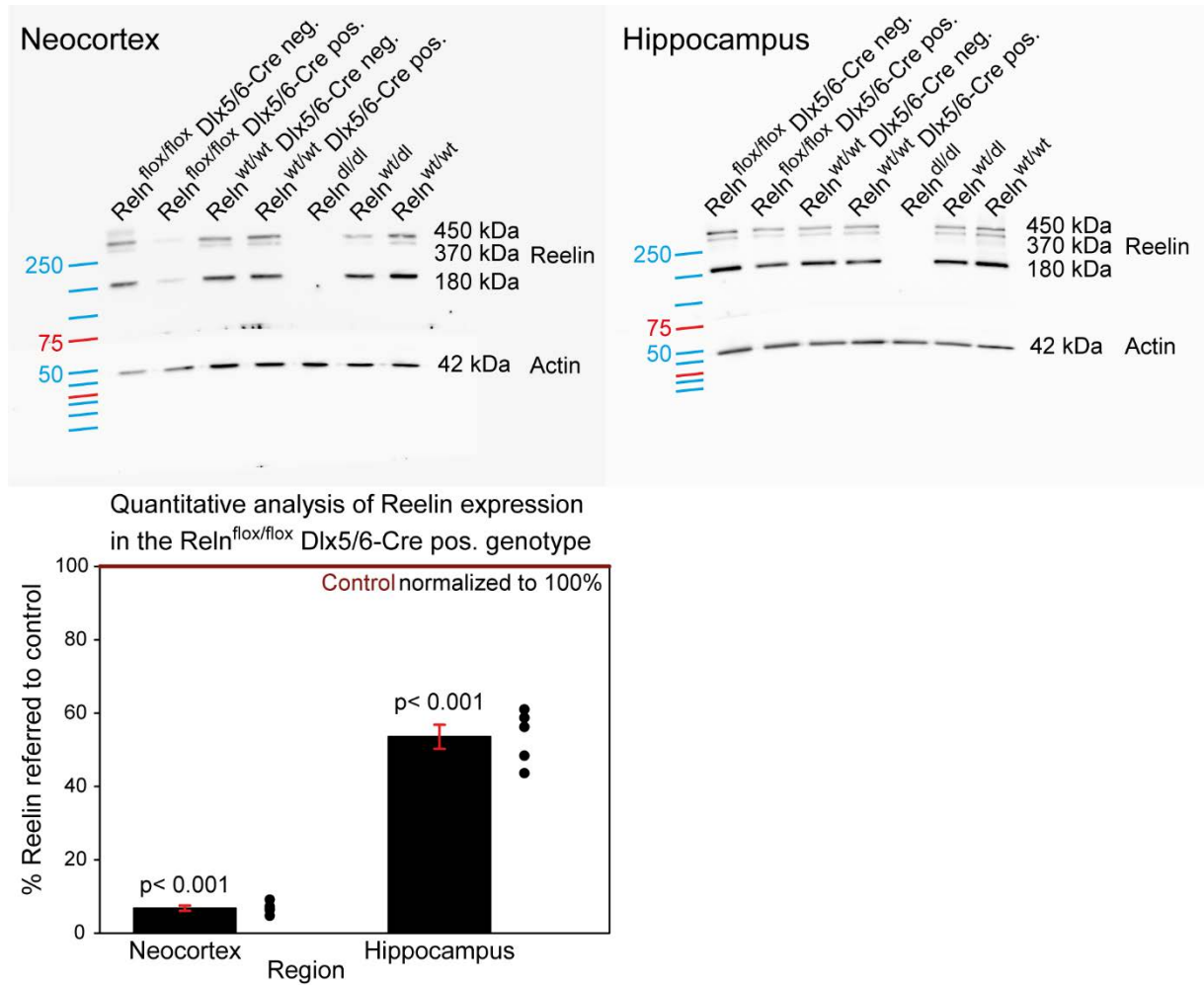


Figure 24: Quantification of Reelin expression in the neocortex and the hippocampus by Western blotting

Western blots were used to quantify the Reelin amount in the neocortex and the hippocampus of seven main genotypes: the interneuron specific Reelin knockout ($ReIn^{flox/flox}$ Dlx5/6-Cre pos.), the control with just loxP sites ($ReIn^{flox/flox}$ Dlx5/6-Cre neg.), the wild type-like control ($ReIn^{wt/wt}$ Dlx5/6-Cre neg.), the wild type-like control with Cre recombinase ($ReIn^{wt/wt}$ Dlx5/6-Cre pos.), the *reeler*-like total knockout deleter ($ReIn^{dl/dl}$), the heterozygous *reeler*-like knockout ($ReIn^{wt/dl}$) and the wild type control ($ReIn^{wt/wt}$). An actin blot had been performed together with the Reelin blot for normalisation and loading control. The used Reelin antibody (G10), binding at the N-terminal of the Reelin protein, detects the full-length Reelin (450 kDa) and the fragments resulting from posttranslational cleavage: the N-terminal and the central part (370 kDa) and the N-terminal fragment (180 kDa). The deleter genotype ($ReIn^{dl/dl}$) displayed no Reelin positive bands neither in the neocortex nor in the hippocampus. The interneuron specific conditional Reelin knockout ($ReIn^{flox/flox}$ Dlx5/6-Cre pos.) exhibited just very faint bands in the neocortex, but in the hippocampus, a clear Reelin signal was present, albeit weaker than in the control. The graph below gives the blot results as a percentage of control ($ReIn^{wt/wt}$ Dlx5/6-Cre neg.) amount of Reelin (100 %). In the neocortex the $ReIn^{flox/flox}$ Dlx5/6-Cre pos. genotype had just 7 % Reelin left, while in the hippocampus there were still 54 % present compared to control. Both results showed high significance in the statistical testing (one-sampled t-test against 100 % control, $N=5$ animals per genotype, $\alpha=0.05$).

Remaining Reelin expression was higher in the hippocampus compared to the neocortex, but a slight decrease in intensity was still detectable compared to all controls. This first

3. Results

impression was confirmed by a quantitative analysis of five independent Western blot samples. All quantifications were corrected based on the reference actin signal. The $\text{ReIn}^{\text{wt/wt}}$ Dlx5/6-Cre positive genotype, as control, was normalized to 100 % (Fig. 24 graph, red reference line). The quantification revealed a highly significant reduction of the amount of Reelin protein in the neocortex ($p < 0.001$, one-sample t-test, $N=5$) to 6.8 ± 0.71 % (mean \pm standard error of the mean (sem)). The amount of Reelin in the hippocampus was also significantly reduced ($p < 0.001$, one-sample t-test, $N=5$), but the remaining Reelin amount was much higher as in the neocortex. There was still 53.57 ± 3.28 % (mean \pm sem) Reelin protein left in the hippocampus. Thus, in the neocortex, the amount of Reelin protein in the $\text{ReIn}^{\text{flox/flox}}$ Dlx5/6-Cre positive knockout was less than 10 % and supported the visual results of the immunohistochemical staining. The Reelin depletion in the hippocampus of around 50 %, compared to the control situation, was most probably based on the high number of Cajal-Retzius cells, which remain as Reelin source in this area. Based on the quantitative analyses of the Western blots, and the visual support from the immunohistochemical staining, it could be stated that the $\text{ReIn}^{\text{flox/flox}}$ Dlx5/6-Cre positive interneuron specific Reelin knockout was successful. No Reelin expression could be found in inhibitory interneurons any more, neither in the neocortex, nor in the hippocampus while the developmental Reelin source (CR cells) was unaffected.

3.3 Analysis of neuronal layering and morphology in the $\text{ReIn}^{\text{flox/flox}}$ Dlx5/6-Cre line

The before mentioned results gave proof of the depletion of Reelin in iIN but not in CR cells of the $\text{ReIn}^{\text{flox/flox}}$ Dlx5/6-Cre mouse line. This means that the main Reelin source for development in this conditional knockout was unaffected. Considering the severe developmental defects of the natural Reelin knockout, the *reeler* mouse, which suffers from abnormal cell position, orientation and morphology (Caviness 1976; Stanfield and Cowan 1979a; D'Arcangelo 2005; Miyata et al. 2010), a closer investigation of the morphology of the $\text{ReIn}^{\text{flox/flox}}$ Dlx5/6-Cre mouse line had been done.

3.3.1 Brain size and weight of the $\text{ReIn}^{\text{flox/flox}}$ Dlx5/6-Cre mouse line

First of all, the whole brain size and weight were compared between the natural mutant *reeler*, a C57BL/6J wild type and males and females from the $\text{ReIn}^{\text{flox/flox}}$ Dlx5/6-Cre mouse line. As the *reeler* mice suffer from developmental defects, the brains of these mice were smaller and exhibited diminished brain areas like the cerebellum. This becomes obvious in comparison to

3. Results

a normal C57BL/6J mouse brain, whereas the brains of the $Re^{flx/flx}$ Dlx5/6-Cre mice did not differ noticeably from the C57BL/6J brain (Fig. 25). A similar result was found regarding brain weight (table 11). While the C57BL/6J and the brains of the $Re^{flx/flx}$ Dlx5/6-Cre mice encompass the same weight range, the *reeler* brain was about 0.1 g lightweight. The retarded development of the *reeler* mouse was clearly visible within this gross comparison of the brains, especially at the cerebellum, while the $Re^{flx/flx}$ Dlx5/6-Cre mice showed no obvious difference to the C57BL/6J mouse brain. This comparison was based on the outward brain appearance but gives no hint about the layering of cell structures within the brain.

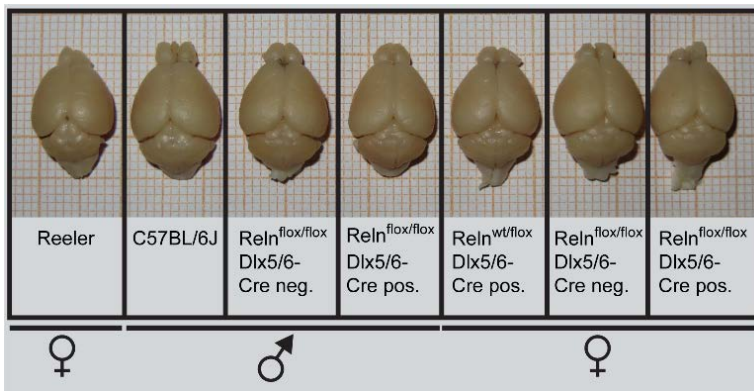


Figure 25: Whole brain comparison

Whole-brain pictures on scale paper for overall size comparison. The natural mutant *reeler* showed a reduction in the overall length and size of the olfactory bulbs, the neocortex, and the cerebellum. The C57BL/6J, the background mouse strain, displayed normal sizes. The interneuron specific Reelin knockout ($Re^{flx/flx}$ Dlx5/6-Cre

pos.), the control with just loxP sites ($Re^{flx/flx}$ Dlx5/6-Cre neg.) and the heterozygous genotype ($Re^{wt/flx}$ Dlx5/6-Cre pos.) were comparable in size to the C57BL/6J. Additionally, no difference in size had been detected between male and female brains.

Table 11: Brain weights for comparisons

Properties for the genotypes presented in figure 25. The obviously smaller size of the *reeler* brain was mirrored by the lighter brain weight of 0.1 g compared to the C57BL/6J. The other brains from the $Re^{flx/flx}$ mouse line were also lighter (0.07-0.02 g) than the C57BL/6J and varied in a range of 0.04 g.

Genotype	Sex	Brain weight	Age
Reeler	female	0.444 g	17 weeks
C57BL/6J	male	0.586 g	25 weeks
$Re^{flx/flx}$ Dlx5/6-Cre neg.	male	0.523 g	25 weeks
$Re^{flx/flx}$ Dlx5/6-Cre pos.	male	0.517 g	25 weeks
$Re^{wt/flx}$ Dlx5/6-Cre pos.	female	0.541 g	25 weeks
$Re^{flx/flx}$ Dlx5/6-Cre neg.	female	0.567 g	25 weeks
$Re^{flx/flx}$ Dlx5/6-Cre pos.	female	0.559 g	25 weeks

3. Results

3.3.2 Overview of the gross cell layering across the brain especially in the neocortex, hippocampus and cerebellum of $ReIn^{flox/flox}$ Dlx5/6-Cre positive mice

In the natural mutant *reeler*, the morphological changes could be seen even by looking at the brain itself. The most obvious change was displayed by a hypoplastic cerebellum which is a result of drastic developmental impairments (Ogawa et al. 1995; Miyata et al. 2010). Likewise affected in this natural mutant was the specific cell layering of different brain areas such as the neocortex, the hippocampus, and the cerebellum (Stanfield and Cowan 1979a, 1979b; Ogawa et al. 1995; Miyata et al. 2010). Although CR cells are known to be most important during this developmental process of neuronal layering, an effect of Reelin expressed by inhibitory interneurons cannot be excluded, especially in the hippocampus, where layering still takes place when inhibitory interneurons start to express Reelin. Immunohistochemical staining against neuronal nuclei (NeuN) and DAPI of sagittal slices from mouse brains of total Reelin depleted *reeler* mice and $ReIn^{dl/dl}$ mice as well, as of the interneuron specific Reelin knockout mice ($ReIn^{flox/flox}$ Dlx5/6-Cre positive), and of control mice ($ReIn^{wt/wt}$ Dlx5/6-Cre negative) were performed for comparison of gross cell layering along the brain (Fig. 26).

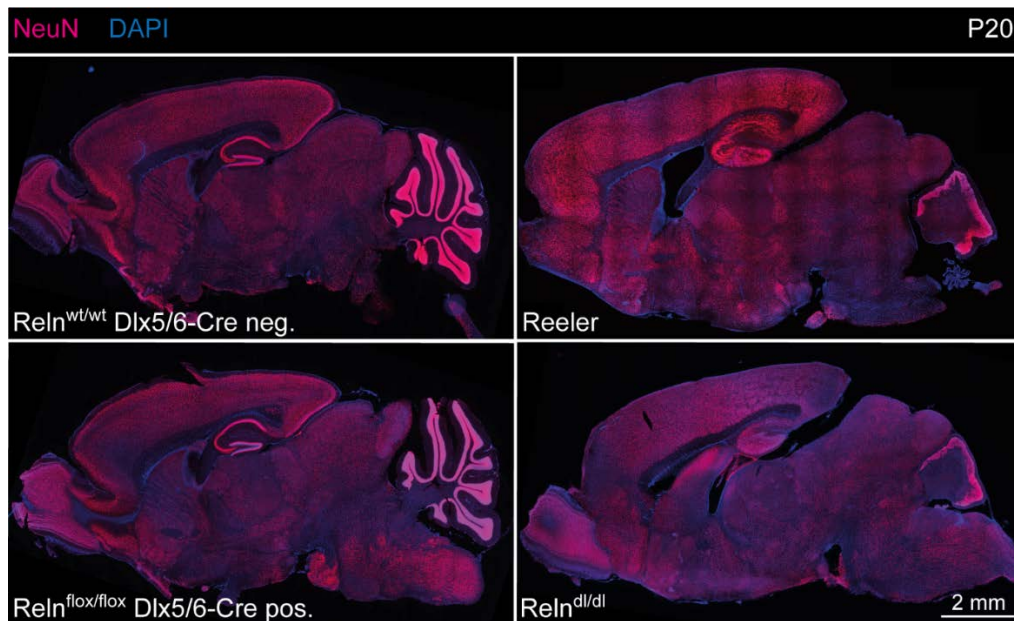


Figure 26: Gross morphological organisation of different brain areas

Sagittal slices of 20 days old mice immunohistochemically stained for NeuN (neuronal nuclei marker) and counterstained with DAPI (DNA marker). The genotype $ReIn^{wt/wt}$ Dlx5/6-Cre neg. illustrated the normal gross morphology in a sagittal slice. The cell layers in the olfactory bulb and the neocortex were recognisable, the double u-shaped form of pyramidal and granule cells in the hippocampus, and the foliation in the cerebellum was clearly highlighted. The same gross morphology organisation could be detected in the $ReIn^{flox/flox}$ Dlx5/6-Cre pos. genotype, the interneuron specific Reelin knockout. The *reeler* mutant did not show any of these structures. The cells in the hippocampus were scattered all over the area and the foliation in the cerebellum was totally absent, while the whole area appeared smaller than in the control genotype. The same disorganisation was found in the deleter ($ReIn^{dl/dl}$).

3. Results

The *reeler* mutant showed a considerable missing of the foliated cell layer in the cerebellum and a scattered cell positioning in the hippocampus, compared to the control (ReIn^{wt/wt} Dlx5/6-Cre negative). The layering in the cerebellum and hippocampus in the ubiquitous Reelin depleted ReIn^{dl/dl} brain was equivalent to the *reeler* phenotype. Whereas the cell-specific depletion in iIN in the ReIn^{flox/flox} Dlx5/6-Cre positive mice led to normal cell positioning in the cerebellum and hippocampus, comparable to the control brain (ReIn^{wt/wt} Dlx5/6-Cre negative). Concerning the neocortex was no precise layering visible at that magnification. By comparing the gross morphology in this sagittal slices, it could be stated, that the iIN specific Reelin knockout (ReIn^{flox/flox} Dlx5/6-Cre positive) resembles strongly the control (ReIn^{wt/wt} Dlx5/6-Cre negative), while the ReIn^{dl/dl} brain, as expected from a ubiquitous Reelin knockout, resembles the *reeler* brain. For better comparison of the layering and cell positioning of the main genotypes in this work (ReIn^{flox/flox} Dlx5/6-Cre positive, ReIn^{dl/dl}, ReIn^{wt/wt} Dlx5/6-Cre negative), the areas of the neocortex, hippocampus and cerebellum had been magnified and opposed in figure 27. The magnification of the neocortex (NC) showed an immunohistochemical staining against Brn2, a transcription factor expressed mainly in layer II but also layers III to V neocortical neurons (Sekine et al. 2011), and Forkhead-Box-Protein P2 (FoxP2), expressed in layer II to VI of neocortical neurons (Ferland et al. 2003), for better discrimination of cell positioning and layering. Using this staining and higher magnification, it was obvious, that the structured composition of the neocortex of the iIN specific Reelin knockout (ReIn^{flox/flox} Dlx5/6-Cre positive, Fig. 27b-b'') equalled the structure of the control neocortex (ReIn^{wt/wt} Dlx5/6-Cre negative, Fig. 27a-a''). On the contrary, the ReIn^{dl/dl} neocortex displayed an inverted layering where Brn2 positive cells were to be found in the area of layer V and VI (Fig. 27c) and FoxP2 positive cells were also present in the molecular layer (Fig. 27c'), where none of these cells were found under normal conditions (Fig. 27a'). This layering of the ReIn^{dl/dl} neocortex was described similarly for the *reeler* brain (Caviness 1976; Boyle et al. 2011). A clearly foliated cell layer and a similar size of the cerebellum (CB) compared to the control (Fig. 27d) could be found in the iIN specific Reelin knockout (Fig. 27e). The same situation could be observed for the hippocampus and dentate gyrus (DG). The pyramidal cell layer and the granule cell layer in the iIN specific Reelin knockout (Fig. 27h) were arranged and positioned comparable to the control (Fig. 27g). In the ReIn^{dl/dl} brain, the cerebellum was obviously underdeveloped and lacking a foliation of the cell layers of Purkinje and granule cells (Fig. 27f).

3. Results

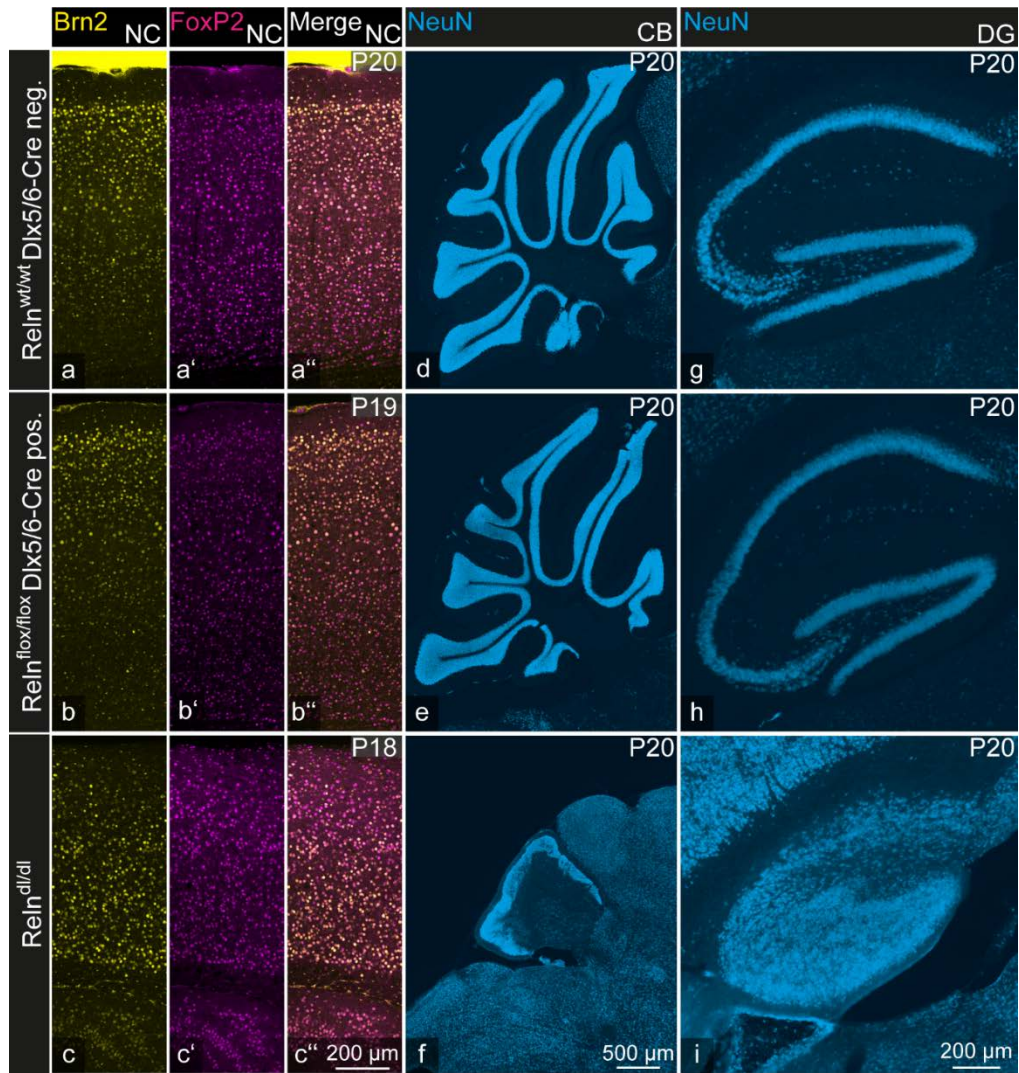


Figure 27: Morphology and cell layering of different brain areas in detail

The areas of the neocortex (NC), cerebellum (CB) and dentate gyrus (DG) had been magnified for the genotype $Reelin^{wt/wt} Dlx5/6-Cre\ neg.$ (control a, a', a'', d, g), the interneuron specific Reelin knockout $Reelin^{flox/flox} Dlx5/6-Cre\ pos.$ (b, b', b'', e, h) and the deleter genotype $Reelin^{dl/dl}$ (c, c', c'', f, i). The NC was immunohistochemically stained against Brn2 (transcription factor and marker for layer II and IV) and Fox P2 (Forkhead-box-protein P2, a marker for layer VI) to detect inverted layering. The staining pattern of control (a, a', a'') and interneuron specific knockout (b, b', b'') were comparable and showed the expected staining of Brn2 in the region of layer II and IV (a, b). The FoxP2 staining scattered along all layers of both NC (a', b'). The merge of both stainings highlighted the equal pattern (a'', b''). The deleter presented an inverted layering, comparable to the *reeler* phenotype, where the Brn2 staining was found in the lower layers of the NC and FoxP2 in the upper layers. For these stainings mice at the age of P20 for control, P19 for interneuron specific knockout and P18 for the deleter were used. The magnification of the CB and DG were taken from immunohistochemical staining against NeuN from P20 mice. The CB showed a proper foliation of the granule cell layer in the control (d) and the interneuron specific Reelin knockout (e) with comparable sizes between the two genotypes. The deleter genotype, on the contrary, displayed a diminished size of the CB and no foliation of the granule cell layer. The DG in the control genotype had a sharp, precise hook-formed pyramidal cell layer and u-shaped granule cell layer (g). The same structure and position of cell layers were found in the interneuron specific Reelin knockout (h). In contrast, the deleter exhibited a scattering of cells all along the area of the DG without the formation of discernible layers (i).

3. Results

The hippocampus and dentate gyrus showed a scattering of cell bodies all across the area without any indications of defined layers of pyramidal and granule cells (Fig. 27i). This situation was also found in the hippocampus of the *reeler* mutant (Fig. 26). With these results regarding the gross morphology of the different brain areas and the cell layering, it could be stated that the iIN specific Reelin knockout ($\text{ReIn}^{\text{flox/flox}}$ Dlx5/6-Cre positive) displayed normal gross morphology and cell layering in the neocortex, hippocampus and cerebellum. The Reelin depletion in iIN did not interfere with the development of morphological properties of the brain. The $\text{ReIn}^{\text{dl/dl}}$ mice showed a *reeler* like phenotype concerning the gross morphology and cell layering in the neocortex, hippocampus, and cerebellum. This gave proof of the effective ubiquitous knockout of Reelin with the loxP and CMV-Cre combination from the beginning of brain development, resulting in a *reeler* phenotype.

3.3.3 Granule cell orientation and layer thickness in the dentate gyrus of the $\text{ReIn}^{\text{flox/flox}}$ Dlx5/6-Cre positive mice

Previous publications described a direct influence of depleted or blocked Reelin on the cell layering in the dentate gyrus. Especially the granule cells were scattered all over the whole dentate gyrus area with no indication of forming a dense layer (Stanfield and Cowan 1979b; Ogawa et al. 1995; Nakajima et al. 1997). Additionally it was shown by various authors (Haas et al. 2002; Heinrich et al. 2006; Frotscher et al. 2009; Haas and Frotscher 2010) that a granule cell dispersion (GCD), found in hippocampi of patients with temporal lobe epilepsy (TLE), was most likely due to a Reelin deficit or blockage of the canonical Reelin pathway. Also, the dendritic orientation was shown to be impaired when the Reelin protein levels were low (Freiman et al. 2011). To investigate these phenomena the $\text{ReIn}^{\text{flox/flox}}$, the $\text{ReIn}^{\text{dl/dl}}$ and the *reeler* mouse line were bred with a mouse line expressing enhanced green fluorescent protein (eGFP) under the Thy-1 cell surface antigen (Thy1) promotor. This resulted in randomly expressed eGFP in neurons of the brain. Figure 28 displays the dentate gyri of a *reeler*, a $\text{ReIn}^{\text{dl/dl}}$, an iIN specific Reelin knockout ($\text{ReIn}^{\text{flox/flox}}$ Dlx5/6-Cre positive) and the control ($\text{ReIn}^{\text{flox/flox}}$ Dlx5/6-Cre negative). The *reeler* and the $\text{ReIn}^{\text{dl/dl}}$ mouse exhibited a scattered position of cell somata over the whole dentate gyrus with randomly oriented dendritic branches.

3. Results

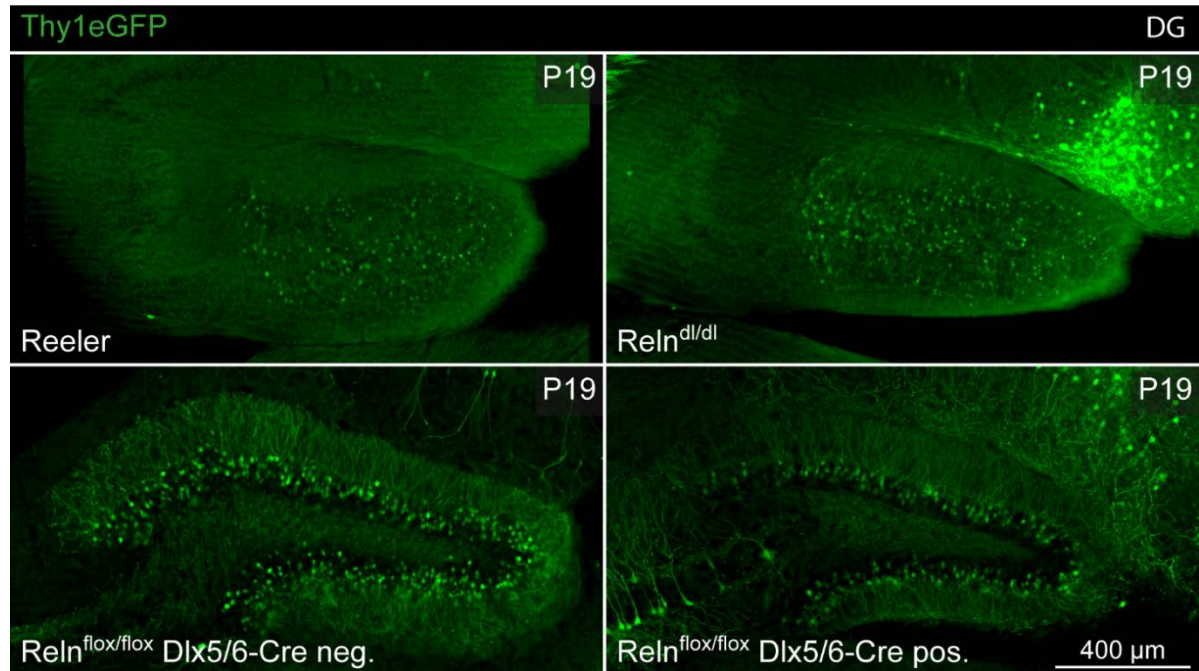


Figure 28: Granule cell orientation in the dentate gyrus

The TG(Thy1-EGFP)MJrs/J mouse line from Feng (Feng et al. 2000) was bred with the $Reln^{flox/flox}$ mouse line resulting in animals randomly expressing an eGFP protein within primary neurons. In the dentate gyrus (DG) the expression of eGFP allowed cell orientation analysis in P19 old mice. The *reeler* genotype showed a scattered distribution of granule cells with dendritic orientation in all directions. The same random positioning and orientation were present in the deleter genotype $Reln^{dl/dl}$. The standard anatomical orientation of cells was found in the control genotype ($Reln^{flox/flox}$ Dlx5/6-Cre neg.). The granule cell somata forming a distinct u-shaped layer spreading their dendritic branches towards the hippocampal fissure and arborizing within the stratum moleculare. An unaltered granule cell positioning and orientation were found in the interneuron specific Reelin knockout ($Reln^{flox/flox}$ Dlx5/6-Cre positive).

While the iIN specific Reelin knockout ($Reln^{flox/flox}$ Dlx5/6-Cre positive) displayed a distinct formed layer of eGFP positive cell somata with dendritic branches oriented towards the stratum moleculare comparable to the control situation in the $Reln^{flox/flox}$ Dlx5/6-Cre negative genotype. This gave again proof that the *reeler* phenotype was able to be simulated with the ubiquitous Reelin knockout $Reln^{dl/dl}$. On the contrary, the $Reln^{flox/flox}$ Dlx5/6-Cre positive genotype showed no impairments regarding layer formation or orientation of granule cells in the dentate gyrus. To evaluate possible granule cell dispersion within the dentate gyrus of the $Reln^{flox/flox}$ Dlx5/6-Cre positive mice, a quantitative measurement of granule layer thickness was performed. Figure 29 depicts the resulting data (Fig. 29A) and a staining example with landmarks of measuring (Fig. 29B). The measurements were performed on an immunohistochemical staining against NeuN in the dentate gyri of adult iIN specific Reelin knockout and control animals. At three landmarks (Fig. 29B) the data were collected and the mean of the granule layer thickness calculated. The mean thickness of iIN specific Reelin

3. Results

knockout (mean±sem: 65.85±1.64 μm) and control animals (ReIn^{wt/wt} Dlx5/6-Cre positive) (66.18±1.46 μm), displayed in Fig. 29A, did not differ significantly regarding the performed two-tailed t-test ($t(8)=-0.15$ $p=0.883$). Five animals per genotype were tested (N=5), with a defined α -error of 0.05. With these results, it could be stated that there was no granule cell dispersion in the iIN specific Reelin knockout. So the granule cell layer was formed, and the granule cells oriented comparable to the control.

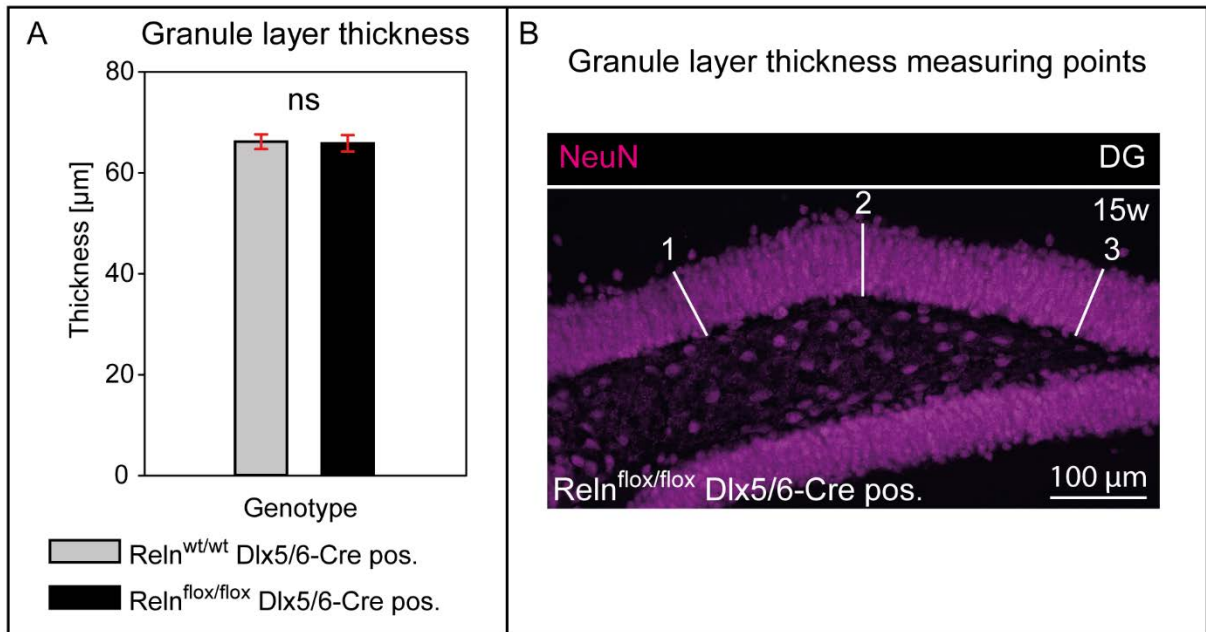


Figure 29: No cell dispersion of the granule cell layer in the ReIn^{flox/flox} Dlx5/6-Cre positive mice

Granule cell dispersion, previously described to occur as a result of reduced Reelin signalling (for example in temporal lobe epilepsy), was quantified by measuring granule cell layer thickness in immunohistochemical stainings against NeuN in 15 week old mice. A: Results of the quantitative analysis of granule cell layer thickness. No significant difference had been found between the control (ReIn^{wt/wt} Dlx5/6-Cre pos.) and the interneuron specific Reelin knockout (ReIn^{flox/flox} Dlx5/6-Cre pos.). The result is presented as mean ± standard error of the mean; statistic: two-tailed t-test $t(8)=-0.15$, $p=0.883$, N=5 animals per genotype, $\alpha=0.05$. B: Example of NeuN stained dentate gyrus with three annotated landmarks of measuring. For statistical analysis the mean of these three measurements was used as the value for each individual animal.

All analyses of the gross and minor morphology of the different brain areas, especially the hippocampus and dentate gyrus, demonstrated clearly that the iIN specific Reelin knockout had no morphologic impairments resulting from development or the Reelin depletion in iIN. In contrast ReIn^{dl/dl} genotype resembles the *reeler* phenotype regarding changes in the layer formation, cell distribution, cell orientation and underdevelopment of the cerebellum. Additionally, it could be stated, that the construct of the loxP sites in combination with either the CMV-Cre or the Dlx5/6-Cre produces the depletion pattern and phenotype expected.

3. Results

3.4 Behaviour of the $ReIn^{flox/flox}$ $Dlx5/6$ -Cre mice

The morphology of the $ReIn^{flox/flox}$ $Dlx5/6$ -Cre positive mice in comparison to controls, *reeler* and *reeler* like phenotypes had been presented beforehand. However, a quite essential part of a living organism is represented by its behaviour. Therefore, it is likely, that neuronal structural changes that occur following interneuron-specific Reelin knockout can subsequently affect behavioural function *in vivo*. For the *reeler* mice and heterozygous *reeler* mice, often used as model for schizophrenia, a lot of behavioural analyses had been done over the years, with contradictory results (Bliss and Errington 1977; Tuetting et al. 1999; Salinger et al. 2003; Krueger et al. 2006; Ognibene et al. 2007; Podhorna and Didriksen 2004; Teixeira et al. 2011). Nevertheless, several forms of behaviour could be focused on in which *reeler*, the heterozygous *reeler*, and wild type mice differed constantly: anxiety-related behaviour, social interaction, working memory, and spatial learning and memory. Consequently, these sections were focused on in the present thesis.

3.4.1 Behavioural tasks used for the pilot group consisting of $ReIn^{flox/flox}$ $Dlx5/6$ -Cre positive and $ReIn^{wt/wt}$ $Dlx5/6$ -Cre negative mice

The pilot group was tested for anxiety-related behaviour, locomotor activity and exploration, learning and memory, plus social interaction. These behavioural functions were evaluated using well-established rodent paradigms consisting of: elevated plus maze (EPM), open field task (OF), Y-maze spontaneous alternation (SA), Novel object recognition (OR) and three-chamber sociability and social recognition test (SI).

3.4.1.1 Behavioural testing for anxiety-related behaviour and locomotor activity and exploration in the pilot group

For the pilot group, mice were tested for innate anxiety and locomotor activity in the EPM and OF tasks, respectively. Previous studies report that *reeler* mouse display hyperactivity in the OF task (Salinger et al. 2003) and the heterozygous *reeler* mouse show less anxiety-related behaviour (Ognibene et al. 2007). Therefore, testing in these tasks was performed to investigate whether iIN specific Reelin knockout mice display a similar phenotype. Figure 30 depicts the results of the two tests. In the EPM (Fig. 30A), anxiety-related behaviour is represented in the time spent in the open arms, given here as the percentage of full trial time of 5 minutes (min).

3. Results

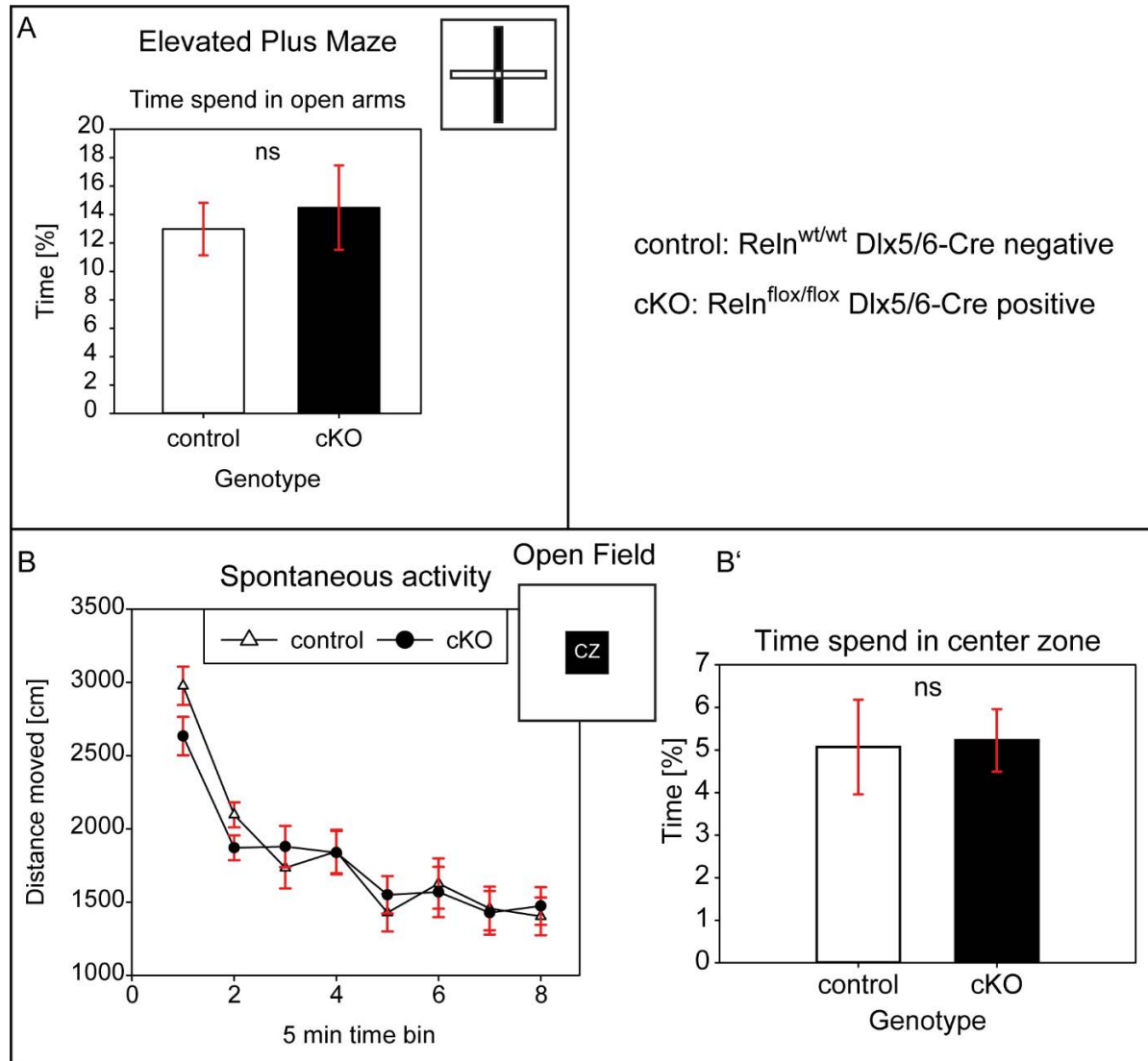


Figure 30: Anxiety-related behaviour, general activity and exploration in the pilot group

The pilot group consisted of 12 male naïve mice with genotypes $Reln^{wt/wt}$ Dlx5/6-Cre neg. (control) and $Reln^{lox/lox}$ Dlx5/6-Cre pos. (conditional knockout, cKO). A: Elevated plus maze results: anxiety-related behaviour was indexed as time spent in open arms as the percentage of all trial time. No significant difference was found in the times spent in the open arms for both genotypes (two-tailed t-test $t(10)=0.43$, $p=0.675$; $N=6$ animals per genotype, $\alpha=0.05$). B and B': Open field results: B: Exploration behaviour and spontaneous activity are presented as the distance moved per time bin of 5 min. A progressing habituation to the surroundings, as an effect of trial time was recognisable in both genotypes (Mixed-design ANOVA (MD ANOVA): effect of time bin: $F(7,70)=29.36$ $p<0.001$ $N=6$ animals per genotype, $\alpha=0.05$), but no effect of genotype (MD ANOVA: genotype: $F(1,10)=0.13$ $p=0.730$). B': Anxiety-related behaviour was indexed as time spent in the centre zone as the percentage of trial time. No significant difference was found between the control and the cKO: two-tailed t-test: $t(10)=0.12$ $p=0.908$, $N=6$ animals per genotype, $\alpha=0.05$, values as mean \pm sem.

The iIN specific Reelin knockout ($Reln^{lox/lox}$ Dlx5/6-Cre positive or cKO) spent $14.49\pm 2.97\%$ time in the open arms and did not significantly differ from the control ($Reln^{wt/wt}$ Dlx5/6-Cre negative) mice, which spent $12.98\pm 1.84\%$ time in the open arms (independent t-test: $t(10)=0.43$ $p=0.675$, $N=6$ animals per genotype, $\alpha=0.05$). The balance

3. Results

between the compulsion to explore novel environments and the anxiety, evoked by the exposed and elevated position of the open arms, was quite comparable between the two genotypes. The same outcome was seen upon exposing the animals to an unprotected open space (represented by the centre zone (CZ) of the box) in the open field task (Fig. 30B, Fig. 30B'). Focusing on the time spent in the CZ, as an index for anxiety-related behaviour (Fig. 30B'), there was no significant difference between the control and the cKO. Both genotype groups spent equal amounts of time (control: 5.07 ± 1.11 %, cKO: 5.23 ± 0.73 %) in the centre zone of the box (independent t-test: $t(10)=0.12$ $p=0.908$, $N=6$ animals per genotype, $\alpha=0.05$). These data support the results of anxiety-related behaviour in the EPM. Additionally, the OF task provides the possibility to analyse spontaneous locomotor activity as an index for exploration, locomotion and general activity. Figure 30B depicts the mean distance (cm) travelled across 5 min time bins, following a 40 min test session. The curve for both genotypes shows a steady decrease in activity levels across time, indicating the progressive habituation to the novel OF environment (Mixed-design ANOVA (MD ANOVA): duration of task as time bins: $F(7,70)=29.36$ $p<0.001$ $N=6$ animals per genotype, $\alpha=0.05$). Meanwhile, the individual curves of the genotype groups remain in close proximity, illustrating comparable activity patterns (RM ANOVA: genotype: $F(1,10)=0.13$ $p=0.730$). Therefore, the $Reln^{lox/lox}$ $Dlx5/6$ -Cre positive and the $Reln^{wt/wt}$ $Dlx5/6$ -Cre negative mice showed equal locomotor activity patterns and exploratory behaviour.

3.4.1.2 Behavioural testing for learning and memory function, and social behaviour in the pilot group

Previous studies show that, while the *reeler* mice are impaired in spontaneous alternation (Bliss and Errington 1977) and show impairments in working memory tasks (Salinger et al. 2003), the heterozygous *reeler* mice (HRM) performed normally in the same tasks (Salinger et al. 2003; Podhorna and Didriksen 2004; Krueger et al. 2006). To test for working memory function in iIN specific Reelin knockout (cKO or $Reln^{lox/lox}$ $Dlx5/6$ -Cre positive) and controls ($Reln^{wt/wt}$ $Dlx5/6$ -Cre negative), the Y-maze spontaneous alternation (SA) task was performed. In this task, the animal had to remember the previously visited arm to avoid exploration failure. The index for normal working memory was represented in the percentage of successful alternations relative to all possible alternations during a trial session. A full alternation was calculated by a triad of consecutive visits to all arms, with no repeated visit of a previously explored arm. The results are represented in figure 31A.

3. Results

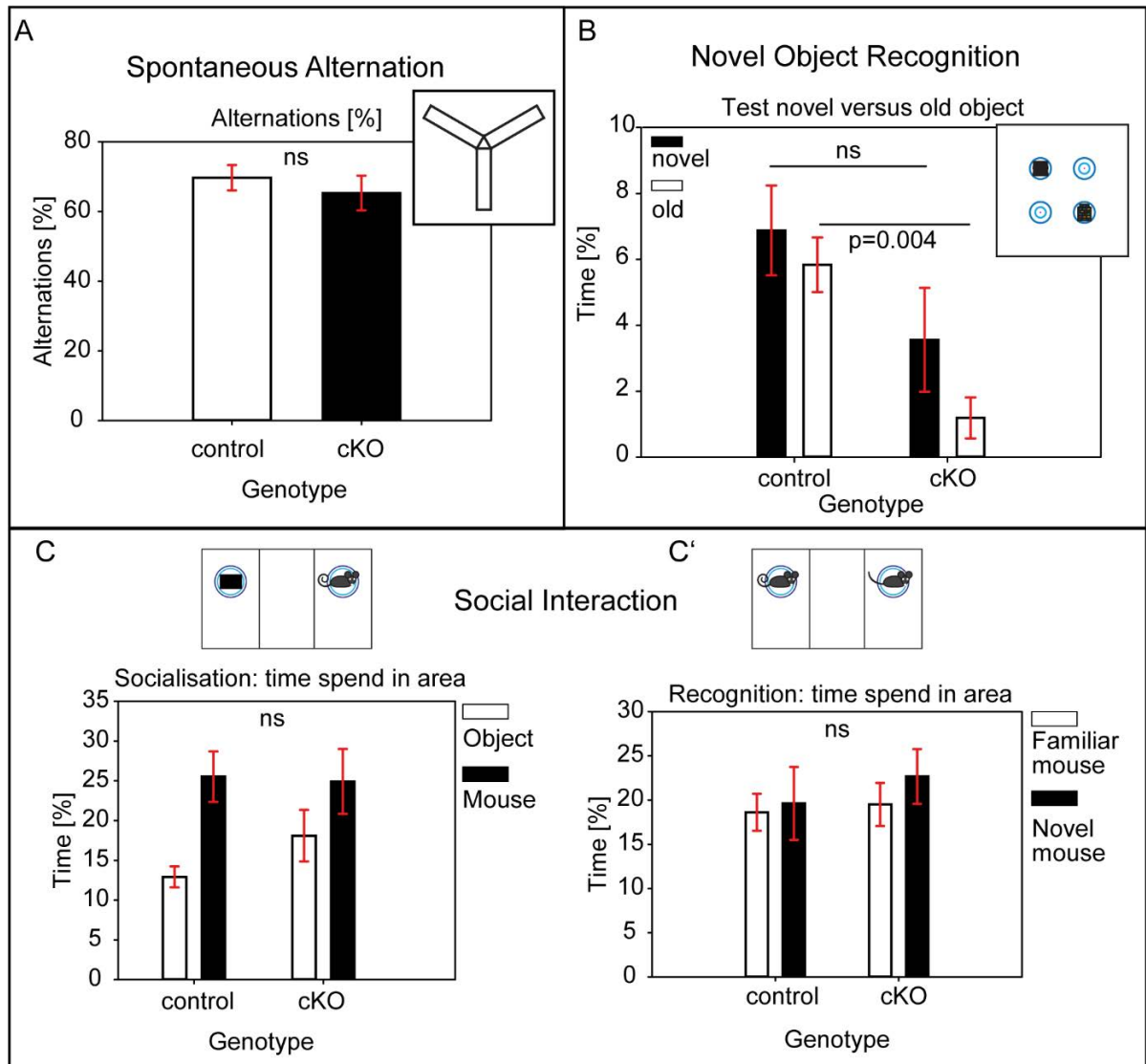


Figure 31: Working memory and social behaviour in the pilot group

A: Y-Maze spontaneous alternation task: working memory was indexed as the percentage of alternations of the maximum alternations possible per trial time. No difference was found between the control and the cKO (two-tailed t-test: $t(10)=-0.71$ $p=0.494$, $N=6$ animals per genotype, $\alpha=0.05$). B: Novel object recognition: as a new object is preferentially examined, the index for working memory is displayed as time spent at the novel object as the percentage of all trial time. There was no difference regarding the preference towards the new object but a significant difference in the time spent at the old object between the genotypes (novel object time: two-tailed t-test: $t(10)=-1.59$ $p=0.142$; old object time: Mann-Whitney-U (MWU): $p=0.004$, $N=6$ animals per genotype, $\alpha=0.05$). Social behaviour was tested with the sociability paradigm and the social novelty paradigm. C: Sociability: The preference for the conspecific was indexed as the time spent in the encounter zone at the conspecific compartment as the percentage of all trial time. The preference for the conspecific was comparable for both genotypes and did not differ between genotypes (time in object zone: two-tailed t-test: $t(10)=1.48$ $p=0.170$; time in encounter zone: two-tailed t-test: $t(10)=-0.12$ $p=0.910$; $N=6$ animals per genotype, $\alpha=0.05$). C': Social novelty: The preference for the unknown (novel) mouse was indexed as the time spent in the encounter zone of the novel mouse as the percentage of all trial time. Both genotypes did not display a clear preference for the novel mouse. There was no significant difference between the control and the cKO (time in encounter zone of familiar mouse: two-tailed t-test: $t(10)=0.28$ $p=0.788$; time in encounter zone of novel mouse: two-tailed t-test: $t(10)=0.59$ $p=0.567$; $N=6$ animals per genotype, $\alpha=0.05$). Values as mean \pm sem.

3. Results

The mean percentage alternation in the control group (69.69 ± 3.66 %) did not differ significantly from cKO mice (65.29 ± 4.99 %) (two-tailed t-test: $t(10) = -0.71$ $p = 0.494$, $N = 6$ animals per genotype, $\alpha = 0.05$). This implied intact working memory in the iIN specific Reelin knockout animals.

The novel object recognition (OR) test is commonly used to assess various aspects of learning and memory, including the capacity to distinguish novel versus familiar objects. Due to the innate preference for novelty in rodents, a novel object should be more interesting to explore compared to previously explored familiar objects. *Reeler* mice showed a higher exploration rate of a novel object (Salinger et al. 2003) in contrast to the HRM, which had less (Ognibene et al. 2007) or equal contact rates (Salinger et al. 2003) compared to controls. The results of the OR task are presented in Fig. 31B, the index for memory and recognition are displayed as the percentage of time spent in contact with the object. As depicted in the graphs, the novel object was visited for longer durations, by both genotypes, than the already familiar, old object: control group: novel object 6.88 ± 1.36 % versus old object: 5.84 ± 0.83 % and iIN specific Reelin knockout (cKO): novel object 3.56 ± 1.57 % versus old object: 1.19 ± 0.62 %. It was clear, that the overall time spent exploring both objects was less in the iIN specific Reelin knockout. Although the time spent exploring the novel object did not differ significantly (two-tailed t-test: $t(10) = -1.59$ $p = 0.142$, $N = 6$ animals per genotype, $\alpha = 0.05$), there was a significant difference from the control mice in the time spent exploring the old object (Mann-Whitney-U (MWU): $p = 0.004$, $N = 6$ animals per genotype, $\alpha = 0.05$). Hence, the cognitive ability to memorise and recognise an object was unimpaired, but there was some significant difference in the time spent to explore the objects between the control and the cKO.

For social behaviour and function, *reeler* mice and the heterozygous *reeler* mice show higher dominance levels in the tube dominance test (Salinger et al. 2003). However, Michetti (Michetti et al. 2014) did not find a difference in the social behaviour of heterozygous male mice when tested for social interaction. The results of the three-chamber sociability and social recognition test (SI) in iIN specific Reelin knockout mice are presented in Fig. 31C and Fig. 31C'. The social preference for a novel conspecific compared with an inanimate object was calculated as the percentage of the time spent in the encounter zone (Fig. 31C). Both genotypes showed a higher preference to interact with a novel conspecific (control: 25.53 ± 3.17 % cKO: 24.93 ± 4.08 %), compared to the time spent exploring the object (control: 12.93 ± 1.32 % cKO: 18.10 ± 3.24 %). The two genotypes, $Reln^{wt/wt}$ Dlx5/6-Cre negative and $Reln^{flx/flx}$ Dlx5/6-Cre positive, did not differ in the time spent at the object (two-tailed t-test:

3. Results

$t(10)=1.48$ $p=0.170$ with $N=6$ animals per genotype and $\alpha=0.05$) or the mouse (two-tailed t-test: $t(10)=-0.12$ $p=0.910$, $N=6$ animals per genotype, $\alpha=0.05$). Therefore, sociability and social approach were comparable for both genotypes. The results from the social recognition phase of the test are presented in figure 31C'. Here, control mice spent a similar amount of time interacting with the familiar mouse and the novel mouse (familiar: $18.62\pm 2.09\%$ novel: $19.62\pm 4.12\%$) without a clear tendency. By contrast, the iIN specific Reelin knockout mice displayed a tendency to spent more time in contact with the novel mouse ($22.67\pm 3.10\%$) than the familiar mouse ($19.51\pm 2.43\%$). Both genotypes did not differ significantly in time spent interacting with the familiar mouse (two-tailed t-test: $t(10)=0.28$ $p=0.788$ with $N=6$ animals per genotype and $\alpha=0.05$) or the novel mouse (two-tailed t-test: $t(10)=0.59$ $p=0.567$, $N=6$ animals per genotype, $\alpha=0.05$). Therefore, the preference for the novel over familiar conspecifics was exhibited by the iIN specific Reelin knockout, indicating normal social recognition. Overall both genotypes did not show any clear preference for either the familiar or the novel mouse. Altogether, the iIN specific Reelin knockout ($\text{Reln}^{\text{flox/flox}}$ Dlx5/6-Cre positive) mice showed normal spontaneous activity, explorative behaviour, and anxiety-like behaviour compared to the control groups.

3.4.2 Behavioural tasks in cohort 1 including all control genotype groups with main focus on hippocampal-dependent spatial learning and memory

Cohort 1 consisted of $\text{Reln}^{\text{wt/wt}}$ Dlx5/6-Cre negative (wt), $\text{Reln}^{\text{wt/wt}}$ Dlx5/6-Cre positive (cre), $\text{Reln}^{\text{flox/flox}}$ Dlx5/6-Cre positive (cKO) and $\text{Reln}^{\text{flox/flox}}$ Dlx5/6-Cre negative (flox) genotypes. After testing for locomotor activity and exploration in the OF, and the anxiety-related behaviour in the EPM (both of which rely on intact hippocampal function (Fanselow and Dong 2010), the focus in this group was to assess hippocampal-dependent spatial learning and memory (Vorhees and Williams 2006; Eichenbaum 2017; Lisman et al. 2017) using the Morris Water Maze task.

3.4.2.1 Anxiety-related behaviour, locomotor activity and exploration behaviour in the cohort 1

These tasks were conducted to compare locomotor activity, exploratory behaviour, and anxiety-related behaviour between the four genotypes. Figure 32A illustrates the results of the EPM task for the $\text{Reln}^{\text{wt/wt}}$ Dlx5/6-Cre negative (wt), $\text{Reln}^{\text{wt/wt}}$ Dlx5/6-Cre positive (cre), $\text{Reln}^{\text{flox/flox}}$ Dlx5/6-Cre positive (cKO) and $\text{Reln}^{\text{flox/flox}}$ Dlx5/6-Cre negative (flox) mice. There was no significant difference between the genotypes for the time spent in the open arms (Kruskal-Wallis $p=0.584$, $N=10$ animals per genotype, $\alpha=0.05$).

3. Results

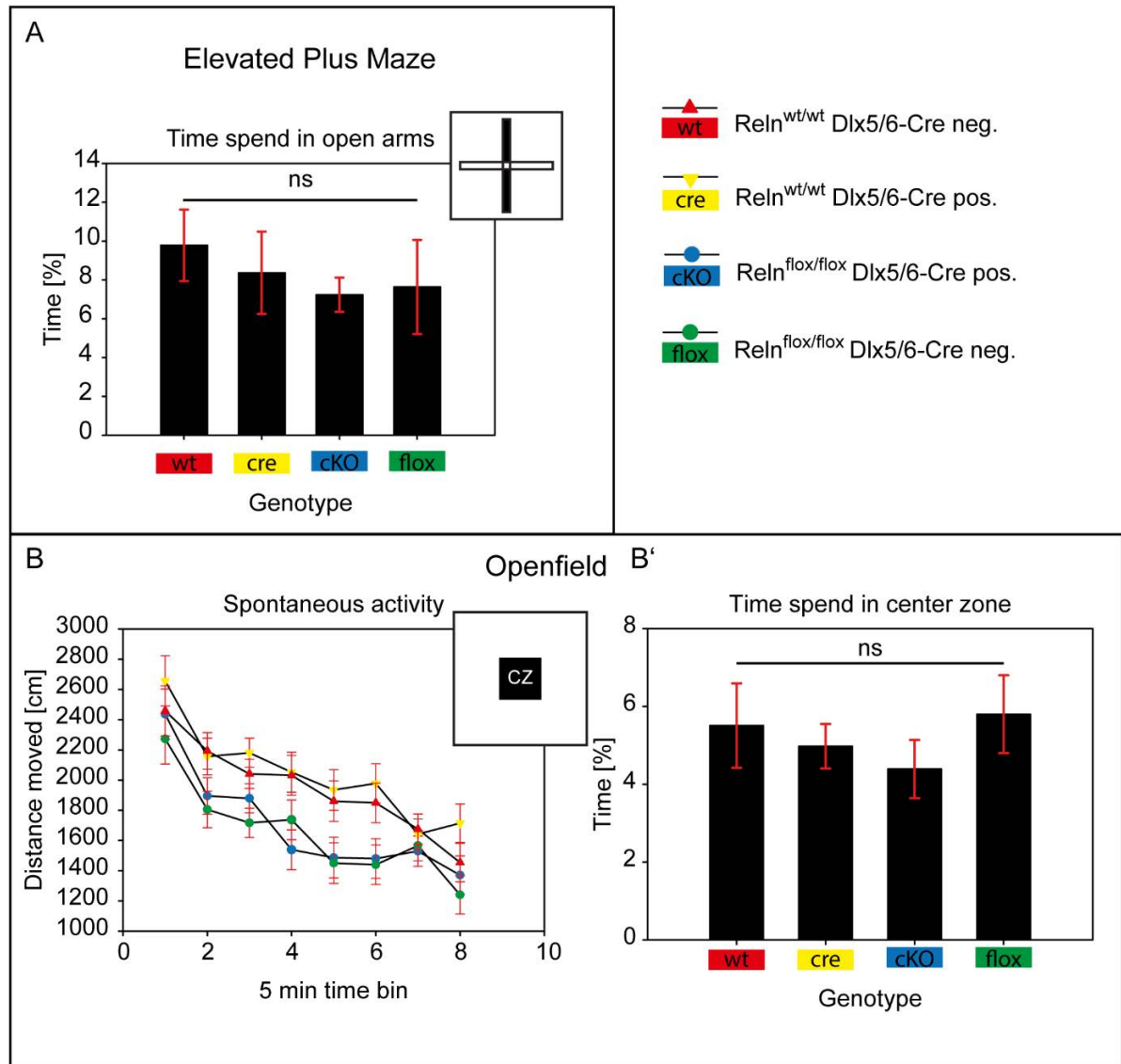


Figure 32: Anxiety-related behaviour, general activity and exploration in cohort 1

Cohort 1 comprised all genetic control groups for the investigation of behavioural changes. The Reln^{wt/wt} Dlx5/6-Cre neg. resembling the wild type (wt, red), the Reln^{wt/wt} Dlx5/6-Cre pos. control with expressed Cre recombinase (cre, yellow), the Reln^{flox/flox} Dlx5/6-Cre neg. control with two loxP sites but no Cre recombinase (flox, green) and the interneuron specific Reelin knockout Reln^{flox/flox} Dlx5/6-Cre pos. (cKO, blue). A: Elevated plus maze results: The percentage of the time spend in the open arms to overall trial time was not significantly different between the four genotypes (Kruskal-Wallis, KW: $p=0.584$, $N=10$ animals per genotype, $\alpha=0.05$). B and B' Open field results: B: Exploration behaviour as a factor of trial time, resulting in a progressing habituation to the environment, was comparable between all genotypes (MD ANOVA time bins: $F(4.87,175.20)=43.98$ Greenhouse-Geisser (GG) correction $p<0.001$, $N=10$ animals per genotype, $\alpha=0.05$). The spontaneous activity indexed as distance travelled within a time bin revealed a genotype effect. Bonferroni post hoc comparison revealed a significant difference between the flox and the cre genotype (MD ANOVA $F(3,36)=4.09$, $p=0.013$, $N=10$ animals per genotype, $\alpha=0.05$; post hoc Bonferroni: flox x cre $p=0.033$; cKO x wt $p=0.424$; cKO x cre $p=0.084$; flox x wt $p=0.191$; wt x cre $p=1.000$). B': Anxiety-related behaviour in the open field: the anxiety-related behaviour indexed as the percentage of time spent in the centre zone from all trial time, displayed no significant difference between the four genotypes (one-way ANOVA $F(3,36)=0.50$ $p=0.684$, $N=10$ animals per genotype, $\alpha=0.05$). Values as mean \pm sem.

3. Results

Although the cKO, with 7.24 ± 0.88 %, and the flox, with 7.64 ± 2.42 %, spent less time in the open arms than the wt, with 9.78 ± 1.84 %, and the cre, with 8.36 ± 2.11 %. In the OF task (Fig. 32B and Fig. 32B'), the locomotor activity patterns were similar for the four genotype groups (Fig. 32B). All groups showed clear habituation to the novel OF arena (MD ANOVA duration of the task as time bins: $F(4.87, 175.20) = 43.98$ Greenhouse-Geisser (GG) correction $p < 0.001$, $N = 10$ animals per genotype, $\alpha = 0.05$). However, the MD ANOVA revealed an effect of genotype ($F(3, 36) = 4.09$, $p = 0.013$, $N = 10$ animals per genotype, $\alpha = 0.05$, and the post hoc test detected a significant difference between the flox and the cre genotype: Bonferroni $p = 0.033$), due to decreased locomotor habituation or exploration in flox and cre genotype groups. All other genotypes did not differ significantly (Bonferroni: cKO x wt $p = 0.424$, cKO x cre $p = 0.084$, flox x wt $p = 0.191$, wt x cre $p = 1.000$). Analysis of anxiety-related behaviour based on the time spent in the centre zone of the OF (Fig. 32B') revealed no significant differences among the four genotype groups (one-way ANOVA $F(3, 36) = 0.50$ $p = 0.684$, $N = 10$ animals per genotype, $\alpha = 0.05$). Comparable to the EP the cKO spent less time in the centre zone 4.39 ± 0.75 % than the other genotypes: flox: 5.80 ± 1.00 %, cre: 4.98 ± 0.57 % and wt: 5.51 ± 1.08 %. Summed up, it could be stated that general behavioural functions in all four genotypes were comparable and not significantly different.

3.4.2.2 Hippocampal-dependent spatial learning and memory in the Morris Water Maze task

The hippocampus is critical for spatial learning and memory (Eichenbaum 2017; Lisman et al. 2017) and one of the most affected brain regions in the *reeler* mouse (Hamburgh 1963). Spatial learning and memory could be addressed with the Morris Water Maze task (MWM) (Morris 1981). *Reeler* mice had not been tested in the MWM task due to their ataxia and impaired mobility, but Krueger (Krueger et al. 2006) reported that heterozygous *reeler* mice show normal performance in this task. The $Reln^{wt/wt}$ *Dlx5/6*-Cre negative (wt) control group was excluded and the more important other two control groups of cre and flox mice were kept for better management during the MWM. Additionally, one mouse had to be euthanized due to health problems, and therefore the control group of the flox mice was diminished by one animal. Reference memory acquisition in the MWM task requires successful navigation to the hidden escape platform, based on extra-maze cues. The results of the acquisition phase are presented in figure 33A. Latency to the hidden platform declines across progressive training days. Successfully acquired spatial learning is represented in the latency (15-20 s) to the escape platform. As depicted in figure 33A, all four genotypes successfully acquired the task after 10 days of training.

3. Results

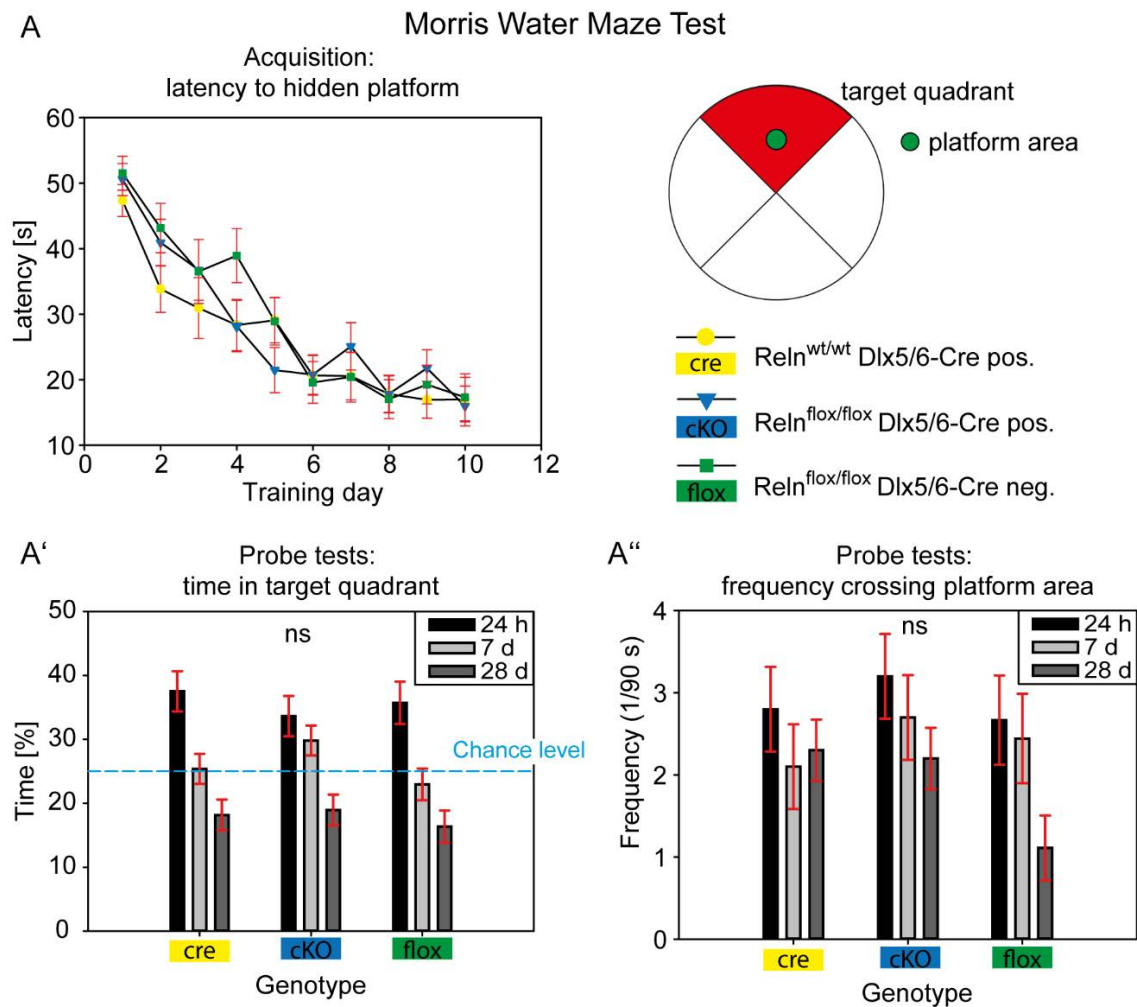


Figure 33: Morris water maze task for hippocampal learning and memory in cohort 1

The Morris water maze (MWM) task was chosen to test hippocampus-dependent spatial learning and memory. In this task, the control genotype wt was excluded and the more important controls kept for better management in the MWM. A: Hippocampal dependent spatial learning: acquisition of platform position as a factor of training day indexed as latency until the platform was found. All four genotypes showed a comparable acquisition of spatial position as factor of training day (mixed design ANOVA training days: $F(9,234)=37.73$ $p<0.001$, $N=9-10$ animals per genotype, $\alpha=0.05$) and showed no effect of genotype (mixed design ANOVA genotype: $F(2,26)=0.62$ $p=0.544$, $N=9-10$ animals per genotype, $\alpha=0.05$). A': Retention of spatial memory and long term memory: probe tests have been performed without in between reinforcement at defined time points (24 hours, 7 days, 28 days). Spatial memory was indexed as percentage time spent in the target quadrant overall trial time above chance level. Long term memory: with increasing time intervals to the last training day, the preference for the target quadrant declines. This effect was equal in all three genotypes (mixed design ANOVA probe day: $F(2.06,53.48)=25.74$ GG $p<0.001$, $N=9-10$ animals per genotype, $\alpha=0.05$). The time spent in the target quadrant was also not different between genotypes (mixed design ANOVA genotype: $F(2,26)=0.66$ $p=0.528$, $N=9-10$ animals per genotype, $\alpha=0.05$). A'': Precision of spatial memory: the precision of acquired spatial memory was indexed as the frequency of crossing the platform area per trial time. The precision declines as effect of trial day (mixed design ANOVA probe trials: $F(3,78)=2.80$ $p=0.045$, $N=9-10$ animals per genotype, $\alpha=0.05$). The precision compared between genotypes did not show any effect of genotype (mixed design ANOVA genotype: $F(2,26)=0.70$ $p=0.505$, $N=9-10$ animals per genotype, $\alpha=0.05$). Values as mean \pm sem.

3. Results

The rate of acquisition across training days was similar for all genotype groups (effect for training day from MD ANOVA $F(9,234)=37.73$ $p<0.001$, $N=9-10$ animals per genotype, $\alpha=0.05$). There were no significant differences amongst the genotypes either (no effect of genotype, based on MD ANOVA $F(2,26)=0.62$ $p=0.544$, $N=9-10$ animals per genotype, $\alpha=0.05$). This indicates, that the learning of the spatial position of the platform was successful for all genotypes. To test the retention of the acquired spatial memory, probe trials had been performed 24 h, 7 d, and 28 d after that last acquisition day, without reinforcement training in between. Two parameters were used to assess memory retention: the proportion of time spent in the target quadrant (Fig. 33A'), and the frequency of crossings at the exact platform area (Fig. 33A''). The percentage of time spent in the target quadrant for the probe trials (Fig. 33A') depicts a clear preference for the target quadrant at probe test one (24 h) for all three genotypes (cre: $37.52\pm 3.15\%$, flox: $35.73\pm 3.32\%$, cKO: $33.64\pm 3.15\%$), which is higher than the chance level (25% indicates random presence in the target quadrant). However, the spatial preference for the target quadrant declined in the longer retention intervals (Fig. 33A'). At the 7 d probe trial the cre group spent $25.38\pm 2.35\%$ of the time in the target quadrant, the flox $22.96\pm 2.47\%$ and the cKO $29.83\pm 2.35\%$. At the 7 d probe trial, while the cre and the flox mouse groups performed at or below the chance level (25%), the cKO still displayed a clear preference for the target quadrant (Fig. 33A'). The probe trial conducted 28 d after acquisition yielded a distinct drop in the time spent in the target quadrant in all three genotypes (cre: $18.17\pm 2.40\%$, flox: $16.35\pm 5.54\%$, cKO: $18.96\pm 2.40\%$), which were below chance levels. This decline was also illustrated by statistics, as effect of time of probe trials (within subjects effect) in the MD ANOVA $F(2.06,53.48)=25.74$ GG $p<0.001$, $N=9-10$ animals per genotype, $\alpha=0.05$. The genotypes, however, did not differ significantly (MD ANOVA between subjects factor genotype: $F(2,26)=0.66$ $p=0.528$, $N=9-10$ animals per genotype, $\alpha=0.05$). The retention of the acquired memory was evident as a clear preference for the target quadrant in the probe trial 24 h later. With the passage of time, the preference for the target quadrant declined in all genotypes. But, the cKO still showed a preference for the target quadrant above chance level in the 7 d probe trial, indicating intact retention and long-term memory. The drop of time spent in the target quadrant at the 28 d probe trial indicated the extinction of memory, as there had been no reinforcement trials. The frequency of platform-area-crossings (Fig. 33A'') indicates the precision of spatial memory. At the 24 h probe trial, the highest frequency of platform-area-crossings was reached by the cKO, with 3.2 ± 0.52 crossings in 90 s trial time, followed by the cre, with 2.8 ± 0.52 crossings per 90 s,

3. Results

and the flox, with 2.67 ± 0.54 crossings. The number of crossings for the cKO and the flox group declined in a similar pattern, like the time spent in the quadrant with increasing timely distance. An exception was the cre group. During the 7 d probe trial, the cKO crossed the platform area 2.7 ± 0.52 times, the flox 2.44 ± 0.54 times, but the cre group dropped to a frequency of 2.1 ± 0.52 times which increased again in the 28 d probe trial to a frequency of 2.3 ± 0.38 times. Concomitant the frequencies of the cKO (2.2 ± 0.38) and the flox (1.11 ± 0.40) dropped clearly. This was statistically supported by the MD ANOVA with slight effect for time of probe trials $F(3,78)=2.80$ $p=0.045$ as within subjects factor, but no effect for genotype as between subjects factor: $F(2,26)=0.70$ $p=0.505$, $N=9-10$ animals per genotype, $\alpha=0.05$. Out of it the precision of the spatial memory drops, except in the cre group, according to the timely distance to the last acquisition training. Altogether, the behavioural tests revealed that inhibitory interneuron specific Reelin knockout ($\text{Reln}^{\text{flox/flox}}$ Dlx5/6-Cre positive) does not alter general behavioural functions or spatial learning and memory.

The next step included a closer look at the morphology at cell levels, Reelin sources, and composition of cell types.

3.5 The Reelin-expressing Cajal-Retzius cells in the $\text{Reln}^{\text{flox/flox}}$ Dlx5/6-Cre mice

Cajal-Retzius (CR) cells were the first appearing Reelin source in the developing brain (D'Arcangelo et al. 1995; Alcántara et al. 1998) and were crucial for layer development in the neocortex (Marín-Padilla 1998; Soriano and Del Río 2005) and hippocampus (Hodge et al. 2013). After the completion of development, the number of CR cells declines dramatically in the layer I of the neocortex (Derer and Derer 1990; Chowdhury et al. 2010), while they remain numerous in the hippocampus (Anstötz et al. 2016).

3.5.1 Quantification of Cajal-Retzius cell numbers in the dentate gyrus of the $\text{Reln}^{\text{flox/flox}}$ Dlx5/6-Cre mice

Previous studies with the natural mutant *reeler* showed quite contradictive results regarding the remaining number of CR cells in the hippocampus. Coulin (Coulin et al. 2001) found higher remaining numbers, while Anstötz (Anstötz et al. 2019) counted lower numbers. Considering these previous studies the number of CR cells was quantified in 12w old iIN specific Reelin knockout ($\text{Reln}^{\text{flox/flox}}$ Dlx5/6-Cre positive) and the control genotype ($\text{Reln}^{\text{wt/wt}}$ Dlx5/6-Cre positive) with immunohistochemical staining against Reelin. Additionally, the animals inherited the reporter allele tdRFP to visualize cells that had undergone Cre dependent DNA recombination.

3. Results

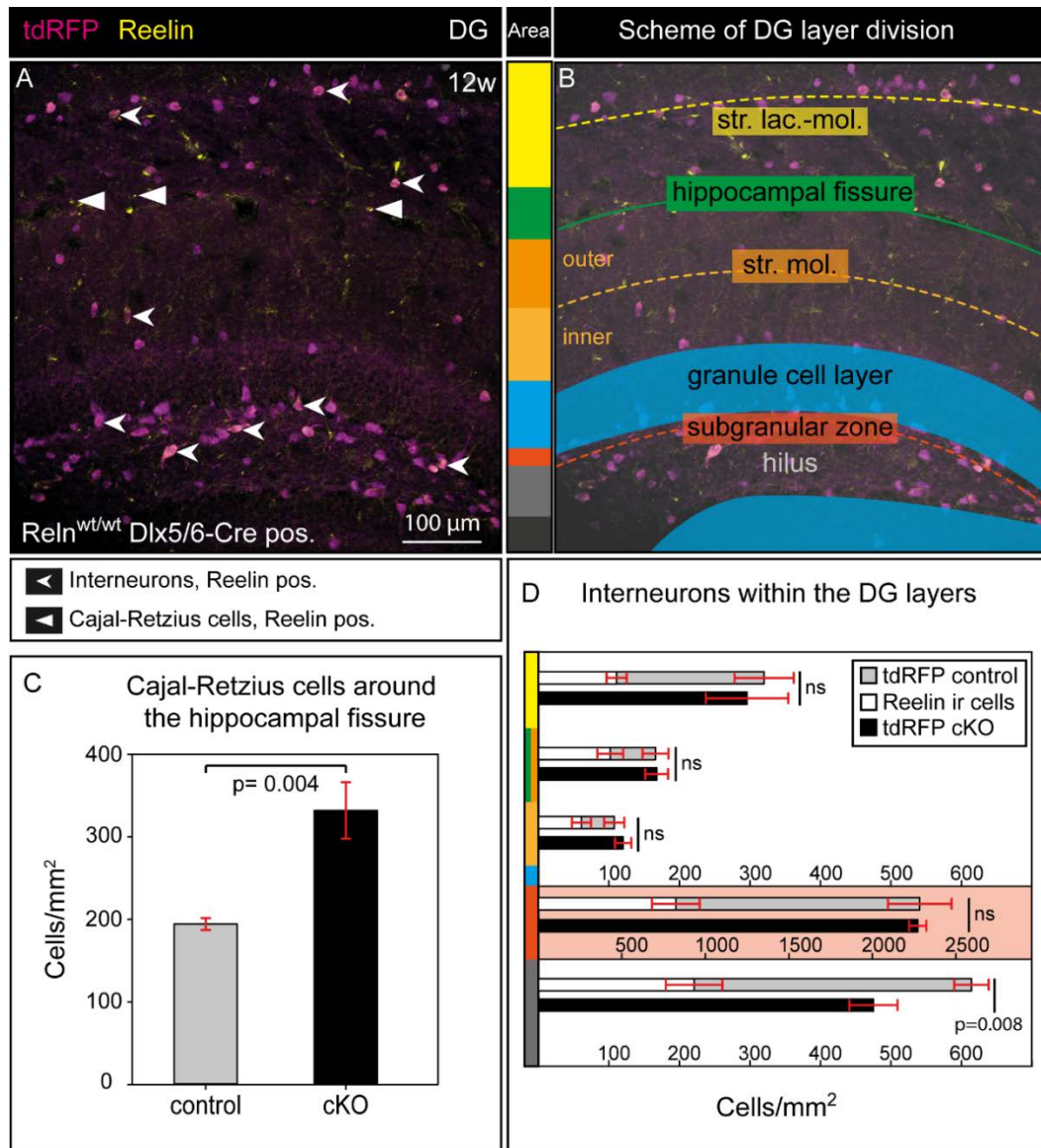


Figure 34: Quantification of Reelin positive Cajal-Retzius cells and inhibitory interneurons in the dentate gyrus

A: The quantification of Reelin-expressing sources in the dentate gyrus, namely Cajal-Retzius cells (CR, arrowheads) and inhibitory interneurons (iIN, dovetailed arrowheads), was performed with tdRFP pos. 12 week old mice, being stained immunohistochemically against Reelin. B: Subdivision of the dentate gyrus according to anatomical layers. C: Quantification of Reelin pos. CR cells for the $Rein^{wt/wt}$ Dlx5/6-Cre pos. (control) and the $Rein^{lox/lox}$ Dlx5/6-Cre pos. (cKO) genotypes, given as mean \pm sem. The counted numbers of Reelin immunoreactive (ir) CR cells per square millimetre of the hippocampal fissure area (green, B) was significantly increased compared to the control situation (two-tailed t-test: $t(8)=3.93$ $p=0.004$, $N=5$ animals per genotype, $\alpha=0.05$). D: The iIN were counted as tdRFP pos., which were either Reelin negative (grey column) or Reelin positive (white column). In $Rein^{lox/lox}$ Dlx5/6 Cre pos. animals all tdRFP positive cells were Reelin negative (black column), as expected. Only in the hilar area (grey, B) the numbers of tdRFP positive cells differed between the genotypes. In this area iIN specific Reelin knockout mice exhibit significantly lower numbers of tdRFP positive interneurons (MWU $p=0.008$, $N=5$ animals per genotype $\alpha=0.05$). The highest density of Reelin-expressing cells was found along the subgranular zone (red, B) followed by the hilar region (grey, B). The highest proportion of interneurons expressing Reelin versus non-expressing interneurons, was found in the outer stratum moleculare (1:1.6) and the inner stratum moleculare (1:1.7).

3. Results

The combination of tdRFP reporter and Reelin staining facilitated the discrimination of Reelin positive iIN and CR cells in the slices (Fig. 34A). The CR cells (arrowheads) along the hippocampal fissure of the dentate gyrus (see Fig. 34B for orientation) presented positive immunoreaction (ir) for Reelin while the iIN (dovetailed arrows) exhibited a double labelling of Reelin and tdRFP. The quantification of Reelin positive CR cells is diagrammed in figure 34C. The cell numbers of CR cells expressing Reelin were quite diverging between the genotypes. In the control 194.48 ± 7.17 cells per mm^2 of the hippocampal fissure towards 331.99 ± 34.29 cells per mm^2 in the iIN specific Reelin knockout (cKO) were counted. This result was highly significant in the two-tailed t-test $t(8)=3.93$ $p=0.004$, $N=5$ animals per genotype, $\alpha=0.05$. The iIN specific Reelin knockout ($\text{Reln}^{\text{flox/flox}}$ Dlx5/6-Cre positive) contained almost double the quantity of CR cells at the hippocampal fissure of the dentate gyrus of the hippocampus at adult age.

3.6 Inhibitory interneurons in the $\text{Reln}^{\text{flox/flox}}$ Dlx5/6-Cre mice

The second important Reelin source in the brain were inhibitory interneurons (iIN). They start to express Reelin in the mouse around postnatal day five and from that point onward remain a Reelin source during the entire mouse life (Alcántara et al. 1998; Pesold, Impagnatiello, et al. 1998).

3.6.1 Layer specific quantification of inhibitory interneurons in the dentate gyri of $\text{Reln}^{\text{flox/flox}}$ Dlx5/6-Cre mice expressing tdRFP

Having found a significant increase in CR cells in the dentate gyrus of the iIN specific Reelin knockout, a quantification of the second main Reelin source had been performed. According to the diverse distribution of iIN within the dentate gyrus (DG), the quantification had been done corresponding to the layers of the DG (Fig. 34B). Mice expressing the tdRFP in iIN at the age of 12 weeks, were immunohistochemically stained against Reelin, and the cell numbers of tdRFP and double labelled cells (tdRFP plus Reelin) quantified. The cell numbers according to the colour-coded layers are presented in figure 34D. The two columns represent the iIN specific Reelin knockout ($\text{Reln}^{\text{flox/flox}}$ Dlx5/6-Cre positive) in black and the grey-white stacked column represents the control ($\text{Reln}^{\text{wt/wt}}$ Dlx5/6-Cre positive). The stacked column in the control illustrates the amount of Reelin-expressing tdRFP positive iIN (white) versus the tdRFP positive cells not expressing Reelin (light grey). In the stratum lacunosum-moleculare (str. lac.-mol., yellow), the control was counted as 320.59 ± 41.90 cells/ mm^2 , thereof 111.38 ± 14.22 cells/ mm^2 Reelin-expressing cells. In the iIN specific Reelin knockout (cKO)

3. Results

296.32±58.46 cells/mm² iIN were counted. This difference was not significant regarding overall cell numbers (MWU p=0.841, N=5 animals per genotype $\alpha=0.05$). 166.57±18.33 cells/mm² with proportionate 102.37±18.32 cells/mm² of Reelin-expressing iIN were counted in the area around the hippocampal fissure (green), including the outer stratum moleculare (str. mol., orange), for the control. This was the highest number of Reelin-expressing interneurons in relation to overall interneuron cell numbers, compared to all other layers. It was followed by the inner stratum moleculare with a ratio of 1:1.6. In the cKO, 168.29±16.12 cells/mm² were counted around the hippocampal fissure. The two-tailed t-test resulted in no significant difference for this area in overall cell numbers (t(8)=0.07 p=0.945, N=5 animals per genotype $\alpha=0.05$). The quantification of the inner stratum moleculare (str. mol., light orange) of the control resulted in overall 107.99±14.27 cells/mm² and 61.46±13.49 cells/mm² interneurons expressing Reelin. For the cKO, 120.77±11.67 cells/mm² interneurons were counted. Even here no significant difference was detected by the two-tailed t-test t(8)=0.69 p=0.508, N=5 animals per genotype, $\alpha=0.05$. Also, in this layer, a high ratio regarding overall cell numbers proportional to Reelin ir cells was found (ratio: 1:1.8). The granule cell layer was inherently free of iIN somata. The next region of the dentate gyrus was the polymorphic layer, here called hilus. This area was subdivided in the subgranular zone (red), a small area the size of 25 μ m below the border of the granule cell layer, and the rest of the hilus (light grey). In the control, the counted numbers of iIN in the subgranular zone were 2,287.06±190.55 cells/mm², thereof 825.50±143.05 cells/mm² Reelin positive cells. In the iIN specific Reelin knockout, 2,275.22±51.57 cells/mm² of interneurons were counted. Both genotypes did not differ in overall cell numbers (two-tailed t-test t(4.58)=-0.06 p=0.955, N=5 animals per genotype $\alpha=0.05$). According to the dentate gyrus layers, no differences in overall interneuron cell numbers between control and iIN specific Reelin knockout were discovered. The counting of the hilar area resulted in a strong significant difference (MWU p=0.008, N=5 animals per genotype $\alpha=0.05$) in cell numbers. For the control 614.65±24.34 cells/mm³ were counted and thereof 221.35±40.16 Reelin-expressing interneurons. In the iIN specific Reelin knockout, 475.59±34.25 cells/mm³ were counted. In summary, regarding the hilar region there was a significant difference in cell numbers of tdRFP expressing inhibitory interneurons, which was not the case for all other layers of the dentate gyrus.

3. Results

3.6.2 Marker specific quantification of inhibitory interneurons in the dentate gyri and neocortices of $\text{Reln}^{\text{flox/flox}}$ Dlx5/6-Cre mice expressing tdRFP

Inhibitory interneurons could be subdivided according to their morphology, their electrophysiological properties, or their expressed marker proteins (Freund and Buzsáki 1996; Danglot et al. 2006; Benarroch 2013; Sultan et al. 2013; Hosp et al. 2014; Mayer et al. 2018). Therefore, a quantification of tdRFP expressing overall inhibitory interneuron numbers was incomplete if not combined with subgroup quantification. Thus, immunohistochemical staining was performed for the most important marker proteins expressed by cortical and hippocampal interneurons. Adult animals (24 w) expressing the tdRFP were used for the staining against Parvalbumin (PV, calcium-binding protein), Vasoactive intestinal polypeptide (VIP), Glutamate decarboxylase isoform 67 (GAD67), Calbindin (CALB, calcium-binding protein), Calretinin (CRET, calcium-binding protein) and cannabinoid receptor 1 (CB1) (Danglot et al. 2006). The staining results of the neocortex (NC) are presented in figure 35. The upper row displays the control ($\text{Reln}^{\text{wt/wt}}$ Dlx5/6-Cre positive) and below, the images of the iIN specific Reelin knockout ($\text{Reln}^{\text{flox/flox}}$ Dlx5/6-Cre positive). With the exception of CB1, all marker proteins could be found in tdRFP expressing cells (dovetail arrows) of the cortices of both, the control (Fig. 35a-e, Fig. 35a'-e', Fig. 35a''-e'') and the iIN specific Reelin knockout (Fig. 35f-j, Fig. 35f'-j', Fig. 35f''-j''). In both cases, CB1 was just stained in the dentate gyrus. The white squares in the images indicate the magnified areas shown below. In both control (Fig. 35a, Fig. 35a' and Fig. 35a'') and iIN specific Reelin knockout (Fig. 35f, Fig. 35f' and Fig. 35f''), Parvalbumin-positive cells were located in the lower layers of the cortex. VIP positive cells could be found adjacent to layer I in the neocortex for controls (Fig. 35b, Fig. 35b' and Fig. 35b''), as well as iIN specific Reelin knockout (Fig. 35g, Fig. 35g' and Fig. 35g''). GAD67 was distributed all over the cortical area in control (Fig. 35c, Fig. 35c' and Fig. 35c'') and iIN specific Reelin knockout (Fig. 35h, Fig. 35h' and Fig. 35h''). CALB positive cells could be found mainly in the upper layers of the neocortex and only a few of them in the lower layers (control: Fig. 35d, Fig. 35d' and Fig. 35d'', iIN specific Reelin knockout: Fig. 35i, Fig. 35i' and Fig. 35i''). CRET could be located in the middle and lower layers of the neocortex (control: Fig. 35e, Fig. 35e' and Fig. 35e'', iIN specific Reelin knockout: Fig. 35j, Fig. 35j' and Fig. 35j'').

3. Results

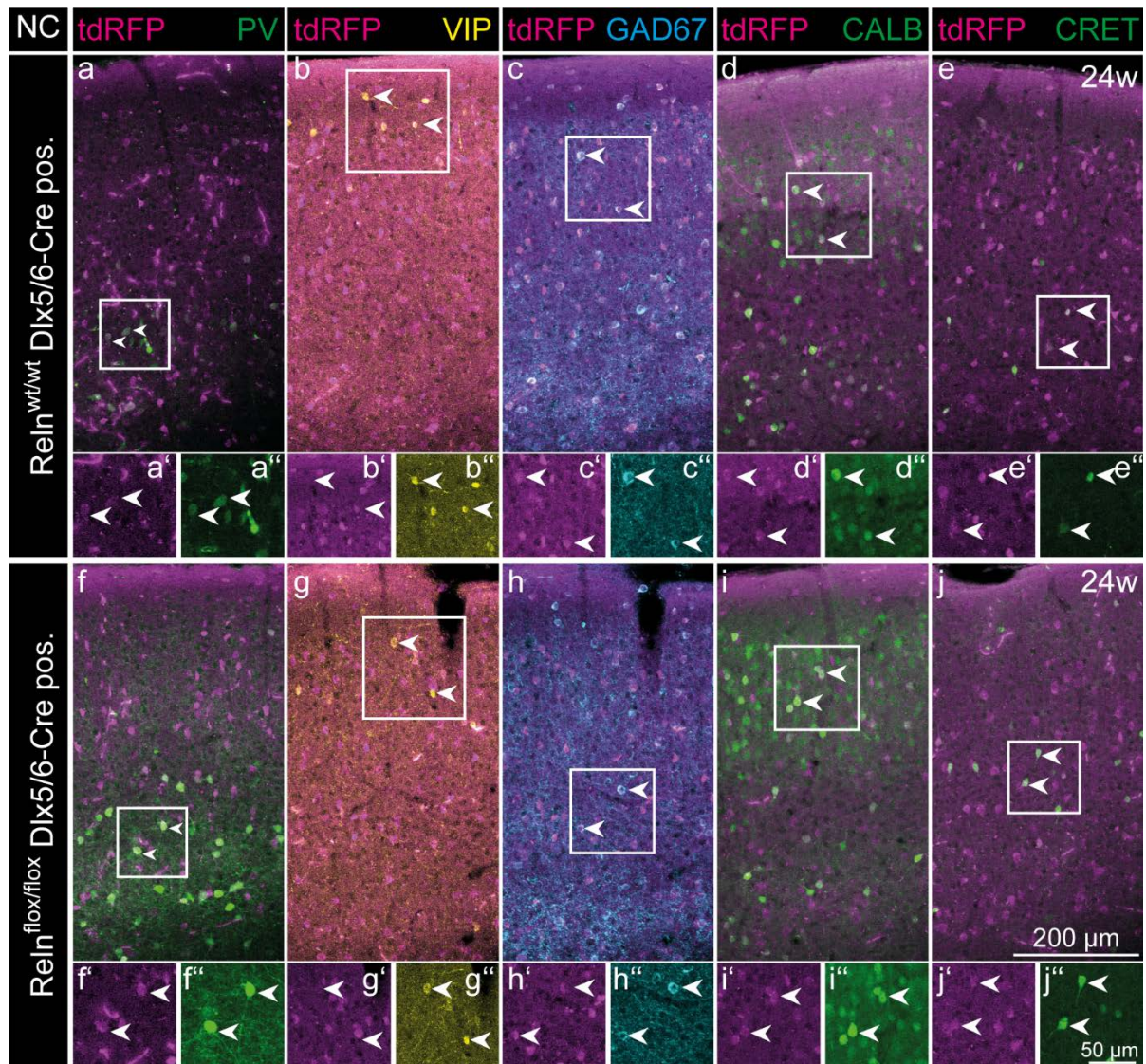


Figure 35: Differentiation of inhibitory interneuron subgroups by reference to their expressed marker proteins in the neocortex

Immunohistochemical stainings for main interneuron marker proteins had been performed in tdRFP positive, 24 week old mice, with $Rein^{wt/wt}$ Dlx5/6-Cre pos. (control) and $Rein^{flox/flox}$ Dlx5/6-Cre pos. (interneuron specific Reelin knockout genotype). The white squares in the big images indicate the magnified area presented below. Dovetailed arrowheads indicate positions of interneurons coexpressing tdRFP and the respective marker protein. Parvalbumin (PV, calcium-binding protein) positive interneurons were found in the lower layers of the neocortex of both genotypes (a, a', a'' and f, f', f''). Vasoactive intestinale polypeptide (VIP, peptide hormone) positive cells were found in both genotypes in the area of layer II (b, b', b'' and g, g', g''). Glutamate decarboxylase isoform 67 (GAD67, enzyme) positive cells were distributed all over the neocortical layers and found in both genotypes in the same pattern (c, c', c'' and h, h', h''). Not all tdRFP expressing cells were found positive for GAD67. Distributed overall neocortical layers, the somata of Calbindin (CALB, calcium-binding protein) ir cells were found in both genotypes (d, d', d'' and i, i', i''). The numbers of Calretinin (CRET, calcium-binding protein) ir cells were sparse and located in the middle of the cortical layers. This staining pattern was found in the control (e, e', e'') and the interneuron specific Reelin knockout (j, j', j'').

3. Results

In summary, in the neocortices all markers were present, and in the same layer location for both control and iIN specific Reelin knockout. The staining results for the dentate gyri (DG) are presented in figure 36. Again, the upper column represents the control, the lower the iIN specific Reelin knockout. The Parvalbumin-positive cells were mainly located in the subgranular and granular area and in rare cases adjacent to the inner stratum moleculare, above the granule cell layer. The dovetail arrows mark the cells magnified in the small images below and the white square indicates the magnified area. Both, control (Fig. 36a, Fig. 36a' and Fig. 36a'') and iIN specific Reelin knockout (Fig. 36f, Fig. 36f' and Fig. 36f''), contained very prominent stained Parvalbumin-positive cells. The same holds true for the GAD67 marked cells. Both genotypes displayed similarly stained cells in the subgranular area and within the stratum moleculare (control: Fig. 36b, Fig. 36b', Fig. 36b'' iIN specific Reelin knockout: Fig. 36g, Fig. 36g', Fig. 36g''). The staining against Calretinin did not just mark cell bodies within the subgranular and hilar region, it also stained an area above the granule cell layer in the adjacent inner stratum moleculare. Cells in the control (Fig. 36c, Fig. 36c', Fig. 36c'') exhibited weaker staining than cells in the iIN specific Reelin knockout (Fig. 36h, Fig. 36h' and Fig. 36h''). Also, the inner stratum moleculare (iML) staining was more intense in the iIN specific Reelin knockout than in the control. This was most obvious in the presented grayscale image of control (Fig. 36d) and iIN specific Reelin knockout (Fig. 36i). In the dentate gyrus, prominent CB1 staining could be found in the inner stratum moleculare (iML) of the iIN specific Reelin knockout (Fig. 36j). The control, however, displayed just very faint staining in this region (Fig. 36e). Cells positive for VIP or CALB, could not be found in the dentate gyri. Summed up, in the dentate gyri of control ($ReIn^{wt/wt}$ Dlx5/6-Cre positive) and iIN specific Reelin knockout mice ($ReIn^{flox/flox}$ Dlx5/6-Cre positive), a similar staining pattern for PV and GAD67 cells could be found. Concerning VIP and CALB immunoreactive cells, none were detected in both genotypes. But the staining against CRET and CB1 differed between the genotypes. According to the presented images, there was more intense staining against CRET and CB1 in the inner stratum moleculare, and cells positive for CRET in the iIN specific Reelin knockout. To support these results, the quantification of cell numbers and an analysis of the intensity of staining with a measured modal intensity were performed. The results are presented in Fig. 37B and Fig. 37C.

3. Results

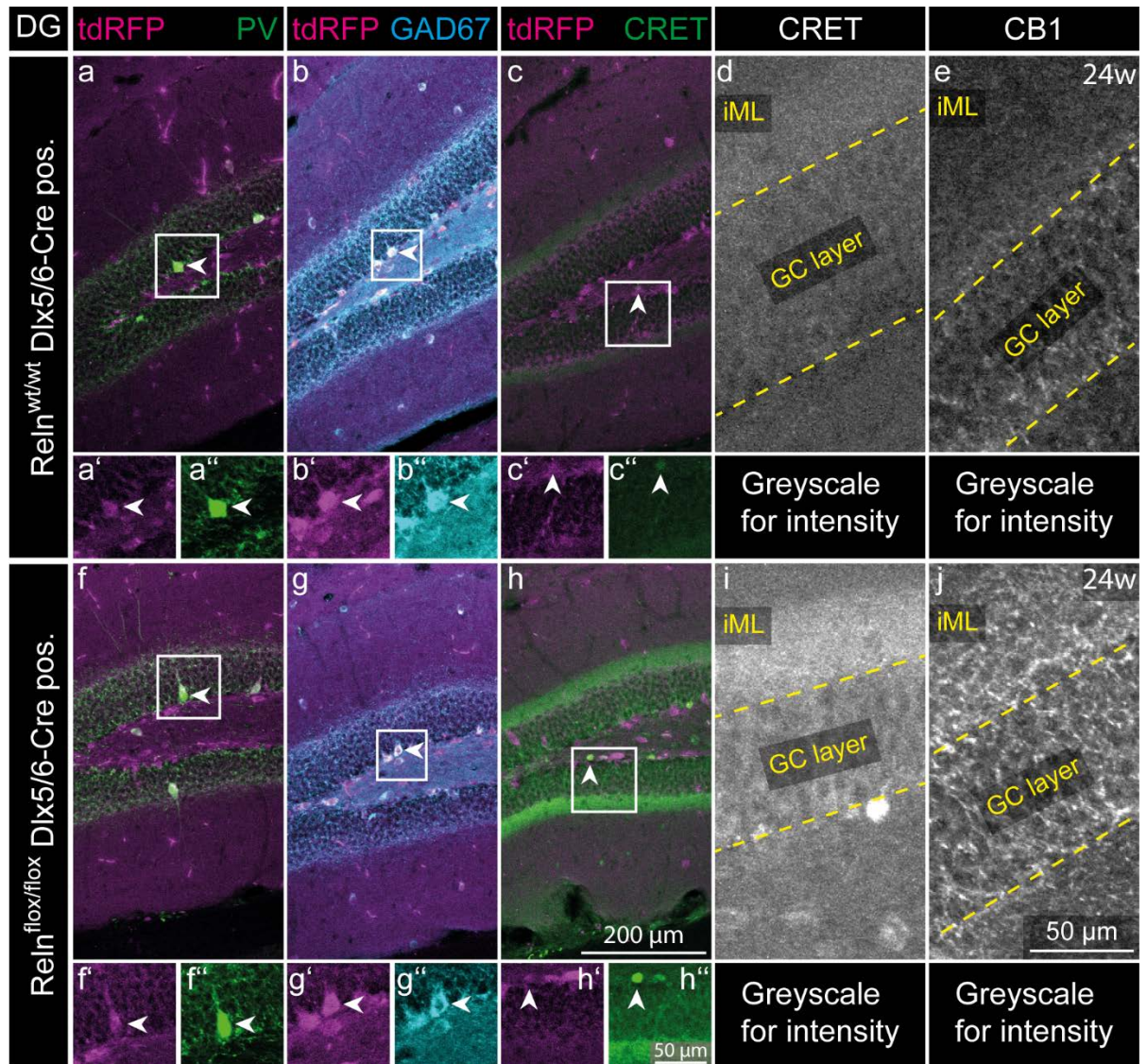


Figure 36: Differentiation of inhibitory interneuron subgroups by reference to their expressed marker proteins in the dentate gyrus

TdRFP positive, 24 week old mice of $Reln^{wt/wt}$ Dlx5/6-Cre pos. (control) and $Reln^{flox/flox}$ Dlx5/6-Cre pos. genotype (interneuron specific Reelin knockout) were stained against main interneuron marker proteins. The white squares indicate the magnified area presented below. Dovetailed arrowheads indicate the position of interneurons coexpressing tdRFP and the respective marker protein. PV positive interneurons were found mainly along the subgranular region and within the granule cell layer (GC layer) in both genotypes (a, a', a'' and f, f', f''). The GAD67 positive cells were distributed all over the dentate gyrus and found in the same pattern in both genotypes (b, b', b'' and g, g', g''). Likewise to the neocortex, not all tdRFP expressing cells were found positive for GAD67. VIP and CALB ir cells were not found in both of the dentate gyri. CRET positive cells were located in the hilus, and showed more intense staining in the interneuron specific Reelin knockout (h, h', h'') than in the control (c, c', c''). Surprisingly, a higher CRET immunoreactive intensity area was present in the inner stratum moleculare (iML) adjacent to the granule cell layer (GC layer, the yellow dotted line represents borders) of the interneuron specific Reelin knockout (i) compared to the control (d). Additional staining against cannabinoid receptor 1 (CB1), in the interneuron specific Reelin knockout, exhibited a higher immunoreactive intensity in the iML, in the same way as the CRET staining (j). This phenomenon was not found in the control (e).

3. Results

The staining intensity found in the inner stratum moleculare of the dentate gyrus for CRET and CB1 were analysed by comparing the modal intensity per μm^2 area. The results are diagrammed in figure 37B. The modal intensity value for CB1 staining was 419.17 ± 36.12 modal intensity/ μm^2 for the control and 587.22 ± 38.09 modal intensity/ μm^2 for the iIN specific Reelin knockout. These values differed significant according to the two-tailed t-test performed ($t(8)=3.20$ $p=0.013$, $N=5$ animals per genotype, $\alpha=0.05$). The impression of higher signal intensity in the immunohistochemically stained image in figure 36j was hereby proven quantitatively for the iIN specific Reelin knockout for CB1 in the inner stratum moleculare. For the same area the CRET staining was analysed with the modal intensity/ μm^2 comparison. For the control a mean of 528.60 ± 41.34 modal intensity/ μm^2 was calculated, and for the iIN specific Reelin knockout a mean of 812.88 ± 53.67 modal intensity/ μm^2 . This difference in modal intensity was highly significant according to the two-tailed t-test performed ($t(8)=4.20$ $p=0.003$, $N=5$ animals/genotype, $\alpha=0.05$). Similar to the expression of the CB1, the expression of the calcium-binding protein Calretinin was significantly increased in the iIN specific Reelin knockout ($\text{ReIn}^{\text{flox/flox}}$ Dlx5/6-Cre positive), in the area of the inner stratum moleculare, an area where afferents of the septum, mossy cell commissures and iIN axons terminate (Leranth and Hajszan 2007).

The quantification for tdRFP and marker proteins was additionally done for the neocortex vertically above the hippocampus. The overall numbers of tdRFP-positive cells in this area amounting to 491.41 ± 21.43 cells/ mm^2 for the control genotype ($\text{ReIn}^{\text{wt/wt}}$ Dlx5/6-Cre positive), and 504.47 ± 34.09 cells/ mm^2 for the iIN specific Reelin knockout ($\text{ReIn}^{\text{flox/flox}}$ Dlx5/6-Cre positive) (Fig. 37A). These results did not differ significantly between genotypes (two-tailed t-test $t(6)=0.32$ $p=0.757$, $N=4$ animals per genotype, $\alpha=0.05$) and indicate comparable cell numbers of tdRFP-positive interneurons in overall numbers in the neocortex. The quantification of the interneuron-specific marker proteins was subdivided. First, all cells positive for the respective marker had been counted in the corresponding area, followed by quantification of all double labelled cells (Fig. 37C). The focus in the dentate gyrus was put on the hilar area, as there had been a significant difference in the analysis presented in figure 34D. The results of the quantification for the hilar area of the dentate gyri and the neocortices are given in figure 37C' and figure 37C''. The following values had been calculated and the resulting p-values were given together with the t-value of the corresponding two-tailed t-test performed to analyse the data (table 12 and table 13):

3. Results

Table 12: Dentate gyrus hilus: Data of the quantification of interneuron markers and tdRFP double labelling, as the mean and standard error of the mean (mean±sem), with statistical values corresponding to Fig. 37C'. Control genotype (control), iIN specific Reelin knockout (cKO), Parvalbumin (PV), double labelling with tandem dimer red fluorescence protein (+tdRFP), Glutamate decarboxylase isoform 67 (GAD67), Calretinin (CRET), t-value with degrees of freedom (t(df)), p-value resulting from two-tailed t-test (p), Mann-Whitney-U test (MWU).

Genotype	control	cKO		
Marker	mean±sem	mean±sem	t(df)	p
PV	85.77±11.04	105.37±17.51	t(8)=0.95	p=0.372
PV+tdRFP	66.72±4.86	83.46±13.48	t(8)=1.17	p=0.276
GAD67	120.37±16.21	93.02±21.4	t(8)=-1.02	p=0.338
GAD67+tdRFP	92.16±16.95	72.82±14.22	t(8)=-0.87	p=0.408
CRET	42.88±14.83	150.33±23.60	t(8)=3.86	p=0.005
CRET+tdRFP	4.63±2.85	20.44±7.13	MWU	p=0.095

Table 13: Neocortex: Data of the quantification of interneuron markers and tdRFP double labelling, as the mean and standard error of the mean (mean±sem), with statistical values corresponding to Fig. 37C''. Control genotype (control), iIN specific Reelin knockout (cKO), Parvalbumin (PV), double labelling with tandem dimer red fluorescence protein (+tdRFP), Vasoactive intestinal polypeptide (VIP), Glutamate decarboxylase isoform 67 (GAD67), Calbindin (CALB), Calretinin (CRET), t-value with degrees of freedom (t(df)), p-value resulting from two-tailed t-test (p).

Genotype	control	cKO		
Marker	mean±sem	mean±sem	t(df)	p
PV	168.65±19.79	178.26±25.34	t(8)=0.30	p=0.773
PV+tdRFP	59.41±8.96	77.27±5.72	t(8)=1.68	p=0.131
VIP	14.28±1.56	18.33±4.31	t(8)=0.88	p=0.403
VIP+tdRFP	1.49±0.66	4.20±1.52	t(8)=1.63	p=0.142
GAD67	114.17±14.01	82.62±21.11	t(8)=-1.25	p=0.248
GAD67+tdRFP	64.36±15.33	49.59±11.36	t(8)=-0.77	p=0.461
CALB	309.44±33.34	283.07±41.56	t(8)=-0.50	p=0.634
CALB+tdRFP	40.71±12.08	45.55±5.04	t(8)=0.37	p=0.721
CRET	47.84±9.18	58.15±6.61	t(8)=0.91	p=0.389
CRET+tdRFP	9.10±3.49	17.95±3.05	t(8)=1.91	p=0.093

The quantification data for interneuron subtypes, analysed according to their expressed markers, elucidated that there was no difference between control and the iIN specific Reelin knockout in the neocortex for the double labelled interneurons or the overall cell number of cells expressing the respective marker protein (Fig. 37C''). This holds also true for the cell numbers counted and analysed in the dentate gyrus hilar area with one exception.

3. Results

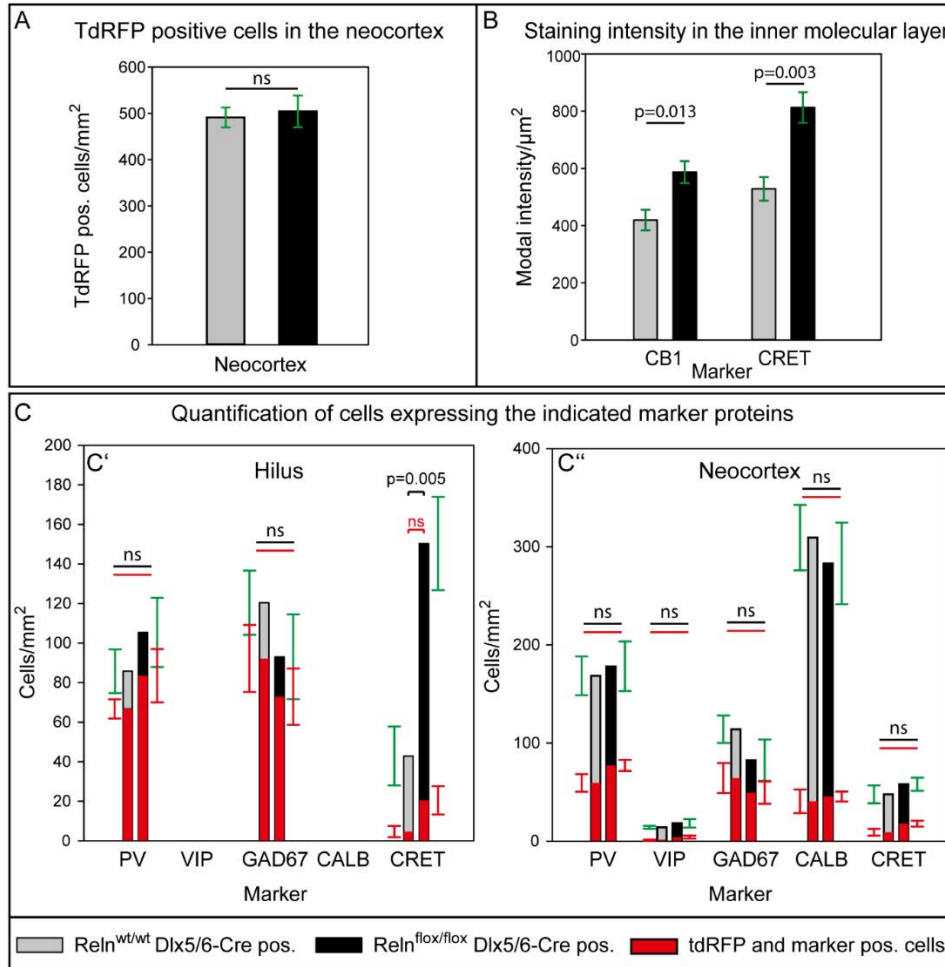


Figure 37: Quantification of inhibitory interneurons by reference to their expressed marker proteins in the neocortex and dentate gyrus

A: Quantification of tdRFP expressing cells along all neocortical layers showed no significant difference for cell numbers per mm² between the control (Reln^{wt/wt} Dlx5/6-Cre pos.) and the interneuron specific Reelin knockout (Reln^{lox/lox} Dlx5/6-Cre pos.) (two-tailed t-test: $t(6)=0.32$, $p=0.757$, $N=4$, $\alpha=0.05$). B: Staining intensity in the inner stratum moleculare for CB1 and CRET were analysed via modal intensity value per μm². The staining intensities for CB1 and CRET resulted in higher modal values in the interneuron specific Reelin knockout than in the control. For the CB1 staining the difference was significant (two-tailed t-test $t(8)=3.20$, $p=0.013$, $N=5$, $\alpha=0.05$), for the CRET staining it was highly significant (two-tailed t-test $t(8)=4.20$, $p=0.003$, $N=5$, $\alpha=0.05$). C: Quantification of cell numbers expressing the marker protein and coexpressing tdRFP in the hilus of the dentate gyrus and the layers of the neocortex ($N=5$, $\alpha=0.05$). C': The cell numbers in the hilar area of the dentate gyrus of PV, GAD67 and of tdRFP coexpressing cells together with PV, GAD67 and CRET, showed similar numbers and no significant difference according to the statistics (two-tailed t-tests: PV: $t(8)=0.95$, $p=0.372$, PV+tdRFP: $t(8)=1.17$, $p=0.276$, GAD67: $t(8)=-1.02$, $p=0.338$, GAD67+tdRFP $t(8)=-0.87$ $p=0.408$; Mann-Whitney-U test: CRET+tdRFP: $p=0.095$). But the numbers of CRET positive cells were higher in the interneuron specific Reelin knockout than in the control and this was a high significant difference (two-tailed t-test: $t(8)=3.86$, $p=0.005$). C'': In the neocortex no difference had been found for the numbers of cells expressing the individual marker proteins nor in the number of cells expressing the marker proteins together with tdRFP (two-tailed t-test: PV: $t(8)=0.30$, $p=0.773$, PV+tdRFP: $t(8)=1.68$, $p=0.131$, VIP: $t(8)=0.88$, $p=0.403$, VIP+tdRFP: $t(8)=1.63$, $p=0.142$, GAD67: $t(8)=-1.25$, $p=0.248$, GAD67+tdRFP: $t(8)=-0.77$, $p=0.461$, CALB: $t(8)=-0.50$, $p=0.634$, CALB+tdRFP: $t(8)=0.37$, $p=0.721$, CRET: $t(8)=0.91$, $p=0.389$, CRET+tdRFP: $t(8)=1.91$, $p=0.093$). Values as mean±sem, N: animals per genotype.

3. Results

The cell number of Calretinin expressing cells, which were not double labelled (no interneurons), differed in a highly significant manner (Fig. 37C'). The iIN specific Reelin knockout ($\text{ReIn}^{\text{flox/flox}}$ Dlx5/6-Cre positive) contained much more Calretinin labelled cells in the hilar area of the dentate gyrus than the control genotype ($\text{ReIn}^{\text{wt/wt}}$ Dlx5/6-Cre positive). The only other cell type known to express Calretinin in this area were mossy cells (Gulyás et al. 1992; Blasco-Ibáñez and Freund 1997; Fujise et al. 1998). Referring to the presented results, it could be stated, that in the iIN specific Reelin knockout higher amounts of Calretinin expressing mossy cells were present in the hilar area, and in the inner stratum moleculare, a higher intensity of Calretinin and cannabinoid receptor 1 immunostaining was detectable.

So far, the effects found, could be due to either, the overall reduction of the secreted Reelin protein in the dentate gyrus, due to the missing expression in iIN, or they may be based on a specific function of Reelin from interneurons. To verify the assumption, that the cell-specific depletion in inhibitory interneurons was responsible for these findings, $\text{ReIn}^{\text{wt/dl}}$ mice were tested. As previously mentioned, the genetic modification of the Cre recombinase in this mouse line was inheritable, resulting in a Reelin depletion of around 50 % from the beginning of expression in both Cajal-Retzius cells and inhibitory interneurons. Thus, regarding overall Reelin expression levels in the hippocampus, these mice resemble iIN specific Reelin knockout mice (Fig. 24), while just the source of Reelin differs between these mouse models.

3.7 The Reelin-expressing Cajal-Retzius cells in the $\text{ReIn}^{\text{wt/dl}}$ mice

For analysis, immunohistochemical staining against Reelin and Calretinin in 24 week old $\text{ReIn}^{\text{wt/wt}}$ as control and $\text{ReIn}^{\text{wt/dl}}$ mice as the 50 % depleted situation was performed. The staining is shown in figure 38A. The dovetailed arrows in the image point at Reelin positive interneurons, while the arrow heads hint at the localization of the Reelin positive Cajal-Retzius cells along the hippocampal fissure.

3. Results

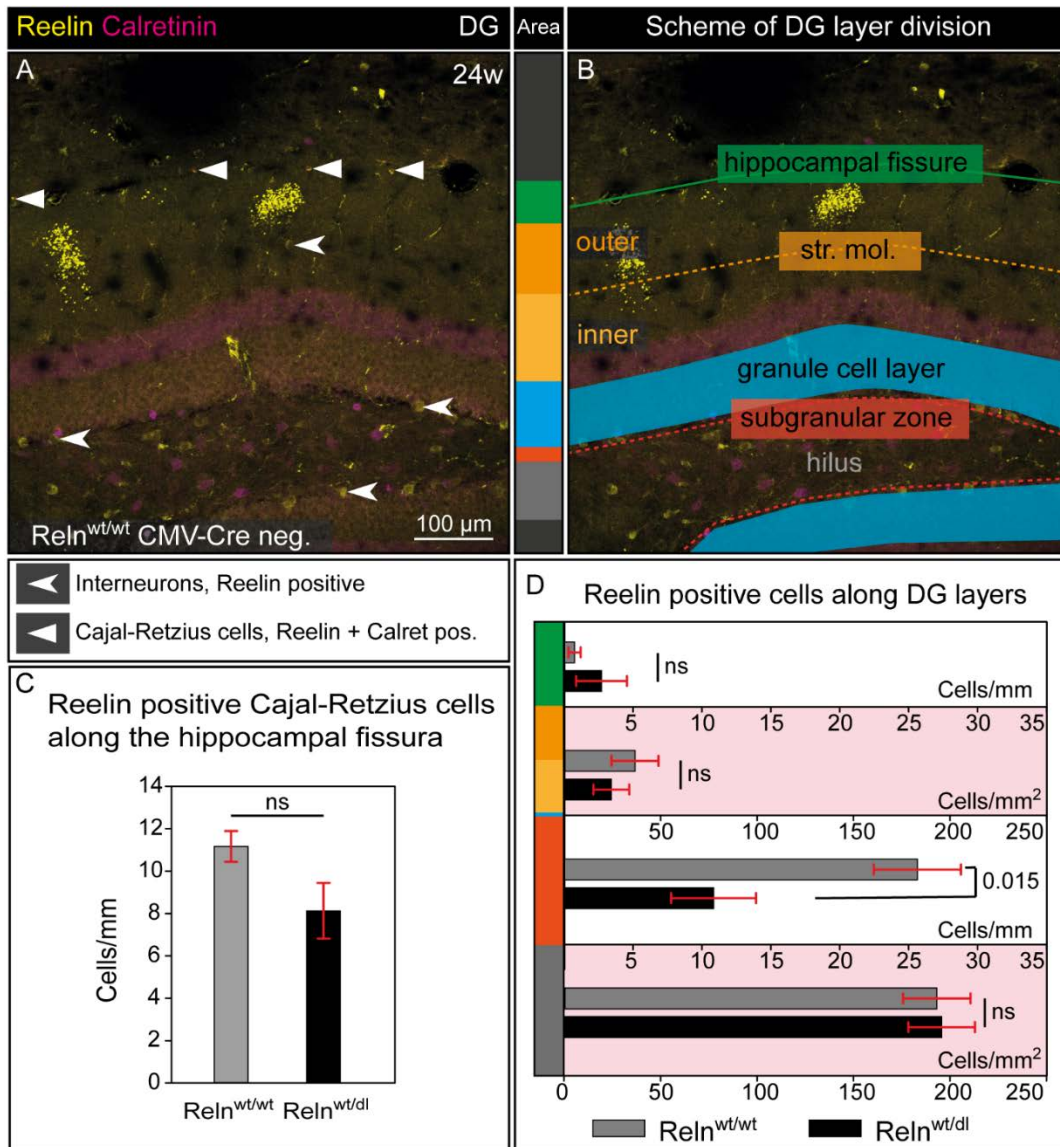


Figure 38: Quantification of Reelin positive Cajal-Retzius cells and inhibitory interneurons in the dentate gyrus of *Rein^{wt/dl}* mice

A: The quantification of the two Reelin-expressing sources Cajal-Retzius cells (CR, arrowheads) and inhibitory interneurons (iIN, dovetailed arrowheads) in the dentate gyrus of *Rein^{wt/dl}* mice, exhibiting 50% reduced total Reelin levels, was performed in 24 week old mice being stained immunohistochemically against Reelin, here with costaining of Calretinin. B: Subdivision of the dentate gyrus according to anatomical layers. C: Quantification of Reelin positive CR cells for the *Rein^{wt/wt}* (control) and the *Rein^{wt/dl}* (heterozygous Reelin knockout) genotypes. The control showed a tendency towards higher numbers of Reelin ir CR cells per mm of the hippocampal fissure (green, B) compared to the *Rein^{wt/dl}* genotype, but this tendency did not reach level of significance (two-tailed t-test: $t(6)=2.02$, $p=0.090$, $N=4$ animals per genotype, $\alpha=0.05$). D: The numbers of iIN ir for Reelin allocated to the different anatomical layers resulted in similar numbers, not reaching level of significance for the hippocampal fissure (green, B, two-tailed t-test: $t(6)=-1.03$, $p=0.342$), the stratum moleculare (light and dark orange, B, two-tailed t-test: $t(6)=0.80$, $p=0.453$) and the hilar area (grey, B, two-tailed t-test: $t(6)=-0.10$, $p=0.921$). Nevertheless, *Rein^{wt/dl}* animals showed a tendency towards more Reelin-expressing cells along the hippocampal fissure and less Reelin-expressing cells in the stratum moleculare. A significant difference was calculated for the numbers of iIN ir for Reelin in the subgranular zone (red, B), which were less in the *Rein^{wt/dl}* genotype (two-tailed t-test: $t(6)=3.35$, $p=0.015$). $N=4$ animals per genotype, $\alpha=0.05$. Values given as mean \pm sem.

3. Results

3.7.1 Quantification of Cajal-Retzius cell numbers in the dentate gyrus of the $Reln^{wt/dl}$ mice

The quantification of Reelin positive Cajal-Retzius cells was done along the hippocampal fissure alone and resulted in a mean of 11.17 ± 0.73 cells per mm hippocampal fissure for the $Reln^{wt/wt}$ and a mean of 8.13 ± 1.32 cells per mm for the $Reln^{wt/dl}$ (Fig. 38C). According to the two-tailed t-test, no significant difference was found between the two means ($t(6)=2.02$, $p=0.090$, $N=4$ animals per genotype, $\alpha=0.05$). On the contrary, the amount of CR cells along the hippocampal fissure of the $Reln^{wt/dl}$, showed a tendency to be less in numbers, while in the iIN specific Reelin knockout significantly more CR cells were counted, compared to the control genotype. This was a reversed result.

3.8 The Reelin-expressing cells in the dentate gyri of $Reln^{wt/dl}$ mice

As previously mentioned, Reelin-expressing inhibitory interneurons were found to be distributed along the different layers of the dentate gyrus. To analyse the distribution and the cell numbers of Reelin-expressing cells, as done in the iIN specific Reelin knockout, the immunohistochemical staining against Reelin and Calretinin in 24 week old $Reln^{wt/dl}$ and $Reln^{wt/wt}$ mice was quantified. The dentate gyri were subdivided as illustrated in figure 38B into the hippocampal fissure, the whole stratum moleculare (no differentiation between outer and inner layer), the subgranular zone adjacent to the granule cell layer and the hilar area. The layers were colour coded for better recognition. Since the $Reln^{wt/dl}$ and $Reln^{wt/wt}$ were not bred with the tdRFP reporter line, there was no tdRFP present in the cell bodies to differentiate between iIN and other cells. Thus, in this experiment, CR cells could only be discriminated by morphological criteria as small cells along the hippocampal fissure.

3.8.1 Layer specific quantification of Reelin-expressing cells in the dentate gyri of $Reln^{wt/dl}$ mice

The results of the layer-specific quantification of Reelin-expressing cells are depicted in figure 38D. Along the hippocampal fissure, the control cell count was 0.76 ± 0.44 cells/mm and the $Reln^{wt/dl}$ 2.72 ± 1.84 cells/mm (green area). Despite the different numbers, the two-tailed t-test revealed no significant difference between the two genotypes ($t(6)=-1.03$, $p=0.342$, $N=4$, $\alpha=0.05$). In the stratum moleculare, the control cell count was 36.53 ± 12.15 cells/mm² and the $Reln^{wt/dl}$ 24.24 ± 9.30 cells/mm². Similarly to the hippocampal fissure values, no significant difference between $Reln^{wt/wt}$ and $Reln^{wt/dl}$ was calculated by the two-tailed t-test ($t(6)=0.80$, $p=0.453$, $N=4$, $\alpha=0.05$). Along the subgranular zone the counted

3. Results

numbers of Reelin-expressing cells for the control were 25.63 ± 3.15 cells/mm and for the $\text{Reln}^{\text{wt/dl}}$ 10.85 ± 3.08 cells/mm². These values showed significant difference in the two-tailed t-test ($t(6)=3.35$, $p=0.015$, $N=4$, $\alpha=0.05$). In the hilar region, 192.91 ± 17.45 cells/mm² Reelin-expressing cells were counted for the control genotype and 195.44 ± 17.23 cells/mm² Reelin-expressing cells for the $\text{Reln}^{\text{wt/dl}}$ genotype. As these values indicate, no significant difference was calculated for the cell numbers of Reelin-expressing cells (two-tailed t-test: $t(6)=-0.10$, $p=0.921$, $N=4$, $\alpha=0.05$). According to the quantification, there were comparable numbers of Reelin-expressing cells found in most areas of the dentate gyri of the $\text{Reln}^{\text{wt/wt}}$ and $\text{Reln}^{\text{wt/dl}}$ mice. Only along the subgranular zone, significantly fewer cell numbers were counted in the $\text{Reln}^{\text{wt/dl}}$ genotype, compared to the control. Along the hippocampal fissure, there was a tendency to higher cell numbers in the $\text{Reln}^{\text{wt/dl}}$ genotype, but this result did not reach the level of significance.

Compared to the iIN specific Reelin knockout, the $\text{Reln}^{\text{wt/dl}}$ genotype, mimicking the heterozygous *reeler* mouse, had fewer CR cells along the hippocampal fissure (albeit not significantly different to the control). A significant difference was found along the subgranular zone with less Reelin-expressing cells, considering the numbers of Reelin-expressing cells along the dentate gyrus' layers. Although a tendency to higher numbers of Reelin-expressing cells was found along the hippocampal fissure, all other areas were comparable to the control genotype.

3.8.2 Cannabinoid receptor 1 and Calretinin quantification in the stratum moleculare and hilus of the dentate gyri of $\text{Reln}^{\text{wt/dl}}$ mice

To examine, if the $\text{Reln}^{\text{wt/dl}}$ mice show a similar intense staining pattern in the inner stratum moleculare for cannabinoid receptor 1 (CB1) and Calretinin (CRET) and also a higher number of Calretinin expressing cells in the hilar area, as the iIN specific Reelin knockout, the corresponding immunohistochemical stainings were quantified. Animals at the age of 24 weeks were used for this experiment. The staining examples are shown in figure 39 as greyscale images for the $\text{Reln}^{\text{wt/wt}}$ (left) and $\text{Reln}^{\text{wt/dl}}$ (right). The quantification of CB1 staining is presented in figure 39A as image and a graph illustrating the results.

3. Results

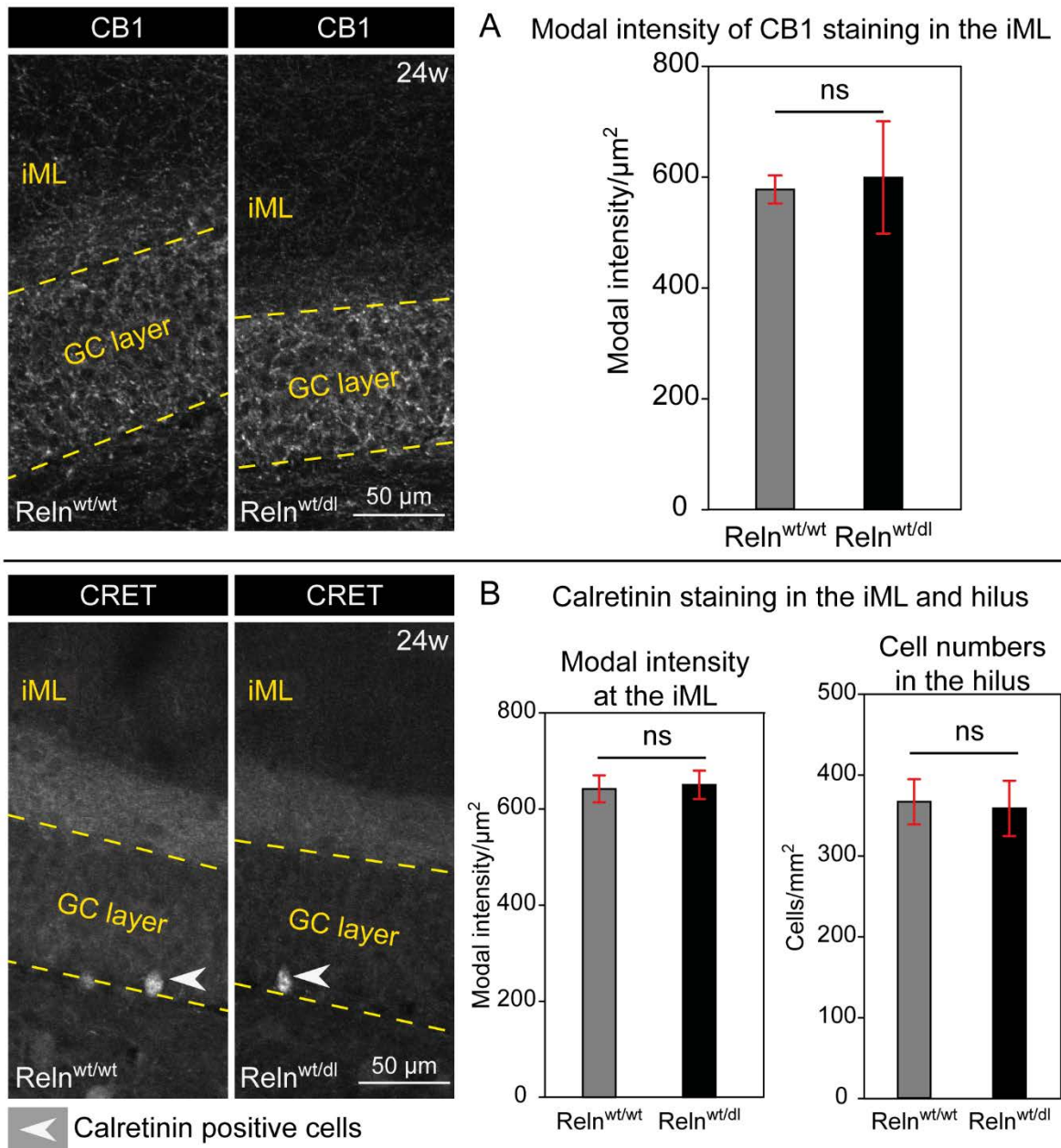


Figure 39: Intensity analysis of cannabinoid receptor 1 and calretinin staining in the inner molecular layer and quantification of calretinin positive cells in the hilus of the dentate gyrus in Reln^{wt/dl} mice

Analysis of modal staining intensity in the inner stratum moleculare (iML), adjacent to the granule cell layer (GC layer) for cannabinoid receptor 1 (CB1, A), and for calretinin (CRET, B). Done for the Reln^{wt/wt} (control) and the Reln^{wt/dl} (heterozygous) genotype in 24 week old mice, presented as a greyscale image. A: The modal intensity of CB1 staining resulted in comparable values for both genotypes, that did not differ significantly (two-tailed t-test: $t(3.374)=0.21$, $p=0.849$, $N=4$, $\alpha=0.05$). B: The calretinin modal intensity (graph left) did not differ significantly between the two genotypes (two-tailed t-test: $t(6)=-0.21$, $p=0.844$) and the cell numbers of calretinin ir cells in the hilar area (graph right) were comparably similar (two-tailed t-test: $t(6)=0.19$, $p=0.859$). $N=4$ animals per genotype, $\alpha=0.05$. Values given as mean \pm sem.

3. Results

The modal intensity analysis resulted in a mean of 577.92 ± 25.34 modal intensity/ μm^2 for the control and 599.42 ± 101.31 modal intensity/ μm^2 for the $\text{ReIn}^{\text{wt/dl}}$ genotype. The two-tailed t-test gave no significant difference for these values ($t(3.374)=0.21$, $p=0.849$, $N=4$, $\alpha=0.05$). Thus, there was no higher intensity of CB1 staining in the inner stratum moleculare for the $\text{ReIn}^{\text{wt/dl}}$ genotype.

Concerning the Calretinin staining in figure 39B, the greyscale image hint also at a similar staining intensity for the inner molecular layer. The cell bodies of Calretinin-positive cells in the hilar area were marked with dovetailed arrows. The modal intensity analysis revealed a mean of 643.17 ± 27.98 modal intensity/ μm^2 for the control, and a mean of 651.50 ± 29.43 modal intensity/ μm^2 for the $\text{ReIn}^{\text{wt/dl}}$ genotype. As indicated by the greyscale image, the two-tailed t-test resulted in no significant difference between the two staining intensities ($t(6)=-0.21$, $p=0.844$, $N=4$, $\alpha=0.05$). The cell count of Calretinin positive cell bodies in the hilus of the dentate gyrus (Fig. 39B right graph) resulted likewise in no significant difference in statistical analysis (two-tailed t-test: $t(6)=0.19$, $p=0.859$, $N=4$, $\alpha=0.05$). A mean of 367.04 ± 27.87 cells/ mm^2 in the hilus was counted for the control and 358.88 ± 34.22 cells/ mm^2 for the $\text{ReIn}^{\text{wt/dl}}$ genotype. Hence, no difference according to the staining intensity of CB1 or CRET and cell count of CRET positive cell bodies in the hilus of the dentate gyrus was found in the $\text{ReIn}^{\text{wt/dl}}$ mice.

The results of higher cell numbers of CR cells along the hippocampal fissure, a higher staining intensity for CB1 and CRET in the inner molecular layer, and higher cell numbers of CRET expressing cells in the hilar area, could not be observed in the $\text{ReIn}^{\text{wt/dl}}$ mice. Thus, all these effects could be clearly ascribed to the cell-specific depletion of Reelin in inhibitory interneurons, and were not due to an overall depletion of Reelin of 50 %, as in the $\text{ReIn}^{\text{wt/dl}}$ mice.

3.9 Adult neurogenesis and stem cell niche structure in the dentate gyrus of $\text{ReIn}^{\text{flox/flox}}$ Dlx5/6-Cre mice

The hilar region of the dentate gyrus is, besides the subventricular zone, an important area for adult neurogenesis (Altman and Das 1965). Adjacent to the granule cell layer in the subgranular zone, stem cell niches were located (Seri et al. 2004; Nicola et al. 2015). There, new granule cells and astrocytes were produced by the division of progenitor cells of glial nature (Seri et al. 2001), the radial glia-like cells (RGLCs). In the *reeler* mouse, Zhao (Zhao et al. 2007) reported diminished adult neurogenesis. Pujadas and Teixeira (Pujadas et al.

3. Results

2010; Teixeira et al. 2012) showed an impairment of adult neurogenesis in conditional *Dab1* knockout mice, in which the canonical Reelin pathway is affected. According to these previous results, an investigation of the hippocampal stem cell niche composition, quantification of neurogenesis and analysis of morphological properties of RGLCs and maturing granule cells were performed.

3.9.1 Composition of the hippocampal stem cell niche in the subgranular zone of *Reln^{flox/flox} Dlx5/6-Cre* mice

The hippocampal stem cell niche was composed of special cell types such as Nestin (intermediate filament protein (Chang and Goldman 2004)) positive RGLCs, young neurons in different maturation stages (D1-D2 or 2a-2b, (Fuentelba et al. 2012; Nicola et al. 2015)) and inhibitory interneurons (Seri et al. 2004; Fuentelba et al. 2012; Nicola et al. 2015). Figure 40 displays immunohistochemical staining against Nestin, Ki-67 (a proliferation marker protein associated with the chromosomes (Cuylen et al. 2016)) and Doublecortin (DCX) (a microtubule-associated protein, expressed in young neurons during maturation (Brown et al. 2003)) of 24 week old dentate gyri. The control genotype *Reln^{wt/flox} Dlx5/6-Cre* negative (Fig. 40A) showed Nestin-positive processes terminating above Ki-67-positive somata or beside them, which were surrounded by DCX positive cell somata grouping in three or four together. The same pattern could be seen in the second control genotype of *Reln^{flox/flox} Dlx5/6-Cre* negative (Fig. 40B), and the iIN specific Reelin knockout *Reln^{flox/flox} Dlx5/6-Cre* positive (Fig. 40D). The Nestin-positive processes start branching within the upper granule cell layer, or in the inner stratum moleculare, where they exhibit profound contacts to blood vessels (Fig. 40D). In contrast, in the *reeler* dentate gyrus the different cell types were distributed all over the area, and not arranged in a special order (Fig. 40C). Additionally, no long and straight formed Nestin processes emerged from the cells, instead, they were short and meandering, compared to the cells in the other genotypes. So, the basic arrangement of the cells belonging to the subgranular stem cell niche of the dentate gyrus was comparable between control genotypes and the iIN specific Reelin knockout. In the *reeler* mouse, no proper composition or arrangement of cells within a stem cell niche was found across the dentate gyrus.

3. Results

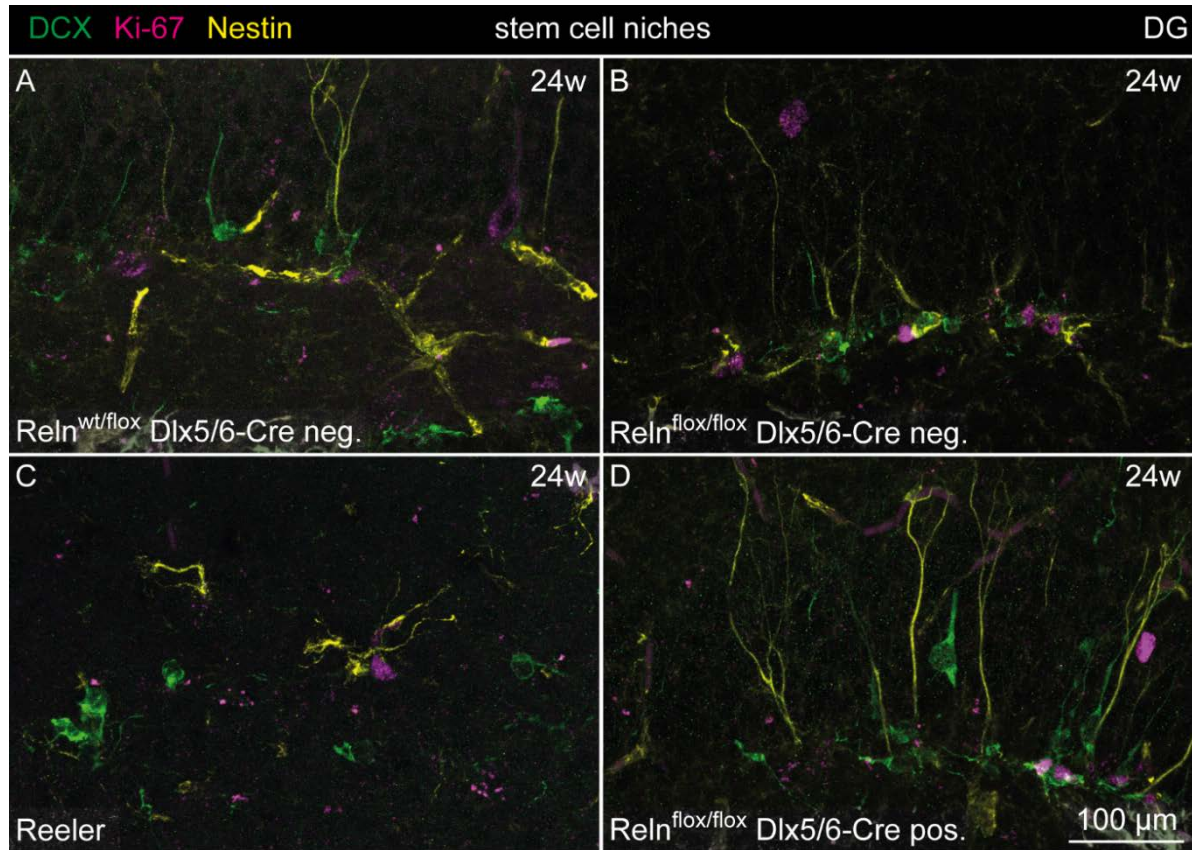


Figure 40: Stem cell niche composition and organisation in the subgranular zone of the dentate gyrus

The stem cell niche composition and organisation along the subgranular zone of the dentate gyrus was illustrated with immunohistochemical triple stainings against Doublecortin (DCX, a marker for young neurons), Ki-67 (a marker for proliferating cells) and Nestin (a filament marker for radial glial-like cells) in 24 week old $ReIn^{wt/flox}$ $Dlx5/6-Cre$ neg. (control, A), $ReIn^{flox/flox}$ $Dlx5/6-Cre$ neg. (control with just loxP sites, B), $ReIn^{flox/flox}$ $Dlx5/6-Cre$ pos. (interneuron specific Reelin knockout, D), and *reeler* (C) mice. The stem cell niche was composed of a stem cell (radial glial-like cell) with a prominent Nestin-positive process, reaching through the whole granule cell layer, sometimes enwrapping a blood vessel (A, B, D). Besides the radial glial-like cell in close proximity, Ki-67-positive, proliferating cells were found and around them young granule cells, immunoreactive for Doublecortin (A, B, D). This composition was not present in the *reeler* mice (C). Here the different cell types were loosely scattered along the whole area.

To determine the exact positioning of Reelin-expressing iIN within the stem cell niche, a reporter mouse line expressing a green fluorescent protein (eGFP) under the control of the proopiomelanocortin (POMC) promotor (in the dentate gyrus exclusively expressed in immature granule cells (Overstreet et al. 2004)), was bred with the $ReIn^{flox/flox}$ $Dlx5/6-Cre$ mice. Subsequently, brain slices of adult mice (24 w) had been immunohistochemically stained against Reelin and glial fibrillary acidic protein (GFAP), to localise Reelin positive cells in relation to radial glia-like cells (GFAP) and immature neurons (POMCeGFP) (Fig. 41A). This staining revealed a close grouping of cells being either Reelin ir or POMCeGFP positive. The white square indicates the magnification of figure 41A'. Within the

3. Results

magnification, it could be seen that the cells were not just grouping together, they also had close contact along their somata. The Reelin ir cell was centred, and surrounded by POMCeGFP-positive young granule cells. The GFAP staining did not display such a clear correlation between Reelin-expressing cells and the GFAP positive processes of radial glia-like cells, although there were some contacts detectable. Having found an interneuron expressing Reelin amidst young granule cells, the next step had been to identify the interneuron subtype. The iIN, with their soma located in the subgranular region, adjacent to the granule cell layer, could be addressed as either basket cells (BC), or hilar commissural-associational pathway related cells (HICAP) (Han et al. 1993; Freund and Buzsáki 1996; Houser 2007). Both cell types could be differentiated by the proteins they expressed. The BC were prominent Parvalbumin (PV) ir while the HICAP cells expressed Cholecystokinin (CCK, a peptide hormone) (Morozov and Freund 2003; Danglot et al. 2006). Figure 41B and figure 41C illustrate two different immunohistochemical stainings against PV, CCK, and Reelin, one with (Fig. 41B), the other without antigen retrieval (Fig. 41C). The white squares indicate the corresponding area to the magnifications in figure 41B' and figure 41C'. The Reelin signal could be localised in the CCK ir cells, but not in PV-positive cells (Fig. 41B', Fig. 41C'). This result demonstrates, that the HICAP cells in the subventricular zone of the dentate gyrus were the Reelin-expressing cells, which are located in close proximity to young granule cells. The results from figures 41A, 41B and 41C, taken together with the information received by the staining in figure 40, and completed by data from Seri, Fuentealba and Nicola (Seri et al. 2004; Fuentealba et al. 2012; Nicola et al. 2015), it was possible to reconstruct a 3D model out of the 2D scheme (transfer from 2D to 3D by Alf Neu) of the stem cell niche within the dentate gyrus (Fig. 41D). The composition of the stem cell niche always showed the same pattern. The centred radial glia-like cells reached out with their process through the whole granule cell layer into the inner stratum moleculare, where they often contacted blood vessels. Besides the radial glia-like cells, young proliferating neurons were located, often grouped in pairs of three to four. Close to the young neurons, even contacting their cell somata, the CCK positive HICAP cells were located. This cell type had been found regularly distributed all over the subgranular area. The PV-positive BC were also found regularly distributed along the subgranular area, but sometimes in proximity, sometimes more distant to the stem cell niche. So, it could be stated, that the stem cell niche in the dentate gyrus subgranular area was mainly composed of one centred radial glia-like cell, surrounded by young proliferating neurons (Type 2a/2b or D1/D2) and a Reelin-expressing HICAP cell.

3. Results

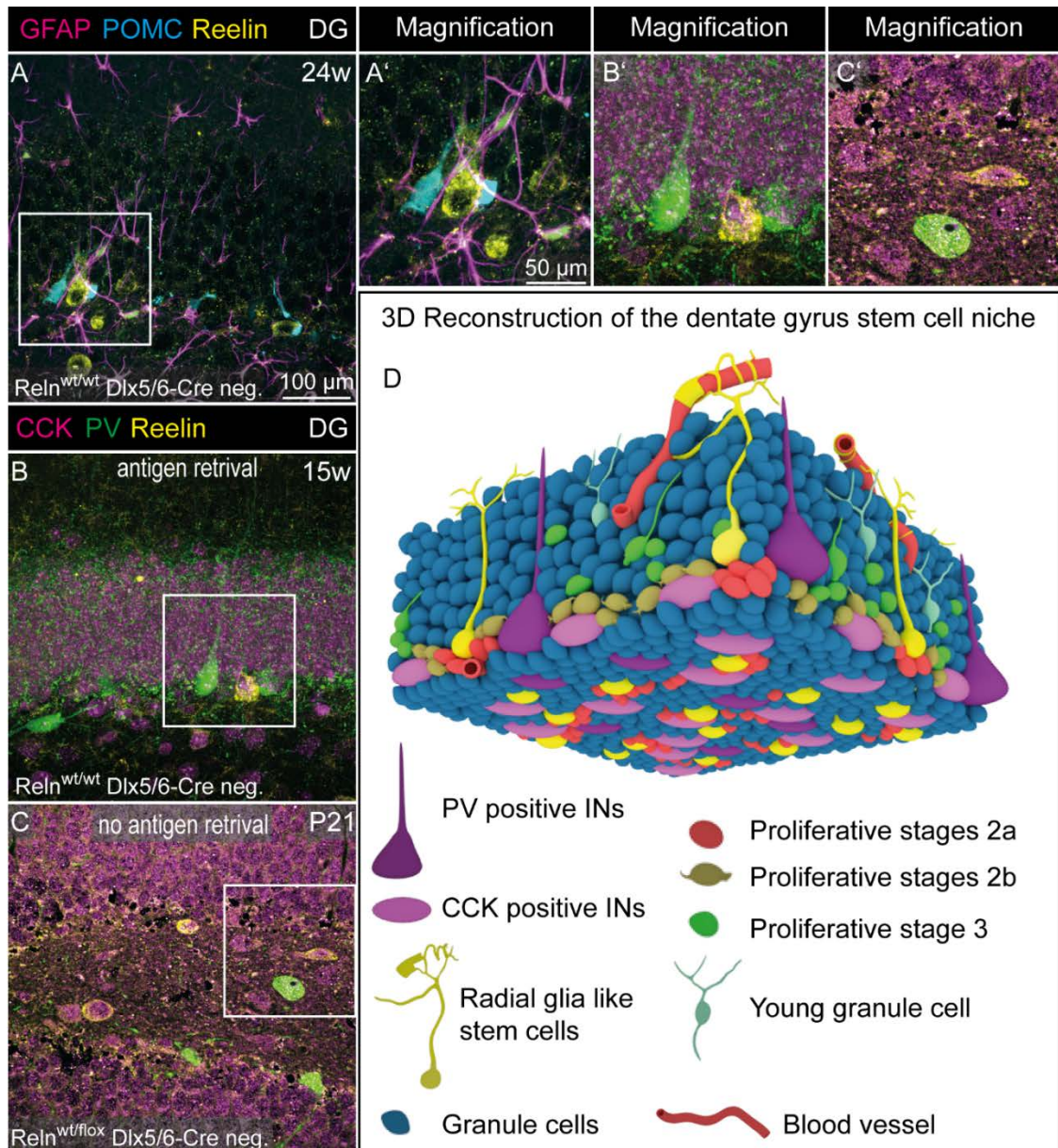


Figure 41: Location of Reelin positive interneurons in the stem cell niche of the dentate gyrus

A: $Rein^{wt/wt}$ $Dlx5/6$ -Cre neg. mice, expressing eGFP under the proopiomelanocortin (POMC) promoter (Overstreet et al. 2004), resulting in labelling of young granule cells, were stained immunohistochemically against Glial fibrillary acidic protein (GFAP, a glia specific intermediate filament marker) and Reelin. The 24 week old mice displayed a Reelin positive interneuron close to young granule cells, while being surrounded by GFAP positive filaments (A'). The white square in A indicates the area of magnification in A'. Stainings against Parvalbumin (PV, a marker for subgranular basket cells) and Cholecystokinin (CCK, a peptide hormone, marker for hilar commissural-associational pathway related cells (HICAP)) were performed, with an antigen retrieval in 15 week old $Rein^{wt/wt}$ $Dlx5/6$ -Cre neg. mice (B), and without antigen retrieval in 21 days old $Rein^{wt/flox}$ $Dlx5/6$ -Cre neg. mice (C), to discriminate the two cell types. White squares in B and C indicate the areas magnified in B' and C'. Both stainings showed the yellow, Reelin positive cell also being positive for CCK, but not for PV. D: The results from the stem cell niche organisation (Fig. 40), and the stainings from A-C and A'-C', together with previous published data from Seri, Fuentealba and Nicola (Seri et al. 2004; Fuentealba et al. 2012; Nicola et al. 2015) allowed the 3D reconstruction of the stem cell niche in the subgranular zone of the dentate gyrus.

3. Results

3.9.2 Pretesting for long time 5-Bromo-2'-deoxyuridine (BrdU) administration to investigate neurogenesis in the $\text{Reln}^{\text{flox/flox}}$ Dlx5/6-Cre mice

A common procedure to quantify neurogenesis was the administration of BrdU into cell culture media or administration to a living organism. For mice this could be achieved by injecting a BrdU solution intra peritoneal (i.p.) or by administering a BrdU-water solution (Wojtowicz and Kee 2006). The injection of animals was quite stressful to them and affected neurogenesis (Cameron and Gould 1994), also it only labelled cells within a time window of 2 h after injection (Cameron and McKay 2001; Buffo et al. 2005). The first approach to investigate neurogenesis within the dentate gyrus was done by i.p. injection. After quantification, it was obvious, that the numbers of stained cells were not satisfactory. To assure a higher number of stained cells, a constant uptake of BrdU during a longer time period was necessary. The administration via drinking water was chosen to achieve this and to quantify neurogenesis for a second time. It was necessary to choose and evaluate a proper method, as Jecker (Jecker et al. 1997) reported less uptake of BrdU-water solution, if presented to the animals without orange juice and Bachmanov (Bachmanov et al. 2002) reported different drinking habits of different mouse strains. A pretesting of the $\text{Reln}^{\text{flox/flox}}$ Dlx5/6-Cre mice was performed, to ascertain the amount of water drunken per mouse per day, and the concentration of sucrose needed to mask the BrdU taste. Figure 42A shows all pretested animals (4 male) and illustrates in stacked columns, the amount of water consumed (blue part) and the uptake of BrdU-water solution (coloured part) per day and mouse. The blue line indicates the mean of drunken water (3.8 ml), the green line indicates the mean of drunken liquid per day of all animals (4.09 ml). The animals were able to choose freely between the water bottle and the BrdU-water-sucrose solution bottle, presented in the cage (two-bottle choice test). With the exception of one individual mouse (1880), all animals preferred the BrdU-water or BrdU-water-sucrose solution instead of pure water. The mean individual liquid uptake during the test phase ranged from 4.64 ml for individual 1878 along 4.21 ml (1880), 3.82 ml (1879) to 3.52 ml for individual 1881. The general liquid uptake in the $\text{Reln}^{\text{flox/flox}}$ Dlx5/6-Cre mice was less than the given mean for their genetic background C57BL/6J, with approximately 6 ml/mouse (Bachmanov et al. 2002).

3. Results

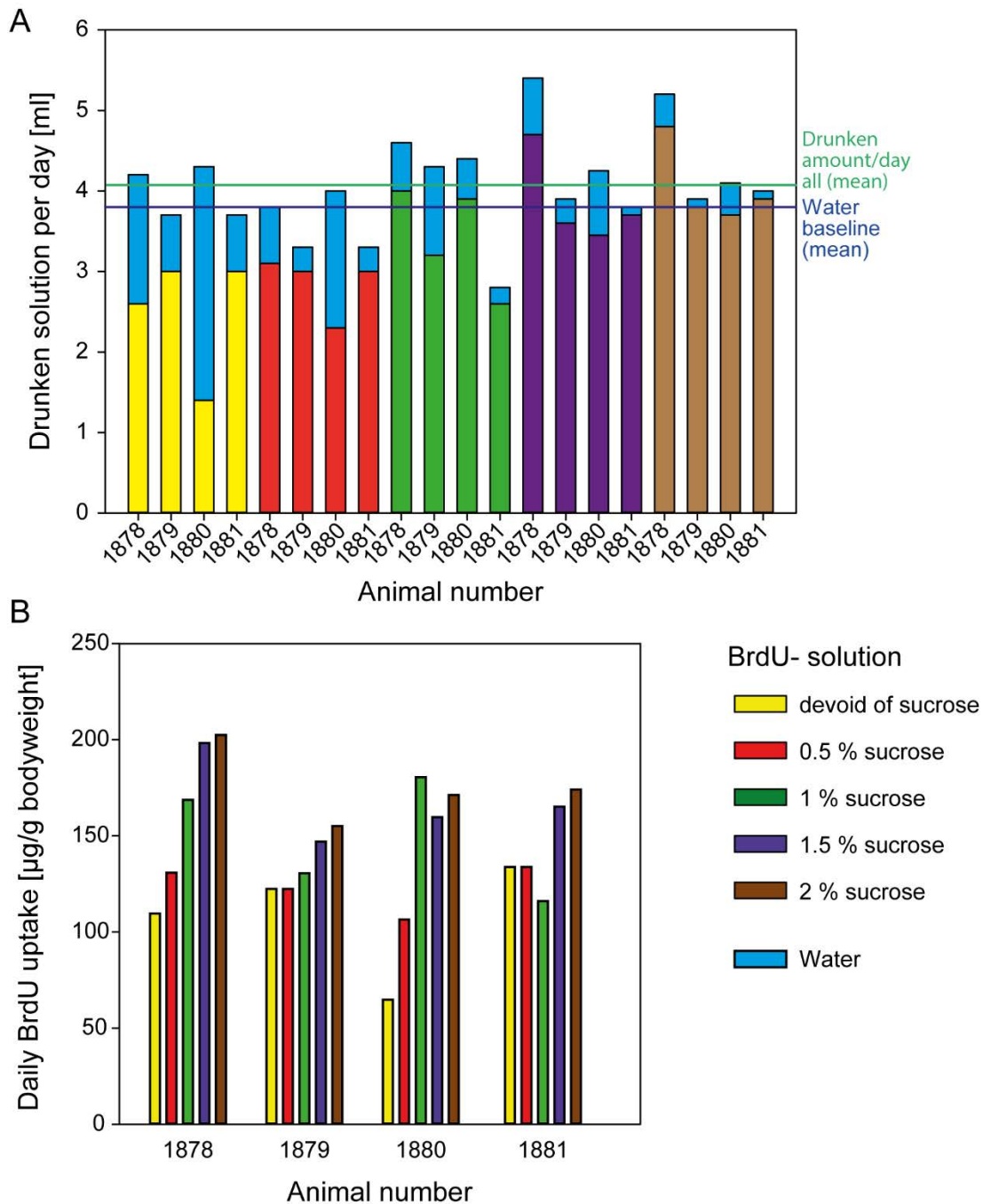


Figure 42: Pilot experiment regarding the administration of 5-Bromo-2'-deoxyuridine (BrdU) via the drinking water to mice

Four naïve male $\text{Reln}^{\text{wt/wt}}$ Dlx5/6-Cre neg. mice were tested for their drinking habits and the acceptance of BrdU water solution (pure or with sucrose) with the two-bottle choice test. A: Individual amount of the offered solutions drunk as the mean: Blue bar: Pure water, coloured bar: BrdU-water-sucrose solution with different amounts of sucrose added, depicted for every individual, blue line: water baseline (amount of water drunken when no other solution is offered, given as the mean of all animals), green line: amount of solution drunken (water and BrdU-water-sucrose) per day as mean out of all animals. The animals accepted the BrdU-water solution devoid of sucrose as their liquid source, but the amount of BrdU uptake increased with the increase in sucrose. B: The daily uptake of total BrdU ranged from $60 \mu\text{g/g}$ body weight up to $200 \mu\text{g/g}$ body weight per mouse, depending on the sucrose concentration of the provided BrdU solution, and the individual drinking habits of the animals.

3. Results

The uptake of pure BrdU-water solution ranged from 1.4 ml to 3.0 ml per mouse. With increasing sucrose concentration, the uptake of the BrdU-water-sucrose solution rose reciprocally, even above the intake of the water base-line. The uptake of BrdU-water solution with 0.5 % sucrose was ranging from 2.3 ml to 3.1 ml per mouse, for the solution with 1 % sucrose from 2.6 ml to 4.0 ml, for the 1.5 % sucrose solution from 3.4 ml to 4.7 ml and for the solution with 2 % sucrose was from 3.7 ml to 4.8 ml per mouse. This experiment illustrated that the mean liquid uptake for $ReIn^{flox/flox}$ $Dlx5/6$ -Cre mice ranged from 3.5 ml to 4.6 ml. The BrdU-water solution without sucrose, was accepted as a liquid source, too, and the higher the sucrose concentration, the higher the BrdU-water-sucrose solution uptake per mouse. The individual uptake of BrdU in μg per g bodyweight (bw) is graphed in figure 42B. The amount of BrdU taken up per g bodyweight ranged between 64.81 $\mu\text{g/g}$ bw and 133.93 $\mu\text{g/g}$ bw for the pure BrdU-water solution. Thus this solution alone was enough to administer approximately 100 $\mu\text{g/g}$ bw BrdU per day. Considering the BrdU-water-sucrose solutions, the increasing amount of drunken solution mirrored an ascending amount of BrdU uptake. The minimum BrdU uptake through the 0.5 % solution was 106.48 $\mu\text{g/g}$ bw the maximum 133.93 $\mu\text{g/g}$ bw. For the 1 % sucrose it was 116.10 $\mu\text{g/g}$ bw to 180.56 $\mu\text{g/g}$ bw, the 1.5 % solution resulted in an uptake range of 146.94 $\mu\text{g/g}$ bw to 198.31 $\mu\text{g/g}$ bw and the 2 % sucrose solution of 155.10 $\mu\text{g/g}$ bw to 202.53 $\mu\text{g/g}$ bw. Hence, it was possible to increase the amount of incorporated BrdU by rising sucrose concentration in the BrdU-water solution, by simultaneously increasing the fluid uptake above normal physiological levels. The concentration of BrdU administered for staining proliferative cells ranged between 50 $\mu\text{g/g}$ bw to 300 $\mu\text{g/g}$ bw in the literature (Gray 1988; Cameron and McKay 2001; Santoso et al. 2006). For the following experiments, a BrdU-water solution (1 mg/ml) together with 1 % of sucrose was chosen to deliver a dosage of 100-150 μg BrdU/g bw per day and mouse.

3.9.3 Analysis of BrdU uptake via the drinking water in the experimental cohort of $ReIn^{flox/flox}$ $Dlx5/6$ -Cre mice and controls

To analyse a possible effect of Reelin from iIN on adult neurogenesis within the dentate gyrus stem cell niche, BrdU was administered to 35 mice via their normal drinking water for 14 days. The animals were mixed regarding gender, genotype and housing conditions. These parameters were examined for their influence on BrdU uptake (Fig. 43). Between male and female mice (Fig. 43A), there was no significant difference found for the amount of BrdU uptake per day (MWU $p=0.755$, $N=15$ (male) + 20 (female), $\alpha=0.05$). The male (σ) mice

3. Results

drunk between 3-7 ml solution per day with a mean of 4.25 ml (median=3.64 ml). The female (♀) mice took up 3-5 ml solution per day with a mean of 3.89 ml (median=3.52 ml). All animals together drunk between 3-7 ml with a mean of 4.05 ml per day (median=3.64 ml). There was a higher variability of BrdU solution uptake per day in the male mice, but the mean did not differ significantly. The housing conditions of the animals, normally grouped, but sometimes single housed, led to different results (Fig. 43B). The MWU test gave a strong significant difference ($p=0.009$) between the two means of single versus group-housed. It needs to be considered that this p-value was based on very different group sizes, as there had been just four single housed animals (all male), and 31 group-housed animals. The single housed animals drunk between 4-7 ml per day (mean=5.58 ml, median=5.61 ml) and the grouped housed 3-6 ml (mean=3.85 ml, median=3.52 ml). The genotypes analysed ($Reln^{wt/wt}$ Dlx5/6-Cre negative, $Reln^{wt/wt}$ Dlx5/6-Cre positive, $Reln^{flox/flox}$ Dlx5/6-Cre positive and $Reln^{flox/flox}$ Dlx5/6-Cre negative) displayed different drinking habits (Fig. 43C). The performed one-way ANOVA showed a high statistical difference ($F(3,31)=11.18$, $p<0.001$, $N=7-11$, $\alpha=0.05$) and the Bonferroni post hoc testing revealed the concrete differences. The genotypes $Reln^{wt/wt}$ Dlx5/6-Cre negative (red box plot) and $Reln^{wt/wt}$ Dlx5/6-Cre positive (yellow box plot) did not differ statistically ($p=1.000$). The same was calculated for $Reln^{flox/flox}$ Dlx5/6-Cre positive (blue box plot) and $Reln^{flox/flox}$ Dlx5/6-Cre negative (green box plot) ($p=1.000$). But the comparison of the iIN specific Reelin knockout ($Reln^{flox/flox}$ Dlx5/6-Cre positive) with the $Reln^{wt/wt}$ Dlx5/6-Cre negative ($p=0.002$) and $Reln^{wt/wt}$ Dlx5/6-Cre positive ($p<0.001$) mice showed high significant differences regarding their means of drunk solution per day per animal. The control genotype $Reln^{flox/flox}$ Dlx5/6-Cre negative showed a significant difference to the $Reln^{wt/wt}$ Dlx5/6-Cre negative genotype ($p=0.043$) and a strong significant difference to the $Reln^{wt/wt}$ Dlx5/6-Cre positive genotype ($p=0.005$). While $Reln^{wt/wt}$ Dlx5/6-Cre negative mice drunk between 3-3.5 ml per day per mouse (mean=3.42 ml, median=3.52 ml), similar to the $Reln^{wt/wt}$ Dlx5/6-Cre positive genotype with 3-3.5 ml per day per mouse (mean=3.23 ml, median=3.27 ml), the $Reln^{flox/flox}$ Dlx5/6-Cre positive genotype drunk 3-5.5 ml per day per mouse (mean=4.61 ml, median=4.82 ml) and the $Reln^{flox/flox}$ Dlx5/6-Cre negative genotype drunk 3-7 ml per day per mouse with mean of 5.04 ml and median of 4.38 ml.

3. Results

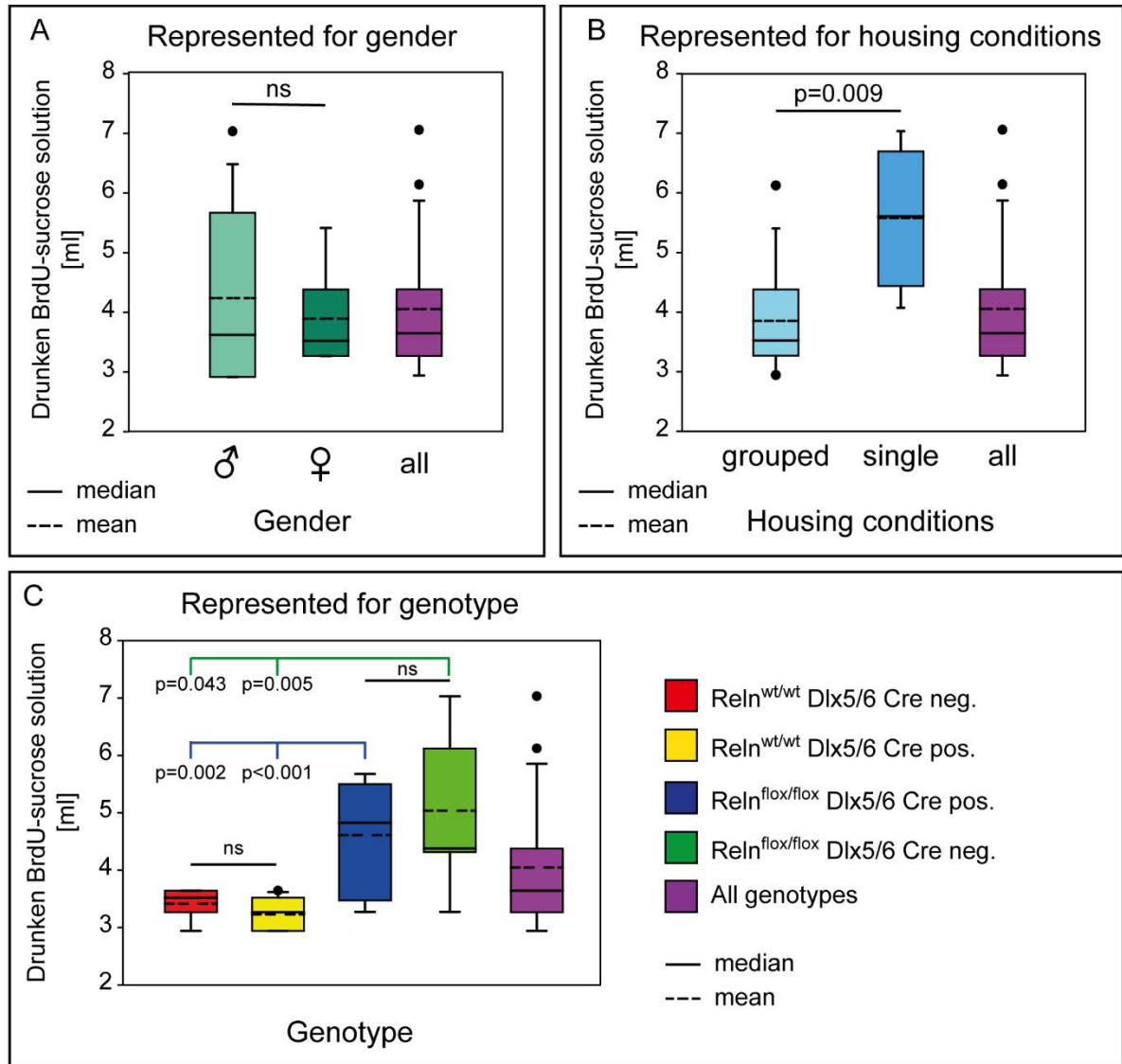


Figure 43: Analysis of BrdU-water-sucrose solution uptake and drinking habits of mice regarding gender, housing and genotype

A: BrdU-water-sucrose solution uptake itemised for gender. Male mice had higher variation and amounts of the drunken solution than female mice, but this did not reach level of significance (MWU $p=0.755$, $N=15$ (male) + 20 (female), $\alpha=0.05$). B: BrdU-water-sucrose solution uptake, itemised for housing conditions. Single housed animals, all male, drunk significantly more than animals housed in groups (MWU $p=0.009$, $N=4$ (single) + $N=31$ (grouped), $\alpha=0.05$). C: BrdU-water-sucrose solution uptake, itemised for genotype. Four genotypes were analysed for their drinking habits of the BrdU-water-sucrose solution: ReIn^{wt/wt} Dlx5/6-Cre neg. (control, red), ReIn^{wt/wt} Dlx5/6-Cre pos. (cre control, yellow), ReIn^{flox/flox} Dlx5/6-Cre pos. (interneuron specific Reelin knockout, blue) and ReIn^{flox/flox} Dlx5/6-Cre neg. (flox control, green). The drunken amounts differed significantly (one-way ANOVA $F(3,31)=11.18$, $p<0.001$, $N=7-11$, $\alpha=0.05$) and the Bonferroni post hoc testing revealed a grouping of control and cre control ($p=1.000$) versus interneuron specific knockout and flox control ($p=1.000$), while constituents of the group differed significant or strong significant from the others. Purple box-whisker plot contains all animals and was given for comparison purpose in all graphs (A-C). All box-whisker plots are annotated with the median (full line) and the mean (dotted line).

3. Results

Nevertheless, a minimum amount of 100µg/g bw per animal per day BrdU had been incorporated with 3 ml solution drunk and a maximum of 233µg/g bw per animal per day was taken up with 7 ml BrdU solution. This covered the intended dose of 100µg/g bw BrdU per day per animal.

Despite the differences between the genotypes, male and female and single versus group housing, a sufficient application of BrdU per day was achieved to quantify the dentate gyrus neurogenesis.

3.9.4 Quantification of proliferation in the adult dentate gyrus using BrdU and Ki-67 in the $ReIn^{flox/flox}$ $Dlx5/6$ -Cre mice

The quantification of adult dentate gyrus neurogenesis was done with three different and independent staining experiments. First with a BrdU staining via a single i.p. injection (count 1), second with BrdU application over 14 days via the drinking water (count 2) and with immunohistochemical staining against proliferation marker Ki-67 (Ki-67) (Kee et al. 2002). Figure 44 illustrates the staining results for $ReIn^{wt/wt}$ $Dlx5/6$ -Cre positive mice on the left column and iIN specific Reelin knockout on the right column ($ReIn^{flox/flox}$ $Dlx5/6$ -Cre positive). Count 1 (Fig. 44A-A') was done in 12 week old mice and BrdU was co-stained with NeuN to highlight the position of the granule cell layer. Count 2 (Fig. 44B-B') was performed in 15 week old mice, with double staining of BrdU and NeuN. The Ki-67 was triple stained with DAPI and Doublecortin (DCX), and is presented in figure 44C-C'. The white arrows hint the position of exemplary BrdU or Ki-67 ir cell bodies in the subgranular zone of the dentate gyri. Whereas the Ki-67 (Fig. 44C-C') and the first BrdU count (Fig. 44A-A') show infrequent immunoreactive cells along the subgranular area, a higher number of BrdU positive cells could be detected in count 2 (Fig. 44B-B'). No obvious differences between staining intensities could be detected comparing control genotype ($ReIn^{wt/wt}$ $Dlx5/6$ -Cre positive) and iIN specific Reelin knockout ($ReIn^{flox/flox}$ $Dlx5/6$ -Cre positive). The quantification results are presented in figure 45. The first BrdU count, depicted in figure 45A, was done for septal, middle, and temporal slices of the hippocampi respectively dentate gyri (for representative images see Fig. A3 in the appendix). The number of cells had been standardised to the length of the subgranular zone. This quantification was done in $ReIn^{wt/wt}$ $Dlx5/6$ -Cre positive (yellow bar) as control, and the iIN specific Reelin knockout ($ReIn^{flox/flox}$ $Dlx5/6$ -Cre positive) mice (blue bar).

3. Results

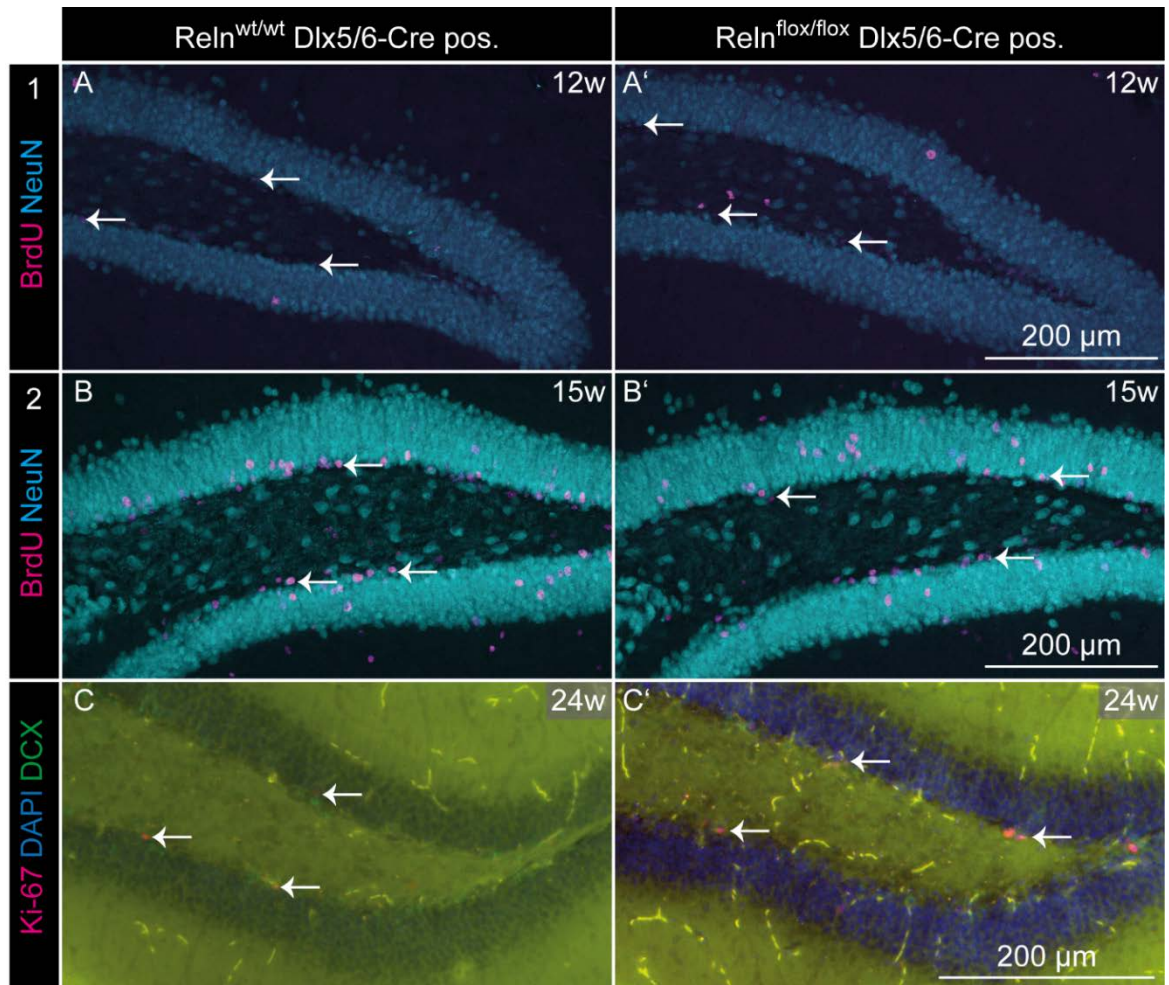


Figure 44: Analysis of adult neurogenesis in the dentate gyrus with BrdU and Ki-67 staining

Immunohistochemical staining examples for $Reln^{wt/wt}$ Dlx5/6-Cre pos. and $Reln^{flox/flox}$ Dlx5/6-Cre pos. animals, for the first BrdU experiment with intra peritoneal injection (1, A, A'), the second BrdU experiment with BrdU administration via the drinking water (2, B, B'), and a staining against Ki-67 (a proliferation marker C, C') in 12 week (A, A'), 15 week (B, B') and 24 week (C, C') old mice. A counterstaining was done with NeuN (a neuronal nuclei marker) in A, A', B, B', and with DAPI together with a costaining against Doublecortin in C, C'. White arrows highlight positions of BrdU or Ki-67 immunoreactive cells in the subgranular area of the dentate gyrus. The number of labelled cells was similar between the genotypes in all three experiments (A-C, A'-C'). The highest number of labelled cells was found in the second BrdU experiment, where BrdU was delivered with the drinking water for 14 days (B, B').

Along the septal subgranular zone (SGZ) a mean of 4.78 ± 1.06 cells/mm SGZ for the control and 3.24 ± 0.87 cells/mm SGZ for the iIN specific Reelin knockout were counted. In the middle area 3.42 ± 0.64 cells/mm SGZ (control) to 2.08 ± 0.40 cells/mm SGZ (iIN specific Reelin knockout) and in the temporal subgranular zone 2.07 ± 0.17 cells/mm SGZ for the control and 2.16 ± 0.78 cells/mm SGZ for the iIN specific Reelin knockout had been quantified. None of these results differed significantly, according to the two-tailed t-test (septal: $t(8)=1.12$, $p=0.295$, middle: $t(8)=1.78$, $p=0.144$, temporal: $t(4.38)=-0.11$, $p=0.921$,

3. Results

N=5 animals per genotype, $\alpha=0.05$), despite a tendency to lesser cell numbers in the septal and middle area in the iIN specific Reelin knockout. The second quantification for BrdU (count 2 Fig. 45B) was focused on the middle area of the dentate gyri since the parallel performed Doublecortin staining and quantification (Fig. 47B) suggested a more pronounced effect in the middle area. The counted cell numbers from the second BrdU quantification (Fig. 45B) were much higher due to the prolonged and continuous BrdU application via the drinking water. Here, all control genotypes were quantified: $Re^{wt/wt}$ Dlx5/6-Cre negative (red bar) 79.36 ± 5.01 cells/mm SGZ, $Re^{wt/wt}$ Dlx5/6-Cre positive (yellow bar) 70.16 ± 3.38 cells/mm SGZ, $Re^{flx/flx}$ Dlx5/6-Cre positive (blue bar) 64.16 ± 4.26 cells/mm SGZ, $Re^{flx/flx}$ Dlx5/6-Cre negative (green bar) 85.79 ± 6.19 cells/mm SGZ. The performed one-way ANOVA showed a significant difference between the genotypes ($F(3,21)=3.96$, $p=0.020$, $N=7$ animals per genotype, $\alpha=0.05$) and Bonferroni post hoc comparison revealed a significant difference between the $Re^{flx/flx}$ Dlx5/6-Cre positive and $Re^{flx/flx}$ Dlx5/6-Cre negative genotypes ($p=0.025$). All other comparisons did not reach statistical significance levels ($Re^{flx/flx}$ Dlx5/6-Cre positive compared to $Re^{wt/wt}$ Dlx5/6-Cre negative: $p=0.213$, to $Re^{wt/wt}$ Dlx5/6-Cre positive: $p=1.000$, $Re^{flx/flx}$ Dlx5/6-Cre negative to $Re^{wt/wt}$ Dlx5/6-Cre negative: $p=1.000$, to $Re^{wt/wt}$ Dlx5/6-Cre positive: $p=0.186$ and $Re^{wt/wt}$ Dlx5/6-Cre negative to $Re^{wt/wt}$ Dlx5/6-Cre positive: $p=1.000$). For the second BrdU quantification with overall higher cell numbers, the iIN specific Reelin knockout showed less BrdU positive cells in the SGZ compared to the three other genotypes, but just reached the level of significance compared to the control genotype $Re^{flx/flx}$ Dlx5/6-Cre negative. Annotation, the $Re^{flx/flx}$ Dlx5/6-Cre negative was the control group, showing comparable BrdU uptake regarding the iIN specific Reelin knockout.

The Ki-67 staining, depicted in figure 45C, was quantified for the septal, middle and temporal dentate gyri with four genotypes. The quantification results are given in table 14:

3. Results

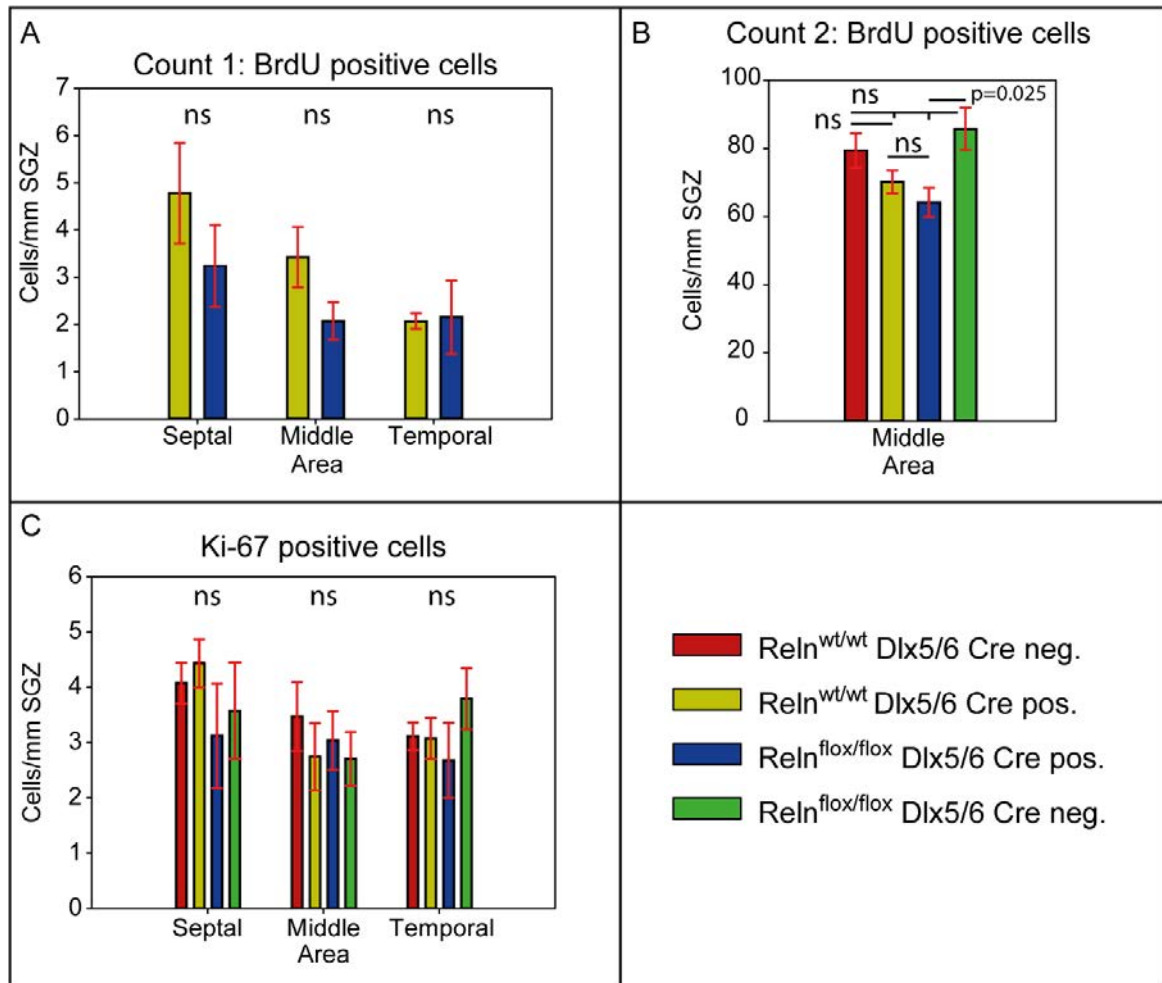


Figure 45: Quantification of adult neurogenesis in the dentate gyrus of Reln^{flox/flox} mice with BrdU and Ki-67 staining

Cell numbers were normalised to the length of the subgranular zone (SGZ) in millimetres (mm). A: BrdU experiment one (intraperitoneal injection): Cell numbers of BrdU positive cells in the area of the septal, middle and temporal dentate gyrus for Reln^{wt/wt} Dlx5/6-Cre pos. (cre control, yellow) and Reln^{flox/flox} Dlx5/6-Cre pos. (interneuron specific Reelin knockout, blue) genotypes. No significant difference had been found between the two genotypes in any area (two-tailed t-tests: septal: $t(8)=1.12$, $p=0.295$, middle: $t(8)=1.78$, $p=0.114$, temporal: $t(4.38)=-0.11$, $p=0.921$, $N=5$ animals per genotype, $\alpha=0.05$). B: BrdU experiment two (administered via drinking water): Cell numbers were counted just for the middle area of the dentate gyrus and for all three controls (Reln^{wt/wt} Dlx5/6-Cre neg. (control, red), Reln^{wt/wt} Dlx5/6-Cre pos. (cre control, yellow), Reln^{flox/flox} Dlx5/6-Cre neg. (flox control, green) and the interneuron specific Reelin knockout (Reln^{flox/flox} Dlx5/6-Cre pos., blue). The interneuron specific Reelin knockout was counted with the lowest cell number per mm SGZ, and did not reach the level of significance compared to the control ($p=0.213$) and the cre control ($p=1.000$), but was significantly different to the flox control ($p=0.025$) in the Bonferroni post hoc comparison (one-way ANOVA: $F(3,21)=3.96$, $p=0.020$, $N=7$ animals per genotype, $\alpha=0.05$). The controls among themselves were not significantly different (control/cre control: $p=1.000$, control/flox control: $p=1.000$, cre control/flox control: $p=0.186$). C: The Ki-67 cell count was done for the septal, middle and temporal and all four genotypes. Similar to the first BrdU experiment, no significant difference was found between the genotypes in all three areas (one-way ANOVA: septal: $F(3,19)=0.63$, $p=0.604$, middle: $F(3,19)=0.39$, $p=0.765$ and temporal: $F(3,19)=0.86$, $p=0.478$). Values given as mean \pm sem.

3. Results

Table 14: Ki-67 staining and quantification in the septal, middle and temporal dentate gyrus: Cell numbers are given as mean±sem cells per mm SGZ. Statistical analysis with one-way ANOVA, F-values with degrees of freedom (F(df1,df2)) and p-value of the respective test given within the column. Genotypes: *Reln*^{wt/flox} *Dlx5/6*-Cre negative (wt), *Reln*^{wt/flox} *Dlx5/6*-Cre positive (het), *Reln*^{flox/flox} *Dlx5/6*-Cre positive (cKO), *Reln*^{flox/flox} *Dlx5/6*-Cre negative (flox). N=4-8 animals per genotype, $\alpha=0.05$

Area	Genotype				Stat. values	
	wt	het	cKO	flox	F(df1,df2)	p-value
Septal	4.07±0.37	4.47±0.43	3.12±0.94	3.58±0.87	F(3,19)=0.63	0.604
Middle	3.47±0.62	2.74±0.61	3.03±0.53	2.71±0.49	F(3,19)=0.39	0.765
Temporal	3.11±0.25	3.07±0.37	2.68±0.68	3.79±0.55	F(3,19)=0.86	0.478

The Ki-67 staining resulted in comparable cell numbers as the BrdU count 1. No statistical differences were detected between the results. Although in the BrdU count 1 a tendency to lower cell numbers in the iIN specific Reelin knockout was indicated, this pattern was not mirrored in the Ki-67 quantification.

In terms of proliferating cells in the SGZ of the dentate gyri in adult mice, there was a tendency towards lower cell numbers in the iIN specific Reelin knockout, but just in the BrdU labelling experiments not in the Ki-67 staining. Additionally, the differences between the genotypes reached only once (BrdU count 2 *Reln*^{flox/flox} *Dlx5/6*-Cre positive to *Reln*^{flox/flox} *Dlx5/6*-Cre negative) the level of significance. These three quantifications indicate, that, if at all, Reelin from iIN has a very faint influence on the proliferating cells in the dentate gyri of adult mice.

3.9.5 Cell numbers and morphology of immature neurons and RGLCs in the adult dentate gyrus in the *Reln*^{flox/flox} *Dlx5/6*-Cre mice

The adult neurogenesis comprises not only the proliferation of progenitor cells, but also the differentiation and maturation of young granule cells along various stages (Imayoshi and Kageyama 2011; Fuentealba et al. 2012; Nicola et al. 2015). The separation, migration, and formation of a proper dendritic tree in young granule cells were essential for integration into the existing granule cell layer (Seri et al. 2004; Fuentealba et al. 2012; Nicola et al. 2015). An influence of Reelin on the outgrowth and arborisation of dendritic trees (Niu et al. 2004; Chai et al. 2014; O'Dell et al. 2015; Santana and Marzolo 2017) on migration and on cytoskeletal components (Chai et al. 2009a, 2009b; Krüger et al. 2010; Courtès et al. 2011) had already

3. Results

been shown in recent literature. Thus, investigations on cell numbers and cell process properties of immature granule cells and Nestin positive progenitor cells were performed. Different markers were used to identify and discriminate between the various stages of development and to localize progenitor cell bodies (Kempermann et al. 2015).

Ki-67 was used to discriminate proliferating and non-proliferating cells. Sox2 (sex determining region y-box2 transcription factor) was used as a marker for progenitor and type 2a cell bodies, facilitating the discrimination between those two cell types. Nestin was used to stain progenitor cell processes. Doublecortin was used as a marker for young granule cells at stages type 2b to 3, and early postmitotic cells, whereas NeuN staining marked early and late postmitotic granule cells. Examples of staining results are depicted in figure 46. The two left columns (Fig. 46a-a' and Fig. 46c-c') illustrate the results for the $ReIn^{wt/wt}$ Dlx5/6-Cre positive control and the two right columns show the iIN specific Reelin knockout ($ReIn^{flox/flox}$ Dlx5/6-Cre positive) (Fig. 46b-b' and Fig. 46d-d'). The quantification for young and early/late postmitotic maturation stages was done in 12 week old animals, while the quantification for progenitor process properties was done in 15 week old mice. The distribution and process orientation in the Doublecortin immunoreactive cells appears to be comparable between control (Fig. 46a-a') and iIN specific Reelin knockout genotype (Fig. 46b-b'). Equivalent results could be discerned for the range, orientation and frequency of Nestin in processes of precursor cells in both genotypes (control: Fig. 46c-c' iIN specific Reelin knockout Fig. 46d-d').

Doublecortin was stained together with BrdU and therefore quantified in the BrdU count 1 and BrdU count 2. NeuN was only co-stained in BrdU count 2 and accordingly only quantified once. Figure 47A graphs the results for the NeuN quantification for all three control genotypes: $ReIn^{wt/wt}$ Dlx5/6-Cre negative (red box plot/bar), $ReIn^{wt/wt}$ Dlx5/6-Cre positive (yellow box plot/bar), $ReIn^{flox/flox}$ Dlx5/6-Cre negative (green box plot/bar) and the iIN specific Reelin knockout ($ReIn^{flox/flox}$ Dlx5/6-Cre positive (blue box plot/bar). NeuN staining was quantified as the intensity of median grey value in BrdU positive cells, to select those cells, which had passed the whole maturation phases since BrdU application (compare Fig. 11 in the introduction). This provided measure whether granule cell maturation was delayed (which would lead to less BrdU/NeuN positive cells) or accelerated (which would lead to more BrdU/NeuN positive cells). In the 1092 analysed cells for the $ReIn^{wt/wt}$ Dlx5/6-Cre negative genotype, the staining intensity for NeuN ranged between 174.00 [au] to 3271.00 [au] with a median of 669.50 [au] and a mean of 816.11 [au].

3. Results

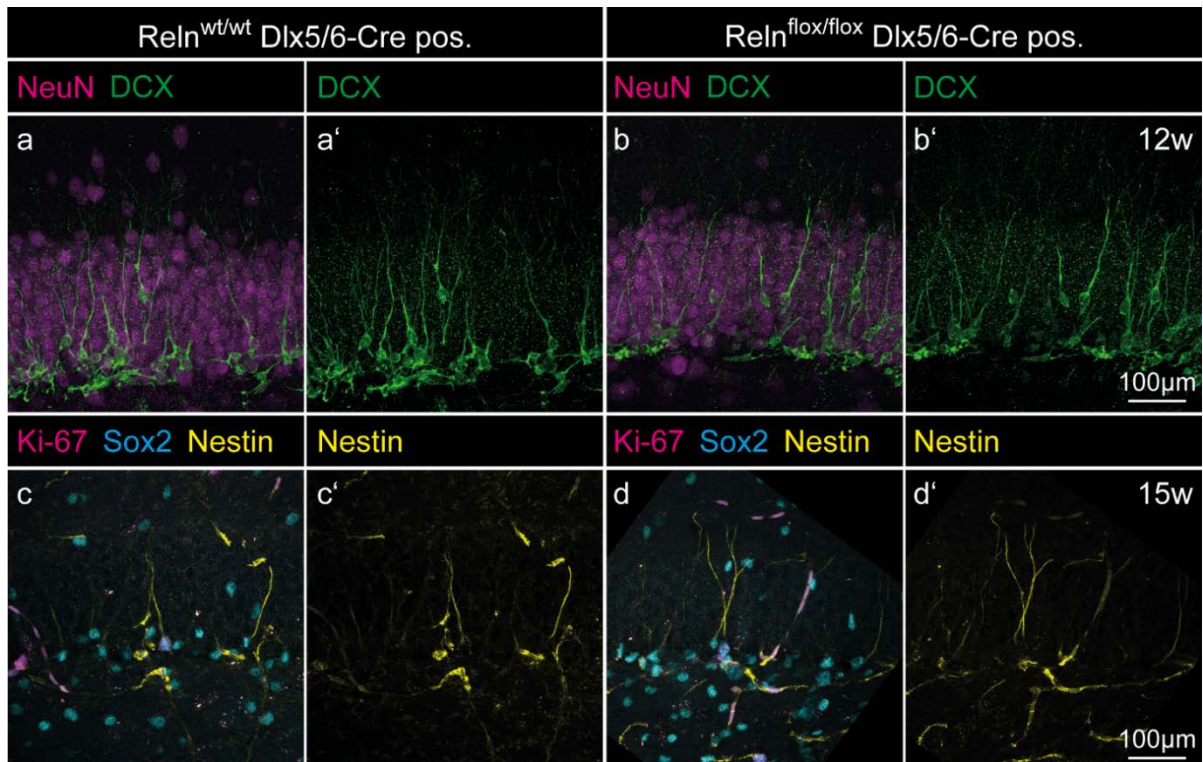


Figure 46: Analysis of appearance and distribution of stem cells and young granule cells in the dentate gyrus of $Reelin^{flox/flox}$ Dlx5/6-Cre positive mice

Young granule cells were stained immunohistochemically against Doublecortin (DCX) and counterstained with NeuN in 12 week old $Reelin^{wt/wt}$ Dlx5/6-Cre pos. (control, a, a') and $Reelin^{flox/flox}$ Dlx5/6-Cre pos. (b, b') mice. Distribution and appearance of DCX positive cells were similar between the control (a, a') and the interneuron specific Reelin knockout (b, b'). Stem cells were analysed according to immunohistochemical staining against Nestin, Ki-67 and Sox2 (sex determining region y-box2 transcription factor, a marker for young cells) in 15 week old mice of $Reelin^{wt/wt}$ Dlx5/6-Cre pos. (c, c') and $Reelin^{flox/flox}$ Dlx5/6-Cre pos. (d, d') genotype. The stem cells showed similar distribution, numbers (c, d), and process morphology (c', d') in both genotypes.

The $Reelin^{wt/wt}$ Dlx5/6-Cre positive control genotype ranged from 170.00 [au] to 1962.00 [au] with a median of 600.00 [au] and a mean of 754.38 [au] from 1579 analysed cells. The $Reelin^{flox/flox}$ Dlx5/6-Cre negative was quantified with 1513 cells, a minimum of 165.00 [au], a maximum of 1904.00 [au], a median of 507.00 [au] and a mean of 635.83 [au]. The iIN specific Reelin knockout had 1135 cells analysed, resulting in a minimum of 169.00 [au], a maximum of 1971.00 [au], a median of 503.00 [au] and a mean of 666.66 [au] of NeuN staining intensity. The analysed cells were taken equally from seven independent animals per genotype. The statistical analysis with the Kruskal-Wallis test reported a high significant difference for the staining intensities with $p < 0.001$. A sample to sample comparison revealed that $Reelin^{wt/wt}$ Dlx5/6-Cre negative to $Reelin^{wt/wt}$ Dlx5/6-Cre positive ($p = 0.668$) and $Reelin^{flox/flox}$ Dlx5/6-Cre positive to $Reelin^{flox/flox}$ Dlx5/6-Cre negative ($p = 0.808$) did not differ significantly. But the iIN specific Reelin knockout differed highly from both control groups $Reelin^{wt/wt}$

3. Results

Dlx5/6-Cre negative ($p < 0.001$) and $ReIn^{wt/wt}$ Dlx5/6-Cre positive ($p < 0.001$). The same results were calculated for the $ReIn^{flox/flox}$ Dlx5/6-Cre negative compared to the $ReIn^{wt/wt}$ Dlx5/6-Cre negative ($p < 0.001$) and $ReIn^{wt/wt}$ Dlx5/6-Cre positive ($p < 0.001$) genotypes. Similar to previous results, there was a clustering of genotypes found. The results between the iIN specific Reelin knockouts did not differ significantly from the direct control group $ReIn^{flox/flox}$ Dlx5/6-Cre negative, but were calculated with a highly significant difference to the other control genotypes $ReIn^{wt/wt}$ Dlx5/6-Cre negative and $ReIn^{wt/wt}$ Dlx5/6-Cre positive, which, however, did not differ between themselves. Thus, the stages passed of maturing cells, having been born within the time window of the BrdU application, were comparable between the iIN specific Reelin knockout and the direct control genotype $ReIn^{flox/flox}$ Dlx5/6-Cre negative. In the other two control genotypes ($ReIn^{wt/wt}$ Dlx5/6-Cre negative and $ReIn^{wt/wt}$ Dlx5/6-Cre positive), maturation stages reached were more advanced at the time point of the sacrifice of the animal. It could be estimated that the newly born granule cells of these genotypes seem to pass the maturation stages faster.

The Doublecortin quantification performed alongside the BrdU count 1 is presented in figure 47B. All three different areas of the hippocampus, respectively the dentate gyrus, had been quantified for the control genotype $ReIn^{wt/wt}$ Dlx5/6-Cre positive (yellow bar) and the iIN specific Reelin knockout (blue bar). The cell numbers were normalised to the length of the subgranular zone (SGZ) analysed. For the septal dentate gyrus, a mean of 107.45 ± 8.60 cells/mm SGZ were counted for the control, and 84.47 ± 8.41 cells/mm SGZ of Doublecortin positive cells for the iIN specific Reelin knockout. Along the SGZ of the middle hippocampus, 87.19 ± 7.09 cells/mm SGZ for the control and 66.44 ± 3.81 cells/mm SGZ for the iIN specific Reelin knockout were counted. In the temporal hippocampus the quantification resulted in 78.33 ± 4.97 cells/mm SGZ in the control and 71.34 ± 3.69 cells/mm SGZ for the iIN specific Reelin knockout. Despite a similar diminished cell number in the septal dentate gyrus, only the quantification in the middle area reached a level of significance (two-tailed t-test: septal: $t(8) = 1.91$, $p = 0.092$, middle: $t(8) = 2.58$, $p = 0.033$, temporal: $t(8) = 1.13$, $p = 0.291$, $N = 5$ animals per genotype, $\alpha = 0.05$). This quantification indicated lower numbers of cells in maturation stages type 2b to early postmitotic in the septal and middle dentate gyrus areas. Only the quantification of the middle area reached the level of significance, which suggested a more pronounced Reelin effect.

3. Results

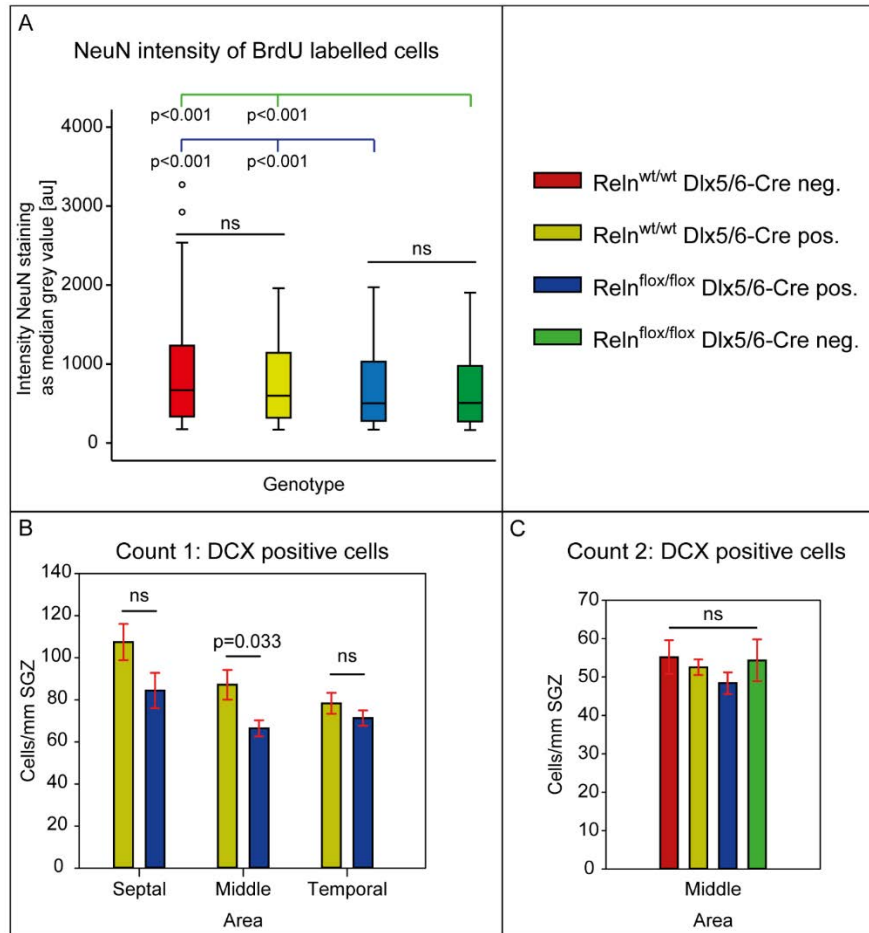


Figure 47: Quantification of main maturity stages of young granule cells in the dentate gyrus of $Reln^{flox/flox}$ Dlx5/6-Cre positive mice

A: The transfer from maturity stages type 2a, 2b and 3 to the early post-mitotic stage are marked by the start of NeuN expression (Kempermann et al. 2015). The number of cells finally reaching the early post mitotic stage was quantified by measuring NeuN staining intensity, as a median grey value in BrdU positive cells (A) in all four genotypes ($Reln^{wt/wt}$ Dlx5/6-Cre neg. (control, red), $Reln^{wt/wt}$ Dlx5/6-Cre pos. (cre control, yellow), $Reln^{flox/flox}$ Dlx5/6-Cre pos. (interneuron specific Reelin knockout, blue), and $Reln^{flox/flox}$ Dlx5/6-Cre neg. (flox control, green)). The statistics revealed a significant difference between the genotypes (Kruskal-Wallis test $p < 0.001$, $N = 1092-1513$ cells from 7 individual animals per genotype, $\alpha = 0.05$). A sample to sample comparison showed no difference between the controls ($p = 0.668$) and between the interneuron specific Reelin knockout to the flox control ($p = 0.808$), but the interneuron specific Reelin knockout differed highly significant to the control ($p < 0.001$) and the cre control ($p < 0.001$). The flox control differed in the same way from the other two controls (control: $p < 0.001$, cre control: $p < 0.001$), indicating a significantly higher expression rate of NeuN in the control and cre control genotypes. Early maturation stages, labelled with DCX, were counted in BrdU experiment one (intraperitoneal injection) (B) and BrdU experiment two (administration via drinking water) (C). Both cell numbers were normalised to the length of the subgranular zone (SGZ) in millimetres. B: The septal, middle and temporal area of the dentate gyrus were quantified for the cre control (yellow) and the interneuron specific Reelin knockout (blue). Only in the middle area a significant difference was found for the DCX positive cell numbers, with lower numbers in the interneuron specific knockout (two-tailed t-test: septal: $t(8) = 1.91$, $p = 0.092$, middle: $t(8) = 2.58$, $p = 0.033$, temporal: $t(8) = 1.13$, $p = 0.291$, $N = 5$ animals per genotype, $\alpha = 0.05$). C: The second BrdU experiment revealed no significant difference between the four genotypes in DCX positive cell numbers in the middle area of the dentate gyrus (one-way ANOVA: $F(3,24) = 0.59$, $p = 0.625$, $N = 7$ animals per genotype, $\alpha = 0.05$). Values in B and C given as mean \pm sem.

3. Results

With this assumption, the second quantification of Doublecortin positive cells, alike the BrdU count 2, was performed only in the middle region of the dentate gyrus. The quantification result is graphed in figure 47C and given for all three control genotypes ($\text{Reln}^{\text{wt/wt}}$ Dlx5/6-Cre negative (red bar), $\text{Reln}^{\text{wt/wt}}$ Dlx5/6-Cre positive (yellow bar), $\text{Reln}^{\text{flox/flox}}$ Dlx5/6-Cre negative (green bar) and the iIN specific Reelin knockout ($\text{Reln}^{\text{flox/flox}}$ Dlx5/6-Cre positive (blue bar)). Seven animals per genotype were counted and resulted in the following mean of cell numbers: $\text{Reln}^{\text{wt/wt}}$ Dlx5/6-Cre negative 55.18 ± 4.42 cells/mm SGZ, $\text{Reln}^{\text{wt/wt}}$ Dlx5/6-Cre positive 52.56 ± 2.03 cells/mm SGZ, $\text{Reln}^{\text{flox/flox}}$ Dlx5/6-Cre negative 54.36 ± 5.45 cells/mm SGZ and $\text{Reln}^{\text{flox/flox}}$ Dlx5/6-Cre positive 48.41 ± 2.82 cells/mm SGZ. The comparison of the means with the one-way ANOVA did not detect a significant difference ($F(3,24)=0.59$, $p=0.625$, $N=7$ animals per genotype, $\alpha=0.05$). The second quantification of Doublecortin positive cells did not confirm the data and statistical difference from the first counting. Seen in numbers, the iIN specific Reelin knockout had fewer Doublecortin positive cells, but this remained just a tendency and did not reach the level of significance.

The analysis of Doublecortin-positive cell processes was presented in figure 48Aa-a'. The data of the main properties of filament length, branching depth and branching points were collected from 10 cells of five independent animals per genotype. The iIN specific Reelin knockout ($\text{Reln}^{\text{flox/flox}}$ Dlx5/6-Cre positive, cKO) was analysed together with the control genotype $\text{Reln}^{\text{wt/wt}}$ Dlx5/6-Cre positive. The filament length described the overall length of the protruding process of the cell. The branching depth, measured as steps from 0-X (at least step 3), was an index for the complexity of filament arborisation (Fig. 48Bb'-b'') and the branching point analysis was used as a reference of the branching frequency itself. For the Doublecortin filament length, a mean of 232.90 ± 14.57 μm was measured in the control and 249.30 ± 22.67 μm in the cKO (Fig. 48Aa'). The statistical analysis with the two-tailed t-test revealed no significant difference between the two genotypes ($t(18)=0.61$, $p=0.550$, $N=10$ cells per genotype, $\alpha=0.05$). The branching depth of the control was analysed with a mean of 2.20 ± 0.44 steps and the cKO with 2.80 ± 0.44 steps (Fig. 48Aa''), the branching points were 2.50 ± 0.60 for the control and 3.50 ± 0.64 for the cKO (Fig. 48Aa''') in numbers. Both parameters did not reach the level of significance, despite the higher numbers in branching depth and points in the cKO (two-tailed t-test: branching depth: $t(18)=0.96$, $p=0.350$, branching points: $t(18)=1.14$, $p=0.268$, $N=10$ cells per genotype, $\alpha=0.05$).

3. Results

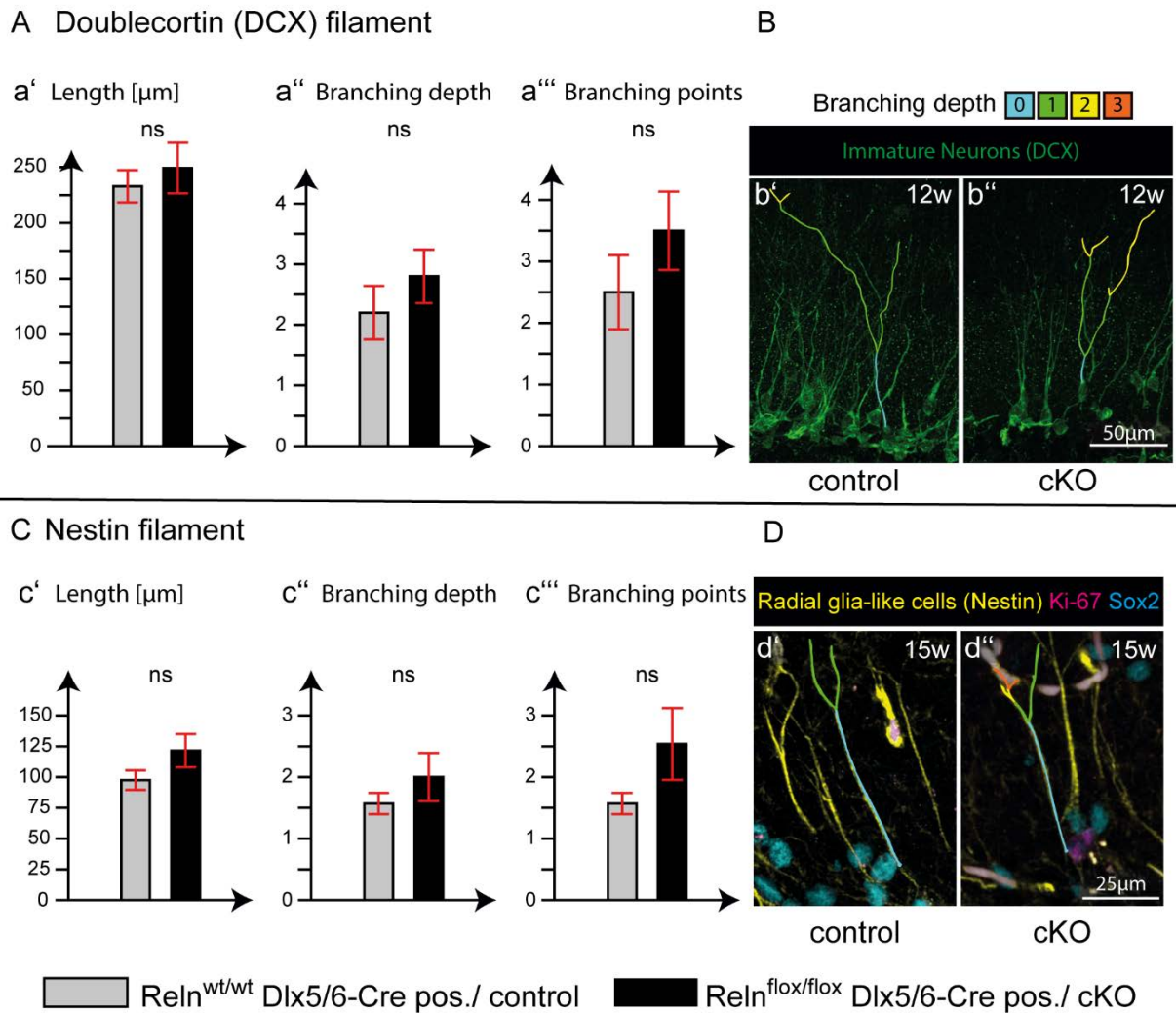


Figure 48: Quantification of stem cell and young granule cell filament properties in the dentate gyrus of $\text{Reln}^{\text{flox/flox}}$ Dlx5/6-Cre positive mice

Filament properties were analysed as filament length, branching depth (B, b, b', D, d, d') and branching points in $\text{Reln}^{\text{wt/wt}}$ Dlx5/6-Cre pos. (control) and $\text{Reln}^{\text{flox/flox}}$ Dlx5/6-Cre pos. (cKO) genotypes. A: Properties of Doublecortin positive cell filaments in 12 week old mice: The filament length (a'), the branching depth (a'') and branching points (a''') did not differ significantly between the two genotypes (two-tailed t-test: filament length: $t(18)=0.61$, $p=0.550$, branching depth: $t(18)=0.96$, $p=0.350$, branching points: $t(18)=1.14$, $p=0.268$, $N=10$ cells of five independent animals per genotype, $\alpha=0.05$), although the cKO showed slightly higher values in all categories. B: Example of DCX filament analysis of branching depth, b': control, b'': cKO. C: Properties of Nestin positive stem cell filaments in 15 week old mice: length (c'), branching depth (c'') and branching points (c''') were comparable between both genotypes despite slightly higher values in all categories for the cKO (two-tailed t-test: length: $t(25)=1.56$, $p=0.132$; branching depth: $t(16.53)=1.00$, $p=0.332$; branching points: $t(14.09)=1.59$, $p=0.135$, $N=13-14$ cells per genotype from two independent animals per genotype, $\alpha=0.05$). D: Example of Nestin filament analysis of branching depth, d': control, d'': cKO. Values given as mean \pm sem.

The cKO revealed a slightly more complex arborisation of the protruding filament, but did not reach the level of significance. The analysis of the Nestin positive filaments is graphed in figure 48Cc'-c'''. Here, the Ki-67 and Sox2 staining helped to localise the associated cell

3. Results

body of the filament (Fig. 48Dd'-d''). The same properties and genotypes as in the Doublecortin filament quantification were used for the Nestin filament quantification. The mean filament length of the control was $97.56 \pm 7.89 \mu\text{m}$ and $121.50 \pm 13.53 \mu\text{m}$ in the cKO. The quantification of the branching depth resulted in 1.57 ± 0.17 steps for the control, and 2.00 ± 0.39 steps for the cKO, the number of branching points was 1.57 ± 0.17 in the control, and 2.54 ± 0.58 in the cKO. Although the cKO results were higher in number regarding filament length, branching depth and number of branching points, the values did not reach the level of significance within the mean analysis of the filament properties (two-tailed t-test: length: $t(25)=1.56$, $p=0.132$, branching depth: $t(16.53)=1.00$, $p=0.332$, branching points: $t(14.09)=1.59$, $p=0.135$, $N=13-14$ cells per genotype from two independent animals per genotype, $\alpha=0.05$). Similar to the Doublecortin filament results, the cKO displayed slightly longer and more complex Nestin filaments within the dentate gyrus than the control, but also without reaching level of significance.

The iIN specific Reelin knockout featured slightly longer and more complex filaments in young granule cells (Doublecortin) and precursor cells (radial glial like cells, Nestin). But both analyses did not diverge enough to reach the level of significance in the performed statistical analysis.

Summary

The established iIN specific conditional Reelin knockout ($\text{ReIn}^{\text{flox/flox}}$ Dlx5/6-Cre positive) mouse line was analysed in various parameters previously shown to be altered in the natural mutant, the *reeler* mouse, or the heterozygous *reeler* mouse, mainly focused on the dentate gyrus and adult stages. The conditional knockout of Reelin was achieved in all inhibitory interneurons, born in the ganglionic eminences which includes all Reelin-expressing inhibitory interneurons of the forebrain. Thus the Reelin depletion in iIN was 100 % whereas other Reelin sources were not affected and expressed Reelin along the timely and spatial schedule comparable to wild type mice. The strongest Reelin depletion was quantified for the neocortex, where the amount of persisting Reelin protein was as low as 7 %. The effect in the hippocampus was lower and Reelin was still present around 50 %. In the inhibitory interneuron specific Reelin knockout, the gross morphology of the main affected brain structures in the *reeler* mouse, like the cerebellum, neocortex, and hippocampus were not affected at all. In the dentate gyrus, where granule cell dispersion and incorrect orientation of cell bodies and filaments were found previously in the *reeler* mouse or other Reelin depletion

3. Results

experiments, none of these impairments could be found in the inhibitory interneuron specific conditional Reelin knockout. Regarding basic behaviour, such as anxiety, locomotor activity, exploration, social abilities, working memory, and spatial long term memory, no severe differences had been revealed by the testing. From gross unchanged structures to smaller entities, quantifications of cell numbers revealed differences. The iIN specific Reelin knockout presented a higher number of Reelin-expressing Cajal-Retzius cells along the hippocampal fissure and lower numbers of interneurons in the hilar area. Stainings against cannabinoid receptor 1 and Calretinin resulted in more intense staining within the inner stratum moleculare and a higher cell number count of Calretinin expressing cells within the hilus. Having been stained with the same markers, these results could not be found in the $ReIn^{wt/dl}$ mice, which resemble the heterozygous *reeler*. Thus, the observed effects were due to the cell-specific depletion in inhibitory interneurons and not based on an overall Reelin depletion. The adult neurogenesis, which depends on an intact stem cell niche structure and a pool of progenitor cells dividing when needed, was found severely impaired in *reeler* mice, but totally unchanged within the iIN specific Reelin knockout, despite the fact that Reelin-expressing interneurons were located within the stem cell niche in close proximity to progenitor cells and young neurons of different maturation stages. Quantifications with BrdU and Ki-67 resulted in statistically insignificant differences regarding numbers of proliferating cells. Although a slight tendency to lower cell numbers in the two BrdU quantifications were present, again below the significance threshold. The refinement of BrdU application via drinking water led to higher staining quality and quantity and turned out to be an easier way for administration. Factors to consider within such an experiment were the housing conditions and drinking habits of the different genotypes. The analysis of cell properties, such as filament length, branching depth and branching points for progenitor cells and immature neurons, based on the known influence of Reelin on the cytoskeleton, revealed no statistically significant differences, but a tendency to slightly longer and more complex filaments in the iIN specific Reelin knockout. All effects found in the iIN specific Reelin knockout were small and often failed to achieve statistical significance, with the exception of the considerably higher expression of cannabinoid receptor 1 and Calretinin in the inner stratum moleculare, the higher cell numbers of Calretinin expressing cells in the hilar area, and the higher cell numbers of Cajal-Retzius cells along the fissure of the dentate gyrus.

4. Discussion

4. Discussion

4.1. Establishment of an interneuron specific conditional Reelin knockout mouse line with a non inducible loxP/Cre system

A numerous variety of *reelin* mouse mutants and conditional knockout lines (review by D'Arcangelo and Curran 1998; Bock and May 2016) are available nowadays. The most of them, spontaneous or targeted, inherit a gene or protein modification or address the Reelin canonical pathway, but none of these mouse lines provided a targeted depletion of Reelin in inhibitory interneurons, being the main adult Reelin source (Alcántara et al. 1998). To address diverse questions of the interplay and effects of Reelin from inhibitory interneurons in the adult brain without affecting the normal development and avoiding regular substance application, an interneuron specific conditional knockout had to be created. The loxP/Cre system was chosen, as it is well established and delivers reliable results (review by Nagy 2000; Kos 2004). The provided floxed mouse line *Reln*^{lox/lox} by Joachim Herz and Hans Bock (Lane-Donovan et al. 2015) contains the loxP nucleotide sequence around the exon 1 (Fig. 17) of the *reelin* gene (D'Arcangelo et al. 1995). This position was chosen, as the exon 1 of the *reelin* gene contains the information for a signalling peptide important for the secretion of the Reelin protein (D'Arcangelo et al. 1995). The sequencing results of the *Reln*^{lox/lox} mice illustrated the exact positions of the two inserted loxP sites encompassing the exon 1 and the adjacent promoter and enhancer region. The sequence was homologue to the human *reelin* promoter and enhancer region containing also its three transcription factor binding sites (Chen et al. 2002; Grayson et al. 2006). The transcription factor binding sites from the mouse *reelin* gene (Royaux et al. 1997) were likewise detectable in the nucleotide sequence. Hence, the modification of transcription was generally possible. The 3' loxP site was located proximal to the end of exon 1 sequence within the following intron, thus the epitope of antibody G10, which was the Reelin antibody used in this study, was unaffected (Royaux et al. 1997; de Bergeyck et al. 1998). The functionality of the loxP sites was shown by breeding the *Reln*^{lox/lox} mouse line with the CMV-Cre mouse line (Schwenk et al. 1995) resulting in an ubiquitous Reelin depletion and a *reeler* like phenotype, in this work addressed as deleter (*Reln*^{dl/dl}). To achieve the inhibitory interneuron specific depletion of Reelin, the *Dlx5/6*-Cre mouse line (Monory et al. 2006) was chosen. The *Dlx5/6* promotor is exclusively active in interneurons emerging from the ganglionic eminence (Zerucha et al. 2000; Ruest et al. 2003; Morozov et al. 2009). The often used calcium calmodulin-dependent protein kinase type II

4. Discussion

(CaMK II)-Cre mouse line was no option at all, as CaMK II is also expressed in non GABAergic neurons (Benson et al. 1992; Bayer et al. 1999) and therefore might have caused undesired effects. With this combination of loxP sites and Dlx5/6-Cre recombinase in the new established mouse line, it was feasible to address the differentiation of the effects of Reelin secreted by Cajal-Retzius cells and inhibitory interneurons. Despite the fact, that the loxP/Cre system is quite effective and widely used, it comes with flaws of the Cre recombinase like maternal inheritance influence (Eckardt et al. 2004) and sometimes inadvertent expression in other tissues (Heffner et al. 2012). In this study the maternal inheritance influence, which finds expression in spontaneous Cre recombinase activity in the female germline, was controlled by strict paternal inheritance of the Cre recombinase. A study of random Cre recombinase expression of the Dlx5/6-Cre along the whole organism was not performed due to the brain focus of this study. Some pronounced expression is expected in the developing limbs, skeletal elements and the tissue between the digits (Simeone et al. 1994; Robledo et al. 2002; Ruest et al. 2003; Díaz-Mendoza et al. 2013). Nevertheless, an analysis of Dlx5/6-Cre recombinase activity in other tissues should be performed to reveal off-target effects.

4.2 Specificity and effectiveness of the loxP/Dlx5/6-Cre system

Reelin-expressing cells have been found in the brain areas of olfactory bulb, neocortex, hippocampus, substantia nigra, ventral tegmental area, nucleus of the optic tract and the cerebellum (D'Arcangelo et al. 1995; Ikeda and Terashima 1997; Schiffmann et al. 1997; Alcántara et al. 1998; Pesold, Impagnatiello, et al. 1998; Ramos-Moreno et al. 2006). Whereas the expression of Reelin in the cerebellum vanishes until it is gone around P24 of the mouse life (Miyata et al. 1996). This expression pattern could be confirmed by immunohistochemical staining against Reelin in wild type mice of the $Rein^{lox/lox}$ Dlx5/6-Cre mouse line. The staining of the iIN specific conditional Reelin knockout showed depletion of Reelin in the neocortex and partly depletion in the hippocampus. Unchanged expression was found in olfactory bulb, substantia nigra, ventral tegmental area and the nucleus of the optic tract. This is due to the fact that iIN are the main Reelin source in the neocortex and hippocampus, in the latter besides the Cajal-Retzius cells (Ogawa et al. 1995; Pesold, Impagnatiello, et al. 1998). The cell types expressing Reelin in other brain areas are not inhibitory or IN, like the mitral and tufted cells in the olfactory bulb (Schiffmann et al. 1997; Ramos-Moreno et al. 2006), the stellate cells of layer II in the entorhinal cortex (Unal et al. 2015; Basu et al. 2016) and the Cajal-Retzius cells in the hippocampus (Ogawa et al. 1995).

4. Discussion

The absence of expression in both genotypes in the cerebellum is due to the loss of expression of Reelin until P24 in this region (Miyata et al. 1996). The specificity of the loxP/Dlx5/6-Cre system depleting Reelin expression just in iIN was confirmed by breeding the tdRFP expressing reporter mouse line by Hans Jörg Fehling (Luche et al. 2007) with the $ReIn^{flox/flox}$ Dlx5/6-Cre mouse line. The cells of the descendants of this breedings, which underwent DNA recombination by the Cre recombinase, subsequently expressed a tdRFP marking them red. The immunohistochemical staining against Reelin in this reporter mice proved, all Reelin-expressing cells in the neocortices of the wild type were also marked with tdRFP and with that identified as iIN. The tdRFP was also present in the neocortices of the iIN specific conditional Reelin knockout, but all red marked cells were ir negative for Reelin. In the dentate gyrus, two Reelin sources were found: the Cajal-Retzius cells, negative for tdRFP, distributed around the hippocampal fissure (Anstötz et al. 2016) and the iIN distributed all over dentate gyrus area (Danglot et al. 2006). All other cells ir positive for Reelin, apart from Cajal-Retzius, were red marked in the dentate gyrus of the wild type, but negative for Reelin in the iIN specific conditional Reelin knockout. Whereas Cajal-Retzius cells showed clear ir for Reelin in both genotypes. The data verified that the loxP/Dlx5/6-Cre system depleted Reelin expression exclusively in iIN and with a 100 % efficiency, while all other sources (e.g. Cajal-Retzius cells, mitral cells, bitufted cells, stellate cells (not shown) (Ogawa et al. 1995; Schiffmann et al. 1997; Ramos-Moreno et al. 2006; Unal et al. 2015) stayed unaffected. However, an inducible loxP/Cre system could at best reach an efficiency of 80-90 % depletion and is strict dosage dependent with the danger of intoxication (Hayashi and McMahon 2002). Additionally, some after treatment activity of the Cre recombinase had been reported by Reinert (Reinert et al. 2012) and this might cause undesired side effects. Since the Dlx5/6-promotor is used in embryonic development (Simeone et al. 1994; Acampora et al. 1999; Ruest et al. 2003) the depletion of Reelin in iIN should be present in the developing dentate gyrus. The immunohistochemical staining against Reelin in P3, P6 and P10 old wild type mice of the $ReIn^{flox/flox}$ Dlx5/6-Cre line illustrated the switch of Reelin expression from Cajal-Retzius cells to iIN around P5 to P7 in the dentate gyrus (Alcántara et al. 1998). The quite strong Reelin expression at P3 in Cajal-Retzius cells declined reciprocally with age while at P6 a faint expression of Reelin was detectable in the hilus of the dentate gyrus increasing reciprocally with age. The iIN specific conditional Reelin knockout showed the same declining pattern regarding Reelin expression in Cajal-Retzius cells but no arising Reelin expression in the hilus of the dentate gyrus around P6. So the embryonic DNA recombination

4. Discussion

in iIN of the $ReIn^{flox/flox}$ $Dlx5/6$ -Cre line was effective. Immunohistochemical stainings are, even if precisely performed after the same protocol and under the same conditions, not optimally suited to acquire quantitative data regarding protein expression. Thus, to quantify Reelin levels in the neocortex and hippocampus, Western blotting for seven different genotypes from the $ReIn^{flox/flox}$ $Dlx5/6$ -Cre and the $ReIn^{flox/flox}$ CMV-Cre line was performed. The results were quite interesting and somehow unexpected. While the wild types, the heterozygous genotypes and the deleter genotype showed expected or the lack of expression levels of the different Reelin fragments stained, the iIN specific conditional Reelin knockout revealed a remnant of Reelin protein in the neocortex of 6.8 %, but surprised with a rather high remaining amount of 53.57 % compared to the control in the hippocampus. Assuming that there was a total depletion of Reelin in iIN as indicated by the immunohistochemical staining results, the reason for this still high expression level in the hippocampus must be found in the only remaining Reelin source, the Cajal-Retzius cells. At that point it seemed as there was either some autocrine effect (Coulin et al. 2001) of Reelin on Cajal-Retzius cells inducing a compensatory reaction or a developmental reason, maybe depending on an altered brain-derived neurotrophic factor (BDNF) expression in Cajal-Retzius cells (Ringstedt et al. 1998). This was a quite surprising result, but just shown for the three fragments, which were detectable with the used G10 antibody. As the Reelin protein contains two cleavage sites for posttranslational modification, a cleavage results in up to five different fragments: the N-terminal part, the single central part, the C-terminal part or the central with N- or C-terminal part. The N-terminal part of the protein contains the G10 epitope (Fig. 2) (de Bergeyck et al. 1998) and with that, just these fragments plus the full length protein are detectable by the G10 antibody. Annotation, even if it is general use to quantify the Reelin protein amount with the G10 antibody (Courtès et al. 2011), a Western blot analysis with antibodies recognising C- and central part of the Reelin protein should be performed to check, if the former results are mirrored for this fragments.

4.3 Unaltered gross brain morphology and cytoarchitecture in the interneuron specific conditional Reelin knockout mouse line

The impacts of Reelin on mouse brain development and especially on brain architecture is well described in literature (Hamburgh 1963; Caviness and Sidman 1973; Caviness 1976; Mariani et al. 1977; Stanfield and Cowan 1979a; Ogawa et al. 1995; Tissir et al. 2002; Badea et al. 2007; Miyata et al. 2010; Boyle et al. 2011). The major impairments besides the smaller

4. Discussion

brain size and weight (Badea et al. 2007) are an inverted or mirrored cell layering in the neocortex (Hamburgh 1963; Caviness 1976; Ogawa et al. 1995; Tissir et al. 2002; Boyle et al. 2011), a irregular formed pyramidal cell layer and scattered distribution of granule cells in the hippocampus (Hamburgh 1963; Caviness and Sidman 1973; Stanfield and Cowan 1979a; Boyle et al. 2011), plus a hypoplastic cerebellum, lacking the typical foliation of Purkinje and granule cells (Hamburgh 1963; Mariani et al. 1977; Miyata et al. 2010). Whereas the heterozygous *reeler* mouse shows a normal outward appearance of the brain and just subtle changes in cytoarchitecture of the brain structures like less Purkinje cells in the cerebellum (Biamonte et al. 2009; Magliaro et al. 2016), smaller numbers of GAD67 and PV positive neurons in the hippocampus (Pappas et al. 2001; Nullmeier et al. 2011), fewer dendritic spines in cortical areas and hippocampus (Pappas et al. 2001), less PV positive cells in the amygdala (Macrì et al. 2010) and striatum (Ammassari-Teule et al. 2009) and an accumulation of nicotinamide-adenine dinucleotide phosphate-diaphorase-d positive neurons in the subcortical white matter (Tueting et al. 1999). Brains of a C57BL/6J, female and male brains of the iIN specific conditional Reelin knockout and the brain of a heterozygous genotype ($ReIn^{wt/flox}$ Dlx5/6-Cre positive) were compared regarding their outward appearance and forms of visible brain structures, which were similar. The *reeler* brain, on the other hand, exhibited a smaller general size and a clear dysplasia of the cerebellum due to developmental defects. The brain weight given for the *reeler* was 0.1 g (25 %) lightweight compared to all others, the iIN specific conditional Reelin knockout brains differed in a range from 0.07 (4 %) to 0.02 g (12 %) of less weight and the heterozygous genotype was 0.04 g (8 %) lightweight compared to the wild type (100 %). These results are comparable with the study of Badea (Badea et al. 2007), which reports a general volume loss in the *reeler* of 19 % and for the heterozygous genotype 6 %. The range of brain weights of the iIN specific conditional Reelin knockout were comparable to the heterozygous *reeler* mouse brain. Regarding the deviations, it should be considered that both studies are based on different background strains. The immunohistochemical staining against NeuN, Brn2 (transcription factor, mainly expressed in layer II) (Sekine et al. 2011) and FoxP2 (Forkhead-Box-Protein P2, mainly expressed in layer II to IV) (Ferland et al. 2003) revealed no gross cytoarchitectonical impairments in the different brain areas of the iIN specific conditional Reelin knockout. The cortical layering, the size of the cerebellum and its foliation, the formed pyramidal and granule cell layer in the hippocampus appeared normal and similar to the wild type cytoarchitecture. The deleter brain, as ubiquitous *reelin* knockout, resembled the *reeler* brain in gross cytoarchitectonical

4. Discussion

composition and layering. So far the brain development and cytoarchitecture appeared unaltered in the iIN specific conditional Reelin knockout. It could therefore be concluded that Reelin of iIN has no functional part in terms of development, especially layering. The performed immunohistochemical staining analysis illustrates just the general visible structures of the different brain areas according to marker proteins, it provided no indication about the cell composition and connectivity in the different brain areas. To exclude the faintest influence on development, as for example found for the heterozygous *reeler* mouse (Pappas et al. 2001; Ammassari-Teule et al. 2009; Biamonte et al. 2009; Macrì et al. 2010; Nullmeier et al. 2011; Magliaro et al. 2016), cell type composition analysis and connectivity investigations should be performed.

4.4 Lack of granule cell dispersion in the interneuron specific conditional Reelin knockout mouse line

In 2002 the study of Haas (Haas et al. 2002) associated the developmental defect of granule cell dispersion (GCD), an over migration of granule cell (GC) neurons into the molecular layer of the dentate gyrus and typical finding in temporal lobe epilepsy (TLE) patients (Houser 1990), with a diminished expression of *reelin* mRNA in Cajal-Retzius cells of human brains (Haas et al. 2002). Supporting this results, the investigation of Heinrich (Heinrich et al. 2006) about the role of adult neurogenesis on GCD, concluded a direct correlation between the induced GCD and the measured decrease in Reelin mRNA synthesis. The review by Haas and Frotscher (Haas and Frotscher 2010), compared the GCD of TLE patients with the anatomical appearance of the *reeler* mouse DG and mentioned the experiments of Nakajima (Nakajima et al. 1997), where the intraventricular injection of the CR50 antibody against Reelin (Ogawa et al. 1995) in the ICR mouse strain led to an impaired development and resulted in a *reeler* like disorganisation of the cell layers in the different brain areas, especially in a slight cell dispersion in the pyramidal cell layer. Duveau (Duveau et al. 2011) added to the GCD topic their findings of an abnormal Reelin processing in Cajal-Retzius cells controlled by the brain-derived neurotrophic factor (BDNF) in mice and Freiman (Freiman et al. 2011) showed an alteration of dendritic furcation and spine density of GC in TLE brains of human patients. In 2016 Orcinha (Orcinha et al. 2016) illustrated that after Kainate injection in organotypic hippocampal slice cultures, the Reelin expression was lost in hilar inhibitory interneurons and GC started migrating into this area. Taken together, these previously published data interrelated GCD and abnormal dendritic furcation and spine density with a

4. Discussion

significant Reelin mRNA deficiency or a loss of Reelin-expressing cells. The exploration of a GCD induction by the loss of Reelin in iIN in the iIN specific conditional Reelin knockout in this study resulted in no detectable GCD. Neither the analysis of arrangement of ThylGFP positive granule cells (resulting from a breeding with the ThylGFP mouse (Feng et al. 2000)) nor the measurement of the GC layer thickness revealed a cell dispersion. A similar result was published by Lane-Donovan (Lane-Donovan et al. 2015), investigating the $ReIn^{flox/flox}$ mouse bred with an inducible Cre mouse line. How to interpret these diverse results? The before mentioned publications induced the GCD via injection of Kainate (Heinrich et al. 2006; Duveau et al. 2011; Orcinha et al. 2016) or showed the reduction of mRNA via in situ hybridization (ISH) or real time PCR in TLE patients (Haas et al. 2002), while Nakajima injected the CR50 antibody against Reelin (Ogawa et al. 1995) in embryonic stages and blocked the canonical Reeling signalling pathway during development (Nakajima et al. 1997). A discrimination between Cajal-Retzius cell-derived Reelin and iIN derived Reelin was not performed and led to the following hypotheses: Reelin from Cajal-Retzius cells, but not from iIN is necessary to establish and maintain the granule cell layer. This is supported by the study of Nakajima (Nakajima et al. 1997), as the injected CR50 antibody was described to mainly recognise Cajal-Retzius cells (Ogawa et al. 1995) and with that presumably tagging just Cajal-Retzius cell derived Reelin protein. This is not unlikely as Furlanis (Furlanis et al. 2019) reported that even closely related cells produce transcript isoforms of the same protein. In the iIN specific conditional Reelin knockout mouse the Reelin expression from Cajal-Retzius cells is unaltered and with that present to establish and maintain the GCL and prevent GCD. The second hypothesis is that the injection of Kainate triggers a special pathway inducing GCD and the reduction of Reelin expression. Considering Ringsted and Duveau (Ringstedt et al. 1998; Duveau et al. 2011), describing an influence of BDNF on the expression level of Reelin in Cajal-Retzius cells, and the studies by Suzuki and Guilhem (Suzuki et al. 1995; Guilhem et al. 1996), illustrating an overexpression of BDNF after Kainate injection in the hippocampus plus the study by Scharfman (Scharfman et al. 2005), showing an increase of adult neurogenesis and ectopic GC positioning after BDNF injection in the hippocampus, one could speculate of an other causal correlation to the appearance of the GCD than Reelin loss triggering the motility and outward migration of GC.

So far the collected and presented data up to that point did not indicate any influence of Reelin expressed by inhibitory interneurons on the brain development, the morphogenesis or

4. Discussion

the cytoarchitecture of brain compartments. Yet, subtle changes in cell numbers and cell composition or connectivity cannot be ruled out. Alterations in the connectivity and physiological variations might be mirrored, if severe, in abnormal behaviour.

4.5 Normal behaviour pattern of the interneuron specific conditional Reelin knockout mouse line

Behavioural testing is a common way to look for cognitive impairments in new established mouse lines or mutant lines. The testing paradigms are quite various and sensitive regarding background strain, used controls and handling (Lewejohann et al. 2006; Crawley 2007; Wahlsten 2011). One has to consider, if the used background strain is vulnerable e.g. for blindness, deafness or other physical handicaps falsifying or interfering with the behavioural testing (Crawley 2007; Wahlsten 2011). Concerning the homozygous *reeler* mice, physical tests are difficult to perform as this mutant suffers from severe ataxia. In contrast, the heterozygous *reeler* mice are physically unimpaired and therefore widely used for studies addressing e.g. pathological alterations in schizophrenia, bipolar disorder, autism and Alzheimer's disease (Moy et al. 2004; Krueger et al. 2006; Teixeira et al. 2011; Lane-Donovan et al. 2015). The variety of studies and tests used are mirrored in different and sometimes contradictory results. For example, while Salinger, Podhorna, Teixeira, Michetti and Schroeder (Salinger et al. 2003; Podhorna and Didriksen 2004; Teixeira et al. 2011; Michetti et al. 2014; Schroeder et al. 2015) found no significant difference between the heterozygous *reeler* mice (HRM) and wild type mice, Tueting (Tueting et al. 1999) reported a diminished prepulse inhibition and less entries into open arms in the elevated plus maze for the HRM, Qiu (Qiu et al. 2006) found a reduced learning ability in the context fear conditioning, Ognibene (Ognibene et al. 2007) showed less anxiety, less impulsivity control and less exploration of a novel object for the HRM. Lane-Donovan (Lane-Donovan et al. 2015), having tested the here used $ReIn^{flox/flox}$ line bred with a tamoxifen inducible Cre recombinase, reported a slightly reduced anxiety in the open field, quite similar results for the elevated plus maze, a small increase in the prepulse inhibition, but no differences in the Morris water maze and context/cued fear conditioning. Comparing all these studies, one might assume there are no clear results for altered behaviour in the HRM. Taking a closer look to all these studies, it has to be mentioned that the used background strains and the paradigms of the tests differed conspicuously. Thus, comparing and interpreting these studies is quite difficult. Nonetheless, it emerged that the highest probability of finding altered

4. Discussion

behaviour might be in the anxiety-related behaviour, locomotor activity and exploration, social interaction, memory and learning. Therefore the iIN specific conditional Reelin knockout was tested for all five categories in two experimental blocks or groups. The first block contained iIN specific conditional Reelin knockout mice compared to wild type mice covering the categories of anxiety-related behaviour (elevated plus maze, open field), locomotor activity and exploration (open field, 2-object novel object recognition), social interaction and working memory (Y-maze spontaneous alternation, 2-object novel object recognition and three chamber sociability and social novelty). No significant differences were found in the behavioural tests and revealed the basic general behaviour being unaltered. The second block contained all three control genotypes for comparison: the wild type ($Reelin^{wt/wt}$ $Dlx5/6$ -Cre negative), the genotype just expressing Cre recombinase, $Reelin^{wt/wt}$ $Dlx5/6$ -Cre positive (abbreviated as Cre, to check for Cre effects) and the $Reelin^{flox/flox}$ genotype comprising the loxP sites but no Cre recombinase (abbreviated as flox, to check for loxP site effects). The Morris water maze paradigm was performed without the wild type animals to facilitate the handling, to ensure a fluent run of the extensive test and to focus on the most important controls (cre and flox). The second group or cohort 1 passed tests for anxiety-related behaviour, locomotor activity and exploration (elevated plus maze, open field) and for learning, spatial and long term memory (Morris water maze). The principle tested with the different paradigms did not result in a significant difference for the genotypes and indicated no aberrant behaviour of the cKO compared to the controls, especially the littermate control flox. However, it can not be excluded that undetected, subtle effects are present in the cKO, which might become more important under pathological conditions and then might lead to a significant change in behaviour.

As the behavioural testing did not reveal any severe alterations in the iIN specific conditional Reelin knockout, the focus of investigation was set on the hippocampus. This brain compartment is severely affected in terms of cell layering, connectivity on spine level and adult neurogenesis in the *reeler* mouse and has a particularly meaning as switch point of learning, integration and formation of new memory. Additionally, it is the only brain compartment still containing numerous Cajal-Retzius cells and interneurons in adulthood to analyse the interplay of both sources.

4. Discussion

4.6 Higher cell numbers of Cajal-Retzius cells in the dentate gyrus of the interneuron specific conditional Reelin knockout mouse line

Cajal-Retzius (CR) cells are the first and main Reelin source during brain development (Derer and Derer 1990; D'Arcangelo et al. 1995; Ogawa et al. 1995; Marín-Padilla 1998). They are distributed in a special pattern along the neocortex layer I and the molecular layer of the hippocampus surrounding the hippocampal fissure (Griveau et al. 2010; Barber et al. 2015; Anstötz et al. 2016). They are morphologically characterised as horizontal oriented cells of a small, ovoid soma sprouting on one pole a thick main dendrite, branching to third level and covered with filopodial protrusions (Ogawa et al. 1995; Anstötz et al. 2016). Any interferences with their development or Reelin expression results in altered cell positioning in the neocortex or hippocampus (Del Río et al. 1997; Nakajima et al. 1997; Supèr et al. 2000). In the neocortex of the mouse brain, the number of Cajal-Retzius cells starts to decrease due to apoptotic cell death around P8 (Derer and Derer 1990) until they are 95 % gone (Chowdhury et al. 2010; Kilb and Frotscher 2016). In the hippocampus, they persist until late adulthood quite numerousness of 15-20 % of original numbers (Anstötz et al. 2016). Investigations in the *reeler* mouse delivered some contradictory results regarding CR cell numbers in the hippocampus. While Coulin (Coulin et al. 2001) counted more remaining CR cells in the *reeler* hippocampus, Anstötz (Anstötz et al. 2019) found less CR cells and Derer (Derer 1985) had no difference in cell numbers at all, but a higher density of cells. The last result was confirmed by Anstötz (Anstötz et al. 2019), measuring a higher cell density at the tip of the dentate gyrus around the hippocampal fissure of *reeler* mice. Based on the already published literature and regarding the high amount of Reelin protein left in the hippocampus of the iIN specific conditional Reelin knockout (cKO) (see Fig. 24), a quantification of CR cells in the cKO and heterozygous deleter mice ($Reln^{wt/dl}$) was performed. The $Reln^{wt/dl}$ resembles the HRM, as they inherited one defective *reelin* allele and therefore express just 50 % (see Fig. 24) of the Reelin protein from the beginning of development in all Reelin-expressing cells. This genotype was analysed to examine, if an overall reduction of Reelin protein elicits the same effects as found in the cKO. The quantification results were quite surprising. The number of Reelin-expressing CR cells in the cKO was significantly higher than in the wild type, but the heterozygous mice were counted with less CR cells compared to the wild type, although not significant. These results indicate three conclusions: first, the higher amount of Reelin protein measured in the cKO hippocampus was due to a higher number of Reelin-expressing CR cells along the hippocampal fissure in the dentate gyrus.

4. Discussion

Second, the longer persistence or the recruiting of more cells expressing Reelin in the cKO hippocampus, which was not detected in the heterozygous deleter and therefore not due to a general depletion of Reelin quantity, implicate a direct coherence of the depletion of Reelin in inhibitory interneurons. Third, the fact that the first Reelin source persisted longer and expressed Reelin, implicates an autocrine effect of Reelin on the CR cells, to regulate its own expression to compensate for the loss of interneuron derived Reelin. One thing can be stated without doubt, the higher numbers of Reelin-expressing CR cells is coherent to the cell-specific depletion in inhibitory interneurons and was responsible for the higher amount of Reelin protein measured in the hippocampus. If the previously discussed absence of a granule cell dispersion (GCD) is added to this deliberations, it seems feasible to assume that the Reelin protein secreted by CR cells might be the key factor to keep the layer architecture of granule cells intact. In conclusion, one could assume that to maintain layer integrity, it was essential to induce either surviving or recruiting of CR cells or upregulate Reelin production, whichever is correct. It remains unclear, if every CR cell of the cKO produces a comparable amount of Reelin protein, as in the wild type cells. It would be interesting to separate the CR cells from the cKO using, for example, CXCR12-eGFP mice (Anstötz et al. 2016), separate the cells with fluorescent activated cell sorting and quantify the Reelin protein amount produced. Additionally there are some other points to think of. It was shown by Ringsted (Ringstedt et al. 1998) that BDNF modulates Reelin expression in CR cells. It would be quite interesting to measure BDNF levels and start some stimulation experiments with cultured CR cells, to see in which dimensions BDNF changes Reelin expression and if BDNF protein level is responsible for the higher Reelin expression in the cKO. Another point to think about are the numbers of CR cells along the hippocampal fissure. Anstötz (Anstötz et al. 2019) presented data about the region specific distribution density of CR cells and its alterations in the *reeler* mouse and Villar-Cerviño (Villar-Cerviño et al. 2013) published the mechanism of contact repulsion mediated via ephrin signalling pathway, which underlies the distribution of CR cells. One might speculate that Reelin, or better the absence of Reelin, influences the distribution pattern of CR cells along the hippocampal fissure, as it was shown that Reelin protein binds to ephrin B receptors and induces ephrin signalling pathway (Bouché et al. 2013). If this influence is present in the cKO, it might be an explanation for the higher cell numbers of CR cells along the hippocampal fissure. But this hypothesis is just useful, if there is a difference between the Reelin protein derived by CR cells and iIN, similar as reported by Furlanis (Furlanis et al. 2019). Concerning the higher cell numbers of Reelin-expressing CR

4. Discussion

cells the question arises, if they persist longer or if just more CR cells were recruited to express Reelin protein. It would be interesting to investigate this fact, as it is strongly connected to the question, if Reelin has an autocrine effect on CR cells, like it has on cells in a neuroblastoma (Becker et al. 2012). So, a time line screening and quantification with apoptotic marker proteins to follow up apoptosis of CR cells in the hippocampus and neocortex of cKO mice might be an interesting experiment. One hypothesis published about the apoptosis of CR cells was the influence of increased calcium influx via the N-methyl-D-aspartate (NMDA) receptor (Mienville and Pesold 1999). This is interesting in that Reelin can change the calcium influx via the NMDA receptor (Chen et al. 2005). To evaluate this influence, the appropriate method would be to perform some two-photon calcium imaging within hippocampal slice cultures (Stoppini et al. 1991), also using a protocol with chemical NMDA receptor antagonist, e.g. 2-amino-5-phosphonopentanoic acid (APV) (Chen et al. 2005). Besides, as the effect is specific for the loss of Reelin from iIN, it would be interesting to investigate the influence of GABAergic interneurons connected to CR cells (Anstötz et al. 2016) on the calcium influx and in succession, possible induction of apoptosis. The coherence of interneuron specific Reelin depletion and the higher numbers of Reelin-expressing CR cells in the hippocampus along the hippocampal fissure of the cKO poses new questions about interrelations and influences on Reelin expression, calcium influx and cell survival. This also led to the question: what about the second Reelin source in the hippocampus, the inhibitory interneurons?

4.7 Distribution and cell numbers of inhibitory interneurons in the interneuron specific conditional Reelin knockout mouse line

The inhibitory interneurons (iIN) are an important part of the brain network (Kepecs and Fishell 2014). They originate from the ganglionic eminences (GE), emerge at embryonic (E) day 9 and migrate tangentially and radially to their later positions (Soriano et al. 1989a, 1989b; Danglot et al. 2006; Morozov et al. 2009; Tricoire et al. 2011; Kepecs and Fishell 2014; Torigoe et al. 2016). This group of inhibitory cells contains a high variability of cell types, which are distinguishable by location, morphology, electrophysiology and marker proteins (Ribak and Seress 1983; Freund and Buzsáki 1996; Danglot et al. 2006; Hosp et al. 2014; Kepecs and Fishell 2014; Wamsley and Fishell 2017; Lim et al. 2018; Mi et al. 2018). Their distribution and combination within a brain area is region specific (see Fig. 6, Fig. 7 and Fig. 8 in introduction for comparison). The expression of Reelin in iIN starts in the neocortex around E18 and increases continuously reciprocally to the decline in CR cell numbers (Alcántara et al. 1998) until they are the main Reelin source in the adult forebrain. In the

4. Discussion

hippocampus, as previously mentioned, the Reelin expression in iIN starts around P5 (Alcántara et al. 1998). In contrast to the neocortex, where iIN are nearly the exclusive Reelin source in the adult brain, iIN are just part of the Reelin-expressing cells in the hippocampus, together with the CR cells, which persist here into adulthood (Alcántara et al. 1998; Pesold, Impagnatiello, et al. 1998; Pesold, Pisu, et al. 1998; Anstötz et al. 2016).

4.7.1 Analysis of Reelin-expressing inhibitory interneuron cell numbers in the dentate gyrus

The difference found in the numbers of CR cells in the cKO and the heterozygous deleter indicated a possible shift in cell numbers of iIN. Therefore, a quantification of Reelin-expressing iIN in the dentate gyrus was performed. The analysis focused on the dentate gyrus, because of the differences in CR cell numbers and the higher amount of remaining Reelin protein here. As the distribution density of iIN is different within layers, the quantification was subdivided according to the dentate gyrus anatomical layers. The advantage of the tdRFP reporter, marking iIN red, helped to count overall cell numbers in relation to the Reelin-expressing cells. In the heterozygous deleter, just Reelin-expressing cells were counted because of the lack of an inbred reporter. The collected data from the quantifications showed interesting facts. First of all, it was possible to address a general distribution of iIN along the dentate gyrus layers and the ratio of Reelin-expressing cells to overall iIN cell numbers. The highest density of iIN was found along the subgranular zone (SGZ), the hilar area (hilus) followed by the stratum lacunosum-moleculare (str. lac.-mol.), which is originally part of the Ammon's horn area of CA1. Interestingly, the highest ratio of Reelin-expressing cells to general numbers of iIN were found in the layers with the lowest cell numbers: hippocampal fissure/outer molecular layer (hf/oML) 1:1.6 (10 out of 16 iIN express Reelin) and the inner molecular layer (iML) with 1:1.8. The other layers showed a ratio of 1:2.8 (SGZ and hilus) and 1:2.9 (str. lac.-mol.). It is interesting to speculate, if the higher probability in encountering a Reelin-expressing iIN is connected to the fact that the molecular layer is the area where entorhinal afferents and associational afferents terminate and commissures pass through (Deller et al. 1995; Seress 2007; Witter 2007). One should keep this in mind, as it will be revisited at a later time point. To the results of the cKO it can be noted, that the amount of iIN along the layers was comparable to the wild type with one exception. In the hilar region, the numbers of iIN counted was significant lower than in the wild type. In addition the heterozygous deleter mice (HDM) was used again as a model for a general non-cell-specific

4. Discussion

decrease of Reelin, and interestingly, resulted in different data. In the HDM the numbers of Reelin-expressing cells in the hilus were comparable to the wild type. In the area of the hf, the oML and iML the numbers were quite similar to the wild type, albeit with the tendency to more (hf) and less (o/iML) numbers of Reelin-expressing cells in the HDM. A difference in cell numbers of Reelin-expressing cells was found in the area of the SGZ, which was significant lower in the HDM. The reason, why the loss of Reelin-expressing interneurons is that strong in the SGZ, which is the location of adult neurogenesis (Altman and Das 1965), is speculative. Perhaps, this is a developmental defect similar to the reported iIN cell loss in the HRM (Ammassari-Teule et al. 2009; Macrì et al. 2010; Nullmeier et al. 2011) as the developmental source of Reelin, the CR cells, are affected in the HDM, too. This publications indicate that there might be an influence on the migration of cells from the hilar area to the outer layers. Brunne (Brunne et al. 2013) reported an impairment of the radial glial cell scaffold in the reeler mouse dentate gyrus and speculated about the role during cell migration. It would be interesting to see, if the lack of iIN and their distribution in the HDM resembles, in a way, the ectopic cell positions in the *reeler* mutant, the ApoE or VLDLR knockout dentate gyri (Trommsdorff et al. 1999), and if the radial glial cell scaffold is affected in any way. Immunohistochemical stainings against Brain lipid-binding protein (BLBP) or Nestin, a density distribution analysis along the dentate gyri and a 3D reconstruction of radial glial cells in the $Reln^{flx/flx}$ mice and the $Reln^{wt/dl}$ mice, both with the tdRFP reporter expressed under the *Dlx5/6* promotor, might be an interesting experiment. It would be an asset to have the tdRFP reporter bred in the $Reln^{wt/dl}$ mice in future experiments, because a more precise analysis of iIN numbers in the dentate gyrus would be possible. The data about the number of iIN in the cKO and Reelin-expressing iIN in the HDM are divergent, nevertheless there seemed to be a Reelin effect in both genotypes, but with different impact on the various layers.

The analyses involved overall iIN cell numbers, but did not separate between the different groups of iIN existing in the dentate gyrus. To see, if the cell numbers of the different iIN subgroups had been impaired, another quantification block was started.

4.7.2 Analysis of marker protein defined subgroups of inhibitory interneuron cell numbers in the neocortex and dentate gyrus

As previously mentioned, the subgroups of iIN can be differentiated according to their expressed marker proteins. To see, if a subgroup of iIN was affected to a special degree, the

4. Discussion

next quantification block was done for the most used iIN markers Parvalbumin (PV), vasoactive intestinal polypeptide (VIP), Calbindin (CALB), Calretinin (CRET), glutamate decarboxylase isoform 67 (GAD67) and cannabinoid receptor 1 (CB1) (Danglot et al. 2006) for the neocortex and the dentate gyrus in tdRFP reporter positive mice. As previous data gave an impression of the overall cell numbers of iIN in the dentate gyrus in wild type and cKO mice, the area of the neocortex vertically adjacent to the hippocampus was quantified for overall cell numbers of iIN expressing tdRF reporter protein, to check for a shift in cell numbers. The quantification resulted in comparable numbers between the cKO and the wild type, indicating no cell loss in the neocortical areas. This was mirrored in the subgroup analysis with the different marker proteins. None of the cell numbers was altered significantly. These data represent just the small area of associational cortex. To be sure that no cell loss actually occurred in the neocortex, one should perform similar quantifications in all areas of the neocortex. Nonetheless, these data indicate no effects or alterations regarding cell numbers and amount of cells in the subgroups of iIN in the neocortex. The data of the dentate gyrus revealed a surprising result. Due to the indicated loss of iIN in the hilar area, only this region was quantified. VIP and CALB staining resulted in no signal at all, which might be due to a changed expression pattern in adult iIN, as it is described for other markers (Verdaguer et al. 2015). PV and GAD67 cell numbers in the cKO were comparable to the wild type, although with a slight tendency to more (PV) and less (GAD67) cells. But most importantly, the number of CRET positive cells was significantly increased in the cKO compared to the wild type. Consulting the numbers of tdRFP expressing cells, it was obvious that not the numbers of CRET expressing iIN was elevated, but the numbers of the other cell population expressing CRET in the hilus, the mossy cells (Gulyás et al. 1992; Blasco-Ibáñez and Freund 1997; Schurmans et al. 1997; Fujise et al. 1998). Co-occurring with this fact, a significant higher staining intensity of CRET in the inner molecular layer of the dentate gyrus was found. This staining might be due to an increased CRET amount in the mossy cell commissures passing through this part of the molecular layer (Blasco-Ibáñez and Freund 1997; Scharfman 2016). The same phenomenon was found for the CB1. The staining intensity of the iML was significantly higher in the cKO than in the wild type. Whereas these effects were not found in the HDM, neither the staining intensity of CRET, nor CB1 was altered nor the number of CRET expressing cells in the hilar area. This indicates that the altered staining intensities in the iML and the high numbers of CRET expressing cells in the hilus were a direct sequel of the Reelin depletion in iIN. One explanation for these phenomena might be

4. Discussion

that CRET is expressed in mossy cells (Gulyás et al. 1992) and functions as a non linear Calcium (Ca^{2+}) buffer, meaning it switches from a slow onset buffer at base line Ca^{2+} levels to a fast buffer at high Ca^{2+} levels and is probably a Ca^{2+} sensor (Schwaller 2014). Thus, a higher expression or accumulation of CRET might be due to a stronger need for a buffering molecule in the cell conditioned by a higher Ca^{2+} influx. This influx might be due to a modification of N-methyl-D-aspartate (NMDA) receptor. Chen (Chen et al. 2005) showed in the hippocampus a modulation of the NMDA receptor by Reelin, enhancing the Ca^{2+} influx into the targeted cell. Such a Ca^{2+} influx could also modulate the production of sn-2-arachidonoylglycerol (2-AG) or N-arachidonoyl ethanolamine (AEA) and induce cannabinoid signalling (Rivera et al. 2014). That would start the cascade of the 2-AG or AEA as retrograde messengers, being produced in the presynapse, then released and subsequently interacting with the cannabinoid receptor 1 (CB1) on the postsynapse of neurons, astrocytes or glial cells and there regulating glutamate or γ -aminobutyric acid (GABA) release (Katona et al. 1999; Zhou et al. 2014; Lutz et al. 2015; Araque et al. 2017). This might be a possible scenario, how Reelin influences the amount of CRET and CB1 in the iML. It was shown by Chiu and Catillo (Chiu and Castillo 2008) that mossy cells also express CB1. Since the mossy cell commissures pass through the iML (Blasco-Ibáñez and Freund 1997; Scharfman 2016), it might be possible that the higher staining intensity in the iML layer may result from an accumulation of CRET and CB1 in mossy cell commissures. But it is also possible that the CB1 signal results, also in part, from a higher expression in dendrites of CCK positive hilar iIN, as they also express CB1 (Katona et al. 1999; Monory et al. 2006; Lee and Soltesz 2011). Despite all that, this interactions are based on literature and speculation and has to be proven by additional experiments. One fact can be stated for sure, the higher amount of CRET and CB1 in the iML is due to the Reelin depletion in iIN in the cKO, as it is totally absent in the HDM. It would be interesting to go deeper into this topic, especially in association with temporal lobe epilepsy (TLE) pathology, which is connected to alterations of mossy cell numbers and cannabinoid signalling, for example: mossy cells loss was shown after repeated seizure appearance (Santhakumar et al. 2005), CB1 was upregulated in animals with TLE (Bhaskaran and Smith 2010), cannabinoids were shown to prevent kainic acid induced epileptic seizures (Monory et al. 2006) and were shown to possess an anti-convulsive role in seizures (Bhaskaran and Smith 2010), CB1 expression was shown to be variable in TLE (Maglóczy et al. 2010) and Sun (Sun et al. 2007) found a loss of hilar Somatostatin and NPY in iIN in status epilepticus.

4. Discussion

One could think of experiments like: synaptosome preparation of mossy cell commissures, GC and iIN dendrites terminating in the iML to identify the amount of CB1 expression; paired recordings of mossy cells and iIN with a protocol to induce seizures via stimulating the perforant path; optogenetic modulation of NMDA receptors; treatment of organotypic slice cultures with Reelin to modulate expression of CRET and CB1. The possibilities are various.

4.8 Stem cell niche composition and adult neurogenesis in the iIN specific conditional Reelin knockout

4.8.1 Analysis of stem cell niche composition and integrity

The dentate gyrus is, besides the subventricular zone, a location for adult neurogenesis (Altman and Das 1965). The stem cell niche, origin of new cells, is located at the rim of the granule cell layer adjacent to the hilus (the SGZ) and contains a special composition of cells (Seri et al. 2004; Fuentealba et al. 2012; Morrens et al. 2012; Lin and Iacovitti 2015). The progenitor cell within the stem cell niche is a radial glial like cell (RGL) also known as radial astrocyte or type 1 cell (Kriegstein and Alvarez-Buylla 2009; Encinas et al. 2011), which extends a radial process through the granule cell layer. With a basal process or an apical extension of its process, either within the subventricular zone or within the inner molecular layer, the RGL cell contacts blood vessels surrounding the stem cell niche (Palmer et al. 2000). In close contact to the RGL cell, different maturation stages of young neurons can be found clustering together. They are discriminable by expressed neuronal marker proteins (Hochgerner et al. 2018) and are named type 2a, 2b, 3 (Hodge et al. 2008; Nicola et al. 2015) or D1-D3 (Seri et al. 2004) or IPC1/2 (intermediate progenitors 1/2), IGC (immature granule cell) (Fuentealba et al. 2012) cells (for overview see introduction Fig. 9). This composition is special to the dentate gyrus subgranular zone. In the *reeler* mutant an altered development impairs the formation of a dense granule cell layer resulting in a scattered pattern of ectopic granule cell bodies (Stanfield and Cowan 1979a) and therefore aggravated the formation of compact stem cell niches. Some previously published investigations of adult neurogenesis in the *reeler* mouse resulted in a diminished neurogenetical capacity and less mitotic and new born cell numbers (Heinrich et al. 2006; Zhao et al. 2007; Sibbe et al. 2015). The studies were done with two independent markers: BrdU, being incorporated in new DNA (Wojtowicz and Kee 2006) and Ki67, marking proliferating cells (Cuylen et al. 2016). Following these studies, the questions arose, if the altered adult neurogenesis in the *reeler* mouse was due to the loss of Reelin, or due to the altered cytoarchitecture, and if similar changes would be found in the

4. Discussion

cKO. The analysis of the stem cell niche structure and composition exhibited similar patterns between the cKO and the wild type. Hence, the cytoarchitectonical prerequisite for adult neurogenesis was intact in the cKO. Another result of this analysis was the close position of Reelin-expressing iIN to young neurons and progenitor cells in the stem cell niche complex. It was shown earlier, that Reelin-expressing cells were located along the subgranular layer and the hilus, respectively (Ramos-Moreno et al. 2006), but the exact position, especially with regard to the participation of the microstructure stem cell niche, and identification was not evaluated. It was possible with the acquired data, on the one hand to identify the Reelin-expressing cell in the subgranular zone as HICAP cell and on the other hand to incorporate the positions of the HICAP cells and the PV expressing basket cells, the second cell type located in the subgranular zone, in a 3D scheme of the stem cell niche. This is presented in that precise form for the first time (Fig. 41D). Thus, the structural prerequisite was unscathed in the cKO, but what about the capacity of neurogenesis, the produced cell numbers and the passing through the different maturation stages?

4.8.2 Quantification of adult neurogenesis proliferation

The generation of new cells was addressed with three different quantification experiments using both markers BrdU and Ki-67. The first quantification was performed after a single intra peritoneal injection of BrdU and resulted in overall small cell numbers of labelled cells and no significant difference between cKO and control animals. Based on the small cell numbers and the really stressful administration method (see below for refinement), this experiment was not repeated. The application method was changed into an oral administration, which enabled an easier dosage of BrdU for a longer time period. With this second experiment, a higher number of labelled cells was achieved. It delivered no statistical difference between the cKO and the two control genotypes (wt and cre), but a significant difference compared to the flox control. Taken into account that the variability of cell numbers counted was quite high between individual animals, this result has to be taken carefully. The Ki-67 staining confirmed the previous result that there was no difference in the numbers of dividing cells at all. These data indicate that the cytoarchitectonical structure of the stem cell niche is the crucial factor for the generation of new cells. As this structure can not be formed properly in the *reeler* mouse, the effects on proliferation and new born cells are severe. Another possibility would be that the CR cell derived Reelin is sufficient to compensate for the iIN derived Reelin loss and thereby sustains normal proliferation.

4. Discussion

Discussing the function of the iIN within the stem cell niche, the PV ir basket cell and the Reelin/CCK ir HICAP cell, it must be mentioned that a regulatory influence on the neurogenesis was mainly shown for the PV ir cells (Moss and Toni 2012; Song et al. 2012, 2013; Alvarez et al. 2016) and not for the Reelin/CCK ir cells. Although Sui (Sui et al. 2013) described an influence on adult neurogenesis in female CCK receptor knockout mice. The hypotheses, how PV ir basket cells influence neurogenesis, range from the spill over effect of GABA (Moss and Toni 2012) to the direct synaptic input on the progenitor cell (Song et al. 2013). This is a point, which has to be clarified by further investigations. It would be interesting to examine the level of neurogenesis in the HRM and HDM, as the cytoarchitecture of the granule cell layer is intact and the Reelin loss is averaged to all sources. Using BrdU for such experiments should be a point of discussion, as Cameron and Mckay (Cameron and Mckay 2001) described an arresting of the cell cycle at high BrdU doses and Duque and Rakic (Duque and Rakic 2011) described an influence of BrdU on the later cell fate. It also has to be considered, if other molecules, like the peptide hormone CCK, play a role in regulating neurogenesis. An alteration of the neurogenesis is also possible, if the new born cells are arrested in a special maturation stage. This was investigated by another quantification, capturing the cells immunoreactive for Doublecortin (DCX), addressing the young maturation stages until type 3, and double stained cells for NeuN and BrdU, addressing the immature neuron stage. The DCX counting was done in combination with the two BrdU stainings, and therefore resulted in two quantification data sets. The first count resulted in a significant difference in cell numbers in the middle area of the hippocampus, which could not be verified by the second count focusing just on the middle area of the hippocampus. For orientation purpose, which area was addressed, see figure A3 in the appendix. According to the divergent results, this experiment should be repeated with equal control genotypes over all hippocampal areas and maybe performed with a fluorescence activated cell sorting (FACS). The analysis of the NeuN staining intensity in BrdU positive cells showed no difference for the two closest related genotypes, the cKO and the flox control, and the wt with the cre control. This grouping, which depends on the progeny, illustrates the necessity to stick to littermates or cousins as control animals, which is strictly recommended by Crawley and Wahlsten (Crawley 2007; Wahlsten 2011). Nevertheless, no recognisable differences in numbers of cells situated in the immature neuron state were found. This data supports the assumption, that besides the proliferation also the maturation of cells in the adult neurogenesis

4. Discussion

in the dentate gyrus of the cKO are unaffected by the depletion of Reelin in inhibitory interneurons.

4.8.3 Analysis of cell properties from progenitor cells and young neurons

The protein Reelin is also known to influence the cytoskeleton (D’Arcangelo et al. 1999; Ayala et al. 2007; Chai et al. 2009b; Krüger et al. 2010; Chai and Frotscher 2016; Santana and Marzolo 2017) and was shown to alter dendritic complexity and branching (Chai et al. 2014; Tensaouti et al. 2018). This raised the question, if the lack of Reelin in iIN, although having no effect on proliferation, eventually might alter the cytoskeleton of young neurons and precursor cells and with that the appearance of the filaments. This was evaluated on reconstructed DCX ir cells and Nestin (marker for intermediate filament of proliferating cells (Michalczyk and Ziman 2005)) ir precursor cells. The analysis of filament length, branching depth (ramification levels of the filament until a specific length of the main branch) and branching points (the number of intersections within a specific range) did not result in any difference between the cKO and the wild type. The loss of interneuron derived Reelin had no influence on the outgrowth of filaments in progenitor cells or immature neurons. Summing up, the data lead to the conclusion, that Reelin secreted by inhibitory interneurons had no effect on the composition of the stem cell niche and the adult neurogenesis, neither on proliferation nor cell maturation nor filament properties. This is a quite interesting finding, as the deletion of an cytosolic component of the canonical Reelin pathway, disabled 1 (Dab1), was reported to lead to dendritic abnormalities and an ectopic migration behaviour in Nestin positive progenitor cells (Teixeira et al. 2012), and was shown to influence proliferation and DCX cell numbers (Korn et al. 2016). All previous data imply that maybe the Reelin produced by Cajal-Retzius cells is able to compensate for the Reelin loss of inhibitory interneurons and is sufficient to maintain cell layer integrity, stem cell composition and branching or CR cells are a priori responsible for these effects. According to Hsieh (Hsieh 2012) niche-derived cell-extrinsic factors and the integration of niche-derived signals by transcription factors are sufficient to control the activity of neuronal stem cells. This supports the hypothesis that it is enough to maintain granule cell layer integrity to sustain the adult neurogenesis in the subgranular zone. Nevertheless, some unanswered questions still remain regarding adult neurogenesis. Are the filament properties and maturation stages in the HRM and HDM affected? Are really all maturation stages (type 2-3) unaffected? Are the quantities of all types of maturation stages equal? Is there an electric modulation of progenitor cells and

4. Discussion

by which cells? Are there other molecules involved in neurogenetic processes, like CCK (Sui et al. 2013) or Nestin or even total different cell types, like astrocytes (Wilhelmsson et al. 2019)? Staining experiments with other markers for the maturation stages, electrophysiology with selected stimulation protocols and the use of knockout mouse lines for other molecules might address these questions in a good way.

Besides all new experiments, one has to consider the living creature being a central part of the experiments. Refining, replacing and reduction are the guidelines to evaluate experiments.

4.9 Refinement of BrdU administration for mice

The administration of BrdU is traditionally done via an intraperitoneal injection while the mouse is hold in a restraining grip, which is quite uncomfortable for the animal (Cameron and Gould 1994). Until today this method is used to label dividing cells and to follow their fate (Ward et al. 1991; Palmer et al. 2000; Wojtowicz and Kee 2006; Brunne et al. 2010; Duque and Rakic 2011; Sui et al. 2013; Podda et al. 2014; Bekiari et al. 2015; Toesca et al. 2016). But the time window for labelling cells with BrdU is limited to 2 h (Cameron and Mckay 2001; Buffo et al. 2005) and this means, to achieve a constant BrdU concentration within the organism to label a progression of cell divisions and differentiations, one has to inject the animal regularly, and thereby stress it. An alternative would be to implant a mini pump under the back skin of the animal, which provides BrdU constantly, but this method requires surgery, drugs and equipment. A much more feasible and long-term way to administer BrdU is to add it to the drinking water of the mice (Gray 1988; Tough and Sprent 1994; Jecker et al. 1997; Santoso et al. 2006). First of all, this is easy to be done without any intrusion into the mouse body. Second, it is easy to administer the drug over a long time period. Third, staining intensity is really good and delivers high and reliable numbers (see Fig. 44B and Fig. 45B). Forth, the animals are less stressed, which prevents influence on physiological processes or on performed behavioural tests (Gould et al. 1997; Kamprath et al. 2006; Palacios-García et al. 2015) . In this work it was taken advantage of this method to deliver a constant daily amount of BrdU between 100 µg/g bw to 233 µg/g bw (recommended standard concentrations by Wojtowicz and Kee (Wojtowicz and Kee 2006)) over a time period of 2 weeks without daily handling and injection. Here, the solution was mixed with 1.5 % sucrose to hide an eventually bad taste of BrdU, but the pilot experiment indicated that the mice would also accept a water/BrdU solution without sucrose, if an intended experiment excludes an administration of additional carbohydrates, for example in obesity studies or similar. Two points should be

4. Discussion

considered before setting up a long-time BrdU application experiment: the housing conditions and genotype dependent drinking habits. According to the presented data, a single housing of mice elevates the daily drunken volume of liquid and the genotypes showed individual drinking habits. So, it may be advisable to pre-test a cohort of animals with different genotypes and housing conditions, to evaluate the influence of these factors on the used strain and then set up a long time experiment according to this data. The advantages of this application method are quite obvious and it would be preferable to change from intraperitoneal injections to water administration of BrdU for refinement.

4.10 Summary of discussion and prospect

The aim of this study to establish a 100 % inhibitory interneuron specific Reelin knockout mouse line without the necessity of drug application was fully achieved. The mice showed no developmental defects or other gross changes in brain and cell architecture. Thus, the second aim of the study, to investigate the effects of the depletion of interneuron derived Reelin on the dentate gyrus of adult mice was feasible. The behavioural testing resulted in no significant differences between the knockout and the wild type, which excludes severe cognitive defects. No granule cell dispersion was found either, so the interneuron derived Reelin seemed not to be necessary for establishing and maintaining granule cell layer integrity. The analysis of adult neurogenesis regarding proliferation, maturation progress of young granule cells and the analysis of cell filament properties showed also no influence of interneuron derived Reelin loss, despite the fact that Reelin-expressing HICAP cells are positioned always close to the radial glial progenitor cells, and the different maturation stages in the subgranular area. Quantification experiments delivered some interesting facts. The number of Reelin-expressing Cajal-Retzius cells was elevated, hinting an autocrine effect to compensate for interneuron derived Reelin loss, which might lead to an underestimation of the real impacts of Reelin derived from iIN. However, the numbers of iIN were not altered, except in the hilar area of the dentate gyrus, where less iIN were counted. Additionally found in the hilar area was a significant increase of Calretinin expressing cell numbers, together with a higher staining intensity of this protein and the cannabinoid receptor 1 in the inner molecular layer of the dentate gyrus. These results were not found in the heterozygous deleter mice and therefore proven to be due to iIN specific depletion of Reelin. The compensatory effect of the CR cells seemed to be compellingly necessary to establish and maintain granule cell layer integrity and stem cell niche structure to provide normal adult neurogenesis. The changed expression

4. Discussion

pattern of CRET and CB1 indicates an influence of interneuron derived Reelin on mossy cells and other CB1 expressing cells having a stake in the iML. This effect could not be compensated for by the CR derived Reelin, which leads to the hypothesis that CR derived Reelin differs from the iIN derived Reelin. This finding should be an issue of further investigations with this conditional knockout. Another very interesting project would be to sort out the function of the HICAP cells located amidst the stem cell niche and their participation in processes of the iML, especially regarding temporal lobe epilepsy pathology. Addressing this topic: the role of the mossy cells and their altered amount of CRET protein should also be incorporated.

The here presented inhibitory interneuron specific Reelin knockout mouse line opens new ways to investigate the role of the two Reelin sources in hippocampal function, adult neurogenesis and their participation in pathologies like Alzheimer`s disease, schizophrenia, bipolar disorder and temporal lobe epilepsy.

Abbreviations

Abbreviations

%	per centum
°C	degree Celsius
µm	micrometre(s)
1x PBS	0.01 mol/l PBS house-made
2-AG	sn-2-arachidonoylglycerol
aa	amino acid
AD	Alzheimer's disease
AEA	N-arachidonylethanolamine
Akt	protein kinase B
apoE	apolipoprotein E
ApoER2	apolipoprotein E receptor 2
BC	basket cells
BDNF	brain-derived neurotrophic factor
BLBP	Brain lipid-binding protein
bp	base pair(s)
BrdU	5-Bromo-2'-deoxyuridine
BSA	bovine serum albumin
bw	bodyweight
C3G	cyanidin-3-glucoside
CA1,2,3	cornu ammonis or Ammon's horn area 1,2,3
CALB	Calbindin
CaMKII	calmodulin-dependent protein kinase type II
cAMP	cyclic adenosine monophosphate
CB	cerebellum
CB1	cannabinoid receptor 1
CCK	Cholecystokinin
Cdc42	GTPase of Rho family
cDNA	coding deoxyribonucleic acid
cKO	conditional knockout, Reln ^{flox/flox} Dlx5/6-Cre positive
CMV	cytomegalovirus
CR	Cajal-Retzius cells
cre	Cre control, Reln ^{wt/wt} Dlx5/6-Cre positive
CRET	Calretinin
Crk	cytosolic adaptor protein
CSF	cerebrospinal fluid
Dab1	Disabled-1
DAPI	4',6-Diamidino-2-phenylindole dihydrochlorid
DCX	Doublecortin
DG	dentate gyrus
Dlx2	distalless homeo box 2

Abbreviations

Dlx5/6	distalless homeo box 5/6
DMSO	dimethyl sulfoxide
DNA	deoxyribonucleic acid
DPBS	Dulbecco`s phosphate-buffered saline
E	embryonic day
E.coli	<i>Escherichia coli</i>
e.g.	for example
EDTA	ethylenediamine-tetraacetic acid
EGF	epidermal growth factor
eGFP	enhanced green fluorescent protein
EP	elevated plus maze
ERK1/2	extracellular signal-regulated kinase 1
FACS	fluorescence activated cell sorting
flox	floxed gene, <i>Reln</i> ^{flox/flox} Dlx5/6-Cre negative
g	gravity
GABA	γ -aminobutyric acid
GAD67	Glutamate decarboxylase isoform 67
GC	granule cell
GCD	granule cell dispersion
GCL	granule cell layer
GE	ganglionic eminence
GFAP	glial fibrillary acidic protein
GSK3 β	glycogen synthase kinase 3 β
GTP	guanosine triphosphate
h	hours
HALT	protease inhibitor cocktail, EDTA-free
HC	hippocampus
HCl	hydrochloric acid
HDM	heterozygous deleter mouse
hf	hippocampal fissure
HICAP	hilar commissural-associational pathway related
hil.	hilus
HRM	heterozygous <i>reeler</i> mouse
IHC	immunohistochemistry
iIN	inhibitory interneuron(s)
iML	inner molecular layer
IN	interneuron(s)
ir	immunoreactive
ISH	in situ hybridization
ITI	inter trial interval
kb	kilobases
kDa	kilodalton
KI	knockin

Abbreviations

LB	Luria-Bertani
LIMK1	LIM domain kinase 1
LTD	long-term depression
LTP	long-term potentiation
m	meter(s)
Mash-1/ASCL1	Achaete-scute homolog 1
MCM2	Minichromosome Maintenance Protein 2
MEK	Mitogen-activated protein kinase/ERK kinase
min	minute(s)
M-Per	mammalian protein extraction reagent
mRNA	messenger ribonucleic acid
mTOR	mechanistic target of rapamycin kinase
MWM	Morris water maze
NaN ₃	sodium azide
NC	neocortex
Nes	Nestin
NeuN	neuronal nuclei
NMDA	N-methyl-D-aspartate
OB	olfactory bulb
OF	open field
oML	outer molecular layer
OR	2-object novel object recognition
P	postnatal day
p	p-value
PBS	phosphate-buffered saline
PCR	polymerase chain reaction
PFA	paraformaldehyde
PI3K	phosphatidylinositol 3-kinase
POMC	proopiomelanocortin
Prox1	Prospero Homeobox 1
PSB	pallial-subpallial boundary
PSD95	postsynaptic density protein 95
PV	Parvalbumin
PVC	polyvinyl chloride
px	pixel(s)
Rap1	ras-related protein 1
RFP	red fluorescence protein
RGL	radial glial-like cell
RNA	ribonucleic acid
ROI	region of interest
rpm	rounds per minute
s	second(s)
SA	spontaneous alternation test

Abbreviations

sem	standard error of the mean
SFK	Src family tyrosin kinase
SGZ	subgranular zone
SI	three-chamber sociability and social novelty test
Sox2	SRY-box transcription factor 2
SST	somatostatin
str. gr.	stratum granulare
str. lac.-mol.	stratum lacunosum-moleculare
str. mol.	stratum moleculare
SVZ	subventricular zone
TAE	Tris-acetic acid-EDTA
tau	microtubule-associated protein tau
Tbr2	T-Box Brain2
TBST20	Tris-buffered saline with TWEEN 20
td	tandem dimer
Thy1	Thy-1 cell surface antigen
TLE	temporal lobe epilepsy
Tris	Tris(hydroxymethyl)aminomethane
TWEEN	Polyoxyethylene-20-sorbitan monolaurate
VIP	Vasoactive intestinal polypeptide
VLDLR	very low-density lipoprotein receptor
w	week
wt	wild type, Reln ^{wt/wt} Dlx5/6-Cre negative, Reln ^{wt/wt}

Bibliography

- Acampora D, Merlo GR, Paleari L, Zerega B, Postiglione MP, Mantero S, Bober E, Barbieri O, Simeone A, Levi G. 1999. Craniofacial, vestibular and bone defects in mice lacking the Distal-less-related gene *Dlx5*. *Development*. 126:3795–3809.
- Alcántara S, Ruiz M, D’Arcangelo G, Ezan F, de Lecea L, Curran T, Sotelo C, Soriano E. 1998. Regional and cellular patterns of reelin mRNA expression in the forebrain of the developing and adult mouse. *J Neurosci*. 18:7779–7799.
- Altman J, Das GD. 1965. Autoradiographic and Histological Evidence of postnatal hippocampal neurogenesis in rats. *J Comp Neurol*. 124:319–336.
- Alvarez DD, Giacomini D, Yang SM, Trincherro MF, Temprana SG, Büttner KA, Beltramone N, Schinder AF. 2016. Regulation of neuronal integration by physiological or pathological stimuli. *Science* (80-). 354:459–466.
- Amaral DG, Scharfman HE, Lavenex P. 2007. The dentate gyrus: fundamental neuroanatomical organization (dentate gyrus for dummies). *Prog Brain Res*. 163:3–22.
- Amaral DG, Witter MP. 1989. The three-dimensional organization of the hippocampal formation: a review of anatomical data. *Neuroscience*. 31:571–591.
- Ammassari-Teule M, Sgobio C, Biamonte F, Marrone C, Mercuri NB, Keller F. 2009. Reelin haploinsufficiency reduces the density of PV+ neurons in circumscribed regions of the striatum and selectively alters striatal-based behaviors. *Psychopharmacology (Berl)*. 204:511–521.
- Andersen P, Morris R, Amaral D, Bliss T, O’Keefe J. 2007. *The Hippocampus Book*. 1st ed. New York, NY: Oxford University Press.
- Anstötz M, Huang H, Marchionni I, Haumann I, MacCafferri G, Lübke JHR. 2016. Developmental Profile, Morphology, and Synaptic Connectivity of Cajal-Retzius Cells in the Postnatal Mouse Hippocampus. *Cereb Cortex*. 26:855–872.
- Anstötz M, Karsak M, Rune GM. 2019. Integrity of Cajal-Retzius cells in the reeler -mouse hippocampus. *Hippocampus*. 29:550–565.
- Araque A, Castillo PE, Manzoni OJ, Tonini R. 2017. Synaptic functions of endocannabinoid signaling in health and disease. *Neuropharmacology*. 124:13–24.
- Assadi AH, Zhang G, Beffert U, McNeil RS, Renfro AL, Niu S, Quattrocchi CC, Antalffy BA, Sheldon M, Armstrong DD, Wynshaw-Boris A, Herz J, D’Arcangelo G, Clark GD. 2003. Interaction of reelin signaling and *Lis1* in brain development. *Nat Genet*. 35:270–

Bibliography

276.

- Ayala R, Shu T, Tsai L-H. 2007. Trekking across the Brain: The Journey of Neuronal Migration. *Cell*. 128:29–43.
- Bachmanov AA, Reed DR, Beauchamp GK, Tordoff MG. 2002. Food intake, water intake, and drinking spout side preference of 28 mouse strains. *Behav Genet*. 32:435–443.
- Bachmanov AA, Tordoff MG, Beauchamp GK. 2001. Sweetener Preference of C57BL/6ByJ and 129P3/J Mice. *Chem Senses*. 26:905–913.
- Badea A, Nicholls PJ, Johnson GA, Wetsel WC. 2007. Neuroanatomical phenotypes in the Reeler mouse. *Neuroimage*. 34:1363–1374.
- Bar I, Lambert De Rouvroit C, Royaux I, Krizman DB, Dernoncourt C, Ruelle D, Beckers MC, Goffinet AM. 1995. A YAC contig containing the reeler locus with preliminary characterization of candidate gene fragments. *Genomics*. 26:543–549.
- Barber M, Arai Y, Morishita Y, Vigier L, Causeret F, Borello U, Ledonne F, Coppola E, Contremoulins V, Pfrieger FW, Tissir F, Govindan S, Jabaudon D, Proux-Gillardeaux V, Galli T, Pierani A. 2015. Migration speed of Cajal-Retzius cells modulated by vesicular trafficking controls the size of higher-order cortical areas. *Curr Biol*. 25:2466–2478.
- Basu J, Zaremba JD, Cheung SK, Hitti FL, Zemelman B V, Losonczy A, Siegelbaum SA. 2016. Gating of hippocampal activity, plasticity, and memory by entorhinal cortex long-range inhibition. *Science* (80-). 351:138–153.
- Bayer K-U, Löhler J, Schulman H, Harbers K. 1999. Developmental expression of the CaM kinase II isoforms: Ubiquitous γ - and δ -CaM kinase II are the early isoforms and most abundant in the developing nervous system. *Mol Brain Res*. 70:147–154.
- Becker J, Fröhlich J, Perske C, Pavlakovic H, Wilting J. 2012. Reelin signalling in neuroblastoma: Migratory switch in metastatic stages. *Int J Oncol*. 41:681–689.
- Bekiari C, Giannakopoulou A, Siskos N, Grivas I, Tsingotjidou A, Michaloudi H, Papadopoulos GC. 2015. Neurogenesis in the septal and temporal part of the adult rat dentate gyrus. *Hippocampus*. 25:511–523.
- Benarroch EE. 2013. Neocortical interneurons: functional diversity and clinical correlations. *Neurology*. 81:273–280.
- Bender RA, Zhou L, Wilkars W, Fester L, Lanowski JS, Paysen D, König A, Rune GM. 2010. Roles of 17 β -estradiol involve regulation of reelin expression and synaptogenesis in the dentate gyrus. *Cereb Cortex*. 20:2985–2995.
- Benson DL, Isackson PJ, Gall CM, Jones EG. 1992. Contrasting patterns in the localization of

Bibliography

- glutamic acid decarboxylase and Ca²⁺ /calmodulin protein kinase gene expression in the rat central nervous system. *Neuroscience*. 46:825–849.
- Bhaskaran MD, Smith BN. 2010. Cannabinoid-mediated inhibition of recurrent excitatory circuitry in the dentate gyrus in a mouse model of temporal lobe epilepsy. *PLoS One*. 5:e10683.
- Biamonte F, Assenza G, Marino R, D'Amelio M, Panteri R, Caruso D, Scurati S, Yague JG, Garcia-Segura LM, Cesa R, Strata P, Melcangi RC, Keller F. 2009. Interactions between neuroactive steroids and reelin haploinsufficiency in Purkinje cell survival. *Neurobiol Dis*. 36:103–115.
- Bielle F, Griveau A, Narboux-Nême N, Vigneau S, Sigrist M, Arber S, Wassef M, Pierani A. 2005. Multiple origins of Cajal-Retzius cells at the borders of the developing pallium. *Nat Neurosci*. 8:1002–1012.
- Blasco-Ibáñez JM, Freund TF. 1997. Distribution, ultrastructure, and connectivity of calretinin-immunoreactive mossy cells of the mouse dentate gyrus. *Hippocampus*. 7:307–320.
- Bliss TVP, Errington ML. 1977. “Reeler” mutant mice fail to show spontaneous alternation. *Brain Res*. 124:168–170.
- Bock HH, May P. 2016. Canonical and Non-canonical Reelin Signaling. *Front Cell Neurosci*. 10:1–20.
- Botella-López A, Burgaya F, Gavín R, García-Ayllón MS, Gómez-Tortosa E, Peña-Casanova J, Ureña JM, Del Río JA, Blesa R, Soriano E, Sáez-Valero J. 2006. Reelin expression and glycosylation patterns are altered in Alzheimer's disease. *Proc Natl Acad Sci*. 103:5573–5578.
- Botella-López A, Cuchillo-Ibáñez I, Cotrufo T, Mok SS, Li Q-X, Barquero M-S, Dierssen M, Soriano E, Sáez-Valero J. 2010. Beta-amyloid controls altered Reelin expression and processing in Alzheimer's disease. *Neurobiol Dis*. 37:682–691.
- Bouché E, Romero-Ortega MI, Henkemeyer M, Catchpole T, Leemhuis J, Frotscher M, May P, Herz J, Bock HH. 2013. Reelin induces EphB activation. *Cell Res*. 23:473–490.
- Boyle MP, Bernard A, Thompson CL, Ng L, Boe A, Mortrud M, Hawrylycz MJ, Jones AR, Hevner RF, Lein ES. 2011. Cell-type-specific consequences of Reelin deficiency in the mouse neocortex, hippocampus, and amygdala. *J Comp Neurol*. 519:2061–2089.
- Brown JP, Couillard-Després S, Cooper-Kuhn CM, Winkler J, Aigner L, Kuhn HG. 2003. Transient expression of doublecortin during adult neurogenesis. *J Comp Neurol*. 467:1–

Bibliography

- 10.
- Brunne B, Franco S, Bouché E, Herz J, Howell BW, Pahle J, Müller U, May P, Frotscher M, Bock HH. 2013. Role of the postnatal radial glial scaffold for the development of the dentate gyrus as revealed by Reelin signaling mutant mice. *Glia*. 61:1347–1363.
- Brunne B, Zhao S, Derouiche A, Herz J, May P, Frotscher M, Bock HH. 2010. Origin, maturation, and astroglial transformation of secondary radial glial cells in the developing dentate gyrus. *Glia*. 58:1553–1569.
- Buffo A, Vosko MR, Erturk D, Hamann GF, Jucker M, Rowitch D, Götz M. 2005. Expression pattern of the transcription factor Olig2 in response to brain injuries: Implications for neuronal repair. *Proc Natl Acad Sci*. 102:18183–18188.
- Cameron HA, Gould E. 1994. Adult neurogenesis is regulated by adrenal steroids in the dentate gyrus. *Neuroscience*. 61:203–209.
- Cameron HA, Mckay RDG. 2001. Adult neurogenesis produces a large pool of new granule cells in the dentate gyrus. *J Comp Neurol*. 435:406–417.
- Cameron HA, Woolley CS, McEwen BS, Gould E. 1993. Differentiation of newly born neurons and glia in the dentate gyrus of the adult rat. *Neuroscience*. 56:337–344.
- Caruncho HJ, Brymer K, Romay-Tallón R, Mitchell MA, Rivera-Baltanás T, Botterill J, Olivares JM, Kalynchuk LE. 2016. Reelin-Related Disturbances in Depression: Implications for Translational Studies. *Front Cell Neurosci*. 10:1–11.
- Caviness VS. 1976. Patterns of cell and fiber distribution in the neocortex of the reeler mutant mouse. *J Comp Neurol*. 170:435–447.
- Caviness VS, Sidman RL. 1973. Retrohippocampal, hippocampal and related structures of the forebrain in the reeler mutant mouse. *J Comp Neurol*. 147:235–253.
- Chai X, Fan L, Shao H, Lu X, Zhang W, Li J, Wang J, Chen S, Frotscher M, Zhao S. 2014. Reelin Induces Branching of Neurons and Radial Glial Cells during Corticogenesis. *Cereb Cortex*. 25:3640–3653.
- Chai X, Förster E, Zhao S, Bock HH, Frotscher M. 2009a. Reelin acts as a stop signal for radially migrating neurons by inducing phosphorylation of n-cofilin at the leading edge. *Commun Integr Biol*. 2:375–377.
- Chai X, Förster E, Zhao S, Bock HH, Frotscher M. 2009b. Reelin stabilizes the actin cytoskeleton of neuronal processes by inducing n-cofilin phosphorylation at serine3. *J Neurosci*. 29:288–299.
- Chai X, Frotscher M. 2016. How does Reelin signaling regulate the neuronal cytoskeleton

Bibliography

- during migration? *Neurogenesis*. 3.
- Chang L, Goldman RD. 2004. Intermediate filaments mediate cytoskeletal crosstalk. *Nat Rev Mol Cell Biol*. 5:601–613.
- Chen Y, Beffert U, Ertunc M, Tang T-S, Kavalali ET, Bezprozvanny I, Herz J. 2005. Reelin Modulates NMDA Receptor Activity in Cortical Neurons. *J Neurosci*. 25:8209–8216.
- Chen Y, Sharma RP, Costa RH, Costa E, Grayson DR. 2002. On the epigenetic regulation of the human reelin promoter. *Nucleic Acids Res*. 30:2930–2939.
- Chiu CQ, Castillo PE. 2008. Input-specific plasticity at excitatory synapses mediated by endocannabinoids in the dentate gyrus. *Neuropharmacology*. 54:68–78.
- Chowdhury TG, Jimenez JC, Bomar JM, Cruz-Martin A, Cattle JP, Portera-Cailliau C. 2010. Fate of Cajal-Retzius neurons in the postnatal mouse neocortex. *Front Neuroanat*. 4:1–8.
- Costa E, Davis J, Grayson DR, Guidotti A, Pappas GD, Pesold C. 2001. Dendritic spine hypoplasticity and downregulation of reelin and GABAergic tone in schizophrenia vulnerability. *Neurobiol Dis*. 8:723–742.
- Coulin C, Drakew A, Frotscher M, Deller T. 2001. Stereological estimates of total neuron numbers in the hippocampus of adult reeler mutant mice: Evidence for an increased survival of Cajal-Retzius cells. *J Comp Neurol*. 439:19–31.
- Courtès S, Vernerey J, Pujadas L, Magalon K, Cremer H, Soriano E, Durbec P, Cayre M. 2011. Reelin controls progenitor cell migration in the healthy and pathological adult mouse brain. *PLoS One*. 6:e20430.
- Crawley JN. 2007. *What's wrong with my Mouse?* 2nd ed. Hoboken, New Jersey: John Wiley & Sons, Inc.
- Cuchillo-Ibañez I, Balmaceda V, Mata-Balaguer T, Lopez-Font I, Sáez-Valero J. 2016. Reelin in Alzheimer's Disease, Increased Levels but Impaired Signaling: When More is Less. *J Alzheimer's Dis*. 52:403–416.
- Cuylen S, Blaukopf C, Politi AZ, Muller-Reichert T, Neumann B, Poser I, Ellenberg J, Hyman AA, Gerlich DW. 2016. Ki-67 acts as a biological surfactant to disperse mitotic chromosomes. *Nature*. 535:308–312.
- D'Arcangelo G. 2005. The reeler mouse: anatomy of a mutant. *Int Rev Neurobiol*. 71:383–417.
- D'Arcangelo G, Curran T. 1998. Reeler: New tales on an old mutant mouse. *BioEssays*. 20:235–244.
- D'Arcangelo G, Homayouni R, Keshvara L, Rice DS, Sheldon M, Curran T. 1999. Reelin is a

Bibliography

- ligand for lipoprotein receptors. *Neuron*. 24:471–479.
- D’Arcangelo G, Miao GG, Chen S-C, Soares HD, Morgan JI, Curran T. 1995. A Protein related to extracellular matrix proteins in the mouse mutant *reeler*. *Nature*. 374:719–723.
- D’Arcangelo G, Nakajima K, Miyata T, Ogawa M, Mikoshiba K, Curran T. 1997. Reelin is a secreted glycoprotein recognized by the CR-50 monoclonal antibody. *J Neurosci*. 17:23–31.
- Danglot L, Triller A, Marty S. 2006. The Development of Hippocampal Interneurons in Rodents. *Hippocampus*. 16:1032–1060.
- de Bergeyck V, Naerhuyzen B, Goffinet AM, Lambert de Rouvroit C. 1998. A panel of monoclonal antibodies against reelin, the extracellular matrix protein defective in *reeler* mutant mice. *J Neurosci Methods*. 82:17–24.
- Del Río JA, Heimrich B, Borrell V, Förster E, Drakew A, Alcántara S, Nakajima K, Miyata T, Ogawa M, Mikoshiba K, Derer P, Frotscher M, Soriano E. 1997. A role for Cajal-Retzius cells and reelin in the development of hippocampal connections. *Nature*. 385:70–74.
- Deller T, Nitsch R, Frotscher M. 1995. Phaseolus vulgaris –leucoagglutinin tracing of commissural fibers to the rat dentate gyrus: Evidence for a previously unknown commissural projection to the outer molecular layer. *J Comp Neurol*. 352:55–68.
- Derer P. 1985. Comparative localization of Cajal-Retzius cells in the neocortex of normal and *reeler* mutant mice fetuses. *Neurosci Lett*. 54:1–6.
- Derer P, Derer M. 1990. Cajal-retzius cell ontogenesis and death in mouse brain visualized with horseradish peroxidase and electron microscopy. *Neuroscience*. 36:839–856.
- DeSilva U, D’Arcangelo G, Braden V V, Chen J, Miao GG, Curran T, Green ED. 1997. The human reelin gene: Isolation, sequencing, and mapping on chromosome 7. *Genome Res*. 7:157–164.
- Díaz-Mendoza MJ, Lorda-Diez CI, Montero JA, García-Porrero JA, Hurlé JM. 2013. Interdigital cell death in the embryonic limb is associated with depletion of Reelin in the extracellular matrix. *Cell Death Dis*. 4:1–7.
- Dlugosz P, Tresky R, Nimpf J. 2019. Differential action of reelin on oligomerization of ApoER2 and VLDL receptor in HEK293 cells assessed by time-resolved anisotropy and fluorescence lifetime imaging microscopy. *Front Mol Neurosci*. 12:53.
- Doetsch F, Caillé I, Lim DA, García-Verdugo JM, Alvarez-Buylla A. 1999. Subventricular Zone Astrocytes Are Neural Stem Cells in the Adult Mammalian Brain. *Cell*. 97:703–

Bibliography

- 716.
- Duque A, Rakic P. 2011. Different Effects of Bromodeoxyuridine and [3H]Thymidine Incorporation into DNA on Cell Proliferation, Position, and Fate. *J Neurosci.* 31:15205–15217.
- Duveau V, Madhusudan A, Caleo M, Knuesel I, Fritschy J-M. 2011. Impaired reelin processing and secretion by Cajal-Retzius cells contributes to granule cell dispersion in a mouse model of temporal lobe epilepsy. *Hippocampus.* 21:935–944.
- Eckardt D, Theis M, Döring B, Speidel D, Willecke K, Ott T. 2004. Spontaneous ectopic recombination in cell-type-specific Cre mice removes loxP -flanked marker cassettes in vivo. *Genesis.* 38:159–165.
- Eichenbaum H. 2017. Prefrontal–hippocampal interactions in episodic memory. *Nat Rev Neurosci.* 18:547–558.
- Encinas JM, Michurina T V, Peunova N, Park JH, Tordo J, Peterson DA, Fishell G, Koulakov A, Enikolopov G. 2011. Division-coupled astrocytic differentiation and age-related depletion of neural stem cells in the adult hippocampus. *Cell Stem Cell.* 8:566–579.
- Eriksson PS, Perfilieva E, Björk-Eriksson T, Alborn A-M, Nordborg C, Peterson DA, Gage FH. 1998. Neurogenesis in the adult human hippocampus. *Nat Med.* 4:1313–1317.
- Falconer DS. 1951. Two new mutants, “trembler” and “reeler”, with neurological actions in the house mouse (*Mus musculus* L.). *J Genet.*
- Fanselow MS, Dong H-W. 2010. Are the dorsal and ventral hippocampus functionally distinct structures? *Neuron.* 65:7–19.
- Fatemi SH, Earle JA, McMenomy T. 2000. Reduction in Reelin immunoreactivity in hippocampus of subjects with schizophrenia, bipolar disorder and major depression. *Mol Psychiatry.* 5:654–663.
- Feng G, Mellor RH, Bernstein M, Keller-Peck C, Nguyen QT, Wallace M, Nerbonne JM, Lichtman JW, Sanes JR. 2000. Imaging neuronal subsets in transgenic mice expressing multiple spectral variants of GFP. *Neuron.* 28:41–51.
- Ferland RJ, Cherry TJ, Preware PO, Morrisey EE, Walsh CA. 2003. Characterization of Foxp2 and Foxp1 mRNA and protein in the developing and mature brain. *J Comp Neurol.* 460:266–279.
- Förster E, Zhao S, Frotscher M. 2006. Laminating the hippocampus. *Nat Rev Neurosci.* 7:259–267.
- Freiman TM, Eismann-Schweimler J, Frotscher M. 2011. Granule cell dispersion in temporal

Bibliography

- lobe epilepsy is associated with changes in dendritic orientation and spine distribution. *Exp Neurol.* 229:332–338.
- Freund TF, Buzsáki G. 1996. Interneurons of the Hippocampus. *Hippocampus.* 6:347–470.
- Frotscher M, Chai X, Bock HH, Haas CA, Förster E, Zhao S. 2009. Role of Reelin in the development and maintenance of cortical lamination. *J Neural Transm.* 116:1451–1455.
- Fuentealba LC, Obernier K, Alvarez-Buylla A. 2012. Adult neural stem cells bridge their niche. *Cell Stem Cell.* 10:698–708.
- Fujise N, Liu Y, Hori N, Kosaka T. 1998. Distribution of calretinin immunoreactivity in the mouse dentate gyrus: II. Mossy cells, with special reference to their dorsoventral difference in calretinin immunoreactivity. *Neuroscience.* 82:181–200.
- Furlanis E, Traunmüller L, Fucile G, Scheiffele P. 2019. Landscape of ribosome-engaged transcript isoforms reveals extensive neuronal-cell-class-specific alternative splicing programs. *Nat Neurosci.* 1546–1726.
- Goffinet AM. 1979. An Early Developmental Defect in the Cerebral Cortex of the Reeler Mouse. *Anat Embryol (Berl).* 157:205–216.
- Gould E, Beylin A, Tanapat P, Reeves A, Shors TJ. 1999. Learning enhances adult neurogenesis in the hippocampal formation. *Nat Neurosci.* 2:260–265.
- Gould E, McEwen BS, Tanapat P, Galea LAM, Fuchs E. 1997. Neurogenesis in the dentate gyrus of the adult tree shrew is regulated by psychosocial stress and NMDA receptor activation. *J Neurosci.* 17:2492–2498.
- Gray D. 1988. Population Kinetics of Rat Peripheral B Cells. *J Exp Med.* 167:805–816.
- Grayson DR, Chen Y, Costa E, Dong E, Guidotti A, Kundakovic M, Sharma RP. 2006. The human reelin gene: Transcription factors (+), repressors (-) and the methylation switch (+/-) in schizophrenia. *Pharmacol Ther.* 111:272–286.
- Griveau A, Borello U, Causeret F, Tissir F, Boggetto N, Karaz S, Pierani A. 2010. A novel role for Dbx1-derived Cajal-Retzius cells in early regionalization of the cerebral cortical neuroepithelium. *PLoS Biol.* 8:e1000440.
- Guidotti A, Auta J, Davis JM, Gerevini VD, Dwivedi Y, Grayson DR, Impagnatiello F, Pandey G, Pesold C, Sharma R, Uzunov D. 2000. Decrease in Reelin and Glutamic Acid Decarboxylase 67 (GAD 67) Expression in Schizophrenia and Bipolar Disorder. *Arch Gen Psychiatry.* 57:1061–1069.
- Guilhem D, Dreyfus PA, Makiura Y, Suzuki F, Onteniente B. 1996. Short increase of BDNF messenger RNA triggers Kainic acid-induced neuronal hypertrophy in adult mice.

Bibliography

- Neuroscience. 72:923–931.
- Gulyás AI, Miettinen R, Jacobowitz DM, Freund TF. 1992. Calretinin is present in non-pyramidal cells of the rat hippocampus-I. A new type of neuron specifically associated with the mossy fibre system. *Neuroscience*. 48:1–27.
- Ha S, Tripathi PP, Mihalas AB, Hevner RF, Beier DR. 2017. C-Terminal Region Truncation of RELN Disrupts an Interaction with VLDLR, Causing Abnormal Development of the Cerebral Cortex and Hippocampus. *J Neurosci*. 37:960–971.
- Haas C a, Dudeck O, Kirsch M, Huszka C, Kann G, Pollak S, Zentner J, Frotscher M. 2002. Role for reelin in the development of granule cell dispersion in temporal lobe epilepsy. *J Neurosci*. 22:5797–5802.
- Haas CA, Frotscher M. 2010. Reelin deficiency causes granule cell dispersion in epilepsy. *Exp Brain Res*. 200:141–149.
- Hamburgh M. 1963. Analysis of the postnatal developmental effects of “reeler,” a neurological mutation in mice. A study in developmental genetics. *Dev Biol*. 8:165–185.
- Han Z-S, Buhl EH, Lörinczi Z, Somogyi P. 1993. A High Degree of Spatial Selectivity in the Axonal and Dendritic Domains of Physiologically Identified Local-circuit Neurons in the Dentate Gyrus of the Rat Hippocampus. *Eur J Neurosci*. 5:395–410.
- Harwell CC, Fuentealba LC, Gonzalez-Cerrillo A, Parker PRL, Gertz CC, Mazzola E, Garcia MT, Alvarez-Buylla A, Cepko CL, Kriegstein AR. 2015. Wide Dispersion and Diversity of Clonally Related Inhibitory Interneurons. *Neuron*. 87:999–1007.
- Hausrat TJ, Muhia M, Gerrow K, Thomas P, Hirdes W, Tsukita S, Heisler FF, Herich L, Dubroqua S, Breiden P, Feldon J, Schwarz JR, Yee BK, Smart TG, Triller A, Kneussel M. 2015. Radixin regulates synaptic GABA A receptor density and is essential for reversal learning and short-term memory. *Nat Commun*. 6.
- Hayashi S, McMahon AP. 2002. Efficient recombination in diverse tissues by a tamoxifen-inducible form of Cre: A tool for temporally regulated gene activation/inactivation in the mouse. *Dev Biol*. 244:305–318.
- Heffner CS, Pratt CH, Babiuk RP, Sharma Y, Rockwood SF, Donahue LR, Eppig JT, Murray SA. 2012. Supporting conditional mouse mutagenesis with a comprehensive cre characterization resource. *Nat Commun*. 3:1218–1219.
- Heinrich C, Nitta N, Flubacher A, Müller M, Fahrner A, Kirsch M, Freiman T, Suzuki F, Depaulis A, Frotscher M, Haas CA. 2006. Reelin deficiency and displacement of mature neurons, but not neurogenesis, underlie the formation of granule cell dispersion in the

Bibliography

- epileptic hippocampus. *J Neurosci.* 26:4701–4713.
- Herz J, Beffert U. 2000. Apolipoprotein E receptors: Linking brain development and alzheimer's disease. *Nat Rev Neurosci.* 1:51–58.
- Herz J, Chen Y. 2006. Reelin, lipoprotein receptors and synaptic plasticity. *Nat Rev Neurosci.* 7:850–859.
- Hochgerner H, Zeisel A, Lönnerberg P, Linnarsson S. 2018. Conserved properties of dentate gyrus neurogenesis across postnatal development revealed by single-cell RNA sequencing. *Nat Neurosci.* 21:290–299.
- Hodge RD, Iii AJG, Elsen GE, Nelson BR, Mussar KE, Reiner SL, Ramirez J-M, Hevner RF. 2013. *Tbr2* expression in Cajal-Retzius cells and intermediate neuronal progenitors is required for morphogenesis of the dentate gyrus. *J Neurosci.* 33:4165–4180.
- Hodge RD, Kowalczyk TD, Wolf SA, Encinas JM, Rippey C, Enikolopov G, Kempermann G, Hevner RF. 2008. Intermediate progenitors in adult hippocampal neurogenesis: *Tbr2* expression and coordinate regulation of neuronal output. *J Neurosci.* 28:3707–3717.
- Hong SE, Shugart YY, Huang DT, Al Shahwan S, Grant PE, Hourihane JO, Martin NDT, Walsh CA. 2000. Autosomal recessive lissencephaly with cerebellar hypoplasia is associated with human *RELN* mutations. *Nat Genet.* 26:93–96.
- Hosp JA, Strüber M, Yanagawa Y, Obata K, Vida I, Jonas P, Bartos M. 2014. Morphophysiological criteria divide dentate gyrus interneurons into classes. *Hippocampus.* 24:189–203.
- Houser CR. 1990. Granule cell dispersion in the dentate gyrus of humans with temporal lobe epilepsy. *Brain Res.* 535:195–204.
- Houser CR. 2007. Interneurons of the dentate gyrus: an overview of cell types, terminal fields and neurochemical identity. *Prog Brain Res.* 163:217–232.
- Hsieh J. 2012. Orchestrating transcriptional control of adult neurogenesis Orchestrating transcriptional control of adult neurogenesis. *Genes Dev.* 26:1010–1021.
- Hu H, Gan J, Jonas P. 2014. Interneurons. Fast-spiking, parvalbumin⁺ GABAergic interneurons: from cellular design to microcircuit function. *Science.* 345:1255–1263.
- Ichihara H, Jingami H, Toh H. 2001. Three novel repetitive units of reelin. *Mol Brain Res.* 97:190–193.
- Ikeda Y, Terashima T. 1997. Expression of reelin, the gene responsible for the reeler mutation, in embryonic development and adulthood in the mouse. *Dev Dyn.* 210:157–172.

Bibliography

- Imayoshi I, Kageyama R. 2011. The role of notch signaling in adult neurogenesis. *Mol Neurobiol.* 44:7–12.
- Impagnatiello F, Guidotti AR, Pesold C, Dwivedi Y, Caruncho H, Pisu MG, Uzunov DP, Smalheiser NR, Davis JM, Pandey GN, Pappas GD, Tuetting P, Sharma RP, Costa E. 1998. A decrease of reelin expression as a putative vulnerability factor in schizophrenia. *Proc Natl Acad Sci U S A.* 95:15718–15723.
- Jecker P, Beuleke A, Dressendörfer I, Pabst R, Westermann J. 1997. Long-term oral application of 5-bromo-2-deoxyuridine does not reliably label proliferating immune cells in the LEW rat. *J Histochem Cytochem.* 45:393–401.
- Jossin Y, Ignatova N, Hiesberger T, Herz J, Lambert de Rouvroit C, Goffinet AM. 2004. The central fragment of Reelin, generated by proteolytic processing in vivo, is critical to its function during cortical plate development. *J Neurosci.* 24:514–521.
- Kamprath K, Marsicano G, Tang J, Monory K, Bisogno T, Di Marzo V, Lutz B, Wotjak CT. 2006. Cannabinoid CB1 Receptor Mediates Fear Extinction via Habituation-Like Processes. *J Neurosci.* 26:6677–6686.
- Kassab R, Alexandre F. 2018. Pattern separation in the hippocampus: distinct circuits under different conditions. *Brain Struct Funct.* 223:2785–2808.
- Katona I, Sperlách B, Sík A, Káfalvi A, Vizi ES, Mackie K, Freund TF. 1999. Presynaptically Located CB1 Cannabinoid Receptors Regulate GABA Release from Axon Terminals of Specific Hippocampal Interneurons. *J Neurosci.* 19:4544–4558.
- Kee N, Sivalingam S, Boonstra R, Wojtowicz J. 2002. The utility of Ki-67 and BrdU as proliferative markers of adult neurogenesis. *J Neurosci Methods.* 115:97–105.
- Kempermann G, Song H, Gage FH. 2015. Neurogenesis in the Adult Hippocampus. *Cold Spring Harb Perspect Biol.* 7:a018812.
- Kepecs A, Fishell G. 2014. Interneuron cell types are fit to function. *Nature.* 505:318–326.
- Kilb W, Frotscher M. 2016. Cajal-Retzius-Zellen: Architekten der kortikalen Entwicklung. *Neuroforum.* 22:124–129.
- Knuesel I, Nyffeler M, Mormède C, Muhia M, Meyer U, Pietropaolo S, Yee BK, Pryce CR, LaFerla FM, Marighetto A, Feldon J. 2009. Age-related accumulation of Reelin in amyloid-like deposits. *Neurobiol Aging.* 30:697–716.
- Kola I, Brookes S, Green AR, Garber R, Tymms M, Papas TS, Seth A. 1993. The Ets1 transcription factor is widely expressed during murine embryo development and is associated with mesodermal cells involved in morphogenetic processes such as organ

Bibliography

- formation. *Proc Natl Acad Sci U S A.* 90:7588–7592.
- Korn MJ, Mandle QJ, Parent JM. 2016. Conditional disabled-1 deletion in mice alters hippocampal neurogenesis and reduces seizure threshold. *Front Neurosci.* 10:1–12.
- Kos CH. 2004. Cre / loxP System for Generating Tissue-specific Knockout Mouse Models. *Nutr Rev.* 62:243–246.
- Kriegstein A, Alvarez-Buylla A. 2009. The Glial Nature of Embryonic and Adult Neural Stem Cells. *Annu Rev Neurosci.* 32:149–184.
- Krueger DD, Howell JL, Hebert BF, Olausson P, Taylor JR, Nairn AC. 2006. Assessment of cognitive function in the heterozygous reeler mouse. *Psychopharmacology (Berl).* 189:95–104.
- Krüger MT, Zhao S, Chai X, Brunne B, Bouché E, Bock HH, Frotscher M. 2010. Role for Reelin-induced cofilin phosphorylation in the assembly of sympathetic preganglionic neurons in the murine intermediolateral column. *Eur J Neurosci.* 32:1611–1617.
- Lane-Donovan C, Philips GT, Wasser CR, Durakoglugil MS, Masiulis I, Upadhaya A, Pohlkamp T, Coskun C, Kotti T, Steller L, Hammer RE, Frotscher M, Bock HH, Herz J. 2015. Reelin protects against amyloid β toxicity in vivo. *Sci Signal.* 8:ra67.
- Lee GH, D’Arcangelo G. 2016. New insights into reelin-mediated signaling pathways. *Front Cell Neurosci.* 10:1–8.
- Lee S-H, Soltesz I. 2011. Requirement for CB1 but not GABAB receptors in the cholecystokinin mediated inhibition of GABA release from cholecystokinin expressing basket cells. *J Physiol.* 589:891–902.
- Lehmann K, Steinecke A, Bolz J. 2012. GABA through the ages: Regulation of cortical function and plasticity by inhibitory interneurons. *Neural Plast.* 2012.
- Lein ES, Hawrylycz MJ, Ao N, Ayres M, Bensinger A, Bernard A, Boe AF, Boguski MS, Brockway KS, Byrnes EJ, Chen L, Chen L, Chen TM, Chin MC, Chong J, Crook BE, Czaplinska A, Dang CN, Datta S, Dee NR, Desaki AL, Desta T, Diep E, Dolbeare TA, Donelan MJ, Dong HW, Dougherty JG, Duncan BJ, Ebbert AJ, Eichele G, Estin LK, Faber C, Facer BA, Fields R, Fischer SR, Fliss TP, Frensley C, Gates SN, Glattfelder KJ, Halverson KR, Hart MR, Hohmann JG, Howell MP, Jeung DP, Johnson RA, Karr PT, Kawal R, Kidney JM, Knapik RH, Kuan CL, Lake JH, Laramee AR, Larsen KD, Lau C, Lemon TA, Liang AJ, Liu Y, Luong LT, Michaels J, Morgan JJ, Morgan RJ, Mortrud MT, Mosqueda NF, Ng LL, Ng R, Orta GJ, Overly CC, Pak TH, Parry SE, Pathak SD, Pearson OC, Puchalski RB, Riley ZL, Rockett HR, Rowland SA, Royall JJ, Ruiz MJ,

Bibliography

- Sarno NR, Schaffnit K, Shapovalova N V, Sivisay T, Slaughterbeck CR, Smith SC, Smith KA, Smith BI, Sodt AJ, Stewart NN, Stumpf KR, Sunkin SM, Sutram M, Tam A, Teemer CD, Thaller C, Thompson CL, Varnam LR, Visel A, Whitlock RM, Wohnoutka PE, Wolkey CK, Wong VY, Wood M, Yaylaoglu MB, Young RC, Youngstrom BL, Yuan XF, Zhang B, Zwingman TA, Jones AR. 2007. Genome-wide atlas of gene expression in the adult mouse brain. *Nature*. 445:168–176.
- Leranth C, Hajszan T. 2007. Extrinsic afferent systems to the dentate gyrus. *Prog Brain Res*. 163:63–85.
- Lewejohann L, Reinhard C, Schrewe A, Brandewiede J, Haemisch A, Görtz N, Schachner M, Sachser N. 2006. Environmental bias? Effects of housing conditions, laboratory environment and experimenter on behavioral tests. *Genes, Brain Behav*. 5:64–72.
- Lim L, Mi D, Llorca A, Marín O. 2018. Development and Functional Diversification of Cortical Interneurons. *Neuron*. 100:294–313.
- Lin R, Iacovitti L. 2015. Classic and novel stem cell niches in brain homeostasis and repair. *Brain Res*. 1628:327–342.
- Lisman J, Buzsáki G, Eichenbaum H, Nadel L, Ranganath C, Redish AD. 2017. Viewpoints: how the hippocampus contributes to memory, navigation and cognition. *Nat Neurosci*. 20:1434–1447.
- Luche H, Weber O, Rao TN, Blum C, Fehling HJ. 2007. Faithful activation of an extra-bright red fluorescent protein in “knock-in” Cre-reporter mice ideally suited for lineage tracing studies. *Eur J Immunol*. 37:43–53.
- Lutz B, Marsicano G, Maldonado R, Hillard CJ. 2015. The endocannabinoid system in guarding against fear, anxiety and stress. *Nat Rev Neurosci*. 16:705–718.
- Macrì S, Biamonte F, Romano E, Marino R, Keller F, Laviola G. 2010. Perseverative responding and neuroanatomical alterations in adult heterozygous reeler mice are mitigated by neonatal estrogen administration. *Psychoneuroendocrinology*. 35:1374–1387.
- Magliaro C, Cocito C, Bagatella S, Merighi A, Ahluwalia A, Lossi L. 2016. The number of Purkinje neurons and their topology in the cerebellar vermis of normal and reelin haplodeficient mouse. *Ann Anat*. 207:68–75.
- Maglóczky Z, Tóth K, Karlócai R, Nagy S, Eröss L, Czirják S, Vajda J, Rásonyi G, Kelemen A, Juhos V, Halász P, Mackie K, Freund TF. 2010. Dynamic changes of CB1-receptor expression in hippocampi of epileptic mice and humans. *Epilepsia*. 51:115–120.

Bibliography

- Mariani J, Crepel F, Mikoshiba K, Changeux JP, Sotelo C. 1977. Anatomical, Physiological And Biochemical Studies Of The Cerebellum From Reeler Mutant Mouse. *Philos Trans R Soc London*. 281:1–28.
- Marín-Padilla M. 1998. Cajal-Retzius cells and the development of the neocortex. *Trends Neurosci*. 21:64–71.
- Markwardt SJ, Dieni C V, Wadiche JI, Overstreet-Wadiche L. 2011. Ivy/neurogliaform interneurons coordinate activity in the neurogenic niche. *Nat Neurosci*. 14:1407–1409.
- Mayer C, Hafemeister C, Bandler RC, Machold R, Batista Brito R, Jaglin X, Allaway K, Butler A, Fishell G, Satija R. 2018. Developmental diversification of cortical inhibitory interneurons. *Nature*. 555:457–462.
- Meadows JP, Guzman-Karlsson MC, Phillips S, Holleman C, Posey JL, Day JJ, Hablitz JJ, Sweatt JD. 2015. DNA methylation regulates neuronal glutamatergic synaptic scaling. *Sci Signal*. 8:ra61 (1-10).
- Mi D, Li Z, Lim L, Li M, Moissidis M, Yang Y, Gao T, Hu TX, Pratt T, Price DJ, Sestan N, Marín O. 2018. Early emergence of cortical interneuron diversity in the mouse embryo. *Science (80-)*. 360:81–85.
- Miao GG, Smeyne RJ, D’Arcangelo G, Copeland NG, Jenkins NA, Morgan JI, Curran T. 1994. Isolation of an allele of reeler by insertional mutagenesis. *Proc Natl Acad Sci U S A*. 91:11050–11054.
- Michalczyk K, Ziman M. 2005. Nestin structure and predicted function in cellular cytoskeletal organisation. *Histol Histopathol*. 20:665–671.
- Michetti C, Romano E, Altabella L, Caruso A, Castelluccio P, Bedse G, Gaetani S, Canese R, Laviola G, Scattoni ML. 2014. Mapping Pathological Phenotypes in Reelin Mutant Mice. *Front Pediatr*. 2:1–12.
- Mienville J-M, Pesold C. 1999. Low resting potential and postnatal upregulation of NMDA receptors may cause Cajal-Retzius cell death. *J Neurosci*. 19:1636–1646.
- Ming G, Song H. 2011. Adult Neurogenesis in the Mammalian Brain: Significant Answers and Significant Questions. *Neuron*. 70:687–702.
- Miyata T, Nakajima K, Aruga J, Takahashi S, Ikenaka K, Mikoshiba K, Ogawa M. 1996. Distribution of a reeler gene-related antigen in the developing cerebellum: An immunohistochemical study with an allogeneic antibody CR-50 on normal and reeler mice. *J Comp Neurol*. 372:215–228.
- Miyata T, Ono Y, Okamoto M, Masaoka M, Sakakibara A, Kawaguchi A, Hashimoto M,

Bibliography

- Ogawa M. 2010. Migration, early axonogenesis, and Reelin-dependent layer-forming behavior of early/posterior-born Purkinje cells in the developing mouse lateral cerebellum. *Neural Dev.* 5:23.
- Miyoshi G, Young A, Petros T, Karayannis T, McKenzie Chang M, Lavado A, Iwano T, Nakajima M, Taniguchi H, Huang ZJ, Heintz N, Oliver G, Matsuzaki F, Machold RP, Fishell G. 2015. Prox1 Regulates the Subtype-Specific Development of Caudal Ganglionic Eminence-Derived GABAergic Cortical Interneurons. *J Neurosci.* 35:12869–12889.
- Monory K, Massa F, Egertová M, Eder M, Blaudzun H, Westenbroek R, Kelsch W, Jacob W, Marsch R, Ekker M, Long J, Rubenstein JL, Goebbels S, Nave KA, During M, Klugmann M, Wölfel B, Dodt H-UU, Zieglgänsberger W, Wotjak CTT, Mackie K, Elphick MR, Marsicano G, Lutz B. 2006. The Endocannabinoid System Controls Key Epileptogenic Circuits in the Hippocampus. *Neuron.* 51:455–466.
- Morozov YM, Freund TF. 2003. Post-natal development of type 1 cannabinoid receptor immunoreactivity in the rat hippocampus. *Eur J Neurosci.* 18:1213–1222.
- Morozov YM, Torii M, Rakic P. 2009. Origin, early commitment, migratory routes, and destination of cannabinoid type 1 receptor-containing interneurons. *Cereb Cortex.* 19:i78–i89.
- Morrens J, van den Broeck W, Kempermann G. 2012. Glial cells in adult neurogenesis. *Glia.* 60:159–174.
- Morris RGM. 1981. Spatial Localization Does Not Require the Presence of Local Cues. *Learn Motiv.* 12:239–260.
- Moss J, Toni N. 2012. A circuit-based gatekeeper for adult neural stem cell proliferation: Parvalbumin-expressing interneurons of the dentate gyrus control the activation and proliferation of quiescent adult neural stem cells. *Bioessays.* 35:28–33.
- Mott DD, Turner DA, Okazaki MM, Lewis D V. 1997. Interneurons of the dentate-hilus border of the rat dentate gyrus: morphological and electrophysiological heterogeneity. *J Neurosci.* 17:3990–4005.
- Moy SS, Nadler JJ, Perez A, Barbaro RP, Johns JM, Magnuson TR, Piven J, Crawley JN. 2004. Sociability and preference for social novelty in five inbred strains : an approach to assess autistic-like behavior in mice. *Genes, Brain Behav.* 3:287–302.
- Muhia M, Yee BK, Feldon J, Markopoulos F, Knuesel I. 2010. Disruption of hippocampus-regulated behavioural and cognitive processes by heterozygous constitutive deletion of

Bibliography

- SynGAP. *Eur J Neurosci.* 31:529–543.
- Müller MC, Osswald M, Tinnes S, Häussler U, Jacobi A, Förster E, Frotscher M, Haas CA. 2009. Exogenous reelin prevents granule cell dispersion in experimental epilepsy. *Exp Neurol.* 216:390–397.
- Nagy A. 2000. Cre recombinase: The universal reagent for genome tailoring. *Genesis.* 26:99–109.
- Nakajima K, Mikoshiba K, Miyata T, Kudo C, Ogawa M. 1997. Disruption of hippocampal development in vivo by CR-50 mAb against reelin. *Proc Natl Acad Sci U S A.* 94:8196–8201.
- Nicola Z, Fabel K, Kempermann G. 2015. Development of the adult neurogenic niche in the hippocampus of mice. *Front Neuroanat.* 9:1–13.
- Niu S, Renfro A, Quattrocchi CC, Sheldon M, D’Arcangelo G. 2004. Reelin Promotes Hippocampal Dendrite Development through the VLDLR/ApoER2-Dab1 Pathway. *Neuron.* 41:71–84.
- Notaras MJ, Vivian B, Wilson C, van den Buuse M. 2017. Interaction of reelin and stress on immobility in the forced swim test but not dopamine-mediated locomotor hyperactivity or prepulse inhibition disruption: Relevance to psychotic and mood disorders. *Schizophr Res.* DOI.
- Nullmeier S, Panther P, Dobrowolny H, Frotscher M, Zhao S, Schwegler H, Wolf R. 2011. Region-specific alteration of GABAergic markers in the brain of heterozygous reeler mice. *Eur J Neurosci.* 33:689–698.
- O’Dell RS, Cameron DA, Zipfel WR, Olson EC. 2015. Reelin Prevents Apical Neurite Retraction during Terminal Translocation and Dendrite Initiation. *J Neurosci.* 35:10659–10674.
- Ogawa M, Miyata T, Nakajima K, Yagyu K, Seike M, Ikenaka K, Yamamoto H, Mikoshiba K. 1995. The reeler gene-associated antigen on Cajal-Retzius neurons is a crucial molecule for laminar organization of cortical neurons. *Neuron.* 14:899–912.
- Ognibene E, Adriani W, Granstrem O, Pieretti S, Laviola G. 2007. Impulsivity-anxiety-related behavior and profiles of morphine-induced analgesia in heterozygous reeler mice. *Brain Res.* 1131:173–180.
- Olson EC, Walsh CA. 2002. Smooth, rough and upside-down neocortical development. *Curr Opin Genet Dev.* 12:320–327.
- Orcinha C, Münzner G, Gerlach J, Kiliyas A, Follo M, Egert U, Haas CA. 2016. Seizure-

Bibliography

- Induced Motility of Differentiated Dentate Granule Cells Is Prevented by the Central Reelin Fragment. *Front Cell Neurosci.* 10:1–13.
- Overstreet LS, Hentges ST, Bumashny VF, de Souza FSJ, Smart JL, Santangelo AM, Low MJ, Westbrook GL, Rubinstein M. 2004. A transgenic marker for newly born granule cells in dentate gyrus. *J Neurosci.* 24:3251–3259.
- Palacios-García I, Lara-Vásquez A, Montiel JF, Díaz-Véliz GF, Sepúlveda H, Utreras E, Montecino M, González-Billault C, Aboitiz F. 2015. Prenatal Stress Down-Regulates Reelin Expression by Methylation of Its Promoter and Induces Adult Behavioral Impairments in Rats. *PLoS One.* 10:e0117680.
- Palmer TD, Willhoite AR, Gage FH. 2000. Vascular niche for adult hippocampal neurogenesis. *J Comp Neurol.* 425:479–494.
- Pappas GD, Kriho V, Pesold C. 2001. Reelin in the extracellular matrix and dendritic spines of the cortex and hippocampus: a comparison between wild type and heterozygous reeler mice by immunoelectron microscopy. *J Neurocytol.* 30:413–425.
- Pesold C, Impagnatiello F, Pisu MG, Uzunov DP, Costa E, Guidotti A, Caruncho HJ. 1998. Reelin is preferentially expressed in neurons synthesizing gamma-aminobutyric acid in cortex and hippocampus of adult rats. *Proc Natl Acad Sci U S A.* 95:3221–3226.
- Pesold C, Pisu MG, Impagnatiello F, Uzunov DP, Caruncho HJ. 1998. Simultaneous detection of glutamic acid decarboxylase and reelin mRNA in adult rat neurons using in situ hybridization and immunofluorescence. *Brain Res Protoc.* 3:155–160.
- Podda M V, Leone L, Barbati SA, Mastrodonato A, Li Puma DD, Piacentini R, Grassi C. 2014. Extremely low-frequency electromagnetic fields enhance the survival of newborn neurons in the mouse hippocampus. *Eur J Neurosci.* 39:893–903.
- Podhorna J and Didriksen M. 2004. The heterozygous reeler mouse: behavioural phenotype. *Behavioural Brain Research.* 153:43-54
- Pujadas L, Gruart A, Bosch C, Delgado L, Teixeira CM, Rossi D, de Lecea L, Martínez A, Delgado-García JM, Soriano E. 2010. Reelin regulates postnatal neurogenesis and enhances spine hypertrophy and long-term potentiation. *J Neurosci.* 30:4636–4649.
- Quattrocchi CC, Wannenes F, Persico AM, Ciafré SA, D’Arcangelo G, Farace MG, Keller F. 2002. Reelin is a serine protease of the extracellular matrix. *J Biol Chem.* 277:303–309.
- Quattrocchio G, Maccaferri G. 2013. Novel GABAergic circuits mediating excitation/inhibition of Cajal-Retzius cells in the developing hippocampus. *J Neurosci.* 33:5486–5498.

Bibliography

- Quattrocchio G, Maccaferri G. 2014. Optogenetic activation of cajal-retzius cells reveals their glutamatergic output and a novel feedforward circuit in the developing mouse hippocampus. *J Neurosci.* 34:13018–13032.
- Qiu S, Korwek KM, Pratt-Davis AE, Peters M, Bergman MY, Weeber EJ. 2006. Cognitive disruption and altered hippocampus synaptic function in Reelin haploinsufficient mice. *Neurobiology of Learning and Memory.* 85:228-242
- Ramos-Moreno T, Clascá F. 2014. Quantitative mapping of the local and extrinsic sources of GABA and Reelin to the layer Ia neuropil in the adult rat neocortex. *Brain Struct Funct.* 219:1639–1657.
- Ramos-Moreno T, Galazo MJ, Porrero C, Martínez-Cerdeño V, Clascá F. 2006. Extracellular matrix molecules and synaptic plasticity: immunomapping of intracellular and secreted Reelin in the adult rat brain. *Eur J Neurosci.* 23:401–422.
- Ranaivoson FM, von Daake S, Comoletti D. 2016. Structural insights into reelin function: Present and future. *Front Cell Neurosci.* 10:1–8.
- Reddy SS, Connor TE, Weeber EJ, Rebeck W. 2011. Similarities and differences in structure, expression, and functions of VLDLR and ApoER2. *Mol Neurodegener.* 6:1–10.
- Reinert RB, Kantz J, Ackermann Misfeldt A, Poffenberger G, Gannon M, Brissova M, Powers AC. 2012. Tamoxifen-induced cre-loxp recombination is prolonged in pancreatic islets of adult mice. *PLoS One.* 7:e33529.
- Ribak CE, Seress L. 1983. Five types of basket cell in the hippocampal dentate gyrus: a combined Golgi and electron microscopic study. *J Neurocytol.* 12:577–597.
- Ringstedt T, Linnarsson S, Wagner J, Lendahl U, Kokaia Z, Arenas E, Ernfors P, Ibáñez CF. 1998. BDNF regulates reelin expression and Cajal-Retzius cell development in the cerebral cortex. *Neuron.* 21:305–315.
- Rivera P, Arrabal S, Cifuentes M, Grondona JM, Pérez-Martín M, Rubio L, Vargas A, Serrano A, Pavón FJ, Suárez J, Rodríguez de Fonseca F. 2014. Localization of the cannabinoid CB1 receptor and the 2-AG synthesizing (DAGL α) and degrading (MAGL, FAAH) enzymes in cells expressing the Ca²⁺-binding proteins calbindin, calretinin, and parvalbumin in the adult rat hippocampus. *Front Neuroanat.* 8:56.
- Robledo RF, Rajan L, Li X, Lufkin T. 2002. The Dlx5 and Dlx6 homeobox genes are essential for craniofacial, axial, and appendicular skeletal development. *Genes Dev.* 16:1089–1101.
- Royaux I, Lambert de Rouvroit C, D’Arcangelo G, Demirov D, Goffinet AM. 1997. Genomic

Bibliography

- organization of the mouse reelin gene. *Genomics*. 46:240–250.
- Ruest L-B, Hammer RE, Yanagisawa M, Clouthier DE. 2003. Dlx5/6-Enhancer Directed Expression of Cre Recombinase in the Pharyngeal Arches and Brain. *Genesis*. 37:188–194.
- Salinger WL, Ladrow P, Wheeler C. 2003. Behavioral phenotype of the reeler mutant mouse: effects of RELN gene dosage and social isolation. *Behav Neurosci*. 117:1257–1275.
- Santana J, Marzolo M-P. 2017. The functions of Reelin in membrane trafficking and cytoskeletal dynamics: implications for neuronal migration, polarization and differentiation. *Biochem J*. 474:3137–3165.
- Santhakumar V, Aradi I, Soltesz I. 2005. Role of Mossy Fiber Sprouting and Mossy Cell Loss in Hyperexcitability: A Network Model of the Dentate Gyrus Incorporating Cell Types and Axonal Topography. *J Neurophysiol*. 93:437–453.
- Santoso A, Kaiser A, Winter Y. 2006. Individually dosed oral drug administration to socially-living transponder-tagged mice by a water dispenser under RFID control. *J Neurosci Methods*. 153:208–213.
- Scharfman H, Goodman J, Macleod A, Phani S, Antonelli C, Croll S. 2005. Increased neurogenesis and the ectopic granule cells after intrahippocampal BDNF infusion in adult rats. *Exp Neurol*. 192:348–356.
- Scharfman HE. 2016. The enigmatic mossy cell of the dentate gyrus. *Nat Rev Neurosci*. 17:562–575.
- Schiffmann SN, Bernier B, Goffinet AM. 1997. Reelin mRNA Expression During Mouse Brain Development. *Eur J Neurosci*. 9:1055–1071.
- Schindelin J, Arganda-Carreras I, Frise E, Kaynig V, Longair M, Pietzsch T, Preibisch S, Rueden C, Saalfeld S, Schmid B, Tinevez JY, White DJ, Hartenstein V, Eliceiri K, Tomancak P, Cardona A. 2012. Fiji: An open-source platform for biological-image analysis. *Nat Methods*. 9:676–682.
- Schroeder A, Buret L, Hill RA, van den Buuse M. 2015. Gene-environment interaction of reelin and stress in cognitive behaviours in mice: Implications for schizophrenia. *Behavioural Brain Research*. 287:304–314
- Schurmans S, Schiffmann SN, Gurden H, Lemaire M, Lipp H-P, Schwam V, Pochet R, Imperato A, Böhme GA, Parmentier M. 1997. Impaired long-term potentiation induction in dentate gyrus of calretinin-deficient mice. *Proc Natl Acad Sci U S A*. 94:10415–10420.

Bibliography

- Schwaller B. 2014. Calretinin: from a “simple” Ca²⁺ buffer to a multifunctional protein implicated in many biological processes. *Front Neuroanat.* 8:1–7.
- Schwenk F, Baron U, Rajewsky K. 1995. A cre-transgenic mouse strain for the ubiquitous deletion of loxP-flanked gene segments including deletion in germ cells. *Nucleic Acids Res.* 23:5080–5081.
- Sekine K, Honda T, Kawauchi T, Kubo K, Nakajima K. 2011. The outermost region of the developing cortical plate is crucial for both the switch of the radial migration mode and the Dab1-dependent “inside-out” lamination in the neocortex. *J Neurosci.* 31:9426–9439.
- Seress L. 2007. Comparative anatomy of the hippocampal dentate gyrus in adult and developing rodents, non-human primates and humans. *Prog Brain Res.* 163.
- Seri B, García-Verdugo JM, Collado-Morente L, McEwen BS, Alvarez-Buylla A. 2004. Cell types, lineage, and architecture of the germinal zone in the adult dentate gyrus. *J Comp Neurol.* 478:359–378.
- Seri B, García-Verdugo JM, McEwen BS, Alvarez-Buylla A. 2001. Astrocytes Give Rise to New Neurons in the Adult Mammalian Hippocampus. *J Neurosci.* 21:7153–7160.
- Sibbe M, Kuner E, Althof D, Frotscher M. 2015. Stem- and Progenitor Cell Proliferation in the Dentate Gyrus of the Reeler Mouse. *PLoS One.* 10:e0119643.
- Simeone A, Acampora D, Pannese M, Esposito MD, Stornaiuolo A, Gulisano M, Mallamaci A, Kastury K, Druck T, Huebner K. 1994. Cloning and characterization of two members of the vertebrate Dlx gene family. *Proc Natl Acad Sci.* 91:2250–2254.
- Simmons PA, Lemmon V, Pearlman AL. 1982. Afferent and efferent connections of the striate and extrastriate visual cortex of the normal and reeler mouse. *J Comp Neurol.* 211:295–308.
- Song J, Sun J, Moss J, Wen Z, Sun GJ, Hsu D, Zhong C, Davoudi H, Christian KM, Toni N, Ming G-L, Song H. 2013. Parvalbumin interneurons mediate neuronal circuitry-neurogenesis coupling in the adult hippocampus. *Nat Neurosci.* 16:1728–1730.
- Song J, Zhong C, Bonaguidi MA, Sun GJ, Hsu D, Gu Y, Meletis K, Huang ZJ, Ge S, Enikolopov G, Deisseroth K, Luscher B, Christian KM, Ming G, Song H. 2012. Neuronal circuitry mechanism regulating adult quiescent neural stem-cell fate decision. *Nature.* 489:150–154.
- Soriano E, Cobas A, Fairén A. 1989a. Neurogenesis of glutamic acid decarboxylase immunoreactive cells in the hippocampus of the mouse. I: regio superior and regio inferior. *J Comp Neurol.* 281:586–602.

Bibliography

- Soriano E, Cobas A, Fairén A. 1989b. Neurogenesis of glutamic acid decarboxylase immunoreactive cells in the hippocampus of the mouse. II: Area dentata. *J Comp Neurol.* 281:603–611.
- Soriano E, Del Río JA. 2005. The cells of cajal-retzius: still a mystery one century after. *Neuron.* 46:389–394.
- Stanfield BB, Caviness VS, Cowan WM. 1979. The organization of certain afferents to the hippocampus and dentate gyrus in normal and Reeler mice. *J Comp Neurol.* 185:461–483.
- Stanfield BB, Cowan WM. 1979a. The development of the hippocampus and dentate gyrus in normal and Reeler mice. *J Comp Neurol.* 185:423–459.
- Stanfield BB, Cowan WM. 1979b. The Morphology of the Hippocampus and Dentate Gyrus in Normal and Reeler Mice. *J Comp Neurol.* 185:393–422.
- Stoppini L, Buchs P-A, Muller D. 1991. A simple method for organotypic cultures of nervous tissue. *J Neurosci Methods.* 37:173–182.
- Strasser V, Fasching D, Hauser C, Mayer H, Bock HH, Hiesberger T, Herz J, Weeber EJ, Sweatt JD, Pramatarova A, Howell B, Schneider WJ, Nimpf J. 2004. Receptor Clustering Is Involved in Reelin Signaling. *Mol Cell Biol.* 24:1378–1386.
- Sui Y, Vermeulen R, Hökfelt T, Horne MK, Stanić D. 2013. Female mice lacking cholecystinin 1 receptors have compromised neurogenesis, and fewer dopaminergic cells in the olfactory bulb. *Front Cell Neurosci.* 7:13.
- Sultan KT, Brown KN, Shi S-H. 2013. Production and organization of neocortical interneurons. *Front Cell Neurosci.* 7:221.
- Sun C, Mchedlishvili Z, Bertram EH, Erisir A, Kapur J. 2007. Selective Loss of Dentate Hilar Interneurons Contributes to Reduced Synaptic Inhibition of Granule Cells in an Electrical Stimulation-Based Animal Model of Temporal Lobe Epilepsy. *J Comp Neurol.* 500:876–893.
- Supèr H, Del Río JA, Martínez A, Pérez-sust P, Soriano E. 2000. Disruption of Neuronal Migration and Radial Glia in the Developing Cerebral Cortex Following Ablation of Cajal–Retzius Cells. *Cereb Cortex.* 10:602–613.
- Suzuki F, Junier M-P, Guilhem D, Sørensen JC, Onteniente B. 1995. Morphogenetic effect of kainate on adult hippocampal neurons associated with a prolonged expression of brain-derived neurotrophic factor. *Neuroscience.* 64:665–674.
- Teixeira CM, Kron MM, Masachs N, Zhang H, Lagace DC, Martinez A, Reillo I, Duan X,

Bibliography

- Bosch C, Pujadas L, Brunso L, Song H, Eisch AJ, Borrell V, Howell BW, Parent JM, Soriano E. 2012. Cell-Autonomous Inactivation of the Reelin Pathway Impairs Adult Neurogenesis in the Hippocampus. *J Neurosci.* 32:12051–12065.
- Teixeira CM, Martín ED, Sahún I, Masachs N, Pujadas L, Corvelo A, Bosch C, Rossi D, Martinez A, Maldonado R, Dierssen M, Soriano E. 2011. Overexpression of Reelin prevents the manifestation of behavioral phenotypes related to schizophrenia and bipolar disorder. *Neuropsychopharmacology.* 36:2395–2405.
- Tensaouti Y, Stephanz EP, Yu T-S, Kernie SG. 2018. ApoE Regulates the Development of Adult Newborn Hippocampal Neurons. *eNeuro.* 5:1–15.
- Terashima T. 1996. Distribution of mesencephalic trigeminal nucleus neurons in the reeler mutant mouse. *Anat Rec.* 244:563–571.
- Tissir F, Lambert de Rouvroit C, Goffinet AM. 2002. The role of reelin in the development and evolution of the cerebral cortex. *Brazilian J Med Biol Res.* 35:1473–1484.
- Toesca A, Geloso MC, Mongiovì AM, Furno A, Schiattarella A, Michetti F, Corvino V. 2016. Trimethyltin Modulates Reelin Expression and Endogenous Neurogenesis in the Hippocampus of Developing Rats. *Neurochem Res.* 41:1559–1569.
- Torigoe M, Yamauchi K, Kimura T, Uemura Y, Murakami F. 2016. Evidence That the Laminar Fate of LGE/CGE-Derived Neocortical Interneurons Is Dependent on Their Progenitor Domains. *J Neurosci.* 36:2044–2056.
- Tough DF, Sprent J. 1994. Turnover of Naive- and Memory-phenotype T Cells. *J Exp Med.* 179:1127–1135.
- Tricoire L, Pelkey K a, Erkkila BE, Jeffries BW, Yuan X, Mcbain CJ. 2011. A Blueprint for the Spatiotemporal Origins of Mouse Hippocampal Interneuron Diversity. *J Neurosci.* 31:10948–10970.
- Trommsdorff M, Gotthardt M, Hiesberger T, Shelton J, Stockinger W, Nimpf J, Hammer RE, Richardson JA, Herz J. 1999. Reeler/disabled-like disruption of neuronal migration in knockout mice lacking the VLDL receptor and ApoE receptor 2. *Cell.* 97:689–701.
- Tuetting P, Costa E, Dwivedi Y, Guidotti A, Impagnatiello F, Manev R, Pesold C. 1999. The phenotypic characteristics of heterozygous reeler mouse. *Neuroreport.* 10:1329–1334.
- Unal G, Joshi A, Viney TJ, Kis V, Somogyi P. 2015. Synaptic Targets of Medial Septal Projections in the Hippocampus and Extrahippocampal Cortices of the Mouse. *J Neurosci.* 35:15812–15826.
- Uribe E, Wix R. 2011. Epigenetic control of the GABAergic interneurons migration and

Bibliography

- NMDA receptor functioning in schizophrenia . *Rev eNeurobiología*. 2:1–13.
- Utsunomiya-Tate N, Kubo K, Tate S, Kainosho M, Katayama E, Nakajima K, Mikoshiba K. 2000. Reelin molecules assemble together to form a large protein complex, which is inhibited by the function-blocking CR-50 antibody. *Proc Natl Acad Sci U S A*. 97:9729–9734.
- van Strien NM, Cappaert NLM, Witter MP. 2009. The anatomy of memory: an interactive overview of the parahippocampal-hippocampal network. *Nat Rev Neurosci*. 10:272–282.
- Verdaguer E, Brox S, Petrov D, Olloquequi J, Romero R, de Lemos ML, Camins A, Auladell C. 2015. Vulnerability of calbindin, calretinin and parvalbumin in a transgenic/knock-in APP^{swe}/PS1^{dE9} mouse model of Alzheimer disease together with disruption of hippocampal neurogenesis. *Exp Gerontol*. 69:176–188.
- Villar-Cerviño V, Molano-Mazón M, Catchpole T, Valdeolmillos M, Henkemeyer M, Martínez LM, Borrell V, Marín O. 2013. Contact repulsion controls the dispersion and final distribution of Cajal-Retzius cells. *Neuron*. 77:457–471.
- Vorhees C V, Williams MT. 2006. Morris water maze: Procedures for assessing spatial and related forms of learning and memory. *Nat Protoc*. 1:848–858.
- Wahlsten D. 2011. *Mouse behavioral testing*. 1st ed. London: Academic Press.
- Wamsley B, Fishell G. 2017. Genetic and activity-dependent mechanisms underlying interneuron diversity. *Nat Rev Neurosci*. 18:299–309.
- Ward JM, Henneman JR, Osipova GY, Anisimov VN. 1991. Persistence of 5-bromo-2'-deoxyuridine in tissues of rats after exposure in early life. *Toxicology*. 70:345–352.
- Wilhelmsson U, Lebkuechner I, Leke R, Marasek P, Yang X, Antfolk D, Chen M, Mohseni P, Lasič E, Bobnar ST, Stenovec M, Zorec R, Nagy A, Sahlgren C, Pekna M, Pekny M. 2019. Nestin Regulates Neurogenesis in Mice Through Notch Signaling From Astrocytes to Neural Stem Cells. *Cereb Cortex*. 29:4050–4066.
- Witter MP. 2007. The perforant path: projections from the entorhinal cortex to the dentate gyrus. *Prog Brain Res*. 163:43–61.
- Wojtowicz JM, Kee N. 2006. BrdU assay for neurogenesis in rodents. *Nat Protoc*. 1:1399–1405.
- Zerucha T, Stühmer T, Hatch G, Park BK, Long Q, Yu G, Gambarotta A, Schultz JR, Rubenstein JLR, Ekker M. 2000. A highly conserved enhancer in the *Dlx5/Dlx6* intergenic region is the site of cross-regulatory interactions between *Dlx* genes in the embryonic forebrain. *J Neurosci*. 20:709–721.

Bibliography

- Zhao S, Chai X, Frotscher M. 2007. Balance between neurogenesis and gliogenesis in the adult hippocampus: role for reelin. *Dev Neurosci.* 29:84–90.
- Zhou Y, Falenta K, Lalli G. 2014. Endocannabinoid signalling in neuronal migration. *Int J Biochem Cell Biol.* 47:104–108.

Publication:

Pahle J, Muhia M, Wagener R, Tippmann A, Bock HH, Graw J, Herz J, Staiger J, Drakew A, Kneussel M, Rune G, Frotscher M, Brunne B. 2019. Selective inactivation of Reelin in inhibitory interneurons leads to subtle changes in the dentate gyrus but leaves cortical layering and behavior unaffected. *Cerebral Cortex*. 10.1093/cercor/bhz196.

Published online 30th of October 2019

Appendix

Appendix

A1 Recipes

Mowiol 4-88 after Carl Roth		amount:	~110 ml	
Chemical substance	formular	volume/mass	stock solution concentration/ molar mass	final concentration
Mowiol 4-88	$(-\text{CH}_2\text{CHOH})_n$	12 g	31.00 g/mol	3.519 mol/l
Millipore water	H_2O	30 ml	18.015 g/mol	
Glycerin, $\geq 99.5\%$ p.a.	$\text{C}_3\text{H}_8\text{O}_3$	30 g	13.681 mol/l	2.961 mol/l
Tris-HCl pH 8.5	$\text{C}_4\text{H}_{11}\text{NO}_3 \cdot \text{HCl}$	60 ml	0.2 mol/l	0.109 mol/l

10x Modified Gitschier buffer		amount:	50 ml	
Chemical substance	formular	volume	stock solution concentration	final concentration
Tris, alkaline pH 8.8	$\text{C}_4\text{H}_{11}\text{NO}_3$	16.75 ml	2 mol/l	0.67 mol/l
Ammonium sulphate	$(\text{NH}_4)_2\text{SO}_4$	8.3 ml	1 mol/l	0.166 mol/l
Magnesium chloride	MgCl_2	3.25 ml	1 mol/l	0.065 mol/l
Double distilled water	H_2O	21.7 ml		

10x Phosphate buffered saline (10xPBS)		amount:	1 l	
Chemical substance	formular	mass	molar mass	final concentration
Sodium chloride	NaCl	80.00 g	58.50 g/mol	1.38 mol/l
Potassium chloride	KCl	2.01 g	74.55 g/mol	0.027 mol/l
Di-sodium hydrogen phosphate dihydrate	$\text{Na}_2\text{HPO}_4 \cdot 2\text{H}_2\text{O}$	17.80 g	177.99 g/mol	0.1 mol/l
Potassium dihydrogen phosphate	KH_2PO_4	2.72 g	136.09 g/mol	0.02 mol/l

Phosphate buffer (PB) stock solutions		amount:	100 ml, 200 ml	
Chemical substance	formular	mass	molar mass	final concentration
Sodium dihydrogen phosphate monohydrate	$\text{NaH}_2\text{PO}_4 \cdot \text{H}_2\text{O}$	13.8 g	137.99 g/mol	1 mol/l
Millipore water	H_2O	fill up to 100 ml		
Di-Sodium hydrogen phosphate dihydrate	$\text{Na}_2\text{HPO}_4 \cdot 2\text{H}_2\text{O}$	35.6 g	177.99 g/mol	1 mol/l
Millipore water	H_2O	fill up to 200 ml		

1x Phosphate buffer (1xPB) pH 7.4		amount:	500 ml	
Chemical substance	formular	concentration stock	volume stock	final concentration
Sodium dihydrogen phosphate monohydrate	$\text{NaH}_2\text{PO}_4 \cdot \text{H}_2\text{O}$	1 mol/l	10.00 ml	0.02 mol/l
Di-Sodium hydrogen phosphate dihydrate	$\text{Na}_2\text{HPO}_4 \cdot 2\text{H}_2\text{O}$	1 mol/l	40.00 ml	0.08 mol/l
Millipore water	H_2O		fill up to 500 ml	
autoclave				

Soriano buffer stock solutions		amount:	10 ml	
Chemical substance	formular	mass	molar mass	final concentration
Ammonium sulphate	$(\text{NH}_4)_2\text{SO}_4$	1.3214 g	132.14 g/mol	1 mol/l
Tris, alkaline pH 8.8	$\text{C}_4\text{H}_{11}\text{NO}_3$	3.152 g	157.6 g/mol	2 mol/l
Magnesium chloride	MgCl_2	2.033 g	203.3 g/mol	1 mol/l
EDTA	$\text{C}_{10}\text{H}_{16}\text{N}_2\text{O}_8$	1.46125 g	292.25 g/mol	0.5 mol/l
Aqua ad iniectionem	H_2O		fill up to 10 ml	

Appendix

Soriano buffer		amount:	10 ml	
Chemical substance	formular	concentration stock	volume stock	final concentration
Ammonium sulphate	(NH ₄) ₂ SO ₄	1 mol/l	1.66 ml	0.166 mol/l
Tris, alkaline pH 8.8	C ₄ H ₁₁ NO ₃	2 mol/l	3.35 ml	0.670 mol/l
Magnesium chloride	MgCl ₂	1 mol/l	0.67 ml	0.067 mol/l
EDTA	C ₁₀ H ₁₆ N ₂ O ₈	0.5 mol/l	0.0013 ml	0.000067 mol/l
2-mercaptoethanol, ≥99 %, p.a.	C ₂ H ₆ OS	14.4 mol/l	0.0348 ml	0.0497 mol/l
Aqua ad iniectionem	H ₂ O		4.284 ml	

50x Tris-acetic acid-EDTA (TAE) buffer pH 8.0-8.3		amount:	1 l	
Chemical substance	formular	mass /volume	concentration stock	final concentration
Tris, alkaline	C ₄ H ₁₁ NO ₃	242 g		1.998 mol/l
Millipore water	H ₂ O	500 ml		
EDTA pH 8.0	C ₁₀ H ₁₆ N ₂ O ₈	100 ml	0.50 mol/l	0.050 mol/l
Acetic acid	C ₂ H ₄ O ₂	57.10 ml	17.485 mol/l	0.998 mol/l
Millipore water	H ₂ O	fill up to 1 l		

6x Loading buffer for agarose gelelectrophoresis		amount:	10 ml	
Chemical substance	formular	mass /volume	final concentration	
Orange G	C ₁₆ H ₁₀ N ₂ Na ₂ O ₇ S ₂	0.025 g	5.5265*10 ⁻⁶ mol/l	
Sucrose ≥99.5% (GC)	C ₁₂ H ₂₂ O ₁₁	4.0 g	1.169 mol/l	
Milliporewater		fill up to 10 ml		

3x Laemmli loading buffer		amount:	10 ml	
Chemical substance	formular	concentration stock/ molar mass	volume/mass stock	final concentration
Tris-HCl pH 6,8	C ₄ H ₁₁ NO ₃ · HCl	1 mol/l	2.4 ml	0.240 mol/l
Sodium dodecyl sulfate (SDS)	C ₁₂ H ₂₅ NaO ₄ S	0.694 mol/l	3.0 ml	0.208 mol/l
Glycerin, ≥99.5 % p.a.	C ₃ H ₈ O ₃	13.681 mol/l	3.0 ml	4.104 mol/l
2-mercaptoethanol, ≥99 %, p.a.	C ₂ H ₆ OS	14.4 mol/l	1.6 ml	2.304 mol/l
Bromphenol blue	C ₁₉ H ₁₀ Br ₄ O ₅ S	669.96 g/mol	0.003-0.006 g	various

10x SDS running buffer pH 8.6		amount:	1 l	
Chemical substance	formular	concentration stock/ molar mass	volume stock	final concentration
Tris, alkaline	C ₄ H ₁₁ NO ₃	121.14 g/mol	30.29 g	0.250 mol/l
Glycin, ≥99 %, p.a.	C ₂ H ₅ NO ₂	75.07 g/mol	144.13 g	1.920 mol/l
Millipore water	H ₂ O		fill up to 1 l	
Sodium dodecyl sulfate (SDS)	C ₁₂ H ₂₅ NaO ₄ S	288.393 g/mol	10 g	0.035 mol/l

10x Transfer buffer pH 8.6		amount:	1 l	
Chemical substance	formular	concentration stock/ molar mass	volume stock	final concentration
Tris, alkaline	C ₄ H ₁₁ NO ₃	121.14 g/mol	30.29 g	0.250 mol/l
Glycin, ≥99 %, p.a.	C ₂ H ₅ NO ₂	75.07 g/mol	142.6 g	1.900 mol/l
Millipore water	H ₂ O		fill up to 1 l	

Tris buffered saline with Tween 20 (TBST20)		amount:	1 l		
Chemical substance	formular	molar mass	concentration stock	volume stock	final concentration
Tris-HCl pH 8.0	C ₄ H ₁₁ NO ₃ · HCl	157.6 g/mol	0.5 mol/l	20 ml	0.010 mol/l
Sodium chloride	NaCl	58.50 g/mol	5 mol/l	30 ml	0.150 mol/l
Tween 20	C ₅₈ H ₁₁₄ O ₂₆	1.228 g/mol	81.433 mol/l	10 ml	0.814 mol/l
Millipore water	H ₂ O			fill up to 1 l	

Appendix

Tris buffered saline (TBS)		amount: 1 l				
Chemical substance	formular	molar mass	concentration stock	volume stock	final concentration	
Tris-HCl pH 8.0	C ₄ H ₁₁ NO ₃ · HCl	157.6 g/mol	0.5 mol/l	20 ml	0.010 mol/l	
Sodium chloride	NaCl	58.50 g/mol	5 mol/l	30 ml	0.150 mol/l	
Millipore water	H ₂ O			fill up to 1 l		

4x SDS loading buffer		amount: 50 ml				
Chemical substance	formular	molar mass	concentration stock	volume stock	final concentration	
Tris-HCl pH 8.0	C ₄ H ₁₁ NO ₃ · HCl	157.6 g/mol	1 mol/l	25 ml	0.500 mol/l	
Sodium dodecyl sulfate (SDS)	C ₁₂ H ₂₅ NaO ₄ S	288.393 g/mol	0.69 mol/l	10 ml	0.138 mol/l	
Glycerin, ≥99.5 % p.a.	C ₃ H ₈ O ₃	92.09 g/mol	13.681 mol/l	10 ml	2.736 mol/l	
Millipore water	H ₂ O			3 ml		
Bromophenol blue salt	C ₁₉ H ₉ Br ₄ O ₅ SNa	691.9 g/mol	0.007 mol/l	2 ml	0.00028 mol/l	
2-mercaptoethanol, ≥99 %, p.a.	C ₂ H ₆ OS	78.13 g/mol	14.4 mol/l	0.2 ml	0.056 mol/l	

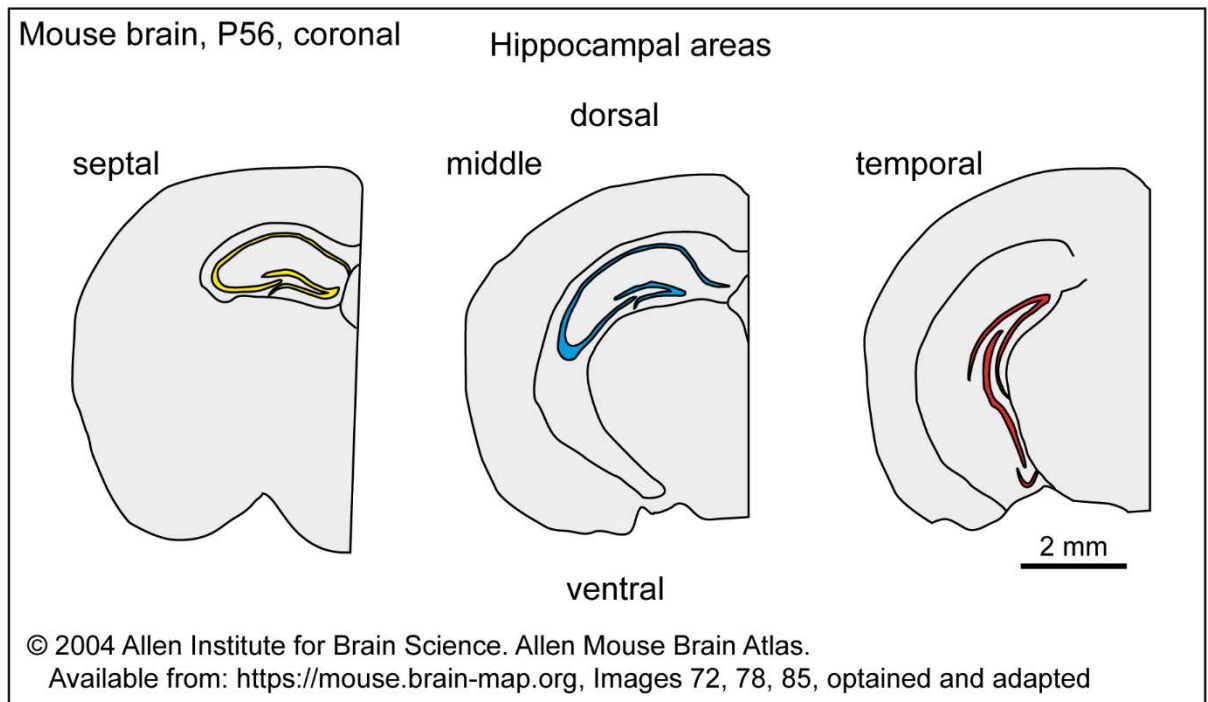
Acrylamid electrophoresis gel 4 / 8 / 15 %		amount: 1 gel					
Chemical substance	formular	molar mass	concentration stock	volume stock (4 %)	volume stock (8 %)	volume stock (15 %)	
Millipore water	H ₂ O			2.18 ml	3.78 ml	1.89 ml	
Acrylamid	C ₃ H ₅ NO	71.08 g/mol	4.2 mol/l	0.50 ml	2.16 ml	4.05 ml	
Tris, alkaline pH 8.8	C ₄ H ₁₁ NO ₃	121.14 g/mol	1.5 mol/l	X	2.03 ml	2.03 ml	
Tris, alkaline pH 6.8	C ₄ H ₁₁ NO ₃	121.14 g/mol	0.5 mol/l	0.95 ml	X	X	
Sodium dodecyl sulfate (SDS)	C ₁₂ H ₂₅ NaO ₄ S	288.393 g/mol	0.35 mol/l	0.040 ml	0.086 ml	0.086 ml	
Ammonium persulfate (APS)	(NH ₄) ₂ S ₂ O ₈	228.20 g/mol	0.44 mol/l	0.080 ml	0.086 ml	0.086 ml	
Tetramethylethyldiamine (TEMED)	C ₆ H ₁₆ N ₂	116.21 g/mol	8.60 mol/l	0.005 ml	0.005 ml	0.005 ml	

Appendix

A2 Score sheet

Annex 7: Scoring list										
Termination criterion of application:										
G14 / 111 Wirkung des Signalproteins Reelin im Gyrus dentatus – Vergleichende Studie zur Reelinwirkung im juvenilen und adulten Gehirn										
Recent Test										
BrdU application via the drinking water										
Monitoring intervals:										
BrdU application with drinking water: 6 hours, 24 hours and 48 hours after the exchange of the drinking water - followed by three times per week										
										Animal number:
Score of burden/termination criterion	date	6h	24h	48h	Wed	Fri	Mon	Wed	Fri	Mon
Monitoring	point rating ^{2,3}									
I Bodyweight										
based on initial weight [X]										
based on control group []	bodyweight:									
unchanged or raised	0									
reduction > 10 %	10									
reduction > 20 %	20									
II General condition										
Fur smooth, shiny, sleek; body orifice clean	0									
Fur dull, ruffled; dull eyes	5									
Clotted or wet body orifice; abnormal posture; high muscle tone; dehydration	10									
Spasms; paralyses; respiratory sounds; animal feels to be cold at touching	20									
III Spontaneous behaviour										
normal behaviour (sleeping, reaction on beeing blow n at and touched, curious, social contacts)	0									
unusual behaviour, restricted motor functions or hyperkinetic	5									
Isolation; pain vocalisation; apathy; pronounced hyperkinetic or rather stereotypy; impairment of coordination	10									
Automutilation	20									
IV Experiment specific criterions										
No uptake of drinking water from the bottles after 6h - if the animal denies to drink water from the scaled bottles, they get their normal drinking bottle with water back after 6 h.	Termination of experiment - see remarks left									
Rating, actions	Sum of points									
not burdened	0									
light burden: watch carefully (1x daily), possible supporting actions (e.g. heat supply, special diet)	5-9									
moderate burden: in certain circumstances initiate medical care (analgesia, antibiotic) if lasting longer than 72 h it's considered as severe burden	10-19									
severe burden: consulting of animal welfare officer; initiate veterinary care; if necessary euthanise animal	20 or higher									
Remarks:										
¹ These points have to be filled in by the applicant.										
² Points (0/5/10/20) are given once per row as soon as the criterion is fulfilled. Even if there are more than one positive finding the sum up of points must not be performed.										

A3 Hippocampal areas



A3: Hippocampal areas

Scheme of the septal, middle and temporal hippocampal areas analysed in this work. Taken from Allen mouse Brain Atlas (Lein et al. 2007) and modified by author.

Appendix

A4 Companies

Company	Address	Homepage
A		
Abcam plc	330 Science Park, Cambridge CB4 0FL, United Kingdom	https://www.abcam.com/
Adobe	345 Park Avenue, San Jose, CA 95110-2704, USA	https://www.adobe.com/de
Agilent (Dako)	5301 Stevens Creek Blvd., Santa Clara, CA 95051, USA	https://www.agilent.com/
AppliChem GmbH	Ottoweg 4, 64291 Darmstadt, Germany	https://www.applichem.com/shop/informationen/
Autodesk Inc.	111 McInnis Parkway, San Rafael, CA 94903, USA	https://www.autodesk.de/
B		
Bitplane AG	Badenerstrasse 682, 8048 Zürich, Switzerland	http://www.bitplane.com/
Bio-Rad Laboratories Inc.	1000 Alfred Nobel Drive, Hercules, CA 94547, USA	http://www.bio-rad.com/de
Biozol Diagnostica Vertrieb GmbH	Obere Hauptstrasse 10b, 85386 Eching, Germany	https://www.biozol.de/en/
Braun B. Melsungen AG	Carl-Braun-Straße 1, 34212 Melsungen, Germany	https://www.bbraun.de/de.html
C		
Corning Inc.	One Riverfront Plaza, Corning, NY 14831, USA	https://www.corning.com/emea/de.html
D		
Dianova Gesellschaft für biochemische, immunologische und mikrobiologische Diagnostik mbH	Warburgstraße 45, 20354 Hamburg, Germany	https://www.dianova.com/
E		
Eppendorf Vertrieb Deutschland GmbH	Peter-Henlein-Straße 2, 50389 Wesseling-Berzdorf, Germany	https://www.eppendorf.com/DE-de/
F		
Fermentas (now ThermoFischer Scientific)	168 Third Avenue, Waltham, MA 02451, USA	https://www.thermo-fisher.com/de/de/home/brands/thermo-scientific/molecular-biology.html
G		
GATC Biotech AG (now eurofins)	Jakob-Stadler-Platz 7, 78467 Konstanz, Germany	https://www.eurofinsgenomics.eu/de/custom-dna-sequencing/gatc-services/
Genaxxon bioscience GmbH	Söflinger Straße 70, 89077 Ulm, Germany	https://www.genaxxon.com/
Gillette (Procter & Gamble Service GmbH)	Sulzbacher Straße 40, 65824 Schwalbach am Taunus, Germany	https://gillette.de/de-de
H		
Hartenstein A. GmbH	Friedrich-Berghaus-Ring 13, 97076 Würzburg, Germany	https://www.laborversand.de/
I		
IBM Deutschland GmbH	IBM-Allee 1, 71137 Ehningen, Germany	https://www.ibm.com/de-de/
Intas Science Imaging Instruments GmbH	Florenz- Sartorius- Straße 14, 37079 Göttingen, Germany	https://www.intas.de/
K		
Keveness Deutschland GmbH	Siemensstraße 1, 63263 Neu-Isenburg, Germany	https://www.keveness.de/
L		
Langenbrinck R. GmbH	Im Hausgrün 13, 79312 Emmendingen, Germany	http://www.langenbrinck.com/home/
Life Technologies (now ThermoFischer Scientific)	168 Third Avenue, Waltham, MA 02451, USA	https://www.thermo-fisher.com/de/de/home/brands/thermo-scientific/molecular-biology.html
LEGO Systems A/S	Aastvej 1, 7190 Billund, Denmark	https://www.lego.com/de-de
Lefranc & Bourgeois Col Art (Colart International Ltd)	21 Evesham Street, London, W11 4AJ, United Kingdom	https://www.colart.com/en/our-brands/lefranc-bourgeois/
M		
Menzel Gerhard GmbH (now ThermoFischer Scientific)	168 Third Avenue, Waltham, MA 02451, USA	https://www.thermo-fisher.com/de/de/home/brands/thermo-scientific/molecular-biology.html
Merck KGaA	Frankfurter Straße 250, 64293 Darmstadt, Germany	http://www.merckmillipore.com/DE/de
N		
Nikon GmbH	Tiefenbroicher Weg 25, 40472 Düsseldorf, Germany	https://www.nikon.de/de_DE/
Noldus Information Technology BV	Nieuwe Kanaal 5, 6709 PA Wageningen, Netherlands	https://www.noldus.com/
O		
Olympus Europa SE & Co. KG	Amsinckstraße 63, 20097 Hamburg	https://www.olympus.de/
P		
Peglab Biotechnologies GmbH	Carl-Thiersch-Str. 2b, 91052 Erlangen	http://www.peglab.de
Q		
Qiagen GmbH - Germany	Qiagen Strasse 1, 40724 Hilden, Germany	https://www.qiagen.com/us/
R		
Roche Deutschland Holding GmbH	Emil-Barell-Straße 1, 79639 Grenzach-Wyhlen, Germany	https://www.roche.de
Roth Carl GmbH + Co. KG	Schoemperlenstraße 1-5, 76185 Karlsruhe, Germany	https://www.carlroth.com/de/de
S		
Santa Cruz Biotechnology Inc.	10410 Finnell Street, Dallas, TX 75220, USA	https://www.scbt.com/scbt/home
Sarstedt AG & Co. KG	Sarstedtstraße 1, 51588 Nümbrecht	https://www.sarstedt.com
Schott AG	Hattenbergstraße 10, 55122 Mainz, Germany	https://www.schott.com/german/index.html
Sigma-Aldrich (now Merck KGaA)	Frankfurter Straße 250, 64293 Darmstadt, Germany	https://www.sigmaaldrich.com/germany.html
Swant Inc.	Rte Ancienne Papeterie, MIC, 1723 Marly 1, Switzerland	https://www.swant.com/
Synaptic Systems Gesellschaft für neurobiologische Forschung, Entwicklung und Produktion mbH	Rudolf-Wissell-Str. 28, 37079 Göttingen, Germany	https://www.sysy.com/
Systat Software Inc.	2107 North First Street, Suite 360, San Jose, CA 95131 USA	https://systatsoftware.com/
T		
TSI GmbH & Co. KG	Südring 26, 27404 Zeven, Germany	https://www.tsi.de

Acknowledgements

Acknowledgements

I would like to thank Prof. Dr. Dr. h.c. Michael Frotscher posthumously for the chance to do my doctorate at his laboratory. He always made time for advice, suggestions, critics and guidance. His enthusiasm for science was inspiring and encouraging.

I thank Prof. Dr. Christian Lohr for supervising me as part of the Department of Biology at the University of Hamburg and for asking the right questions to further my scientific work.

Prof. Dr. Matthias Kneussel I like to thank for assuming the responsibility for all of us after the unexpected death of Prof. Frotscher in 2017. Furthermore, I would like to thank him for supervising my doctorate and giving me access to his behavioural laboratory to perform my work.

Additionally, I thank Dr. Bianka Brunne, who supervised me during the years of my scientific work and funded my position.

Dr. Mary Muhia I would like to thank for her help with the behavioural experiments and for urging me to learn and use statistics properly.

For the supply with the floxed mouse line, I thank Prof. Dr. Hans Bock and Prof. Dr. Joachim Herz, Prof. Dr. Hans Jörg Fehling for providing us with the tdRFP reporter mouse line and Prof. Gary Westbrook for the POMCeGFP mouse line.

I also like to thank our technicians, especially Bettina Herde and Janice Graw, for their support within the laboratory.

For handling and housing our mouse lines, I would like to thank the animal caretakers of the ZMNH, especially Hiltrud Voss, Eva Kronberg, and Silvana Deutsch.

Thank you, Mrs Suciu, for your support and proofreading.

Thank you, Angelika, for support and encouraging words.

Very cordially thanks go to my friend Alf, once for the help with the 3D construction of the stem cell niche and second, together with my friend Kordula, for their encouraging support and proofreading.

You can not make it without good friends luckily I have the best!

Thank you, Björn, for being the friend with the alternative perspective and heart!

Thank you, Jasper, for your scientific inspiration and your humour!

Thank you, Victoria! Without you, I would not have finished my work! And thank you for the best godson in the whole world!

In the end, I want to thank the most important person who has always encouraged me to walk my ground and stand by myself, my mother Emmi. Danke Mama!